Fisheries and Oceans Canada
Canada
Ecosystems and Oceans Science

Pêches et Océans
Canada
Sciences des écosystèmes
et des océans

Canadian Science Advisory Secretariat (CSAS)

Research Document 2015/064

National Capital Region

Transport and dispersal of sea lice bath therapeutants from salmon farm net-pens and well-boats

F.H. Page[1], R. Losier[1], S. Haigh[1], J. Bakker[1], B.D. Chang[1], P. McCurdy[1], M. Beattie[2], K. Haughn[1], B. Thorpe[2], J. Fife[1], S. Scouten[1], D. Greenberg[3], W. Ernst[4], D. Wong[1], and G. Bartlett[1]

[1]Fisheries and Oceans Canada
St. Andrews Biological Station
531 Brandy Cove Road
St. Andrews, New Brunswick, E5B 2L9

[2]New Brunswick Department of Agriculture, Aquaculture and Fisheries
850 Lincoln Road
Fredericton, New Brunswick, E3B 3H2

[3]Fisheries and Oceans Canada
Bedford Institute of Oceanography
1 Challenger Drive
Dartmouth, Nova Scotia, B2Y 4A2

[4]Environment Canada
45 Alderney Drive
Dartmouth, Nova Scotia, B2Y 2N6

December 2015

Canada

Foreword

This series documents the scientific basis for the evaluation of aquatic resources and ecosystems in Canada. As such, it addresses the issues of the day in the time frames required and the documents it contains are not intended as definitive statements on the subjects addressed but rather as progress reports on ongoing investigations.

Research documents are produced in the official language in which they are provided to the Secretariat.

Published by:

Fisheries and Oceans Canada
Canadian Science Advisory Secretariat
200 Kent Street
Ottawa ON K1A 0E6

http://www.dfo-mpo.gc.ca/csas-sccs/
csas-sccs@dfo-mpo.gc.ca

© Her Majesty the Queen in Right of Canada, 2015

ISSN 1919-5044

Correct citation for this publication:

Page, F.H., Losier, R., Haigh, S., Bakker, J., Chang, B.D., McCurdy, P., Beattie, M., Haughn, K., Thorpe, B., Fife, J., Scouten, S., Greenberg, D., Ernst, W., Wong, D., and Bartlett, G. 2015. Transport and dispersal of sea lice bath therapeutants from salmon farm net-pens and well-boats. DFO Can. Sci. Advis. Sec. Res. Doc. 2015/064. xviii +148 p.

TABLE OF CONTENTS

ABSTRACT xv

RÉSUMÉ xvii

INTRODUCTION 1

NET-PENS 1

- Background 1
  - The Treatment Process 1
  - Concentration within Cages 8
  - Flushing from Cages 12
- Mixing and Flushing within Net-Pen 13
  - Methods 13
  - Observations 15
  - Mixing and Flushing Summary 24
- Transport and Dispersal away from Net-Pen 25
  - Background 25
  - Horizontal Transport and Dispersion 29
  - Vertical Distribution and Mixing 41
- Theory and Models 57
  - Dilution of Therapeutant 57
  - FVCOM Modelling 60
- Comparisons between Models and Observations 73
  - Patch Size 73
  - Patch Trajectories: Current Meters 75
  - Patch Trajectories: FVCOM 79
  - Dilution of Concentrations: Okubo-Based Approach 90
  - Dilution of Concentrations: FVCOM-Based Approach 92
  - Model Limitations and Potential Areas for Improvement 94
  - Comparison with SEPA Model 98
  - Summary of Net-Pen Model Results 100

WELL-BOATS 102

- Background 102
  - The Treatment Process 102
  - Initial Distribution within the Well 103
- Transport and Dispersal Once Released into the Receiving Environment 107
  - Background 107
  - Methods 109
  - Observation 111
  - Models 133

CHEMISTRY 138

- Chemical-Dye Relationships 138
- Chemical Persistence 140

SUMMARY AND CONCLUSIONS 143
  Factors Influencing Net-Pen Transport and Dispersal 143
  Factors Influencing Well-Boat Transport and Dispersal 143
  Conclusions for Tarp Treatments 144
  Conclusions for Well-Boats 145
  Conclusions Common to Both Tarp and Well-Boat Treatments 145
  Conclusions Based on the Theories and Observations Examined 146
ACKNOWLEDGEMENTS 147
REFERENCES CITED 147

TABLE OF TABLES

Table 1. Dimensions and volume estimates for tarped circular fish cages under different assumptions of cage size and volume shape....11

Table 2. Calculated estimates of the time, in units of minutes, needed for ambient water currents to advect or transport therapeutant out of the treated cage in an ideal case without farm infrastructure. 12

Table 3. Summary of net-pen dye release experiments including characterizations of current regime and mixing and flushing times....14

Table 4. Distance traveled over time durations of 1 and 3 hours. 38

Table 5. Summary of horizontal eddy diffusivities estimated from dye releases conducted in southwest New Brunswick during 2010-11. The values were estimated from the lengths of the major and minor axes of each plume perimeter and the associated times since release. The single value for each site was estimated from the composite of all data for the site. 40

Table 6. Estimated order of magnitude time scales for vertical mixing over a range of depths when K_z has values of 0.01 m^2/s and 0.1 m^2/s. 41

Table 7. Summary of data associated with vertical dye concentration profiles obtained during dye releases conducted from salmon net-pen therapeutant treatments conducted in southwest Brunswick during 2010-11. Descriptions of the contents of the columns occur in the text. 43

Table 8. Mean values of comparisons of tidal amplitudes and phases of FVCOM run with observed values. 63

Table 9. M2 tidal elevation amplitudes and phases from the tidal analysis of sea surface heights from ADCP data and FVCOM model results for deployments located in the vicinity of dye release Site A. 64

Table 10. M2 tidal ellipse parameters from the tidal analysis currents from ADCP data and FVCOM model results for deployments located in the vicinity of dye release Site A. The results have been vertically averaged over the sigma layers and only include the range of sigma layers for which ADCP data exist. 64

Table 11. M2 tidal elevation amplitudes and phases from the tidal analysis of sea surface heights from ADCP data and FVCOM model results for deployments located in the vicinity of dye release Site B. 66

Table 12. M2 tidal ellipse parameters from the tidal analysis currents from ADCP data and FVCOM model results for deployments located in the vicinity of dye release Site B. The results have been vertically averaged over the sigma layers and only include the range of sigma layers for which ADCP data exist. 67

Table 13. M2 tidal elevation amplitudes and phases from the tidal analysis of sea surface heights from ADCP data and FVCOM model results for deployments located in the vicinity of dye release Site C. 68

Table 14. M2 tidal ellipse parameters from the tidal analysis currents from ADCP data and FVCOM model results for deployments located in the vicinity of dye release Site C. The results have been vertically averaged over the sigma layers and only include the range of sigma layers for which ADCP data exist. 68

Table 15. Summary of fieldwork on dye dispersal from well-boats. 110

TABLE OF FIGURES

Figure 1. Pictures showing the introduction of therapeutant and dye into a tarped fish cage. The top left shows the therapeutant being added to a mixing tank on a farm vessel tethered to the side of the fish cage to be treated. The top right picture shows a solution of dye being added to the mixing tank. The middle photograph shows the pump and hoses used to deliver the therapeutant and dye into the tarped cage. The bottom left shows the therapeutant being hosed into the cage and the bottom right shows the therapeutant being pumped into the cage through two perforated hoses stretched across the diameter of the cage. 3

Figure 2. Photographs showing an example of the temporal evolution of the spread of dye and associated therapeutant throughout a tarped fish cage. The photographs were taken before the dosing began (top left), 0.5 minutes (top right), 2 minutes (middle left), 4 minutes (middle right), 6 minutes (bottom left) and 12.5 minutes (bottom right) after dosing began. 4

Figure 3. Underwater photograph showing cultured Atlantic salmon swimming through a mixture of therapeutant and fluorescein dye. 5

Figure 4. Example of a treatment tarpaulin being dropped and withdrawn from a net-pen showing how the dye begins to leave the cage. The photographs were taken when the net-pen was fully tarped (top left), the tarpaulin was containing the dye/therapeutant (top right), the tarpaulin was just beginning to be dropped (middle left), the tarpaulin was beginning to be pulled under (middle right), the tarpaulin was pulled further under (bottom left), and the tarpaulin was withdrawn (bottom right). 6

Figure 5. A series of photographs showing the temporal evolution of dye, and hence therapeutant, leaving a tarped fish cage. The photographs were taken just prior to the beginning of flushing (top left), 5 minutes (top right), 10 minutes (middle left), 15 minutes (middle right), 20 minutes (bottom left) and 24.5 minutes (bottom right) after flushing began. 7

Figure 6. A second series of photographs showing the temporal evolution of dye, and hence therapeutant, flushing from a different tarped fish cage. The photographs were taken just prior to the beginning of flushing (top left), 20 minutes (top right), 50 minutes (middle left), 80 minutes or 1.3 hours (middle right), 110 minutes or 1.8 hours (bottom left) and 170 minutes or 2.8 hours (bottom right) after flushing began. 8

Figure 7. Dye and pesticide concentrations inside the treated cage at Site B, the 8th of September 2010. Fluorescence plateaus during treatment because dye concentrations exceed the detection limit of the fluorometers. A (upper left): Diagram of sampling stations and treatment equipment inside the treatment cage. B (upper right): Time series of dye concentrations during mixing (before dye concentrations exceeded instrument limitations). C (bottom half): Time series of dye and pesticide concentrations throughout treatment and flushing. 16

Figure 8. Dye and pesticide concentrations inside the treated cage at Site B, the 10th of September 2010. Fluorescence plateaus during treatment because dye concentrations exceed the detection limit of the fluorometers. No fluorometry data were available at station A due to an instrument malfunction. A (top left): Diagram of sampling stations and treatment equipment inside the treatment cage. B (top right): Time series of dye concentrations during mixing (before dye concentrations exceeded instrument limitations). C (bottom): Time series of dye and pesticide concentrations throughout treatment and flushing. 17

Figure 9. Dye and pesticide measurements inside the tarped treatment cage at Site B, the 14th of September 2010. Fluorescence plateaus during treatment because dye concentrations exceed the detection limit of the fluorometers. No fluorometry data were available at sampling station A due to an instrument malfunction. A(top left): Diagram of sampling stations and treatment equipment inside the treatment cage. B(top right): Time series of dye concentrations during mixing (before dye concentrations exceeded instrument limitations). C(bottom): Time series of dye and pesticide concentrations throughout treatment and flushing. The time of the last pesticide sample was interpolated...............19

Figure 10. Dye measurements inside the tarped treatment cage at Site F, the 13th of October 2010. Fluorescence plateaus during treatment because dye concentrations exceed the detection limit of the fluorometers. A (top left). Diagram of sampling stations and treatment equipment inside the treatment cage. B (bottom): Time series of dye concentrations throughout treatment and flushing..20

Figure 11. Dye measurements inside the tarped treatment cage at Site C, the 27th of October 2010. Fluorescence plateaus during treatment because dye concentrations exceed the detection limit of the fluorometers. A (top left): Diagram of sampling stations and treatment equipment inside the treatment cage. B (top right): Time series of dye concentrations during mixing (before dye concentrations exceeded instrument limitations). C (bottom): Time series of dye concentrations throughout treatment and flushing. 21

Figure 12. Dye and pesticide concentrations inside the treated cage at Site B, the 22nd of September 2010. Fluorescence plateaus during treatment because dye concentrations exceed the detection limit of the fluorometers. A (top left): Diagram of sampling stations and treatment equipment inside the treatment cage. B (bottom): Time series of dye and pesticide concentrations throughout treatment and flushing...23

Figure 13. Dye and pesticide concentrations inside the treated cage at Site J, on the 6th of October 2010. Fluorescence plateaus during treatment because dye concentrations exceed the detection limit of the fluorometers. A (top left): Diagram of sampling stations and treatment equipment inside the treatment cage. B (bottom): Time series of dye concentrations throughout treatment and flushing..24

Figure 14. Map showing the outlines of dye patches (coloured polygons), surface and drogued drifter trajectories (broken lines) and the location of the release cage (circle) for the 10th of August 2010 dye release at Site A. These outlines correspond with the dye plumes shown in Figure 15...30

Figure 15. Pictures showing the evolution of the dye plume resulting from a dye release from Site A on the 10th of August 2010...31

Figure 16. Map showing the outlines of dye patches (coloured polygons), surface and drogued drifter trajectories (broken lines) and the location of the release cage (circle) for the 11th of August 2010 dye release at Site A. 32

Figure 17. Map showing the outlines of dye patches (coloured polygons), surface and drogued drifter trajectories (broken lines) and the location of the release cage (circle) for the 17th of August 2010 dye release at Site A. 33

Figure 18. Map showing the outlines of dye patches (coloured polygons), surface and drogued drifter trajectories (broken lines) and the location of the release cage (circle) for the 8th of September 2010 dye release at Site B...34

Figure 19. Map showing the outlines of dye patches (coloured polygons), surface and drogued drifter trajectories (broken lines) and the location of the release cage (circle) for the 10th of September 2010 dye release at Site B...35

Figure 20. Map showing the outlines of dye patches (coloured polygons), surface and drogued drifter trajectories (broken lines) and the location of the release cage (circle) for the 14th of September 2010 dye release at Site B. 36

Figure 21. Map showing the outlines of dye patches (coloured polygons), surface and drogued drifter trajectories (broken lines) and the location of the release cage (circle) for the 27th of October 2010 dye release at Site C. 37

Figure 22. The distance of dye patch centers from the treatment cage vs. time after dye release. 38

Figure 23. Temporal variation in the variance of dye plumes for tarp treatments. The left/ panel shows the variances along the major axes of the dye plumes. The right panel shows the variances along the minor axes of the dye plumes. 39

Figure 24. Vertical dye concentration profiles (left panel) and cumulative dye concentration versus depth curves (right panel) associated with dye releases conducted at Site A. The average site depth at mean low tide is 16.2 m. VP = Vertical Profile; p.r. = post release.45

Figure 25. Vertical dye concentration profiles (left panel) and cumulative concentration versus depth curves (right panel) associated with dye releases from tarps conducted at Site B. At Site B, the average site depth at mean low tide was 33.5 m, below the axis of the graph. VP = Vertical Profile. p.r. = post release. 47

Figure 26. Temperature, salinity and density profiles of the water column collected during tarp dye studies at Site B. 48

Figure 27. Vertical dye concentration profiles (top panel) and cumulative dye concentration versus depth curves (bottom panel) associated with dye releases conducted at Site C. The average site depth at mean low tide is 12.7 m. VP = Vertical Profile. p.r. = post release. 49

Figure 28. Temperature, salinity and density profiles of the water column collected during tarp dye studies at Site C. 50

Figure 29. Vertical dye concentration profiles both inside and inside out the skirted treatment cage at Site J. The average site depth at mean low tide is 18.3 m. VP = Vertical Profile. p.r. = post release 51

Figure 30. Temperature, salinity and density profiles of the water column collected during a skirt study at Site J. 51

Figure 31. Vertical dye concentration profiles inside and outside the skirt during treatment (top panels), vertical dye concentration profiles post treatment (bottom left panel) and cumulative concentration versus depth curves (bottom right panel) associated with dye released from a skirt conducted at Site B. The average site depth at mean low tide is 35.3 m. VP = Vertical Profile. p.r. = post release 53

Figure 32. Temperature, salinity and density profiles of the water column collected during a skirt dye study at Site B. 54

Figure 33. Composite of the maximum depth that dye was detected in each profile taken in association with tarp and skirt releases. 55

Figure 34. The maximum depth at which dye was detected in vertical profiles of fluorescent based estimates of dye concentration. Only dye concentrations greater than 1 µg/L were considered in this analyses to ensure concentrations were above background fluorescence levels. All profiles included in the analyses were taken post release of tarps or skirts. 56

Figure 35. Fickian and Okubo model estimates of the temporal decrease in the standardized dye or therapeutant concentration (C(t)/C(t=0)) after release from a tarped cage. The Fickian curves are based on equation 16. The Okubo curves with no cage effects are based on equation 31. The Okubo curves with cage effect incorporates an initial increase in the rate of horizontal patch spread. Red curves assume a constant depth of 5 m and values of $K_x = K_y = 0.1$ m^2/s. The Okubo dilution assumes an Okubo increase in the horizontal size of the patch and a patch depth that remains at a constant depth of 5 m. ..59

Figure 36. a) FVCOM model grid domain with locations of observation stations used for model sea level and current calibration. The area in the square is enlarged in the other two frames. b) locations of observation stations in southwest NB used for model calibration; c) all stations in southwest New Brunswick. 61

Figure 37. Comparison of M2 tidal ellipse parameters at Site A, ADCP deployment A2. Squares are the results from the tidal analysis of the ADCP data. Circles are the results from the tidal analysis of the FVCOM model run. The vertical axis scale (σ) goes from 0 at the sea surface to -1 at the sea bottom..........65

Figure 38. Comparison of M2 tidal ellipse parameters at Site B, ADCP deployment B2. Squares are the results from the tidal analysis of the ADCP data. Circles are the results from the tidal analysis of the FVCOM model run. The vertical axis scale (σ) goes from 0 at the sea surface to -1 at the sea bottom..........67

Figure 39. Comparison of M2 tidal ellipse parameters at Site C ADCP deployment C1. Squares are the results from the tidal analysis of the ADCP data. Circles are the results from the tidal analysis of the FVCOM model run. The vertical axis scale (σ) goes from 0 at the sea surface to -1 at the sea bottom..........69

Figure 40. Horizontal dilution curves. Red (blue) symbols are for runs with the particles initially randomly distributed over the surface 3 m (10 m). The concentration at a given time is calculated by multiplying the horizontal surface area occupied by the particles and multiplying them by a constant depth of 10 m. The concentration is divided by the initial concentration C(t=0) which is equal to the total number of particles divided by the volume of the cylinder over which the particles are initially randomly distributed. 71

Figure 41. Vertical cumulative concentrations for eight different particle tracking runs comparing the type of diffusion included (no diffusion, horizontal only, vertical only, both horizontal and vertical) and the depth over which the particles are initially distributed (3 m and 10 m). The cumulative vertical concentration for a given depth is computed by determining the number of particles located in the surface layer up to that depth (regardless of horizontal location) and dividing by the total number of particles. Solid lines are the modelled results and dotted lines are the observations. The results are compared at 10 minutes (blue), 40 minutes to 55 minutes (green) and 130 minutes (magenta) post release time..........72

Figure 42. Okubo variance versus time for the dye releases associated with tarpaulin treatments conducted at the three 2010 study sites described here (A, B, C) and the Ernst et al. (2001) study sites (Passamaquoddy Bay). 74

Figure 43. Okubo apparent diffusivity versus time for the dye releases associated with tarpaulin treatments conducted at the three 2010 study sites described here (A, B, C) and the Ernst et al. (2001) study sites (Passamaquoddy Bay). 75

Figure 44. Simulations of a dye patch transport and dispersal pattern at Site A using two different current meter records to advect the patch and the Okubo relationship to estimate the evolving area of the patch. The red polygons are the perimeter of the observed dye patches at the end of the simulation. The shaded blue area is the predicted path of advection. The large circles are centered over the advection trajectory and have a diameter that grows with time according to the Okubo (1974) relationship. The circle diameter is $l=3\sigma$, ...77

Figure 45. Simulations of a dye patch transport and dispersal pattern at Site B using two different current meter records to advect the patch and the Okubo relationship to estimate the evolving area of the patch. The red polygons are the perimeter of the observed dye patches at the end of the simulation. The shaded blue area is the predicted path of advection. The large circles are centered over the advection trajectory and have a diameter that grows with time according to the Okubo (1974) relationship. The circle diameter is $l=3\sigma$, ...78

Figure 46. Simulations of a dye patch transport and dispersal pattern at Site C using two different current meter records to advect the patch and the Okubo relationship to estimate the evolving area of the patch. The red polygons are the perimeter of the observed dye patches at the end of the simulation. The shaded blue area is the predicted path of advection. The large circles are centered over the advection trajectory and have a diameter that grows with time according to the Okubo (1974) relationship. The circle diameter is $l=3\sigma$, ...79

Figure 47. Comparison of results of particle tracking model to dye perimeter data for the dye experiment at Site A on the 10th of August 2010. The dye release location is indicated by a black dot. Observational data include the drifter locations (blue circle), the perimeter of the dye (red line) and the location of ADCP A1 (black square). The particle patch is shown in cyan. Times are given in minutes past the release time. 81

Figure 48. Comparison of results of particle tracking model to dye perimeter data for the dye experiment at Site A on the 11th of August 2010. The dye release location is indicated by a black dot. Observational data include the drifter locations (blue circle), the perimeter of the dye (red line) and the location of ADCP A1 (black square). The particle patch is shown in cyan. Times are given in minutes past the release time. 82

Figure 49. Comparison of results of particle tracking model to dye perimeter data for the dye experiment at Site A on the 17th of August 2010. The dye release location is indicated by a black dot. Observational data include the drifter locations (blue circle) and the perimeter of the dye (red line). The particle patch is shown in cyan. Times are given in minutes past the release time. 83

Figure 50. Comparison of results of particle tracking model to dye perimeter data for the dye experiment at Site B on the 8th of September 2010. The dye release location is indicated by a black dot. Observational data include the drifter locations (blue circle) and the perimeter of the dye (red line). The particle patch is shown in cyan. Times are given in minutes past the release time. 85

Figure 51. Comparison of results of particle tracking model to dye perimeter data for the dye experiment at Site B on the 10th of September 2010. The dye release location is indicated by a black dot. Observational data include the drifter locations (blue circle) and the perimeter of the dye (red line). The particle patch is shown in cyan. Times are given in minutes past the release time. 86

Figure 52. Comparison of results of particle tracking model to dye perimeter data for the dye experiment at Site B on the 14th of September 2010. The dye release location is indicated by a black dot. Observational data include the drifter locations (blue circle) and the perimeter of the dye (red line). The particle patch is shown in cyan. Times are given in minutes past the release time. 87

Figure 53. Comparison of results of particle tracking model to dye perimeter data for the dye experiment at Site C on the 27th of October 2010. The dye release location is indicated by a black dot. Observational data include the drifter locations (blue circle) and the perimeter of the dye (red line). The particle patch is shown in cyan. Times are given in minutes past the release time. 89

Figure 54. Comparisons of Fickian (red curves) and modified Okubo (black curves) based dilution models with observed concentrations of dye and therapeutant. Fickian and Okubo model estimates of the temporal decrease in the standardized dye or therapeutant concentration ($C(t)/C(t=0)$) after release from a tarped cage. The Fickian curves are based on equation 16. The Fickian curves assume a constant depth of 5 m and values of $K_x = K_y = 0.1$ m^2 s^{-1}.The Okubo curves include an initial increase in the rate of horizontal patch spread due to cage effects and a patch depth that remains at a constant depth of 5 m. 91

Figure 55. Comparison of measured and calculated dye concentrations in dye plumes resulting from tarpaulin treatments of net-pens. 92

Figure 56. Predicted and measured dilution after salmon cage and tarp releases at three sites. Predicted dilution are based on FVCOM particle tracking model results (see above for more detail). Empirical data are average concentrations measured in vertical profiles from the surface to the maximum depth where less than 99% of the dye is contained. 93

Figure 57. Comparison of the results of particle tracking model for the dye experiment at Site B when the effects of fish cage drag are included in the model. The dye release location is indicated by a black dot. Observational data include the drifter locations (blue circle) and the perimeter of the dye (red line). The particle patch is shown in cyan. Times are given in minutes past the release time. 96

Figure 58. Comparison of different ways to incorporate effect of fish cage drag on the results of particle tracking model for the dye experiment at Site B on the 10th of September 2010. The dye release location is indicated by a black dot. Observational data include the drifter locations (blue circle) and the perimeter of the dye (red line). The particle patch is shown in cyan. Times are given in minutes past the release time. 97

Figure 59. Comparison of results of FVCOM particle tracking model with particles released over entire tidal cycle with all observed dye patch perimeters at studies Sites A (top left), B (top right) and C (bottom left). 101

Figure 60. Photographs of a flushing discharge directed away from fish cages (top photo) and one directed into a fish cage (bottom photo). 103

Figure 61. The time series of dye concentration within the starboard well of the Colby Perce as measured by a Cyclops 7 fluorometer hung through the well hatch on the 14th of December 2010. The amount of dye added to the well was 50 g so the homogeneous concentration would have been 151 µg/L. 106

Figure 62. The time series of normalized dye concentration within the starboard well of the Colby Perce during the flushing period conducted on the 14th of December 2010. The two plots show the same data as in Figure 61. The data in the left panel are plotted on an arithmetic scal;, that in the right panel on a logarithmic scale. 106

Figure 63. The time series of dye concentration within the starboard well of Well-boat C as measured by a Turner Designs Cyclops 7 fluorometer hung through the well hatch on the 5th of August 2011. The grey line is the unsmoothed data and the green line is the data smoothed by a 5 minute running mean. The amount of dye added to the well was 1.5 kg so the estimated homogeneous concentration would have been 4545 µg/L, a value well above the upper detection limit of the fluorometer. 113

Figure 64. The time series of dye concentration within the flushing discharge jet associated with the starboard well dye treatment conducted on the Well-boat C on the 5th of August 2011. The open black symbols are the unsmoothed time series of dye concentration at depth of 0.5 m and a distance of 6 m from the point of discharge. The heavy red line s the predicted time series of concentration (see text for details). The thin grey and heavy green lines are the concentrations within the well and are the same as those shown in the previous Figure 63. 114

Figure 65. The time series of observed and predicted dye concentrations within the well and flushing discharge jet at a distance of 6 m from the discharge pipe. The observations are associated with the starboard well dye treatment conducted on the Well-boat C on the 5th of August 2011. The straight line predictions (heavy black lines) are based on equation 37. The heavy red line prediction is a scaled version of the smoothed observations taken from inside the well (green line). The blue line is the time series of observations taken from within the well. The open black symbols are the unsmoothed time series of dye concentration at depth of 0.5 m and a distance of 6 m from the point of discharge. 115

Figure 66. Predictions of therapeutant dilution as a function of time and distance (x) from the mouth of the discharge pipe. The predictions are based on the equation 37. 116

Figure 67. Map showing the outlines of dye patches (coloured polygons), and the location of the release (circle) for the 5th of August 2011 dye release from a well-boat treatment at Site B. 117

Figure 68. Map showing the outlines of dye patches (coloured polygons), and the location of the second release (circle) for the 5th of August 2011 dye release from a well-boat treatment at Site B. 118

Figure 69. Map showing the outlines of dye patches (coloured polygons), and the location of the release (circle) for the 17th of November 2011 dye release from a well-boat treatment at Site K. 119

Figure 70. Temperature, salinity and density profiles of the water column collected during a well-boat dye study at Site H from well-boat C on the 16th of December 2010. 120

Figure 71. Vertical dye concentration profiles (left panel) and cumulative concentration versus depth curves (right panel) associated with two dye releases from Well-boat C at Site H on the 16th of December 2010. The average site depth at mean low tide is 33.7 m. VP = Vertical Profile. p.r. = post release 121

Figure 72. Vertical dye concentration profiles (left panel) and cumulative concentration versus depth curves (right panel) associated with dye releases from Well-boat C conducted at Site K. The average site depth at mean low tide is 8.2 m. VP = Vertical Profile, p.r. = post release 122

Figure 73. Vertical dye concentration profiles (left panel) and cumulative concentration versus depth curves (right panel) associated with dye releases from Well-boat A at Site B. The average site depth at mean low tide is 35.3 m. NOTE: Cumulative profiles for the incomplete profiles (B and C) are presented in this figure; insufficient dye data at deeper depths may skew the cumulative profiles. VP = Vertical Profile, p.r. = post release 123

Figure 74. Vertical dye concentration profiles (left panel) and cumulative concentration versus depth curves (right panel) associated with dye releases from Well-boat C at Site B. The average site depth at mean low tide is 35.3 m. VP = Vertical Profile, p.r. = post release. 124

Figure 75. Temperature, salinity and density profiles of the water column collected during well-boat dye studies at Site B. 125

Figure 76. Vertical dye concentration profiles (left panel) and cumulative concentration versus depth curves (right panel) associated with dye releases from Well-boat A conducted at Site D. At Site D, the average site depth at mean low tide is 20.5 m. VP = Vertical Profile, p.r. = post release 126

Figure 77. Temperature, salinity and density profiles of the water column collected during well-boat dye studies at Site D. 126

Figure 78. Vertical dye concentration profiles (left panel) and cumulative concentration versus depth curves (right panel) associated with dye releases from Well-boat B conducted at Site E. The average site depth at mean low tide is 15.7 m. NOTE: Cumulative profiles for the incomplete profiles (G and H) are presented in this figure; insufficient dye data at deeper depths may skew the cumulative profiles. VP = Vertical Profile, p.r. = post release. 127

Figure 79. Temperature, salinity and density profiles of the water column collected during a well-boat dye study at Site E. 128

Figure 80. Vertical dye concentration profiles (left panel) and cumulative concentration versus depth curves (right panel) associated with dye releases from Well-boat B at Site G. The average site depth at mean low tide is 20.6 m. VP = Vertical Profile, p.r. = post release 129

Figure 81. Temperature, salinity and density profiles of the water column collected during a well-boat dye study at Site G. 130

Figure 82. Comparison of measured and calculated dye concentrations in dye plumes resulting from well-boat treatments 131

Figure 83. Maximum depth of dye detected through time, post the start of flushing of well. Concentrations greater than 1 µg/L considered 133

Figure 84. Comparison of particle tracking model with particles continuously released over 55 minutes and well-boat release at Site B on the 5th of August 2011 at 13:11. The dye release location is indicated by a black dot. The red lines indicate the observed perimeters of the dye patches. The particle patch is shown in cyan. Times are given in minutes past the release time. 135

Figure 85. Comparison of particle tracking model with particles continuously released over 63 minutes and well-boat release at Site B on the 5th of August 2011 at 15:05. The dye release location is indicated by a black dot. The red lines indicate the observed perimeters of the dye patches. The particle patch is shown in cyan. Times are given in minutes past the release time. 136

Figure 86. Comparison of particle tracking model with particles continuously released over 22 minutes and well-boat release at Site K on the 17th of November 2011 at 14:37. The dye release location is indicated by a black dot. The red lines indicate the observed perimeters of the dye patches. The particle patch is shown in cyan. Times are given in minutes past the release time. 137

Figure 87. Relationship between dye and azamethiphos concentrations in effluents from salmon aquaculture treatments. Dye concentrations were standardized to the initial concentration (measured concentration/initial dye concentration). The straight line is a linear regression for tarp samples only (R-squared of 0.96). 139

Figure 88. Relationship between dye and pesticide deltamethrin concentrations in effluents from salmon aquaculture treatments. Dye concentrations were standardized to the initial concentration (measured concentration/initial dye concentration). Samples below detection limits are presented as 0. The black regression line through the data includes all of the data. 139

Figure 89. Same plot as in Figure 88, with the exception that the data being designated as having concentrations below the detection limit has been removed from the plot and regression analyses. The black regression line through the data includes all of the data. 140

Figure 90. Photograph of the temperature bath system used to determine the change in therapeutant concentration over time. The beakers in the picture are 5-L jacketed beakers containing a stirring bar and they are sitting on top of a magnetic stirring plate. 141

Figure 91. Temporal evolution of the concentration of Paramove® 50 hydrogen peroxide at several water temperatures (5 °C – top, 10 °C – middle, 20 °C – bottom). 142

ABSTRACT

Salmon aquaculture sea lice bath treatments result in the release of the bath water containing the pesticide into the ambient environment. The consequence of these releases to non-target organisms in the receiving environment depends upon the dilution and toxicity of the therapeutant, and whether the non-target organisms get exposed to the released therapeutant. This report summarizes work conducted during 2010 in relation to measuring and modelling the transport and dispersal of sea lice pesticide effluents from sea lice treatments associated with commercial net-pen salmon farming in the southwest New Brunswick area of the Bay of Fundy in eastern Canada. The work involved commercial tarp and skirt based treatments of net-pens as well as the use of well-boats. Field studies were conducted on local salmon farms during an active and particularly severe outbreak of sea lice. In all cases fluorescein dye, either alone or in combination with a pesticide, was added into the treatment volume that contained commercial quantities of salmon. The concentration of dye and, at times, pesticide was measured within the treatment volume prior to its release into the receiving environment and for several hours after its release. Treatments were accompanied by measurements of the temporal evolution of the horizontal and vertical distributions of the dye concentration, and by measurements of water currents using moored current meters and near-surface GPS drifters.

The purpose of this report is to summarize the dilution and transport of the released dye gathered from the treatment field studies. The report is organised into five main sections: Section one presents a brief context for the work; Section two describes the net-pen treatment process and the work conducted in association with tarped and skirted net-pens treatments; Section three describes the well-boat based treatment process and the work conducted in association with well-boat based treatments; Section four describes results of chemical analyses of water samples taken during the treatment studies and, in addition, on laboratory experiments involving pesticides; and finally, Section five summarizes the work and presents some preliminary conclusions.

The process of conducting a tarpaulin or skirt bath treatment of a net-pen involves several steps. Initially, the outside perimeter of the fish cage net is shallowed to a depth of about 3-4 meters. Next, either a tarpaulin is deployed around and under the net or a skirt is deployed around the net. Subsequently, the pesticide is pumped into the treatment volume and is assumed to become mixed throughout the enclosed volume by the movements of the fish and the water movement generated by the oxygenation system. Finally, at the end of the treatment period, the tarpaulin or skirt is removed, the cage net is allowed to drop to its normal depth, and the pesticide begins to leave the cage and advect into the ambient receiving waters. During the field studies, dye was added to tarped and skirted pens during treatment to allow visualization of the treatment water both within and outside of the treatment volume. Both horizontal and vertical distribution of the dye was measured after release from the treated pens. The data indicate that the rate of horizontal dispersion initially exceeded that estimated by Okubo's empirical relationship for the temporal spread of a conservative substance in the coastal ocean but at approximately one hour post-release the evolution of the area occupied by the released substance evolved at a rate similar to that predicted by Okubo. The concentrations of the dye and pesticide as a function of time after release were measured: the released material is diluted by approximately a factor of 10 after 30 minutes, a factor of 100 after 1 hour and a factor of 1000 after 3 hours. A passive particle tracking model based on an implementation of the FVCOM water circulation model for the local area was used to predict the advection and dispersion of the treatment water in the ambient waters. The model gives a reasonable estimate of the observed horizontal distributions of released dye but did not perform well in the vertical.

In southwest New Brunswick well-boats are used to treat salmon for sea lice. A well-boat is a 100-200 foot long vessel in which the cargo holds can be filled with water. The holds are called the wells and the water inside them is mechanically recirculated and aerated. During sea lice treatment, fish are pumped into the wells where they are treated with pesticides. When the water is discharged from the wells it is pumped through one or more pipes (each ~12-14" in diameter) that exit the side or bottom of the boat. The pumping rate varies among vessels. During the study, dye was added to the treatment water along with the pesticide in order to observe the temporal evolution of dye within the well of the well-boat and to measure the temporal evolution of concentration, horizontal area and vertical distribution of dye within the discharge jet generated by well-boat treatments. The data indicate that discharges from well-boat treatments are quantitatively consistent with jet dynamics and are diluted more rapidly than from net-pen treatments. It was observed that the discharge dynamics vary between well-boats, which is due to each well-boat having unique structural features and different discharge characteristics. A particle tracking model based on the FVCOM generated circulation to predict the dispersion of treatment water into the receiving waters was explored but it was determined that, in its present state, the model is unable to give a reasonable estimation of the horizontal trajectory of the dye plume.

Although the purpose of the work was to gain insight into the distribution, mixing, transport and dispersal of pesticides, the results summarized above pertain to the distribution, mixing, transport and dispersal of the fluorescein dye. Analyses of water samples obtained from the released plumes of dye and pesticide as well as laboratory experiment results indicate that there was a linear correspondence between pesticide (azamethiphos and deltamethrin) and dye concentrations but that the temporal decay of hydrogen peroxide is very slow and negligible on time scales of a few hours.

Transport et dispersion des agents thérapeutiques des bains contre le pou du poisson à partir des parcs en filet et des bateaux viviers des installations salmonicoles

RÉSUMÉ

Les bains de traitement utilisés contre le pou du poisson en salmoniculture entraînent le rejet des eaux du bain contenant le pesticide dans l'environnement ambiant. Les conséquences de ces rejets sur les organismes non ciblés dans le milieu récepteur dépendent de la dilution et de la toxicité des agents thérapeutiques, ainsi que de l'exposition ou non des organismes non ciblés à l'agent thérapeutique libéré. Le présent rapport résume les travaux menés en 2010 pour mesurer et modéliser le transport et la dispersion des effluents de pesticide issus des traitements contre le pou du poisson appliqués dans des parcs en filet d'entreprises salmonicoles commerciales au Nouveau-Brunswick, dans la partie sud-ouest de la baie de Fundy, dans l'est du Canada. Ces travaux visaient à placer des bâches ou des jupes sur les parcs en filet et à utiliser des bateaux viviers. Des études sur le terrain ont été réalisées dans des fermes salmonicoles locales lors d'une pullulation active et particulièrement grave de poux du poisson. Dans tous les cas, de la fluorescéine, employée seule ou en combinaison avec un pesticide, a été ajoutée à l'eau de traitement, qui contenait des saumons destinés au commerce. La concentration du colorant et, par moments, du pesticide a été mesurée dans l'eau de traitement avant son rejet dans l'environnement récepteur et pendant plusieurs heures après le rejet. Les traitements étaient accompagnés de mesures de l'évolution temporelle des distributions horizontales et verticales de la concentration de colorant, et de mesures des courants marins prises à l'aide de courantomètres amarrés et de bouées dérivantes GPS proches de la surface.

L'objectif du présent rapport est de résumer les données sur la dilution et le transport du colorant rejeté recueillies dans le cadre des études sur le terrain. Le rapport est organisé en cinq sections principales : la section un dresse brièvement le cadre des travaux; la section deux décrit le processus de traitement dans les parcs en filet et le travail mené avec des parcs en filet munis de bâches ou de jupes; la section trois décrit le processus de traitement à l'aide d'un bateau vivier et le travail effectué dans le cadre des traitements nécessitant l'utilisation de bateaux viviers; la section quatre décrit les résultats des analyses chimiques des échantillons d'eau recueillis au cours des études de traitement et lors d'expériences en laboratoire avec des pesticides; la section cinq résume les travaux et présente quelques conclusions préliminaires.

Le processus visant à appliquer un bain de traitement dans un parc en filet muni d'une bâche ou d'une jupe comporte plusieurs étapes. D'abord, le périmètre extérieur de la cage à poissons est plongé à une profondeur d'environ 3 à 4 mètres. Puis, on déploie soit une bâche autour et sous le filet, soit une jupe autour du filet. Ensuite, on pompe le pesticide dans l'eau de traitement, dans laquelle il est censé se mélanger sous l'effet des mouvements des poissons et du mouvement d'eau provoqué par le système d'oxygénation. Enfin, on retire la bâche ou la jupe à la fin de la période de traitement, la cage peut redescendre à la profondeur normale et le pesticide commence à quitter la cage et à se propager par advection dans l'eau environnante. Pendant les études sur le terrain, on a ajouté du colorant aux parcs en filet munis d'une bâche ou d'une jupe au cours du traitement pour visualiser l'eau traitée à l'intérieur et à l'extérieur du volume traité. On a mesure la distribution horizontale et verticale du colorant après le rejet des parcs en filet traités. Les données indiquent que le taux de dispersion horizontale dépassait initialement celui estimé par la relation empirique du modèle Okubo pour l'étalement temporel d'une substance rémanente dans les eaux côtières, mais environ une heure après le rejet, la

zone occupée par la substance rejetée avait évolué à un taux similaire à celui prévu par le modèle Okubo. On a mesuré les concentrations du colorant et du pesticide dans le temps après le rejet : la substance rejetée est diluée par un facteur d'environ 10 après 30 minutes, un facteur de 100 après 1 heure et un facteur de 1000 après 3 heures. Un modèle de suivi des particules passives axé sur le modèle de circulation de l'eau dans un volume fini dynamique des eaux côtières pour la zone locale a été utilisé pour prédire l'advection et la dispersion de l'eau de traitement dans l'eau environnante. Le modèle donne une estimation raisonnable des distributions horizontales observées du colorant rejeté, mais n'a pas été efficace pour les distributions verticales.

Dans le sud-ouest du Nouveau-Brunswick, les bateaux viviers sont utilisés pour traiter les saumons contre le pou du poisson. Un bateau vivier est un bâtiment de 100 à 200 pieds de long dont les soutes peuvent être remplies d'eau. Les soutes sont appelées « viviers » et l'eau qui s'y trouve est remise en circulation et aérée mécaniquement. Pendant un traitement contre le pou du poisson, les poissons sont pompés dans les viviers, où ils sont traités avec les pesticides. Lorsque l'eau est expulsée des viviers, elle est pompée par un ou plusieurs tuyaux (ayant chacun un diamètre d'environ 12 à 14 pouces) qui sortent par le côté ou le fond du bateau. Le débit de pompage varie suivant les bâtiments. Lors de l'étude, on a ajouté le colorant à l'eau de traitement conjointement au pesticide afin de pouvoir observer l'évolution temporelle du colorant dans le vivier du bateau et de mesurer l'évolution temporelle de la concentration, la surface horizontale et la distribution verticale du colorant dans le jet de rejet généré par les traitements appliqués à l'aide de bateaux viviers. Les données indiquent que les rejets liés aux traitements appliqués à l'aide de bateaux viviers sont quantitativement cohérents avec la dynamique des jets et sont dilués plus rapidement que ceux provenant des traitements appliqués dans les parcs en filet. On a observé que la dynamique des rejets varie suivant les bateaux viviers, ce qui s'explique par le fait que chaque bateau vivier possède des caractéristiques structurelles uniques et des caractéristiques de rejet différentes. On a étudié un modèle de suivi des particules passives axé sur la circulation générée par le FVCOM afin de prédire la dispersion de l'eau de traitement dans l'eau environnante, mais la conclusion a été que dans son état actuel, le modèle est incapable de fournir une estimation raisonnable de la trajectoire horizontale du panache de colorant.

Bien que l'objectif de ces travaux soit de mieux connaître la distribution, le mélange, le transport et la dispersion des pesticides, les résultats résumés précédemment concernent la distribution, le mélange, le transport et la dispersion de la fluorescéine. Les analyses des échantillons d'eau recueillis dans les panaches de colorant et de pesticide rejetés et les résultats des expériences en laboratoire indiquent qu'il existe une corrélation linéaire entre les concentrations de pesticide (azaméthiphos et deltaméthrine) et de colorant, mais que la dégradation du peroxyde d'hydrogène est très lente et négligeable sur une échelle de quelques heures.

INTRODUCTION

Salmon farmers in southwest New Brunswick and elsewhere in Canada and the world need to control the abundance of sea lice on the fish within their net-pens. There are several methods available for accomplishing this. One method is to administer pesticides in the feed given to the fish. The environmental fate of these in-feed treatments is not the subject of this report. Another method is the use of chemical pesticide bath treatments. These treatments either require the in situ tarping or skirting of the fish within each net-pen or the pumping of fish into well-boat wells. In both cases the pesticide is introduced into the volume of water containing the fish, the fish are allowed to swim through the pesticide bath for a specified period of time, and the water containing the pesticide is released into the ambient environment after the treatment period.

The exposure to the released therapeutant that non-target or wild organisms will experience is controlled by the local transport and dispersal processes. These processes control the dilution rate, spatial trajectory and rate of transport of the released therapeutants. These aspects are essential factors and considerations contributing to the impact and predicted potential for impact in non-target organisms.

The purpose of this report is to explore some of the general factors that influence the exposure of non-target organisms to bath treatments (well-boat, skirt and tarp applications) and their relative importance in different salmon-production environments. This report focuses on some recent work done by a team lead by DFO to describe and predict the transport and dispersal of the pesticides released from tarp and well-boat bath treatments, specifically in the southwest New Brunswick region. Bath treatments are conducted in different environments in Canada but they all follow the same general processes: mixing inside, release from the source, subsequent transport and dispersal. The report is divided into two main sections. The first section focuses on tarp treatments of fish net-pens. The second section focuses on well-boat treatments. In each of these sections there are a series of sub-sections that describe the concepts and theories as well as observations associated with distinct stages in the therapeutant release sequence. It should be noted that the analyses associated with this work will continue for some time. Hence, the present document should be considered as a reflection of the state-of-knowledge at the time of this writing as well as an opportunity for stimulating discussion.

NET-PENS

BACKGROUND

The Treatment Process

The process of conducting a tarpaulin bath treatment of a net-pen involves several steps. Initially, the outside perimeter of the net on the fish cage is shallowed to a depth of about 3-4 meters. The net in the middle of the cage sags and is deeper than the net along the perimeter by a few meters. This raising of the net, concentrates the fish in the cage to within a reduced volume. Once the nets are shallowed, either a tarpaulin is deployed around or under the net or a skirt is deployed around the net. In the case of a tarpaulin, the edges of the tarpaulin are then pulled out of the water and tied at regular intervals to the hand rails of the cage. Once fully deployed the tarpaulin forms a bag surrounding the fish and since water does not flow through the tarpaulin material, and the fish are enclosed within a stagnant pool of water. In the case of a skirt deployment, several panels of tarpaulin material are hung around the edge of the cage and attached to cage railing to keep the skirt above water. The panels overlapped to help mitigate the loss of water through the skirt wall. Each panel extends to about 7 m so the bottom of the skirt is below the depth of the pursed net. In both tarping and skirting approaches, air and/or oxygen is injected into this enclosed water in an effort to maintain oxygen levels adequate for the fish do avoid hypoxia related stress. No attempts are made to mechanically circulate the waters within the tarps.

Once the enclosed fish seem to be "comfortable" in the reduced volume of water, the therapeutant is pumped into the treatment volume (Figure 1). The therapeutant is assumed to become mixed throughout the enclosed volume by the movements of the fish and the water movement generated by the oxygenation system; no mechanical mixing is provided (Figure 2). The fish may avoid the therapeutant until it becomes mixed throughout the treatment volume, at which time they are immersed in the bath treatment (Figure 3). At the end of the treatment period the tarpaulin or skirt is dropped by untying the ropes attached to the hand rails and pulling the tarp or skirt away from the shallowed net. This allows the therapeutant to begin leaving the cage (Figure 4). Once this is done the cage net is allowed to drop to its normal depth and the water containing the therapeutant begins to be advected from the cage into the ambient receiving waters (Figure 5 and Figure 6). The manner in which the dye leaves the net-pen varies between treatments. For example, in Figure 5 the dye is advected out of the net-pen as a narrow plume and is completely flushed from the net-pen within 25 minutes of the tarp being dropped. In contrast, in Figure 6 the dye leaves the net-pen within 170 minutes and no distinct plume is formed within the net-pen.

The duration of a commercial treatment is defined as the amount of time between the start of the introduction of the therapeutant to the beginning of the dropping of the tarpaulin or removal of the skirt. This time is usually between 30 and 60 minutes, with the exact time depending upon considerations such as the therapeutant being used, the health of the fish, water temperature and the oxygen content of the water within the enclosed water.

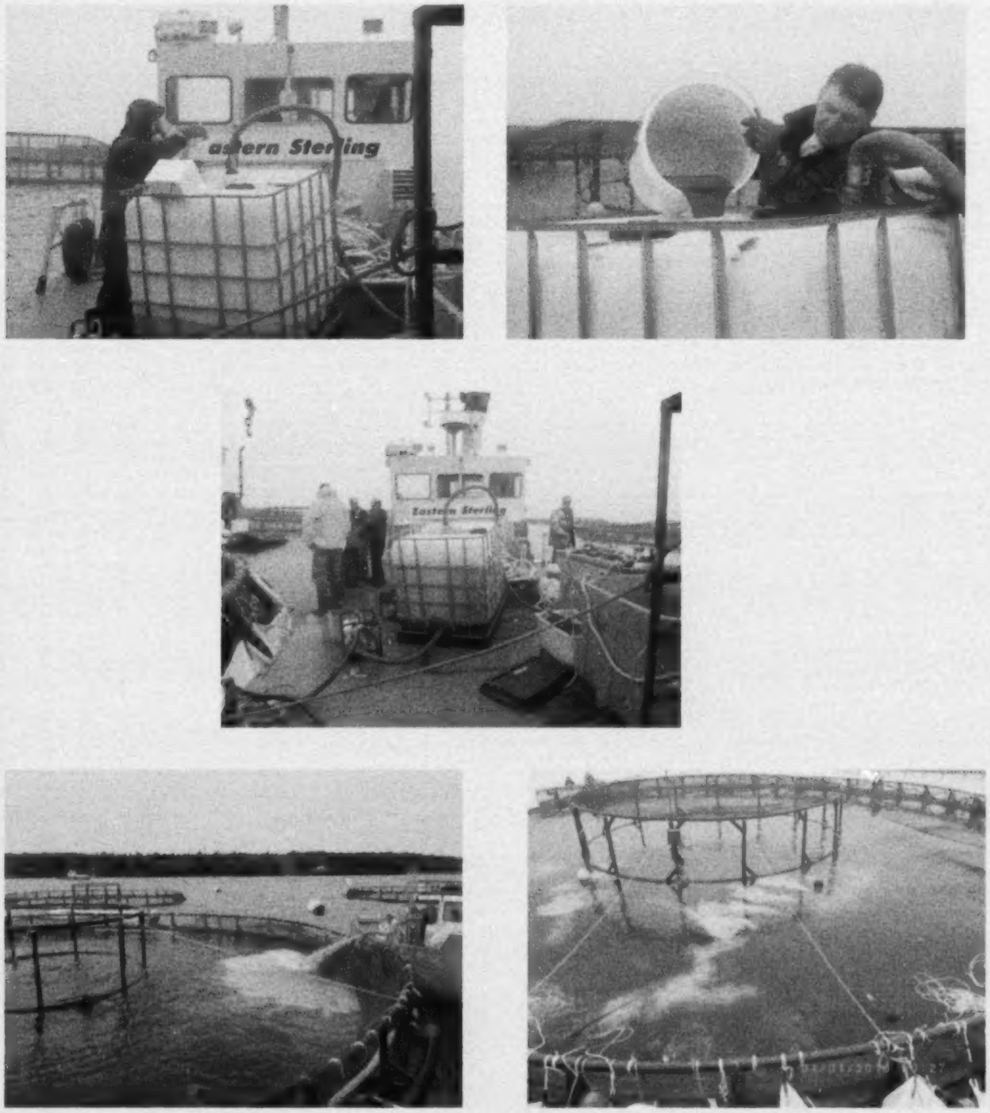

Figure 1. Pictures showing the introduction of therapeutant and dye into a tarped fish cage. The top left shows the therapeutant being added to a mixing tank on a farm vessel tethered to the side of the fish cage to be treated. The top right picture shows a solution of dye being added to the mixing tank. The middle photograph shows the pump and hoses used to deliver the therapeutant and dye into the tarped cage. The bottom left shows the therapeutant being hosed into the cage and the bottom right shows the therapeutant being pumped into the cage through two perforated hoses stretched across the diameter of the cage.

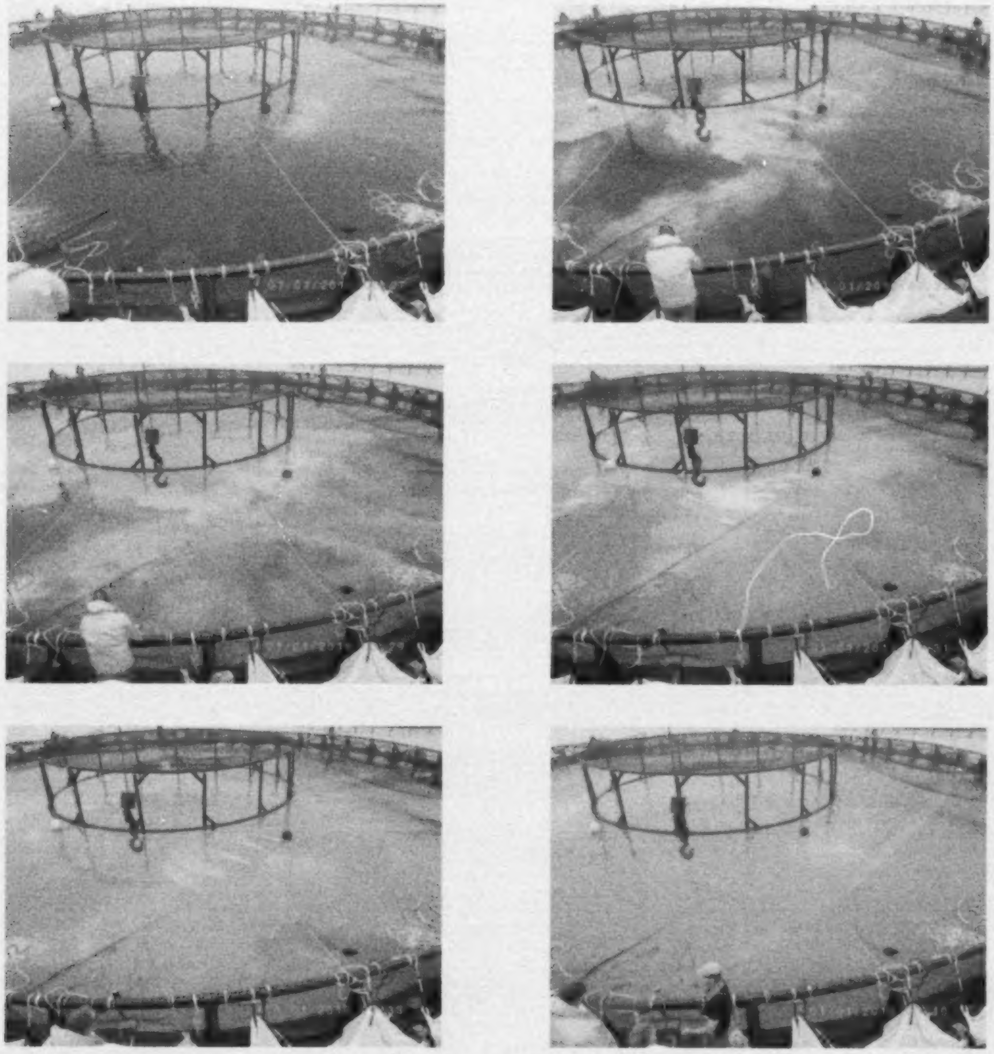

Figure 2. Photographs showing an example of the temporal evolution of the spread of dye and associated therapeutant throughout a tarped fish cage. The photographs were taken before the dosing began (top left), 0.5 minutes (top right), 2 minutes (middle left), 4 minutes (middle right), 6 minutes (bottom left) and 12.5 minutes (bottom right) after dosing began.

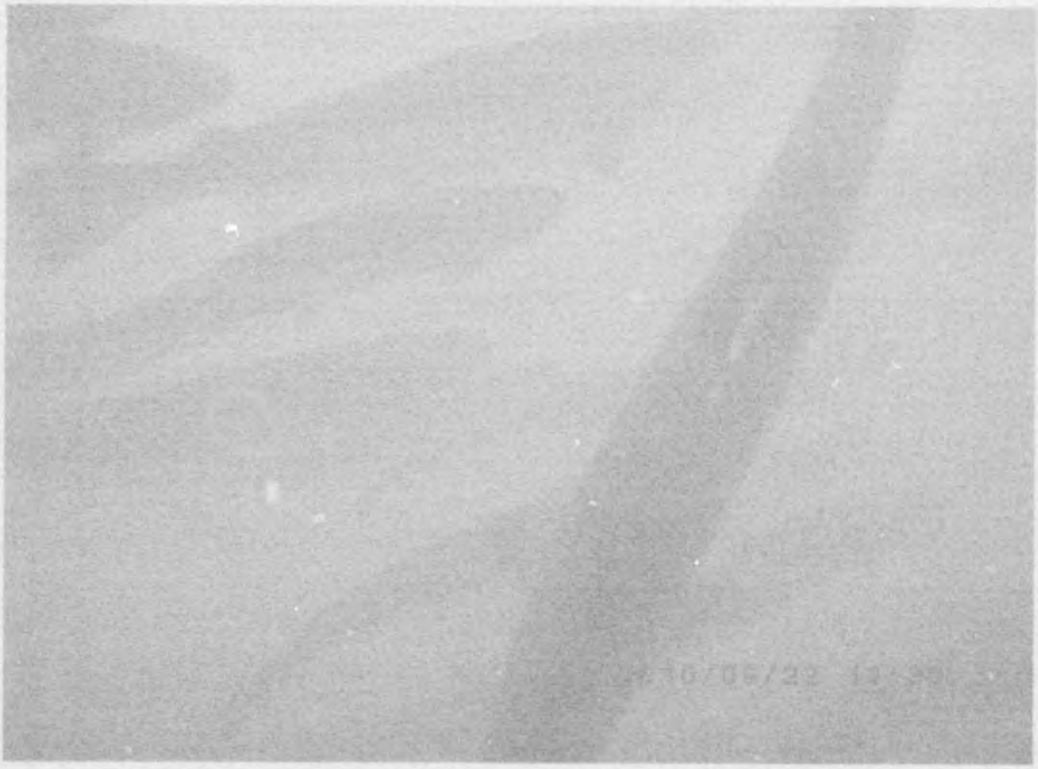

Figure 3. Underwater photograph showing cultured Atlantic salmon swimming through a mixture of therapeutant and fluorescein dye.

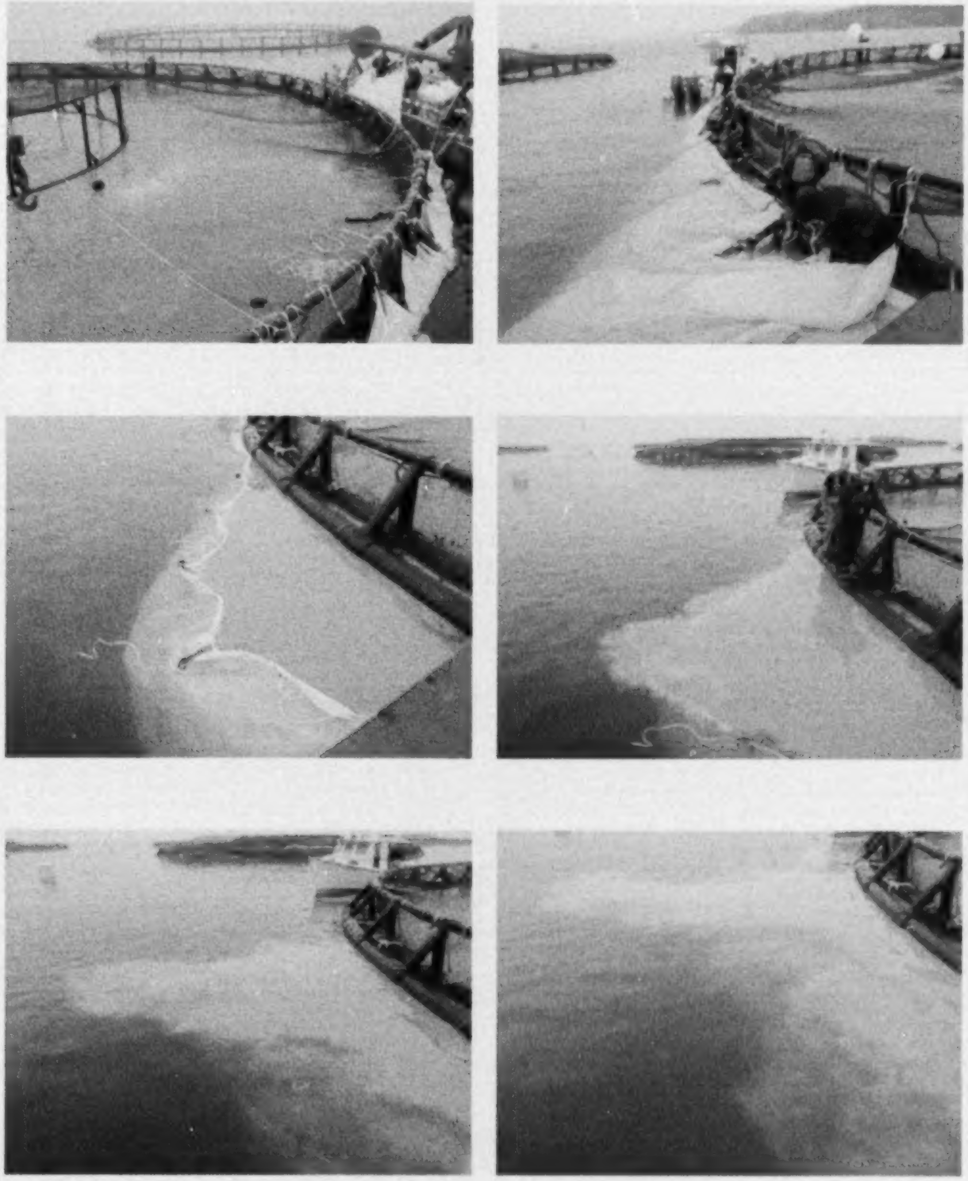

Figure 4. Example of a treatment tarpaulin being dropped and withdrawn from a net-pen showing how the dye begins to leave the cage. The photographs were taken when the net-pen was fully tarped (top left), the tarpaulin was containing the dye/therapeutant (top right), the tarpaulin was just beginning to be dropped (middle left), the tarpaulin was beginning to be pulled under (middle right), the tarpaulin was pulled further under (bottom left), and the tarpaulin was withdrawn (bottom right).

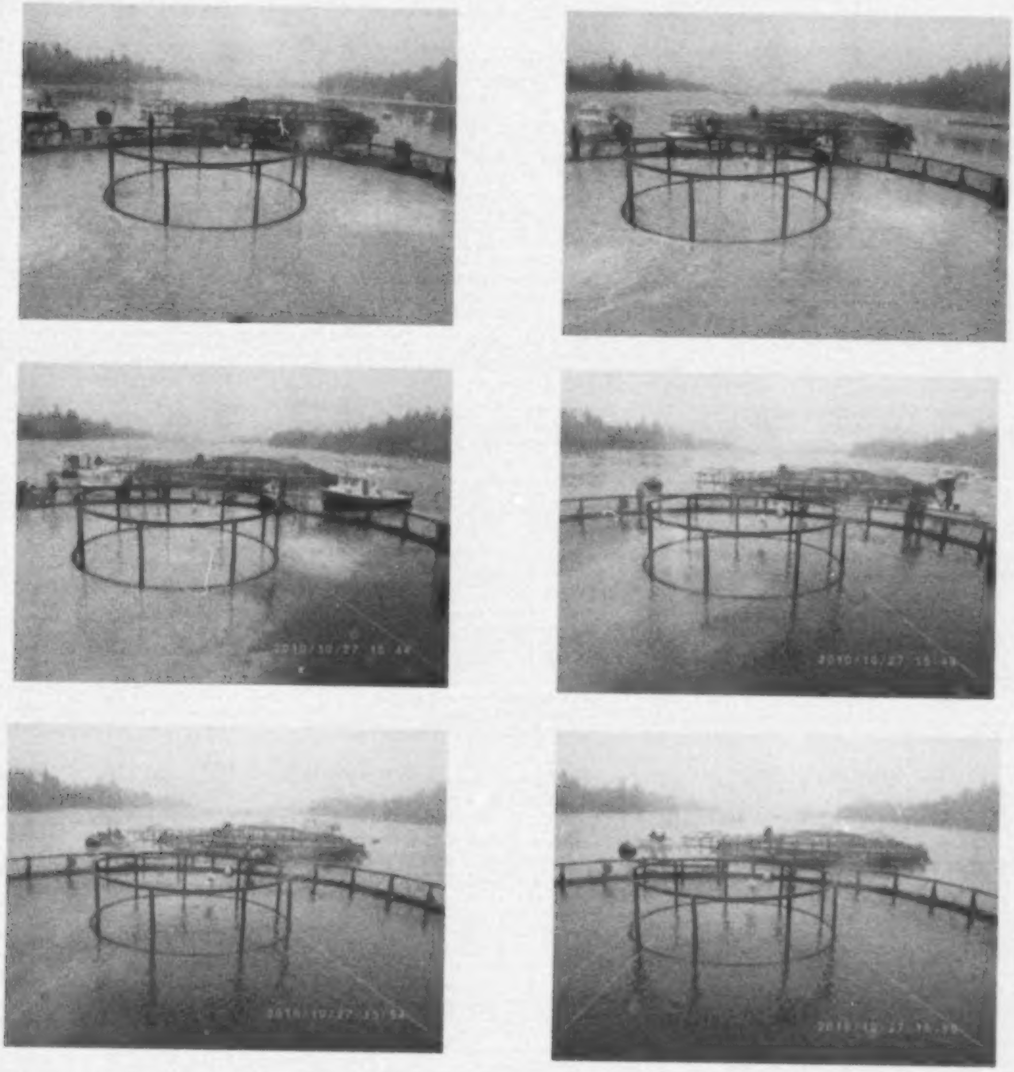

Figure 5. A series of photographs showing the temporal evolution of dye, and hence therapeutant, leaving a tarped fish cage. The photographs were taken just prior to the beginning of flushing (top left), 5 minutes (top right), 10 minutes (middle left), 15 minutes (middle right), 20 minutes (bottom left) and 24.5 minutes (bottom right) after flushing began.

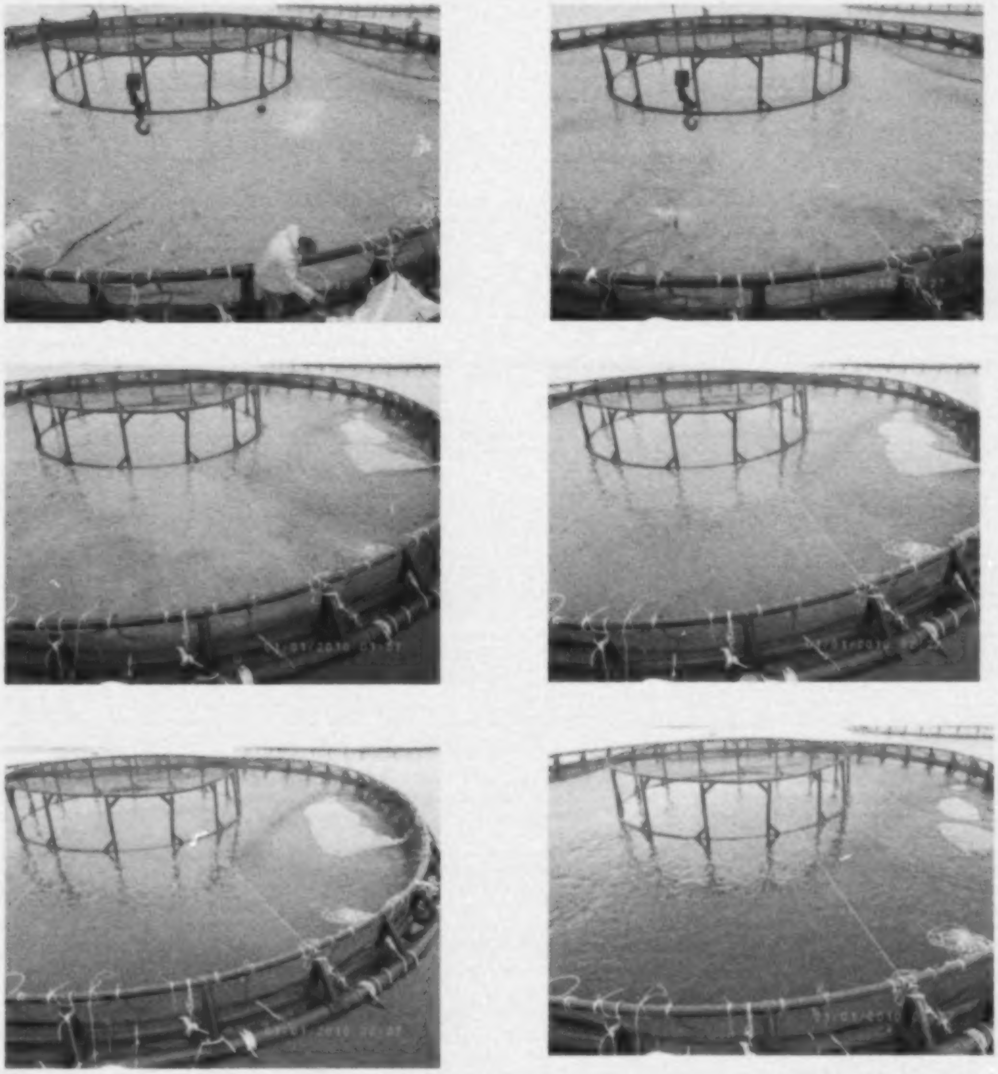

Figure 6. A second series of photographs showing the temporal evolution of dye, and hence therapeutant, flushing from a different tarped fish cage. The photographs were taken just prior to the beginning of flushing (top left), 20 minutes (top right), 50 minutes (middle left), 80 minutes or 1.3 hours (middle right), 110 minutes or 1.8 hours (bottom left) and 170 minutes or 2.8 hours (bottom right) after flushing began.

Concentration within Cages

As mentioned above, the initial concentration of therapeutant within a tarped cage is somewhat uncertain. Operationally, the desired concentration is specified by the veterinarian-in-charge and the mass of therapeutant needed to achieve this target is estimated by multiplying the desired target concentration (C_0) by an estimate of the volume (V) of water enclosed by the tarpaulin. Whether the target concentration is achieved depends upon the accuracy of the volume estimate and the degree to which the therapeutant gets mixed throughout the enclosed volume of water.

The volume of water within the bath treatment is influenced by the shape of the tarp and skirt. In the case of a tarp, the shape varies among and within treatments in response to the speed of the ambient water current. During slack water the shape may be like a cylinder or a half sphere, whereas at times of stronger current, the upstream end of the tarpaulin may be forced toward the surface leaving the downstream end as a bag containing the fish and therapeutant. In the case of a skirt, the water current may change the drop angle of the skirt.

From a practical perspective the volume of water enclosed within a tarp is estimated by assuming the tarp around the raised net forms a relatively simple shape. The volumes associated with a variety of assumed cage sizes and tarpaulin shapes are presented in Table 1. All cages are assumed to be circular since few square cages are used in southwest New Brunswick. The circumference or perimeter (P) of the cages are assumed to be 70, 100, 120 or 150m. The corresponding diameters (d) or length scales ($l_{cage\_x} = l_{cage\_y}$) of these cages are approximately 22, 32, 38 and 48 m, respectively, where the diameters or length scales are estimated as $d = l = P/\pi$. The depth of the tarp along the outside edge of the cage is assumed to be approximately 4m. When the tarp is assumed to be deeper in the middle than at the edge, the depth in the center is assumed to be 6 m. For the purpose of applying analytical equations to the dispersion of therapeutant when it is released from a cage, the initial distribution of the therapeutant patch is often assumed to be a three dimensional Guassian or normal curve shape with initial horizontal and vertical standard deviations of $\sigma_{x0} = \sigma_{y0} = l/4 = d/4$ or $\sigma_{r0} = l/3$ when a radially symmetrical shape is assumed (Okubo 1971, 1974). The vertical standard deviation is usually given as $\sigma_{z0} = h/2$. These standard deviations are also included in Table 1. The minimum volume is obtained by assuming the shape of the tarped cage is a perfect cylinder

$$V = \pi r^2 h_e = \frac{\pi d^2 h_e}{4} \qquad (1)$$

where h_e is the depth of the tarp at the cage edge. For the dimensions listed in Table 1, the minimum estimates of the enclosed volume range from 1560 to 7162 m^3 as the cage size increases from a perimeter of 70 to 150 m. When the volume is estimated as a cylinder with a depth equal to the depth at the center of the cage, h_c, the volumes range from 2340 to 10743 m^3.

The maximum volume estimate is obtained by assuming the tarped volume is cubed shaped. In this case the volume is estimated by equation 2.

$$V = l_x l_y l_z \qquad (2)$$

where $l_x = d = 4\sigma_x$, $l_y = d = 4\sigma_y$, and $l_z = \sigma_z = 2h_c$. These volume estimates range from 2979 to 13678 m^3. The maximum estimates are approximately a factor of 2 higher than the minimum estimates.

Some other ways of estimating the volume are also included in Table 1. For example, the volume estimated by assuming the tarp is a cube with horizontal length scales $l_x = l_y = d$, and a vertical length equal to the depth of the tarp at the edge of the cage ($l_z = h_e$) range from 1986 to 9119 m^3 and are a factor of 1.1 times the cylinder plus cone estimates. When the volume is estimated as a semi-ellipsoid

$$V = \frac{\frac{4}{3}\pi r^2 h_c}{2} \tag{3}$$

the volumes range from 1560 to 7162 m^3. When the volume is estimated by assuming the tarped volume has the shape of an upper cylinder with cone added to it representing the central sagging of the net, the volume is estimated as

$$V = \pi r^2 h_e + \frac{1}{3}\pi r^2 (h_c - h_e) \tag{4}$$

where h_e is the depth of the raised net around the outside edge of the cage, h_c is the depth at the center of the cage and $h_c - h_e$ is the height of the cone underlying the upper cylinder. These volume estimates range from 1820 to 8356 m^3. When the volume is estimated as a surface cylinder plus a subsurface semi-ellipsoid

$$V = \pi r^2 h_e + \frac{\frac{4}{3}\pi r^2 (h_c - h_e)}{2} \tag{5}$$

the volumes range from 2080 to 9549 m^3.

The volume estimated by assuming a cylinder with an average depth of $(h_c + h_e)/2$ is perhaps the easiest to calculate, gives a volume estimate that is closest to the average of all the volume estimates, is within 30% of the minimum and maximum estimates, and the maximums are approximately one and a half times the minimums for each cage size. These uncertainties increase when the assumption of a square cage is included in the considerations; the maximum volumes become about 1.9 times the minimum volumes. Unfortunately, we do not have empirical measurements allowing independent estimates of the volumes for a series of bath treatments to compare with the volumes estimated from the assumed shapes.

The uncertainty in the volume of water within the tarped cage translates into uncertainty in the treatment concentration. Calculations estimating the concentration of an assumed addition of M units of therapeutant show that the ratio of the maximum to minimum concentration is 1.9 (Table 1). For the shapes, cage perimeters and masses assumed here, the range in volume and concentration estimates increase somewhat as the estimates of the tarp depths decrease. However, the maximum to minimum range is still of order 2.

Table 1. Dimensions and volume estimates for tarped circular fish cages under different assumptions of cage size and volume shape.

Dimension Type	**Dimension Values**			
Cage Perimeter or Circumference (P in m)	70	100	120	150
Cage Diameter (d in m)	22.3	31.8	38.2	47.7
Cage Radius (r in m)	11.1	15.9	19.1	23.9
Horizontal Length scale ($\sigma_x = \sigma_y = d/4$ in m)	5.6	8.0	9.5	11.9
Radial Length scale ($\sigma_r = d/3$ in m)	7.4	10.6	12.7	47.7
Net Depth at cage edge (h_e in m)	4	4	4	4
Net Depth at cage center (h_c in m)	6	6	6	6
Vertical Length scale ($\sigma_z = h_e/2$ or $\sigma_z = h_c/2$ in m)	2 or 3	2 or 3	2 or 3	2 or 3
Volume (V) enclosed (m^3)				
Cylinder $h=h_e$	1560	3183	4584	7162
Cylinder $h=h_c$	2340	4775	6875	10743
Semi-Ellipsoid	1560	3183	4584	7162
Cylinder plus cone	1820	3714	5348	8356
Cylinder to h_e plus semi-ellipsoid for h_c-h_e	2080	4244	6112	9549
Cylinder $h=(h_e+h_c)/2$	1950	3979	5730	8952
Cube $\sigma_z = h_e/2$	1986	4053	5836	9119
Cube $\sigma_z = h_c/2$	2979	6079	8754	13678
Ratio of V_{max}/V_{min}	1.9	1.9	1.9	1.9
Ratio of Min/Cylinder plus cone	0.9	0.9	0.9	0.9
Ratio of Max/Cylinder plus cone	1.6	1.6	1.6	1.6
Ratio of cube $\sigma_z = h_e/2$/cylinder plus cone	1.1	1.1	1.1	1.1
Mass (M)	1000	1000	1000	1000
Maximum Concentration ($C_{max} = M/V_{min}$)	0.64	0.31	0.22	0.14
Minimum Concentration ($C_{min} = M/V_{max}$)	0.34	0.16	0.11	0.07
Ratio of C_{max}/C_{min}	1.9	1.9	1.9	1.9

Flushing from Cages

Once a tarpaulin is removed from a cage, the release of the therapeutant into the receiving waters begins. This release is characterized by a combination of transport and dispersal processes. The transport or advection processes cause the therapeutant to be carried with the ambient water as it flows through the treated cage and farm site and eventually away from the farm. During this translation, the initial concentration of therapeutant becomes diluted by ambient eddy dispersion processes.

The speed at which the therapeutant leaves the treated cage depends upon many factors including the size of the cage, the rate of water flow through the cage, the size of the net mesh and the degree of bio-fouling on the mesh. The rate at which the therapeutant subsequently moves away from the cage and disperses depends upon the ambient current velocities and rates of ambient eddy mixing. Unfortunately, all of these aspects are somewhat site, cage and time specific since they depend upon site specific oceanography, farm layout and farm husbandry.

In the absence of the fish cage, fish net, adjacent fish cages and their nets and all of the other farm infrastructure, an estimate of the flushing time of the cage or the time to transport the therapeutant out of the cage is $t_{fl} = d/U$, where d is the diameter of the cage and U is the speed of the ambient current running through the cage. Table 2 shows estimates for a range of water speeds and cage sizes. For speeds between 5 and 50 cm s^{-1}, the times range from less than a minute to about 16 minutes. Under these circumstances the initial therapeutant patch would be transported away from the cage and farm in a matter of minutes and the dispersion of the therapeutant could be approximated by the theories described below. For the slower speed of 2 cm s^{-1}, the flushing time of the cage is a few tens of minutes.

Table 2. Calculated estimates of the time, in units of minutes, needed for ambient water currents to advect or transport therapeutant out of the treated cage in an ideal case without farm infrastructure.

Water Speed (m s^{-1})	**Cage Size (m)**			
	$P = 70$ **$d = 22.3$**	**$P = 100$** **$d = 31.8$**	**$P = 120$** **$d = 38.2$**	**$P = 150$** **$d = 47.7$**
0.02	18.6	26.5	31.8	39.8
0.05	7.4	10.6	12.7	15.9
0.10	3.7	5.3	6.4	8.0
0.20	1.9	2.7	3.2	4.0
0.30	1.2	1.8	2.1	2.7
0.40	0.9	1.3	1.6	2.0
0.50	0.4	0.6	0.7	0.9

MIXING AND FLUSHING WITHIN NET-PEN

Methods

In order to empirically investigate the mixing and flushing rates of the therapeutant inside treatment cages, fluorescein dye was mixed with the therapeutant prior to addition into the treatment cage (Figure 1).

The temporal evolution of concentrations of fluorescein dye and pesticides were monitored during and post treatments. A summary of the studies undertaken can be found in Table 3. The table contains information such as time to reach a well-mixed state and the time to flush for each relevant treatment based on fluorometry data. As the dye and therapeutant spread throughout the bath volume the fish became immersed in the solution (Figure 3). For the most part the tarpaulins contained the dye, and by inference, the therapeutant, within the bath volume. When the tarpaulins and skirts were removed, the dye began to leave the cage (Figure 4). For the skirts, the dye, and therapeutant by inference, was not always contained during the skirt volume during treatment.

For each treatment, time series photographs showing the dye within the treatment cage were recorded and fluorometers were deployed within the treatment cage. For some treatments, water samples were also collected at approximately five minute intervals at the same sampling stations as the fluorometers. These were analyzed for pesticide concentration at the Research and Productivity Council in Fredericton, New Brunswick.

The photographs were taken by mounting digital Pentax Optio cameras at several locations around the cage and setting the cameras to take pictures at 10 second intervals. The fluorometers, Turner Designs Cyclops 7's attached to Data Banks, were deployed at various locations and depths inside the treatment cages. Most were suspended at a distance of 1-2 meters from the cage perimeter and at depths of about 1 m. On some occasions a fluorometer was suspended from the bird ring in the middle of the cage. All of the instruments were set to record dye concentrations at 2 or 3 second intervals. For several of the tarp treatments, large amounts of dye were added to the treatment cages (labelled "2nd dye addition" on the graphs) in order to be able to follow the dye plumes following the end of the treatment. This resulted in dye concentrations exceeding the detection limit of the fluorometers. Prior to each dye study, each fluorometer was calibrated for a 1x gain setting using a 200 µg/L sodium fluorescein dye in water from Brandy Cove, St Andrews NB prior to each study day. Laboratory testing established the range of fluorescence that dye concentration was linearly proportional to fluorescence. Auto gain settings were not used since the patchiness of the dye caused the instruments to be constantly searching for an appropriate gain.

The therapeutant dye mixture was injected into the cages generally using two perforated hoses extended nearly the diameter of the cage in a V shape just below the sea surface; however at one release a single perforated hose was used to inject the mixture and at one other site, a fire hose was used to spray the mixture on the surface (Figure 1).

The photographs from one of the releases help visualize the mixing within the bath treatment (Figure 2). These photographs show the dye being injected into the cage through two perforated hoses stretched across the diameter of the cage. The subsequent photographs show the distribution of the dye at several time intervals. The injection of the mixing tank flushing water approximately 4 minutes after dosing began is shown in the middle right panel.

The photographs also show that the dye takes the longest time to reach the side furthest from the dosing platform.

Other photographs help illustrate the observed patterns of flushing (Figure 5 and Figure 6). In the first example (Figure 5) ambient water initially entered the cage from one side and the left as an elongated streamer, rather than as an intact circular patch. The dye had completely left the cage in about 25 minutes. In the second example (Figure 6), the dye slowly dispersed from the cage over a 2-3 hour period. The dye remaining in the cage seemed to remain distributed throughout the cage rather than form a narrow strip.

The time series of dye concentrations recorded inside each quadrant of the cages are shown below. The temporal patterns are consistent with the above visual impressions in that they show the initial mixing of the dye throughout the tarp as well as a subsequent decrease in concentration after the tarp has been removed. For most studies the concentration during much of the treatment was above the upper detection threshold of the instruments.

Table 3. Summary of net-pen dye release experiments including characterizations of current regime and mixing and flushing times.

Treatment	Site and Date	Cage Circumference (m)	Treatment Duration (min)	Dye Mixing Time (min)	Pesticide Mixing at Treatment End (Stations)	Flushing Time (min)	Current Speed[5] (cm/s)
None[6]	Site A 10 Aug. 2010	100	NAV	NAV	NAV	NAV	3.4-11.7
None[6]	Site A 11 Aug 2010	100	NAV	NAV	NAV	NAV	4.8-11.8
None[6]	Site A 17 Aug 2010	100	NAV	NAV	NAV	NAV	0.4-14.9
Tarp	Site B 8 Sept. 2010	100	42	NAV[1]	Yes[2]	165	0.5-44.2
Tarp	Site B 10 Sept. 2010	100	25	>25	No[3]	80	0.3-22.8
Tarp	Site B 14 Sept. 2010	100	44	NAV[1]	Not yet[4]	175	0.2-20.3
Tarp	Site F 13 Oct. 2010	70	66	50	NAV[2]	7	5.1-29.9
Tarp	Site C 27 Oct. 2010	70	29	NAV[1]	NAV[2]	30	0.2-29.9
Skirt	Site B 22 Sept. 2010	100	40	NAV[3]	Not yet (4)	150	0.8-22.8
Skirt	Site J 6 Oct. 2010	70	67	40[4]	NAV[2]	25	NAV

* Mixing time is defined as the time taken for the dye to become well mixed in the cage, i.e., when fluorometers measure the same concentration of dye and persist at that concentration until treatment

end. Flushing time is defined as the time taken following the end of treatment until concentrations of all fluorometers inside the cage reach and stays below the detection level.

[1] The dye was not mixed before dye concentrations exceeded instrument detection limits.

[2] No pesticide samples were collected to assess mixing.

[3] Dye concentrations never became mixed during the treatment.

[4] Dye concentrations became uniform among stations but the concentration decreased for the rest of the treatment.

[5] Current are measured in the upper 3.5 m from the surface and the observation time period is from 30 minutes prior to commencement of the treatment to 30 minutes post-treatment. These values were obtained from 2 to 16 current meters deployed within and around the dye release site (unpublished data).

[6] Dye was released into a net-pen with a surface collar with no net.

NAV = Not available

Observations

Site B – 8th of September 2010

Figure 7 shows the relative location of the recording fluorometers and the time series of dye concentrations recorded at each location during the 8th of September 2010 treatment. In this treatment, azamethiphos was the chemical treatment used and the dye-chemical mixture was added in two pulses; the first was a low concentration of dye pulse in an effort to ensure the upper detection limit of the fluorometers would not be exceeded. The second pulse (dye only) was added several minutes later in order to raise the dye concentration within the bath so it could be followed after release into the receiving water. Near-surface current speeds during this treatment ranged from 0.5-44.2 cm/s (Table 3). Following the first dye addition, fluorometers located at stations closest to the therapeutant injection hoses detected the dye before stations located farther away from the hoses. The instruments deployed at the same stations at different depths responded more similarly than the instruments at the same depth located at different stations. The concentrations of dye did not become well mixed (or uniform) in the 15 minutes prior before the second addition of dye, at which point the concentrations of dye were above the limits of the fluorometers.

The pesticide data collected from three of the water sampling stations indicate a similar temporal sequence to the dye; there was high variation in pesticide concentrations initially and then similar concentrations just prior to the dropping of the tarp. The latter two data points suggest that the contents of the cage were well mixed or reaching a well-mixed stage by the end of the approximately 45 min treatment.

The time needed for the dye to flush from the cage was over two hours, with some recording stations detecting the dye longer than others. Station E detected dye for 45 minutes longer than Station A.

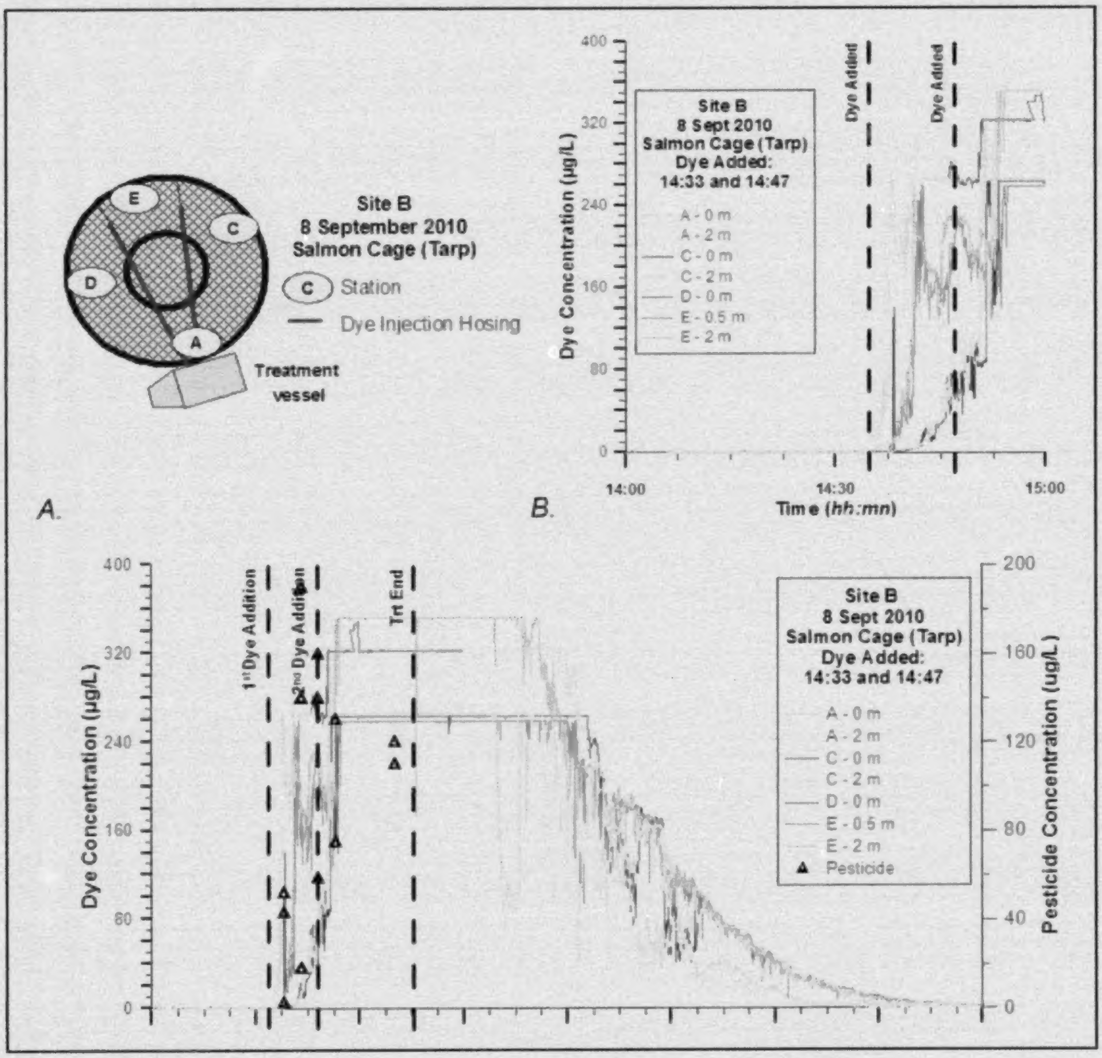

Figure 7. Dye and pesticide concentrations inside the treated cage at Site B, the 8th of September 2010. Fluorescence plateaus during treatment because dye concentrations exceed the detection limit of the fluorometers. A (upper left): Diagram of sampling stations and treatment equipment inside the treatment cage. B (upper right): Time series of dye concentrations during mixing (before dye concentrations exceeded instrument limitations). C (bottom half): Time series of dye and pesticide concentrations throughout treatment and flushing.

Site B – 10th of September 2010

Figure 8 shows the relative location of the recording fluorometers and the time series of dye concentrations recorded at each location during the 10th of September 2010 treatment. In this treatment, azamethiphos was the chemical treatment used and the dye-chemical mixture was added in two pulses; the first was a low concentration of dye pulse in an effort to ensure the upper detection limit of the fluorometers would not be exceeded. The second pulse (dye only) was added several minutes later in order to raise the dye concentration within the bath so it could be followed after release into the receiving water. Near-surface current speeds during this treatment ranged from 0.3-22.8 cm/s (Table 3). Following the first addition of dye, fluorometers at all three stations detected dye within three minutes. The concentrations of dye did not become well mixed (or uniform) in the 15 minutes prior to the second addition of dye, at which point the concentrations of dye were above the limits of the fluorometers. The pesticide data indicate that the contents of the cage were not well mixed by the end of the approximately 25 min treatment, given that differences of up to 150 µg/L of pesticide existed among sampling stations at the last sampling point just prior to tarp release.

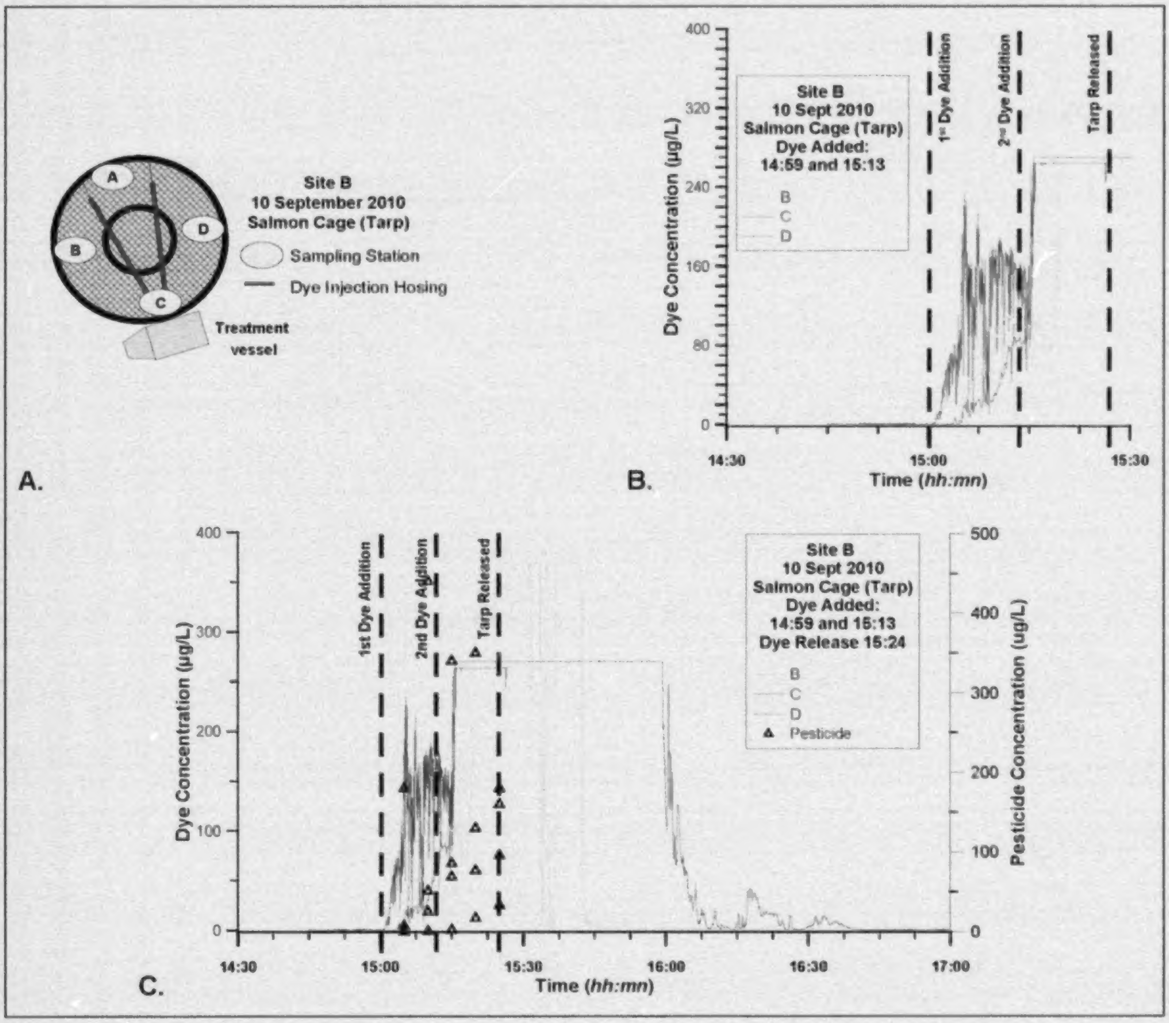

Figure 8. Dye and pesticide concentrations inside the treated cage at Site B, the 10th of September 2010. Fluorescence plateaus during treatment because dye concentrations exceed the detection limit of the fluorometers. No fluorometry data were available at station A due to an instrument malfunction. A (top left): Diagram of sampling stations and treatment equipment inside the treatment cage. B (top right): Time series of dye concentrations during mixing (before dye concentrations exceeded instrument limitations). C (bottom): Time series of dye and pesticide concentrations throughout treatment and flushing.

Estimates of the flushing time varied among fluorometers. The station B data indicated a flushing time of approximately 20 minutes whereas the sampling station D data indicated a time of 80 minutes.

Site B – 14th of September 2010

Figure 9 shows the relative location of the recording fluorometers and the time series of dye concentrations recorded at each location during the 14th of September 2010 treatment. In this treatment, azamethiphos was the chemical treatment used and the dye-chemical mixture was added in two pulses; the first was a low concentration of dye pulse in an effort to ensure the upper detection limit of the fluorometers would not be exceeded. The second pulse (dye only) was added several minutes later in order to raise the dye concentration within the bath so it could be followed after release into the receiving water. Near-surface current speeds during this treatment ranged from 0.2-20.3 cm/s (Table 3). Almost immediately following the first addition of dye to the tarped cage, fluorometers at two of the four stations inside the cage detected dye. At the remaining two stations, dye was detected shortly after, between 5 and 10 minutes after the start of dye addition. Initial detection of fluorescence was sometimes coupled with sharp peaks in dye concentration that quickly diminished. The station which detected dye last, consistently measured much lower concentrations than the other three stations over the initial mixing time period. The concentrations of dye did not become well mixed (or uniform) in the 15 minutes prior to the second addition of dye, at which point the concentrations of dye were above the limits of the fluorometers.

The pesticide data suggests that the concentrations at the four sampling stations were beginning to converge by the end of the approximately 45 minutes treatment, with the concentrations from all stations being within a 20 μg/L range, a much narrower range than the 150 μg/L range observed during the 10th of September 2010 treatment.

The flushing time for this treatment was particularly long; with the dye at all four monitoring stations remaining in the cage for over 2.5h after the tarpaulin was removed.

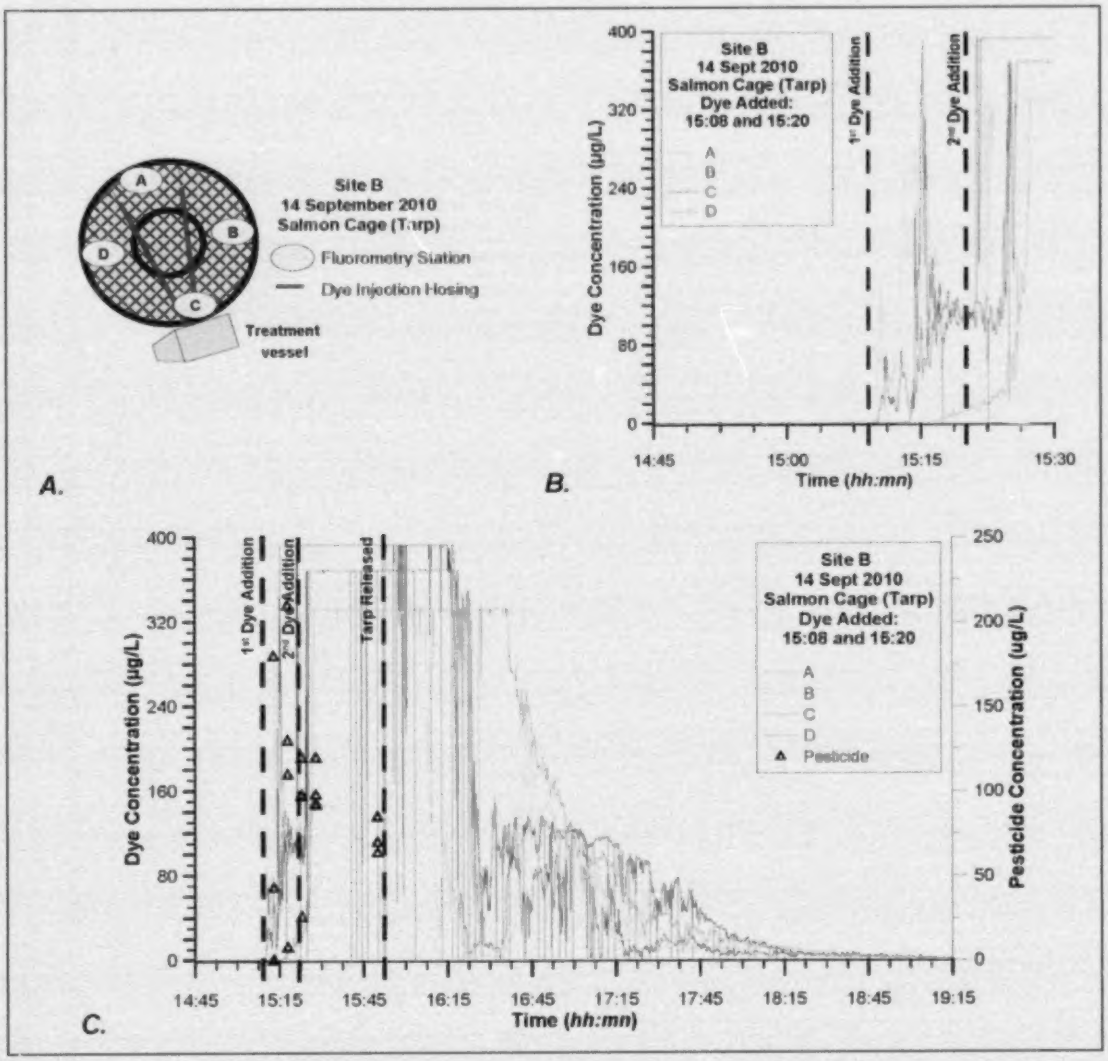

Figure 9. Dye and pesticide measurements inside the tarped treatment cage at Site B, the 14th of September 2010. Fluorescence plateaus during treatment because dye concentrations exceed the detection limit of the fluorometers. No fluorometry data were available at sampling station A due to an instrument malfunction. A(top left): Diagram of sampling stations and treatment equipment inside the treatment cage. B(top right): Time series of dye concentrations during mixing (before dye concentrations exceeded instrument limitations). C(bottom): Time series of dye and pesticide concentrations throughout treatment and flushing. The time of the last pesticide sample was interpolated.

Site F – 13th of October 2010

Figure 10 shows the relative location of the recording fluorometers and the time series of dye concentrations recorded at each location during the 13th of October 2010 treatment. In this treatment, azamethiphos was the chemical treatment used and the dye-chemical mixture was added in one pulse; a low concentration of dye pulse was added in an effort to ensure the upper detection limit of the fluorometers would not be exceeded in order to assess the mixing in the tarp for the duration of the treatment. Following the addition of the dye, three of the stations detected dye within 5 minutes and peaked above instrument limits for 7-30 minutes. The remaining station detected an initial momentary spike in dye concentration, and then detected no dye for a further 10 minutes. From 14:30 to 15:00, dye appeared to have been concentrated in certain areas in the tarp, represented by the two stations with high concentrations compared to the two stations with comparatively lower fluorescence values. Through time, the dye concentrations measured at the four stations converged, suggesting the dye was gradually becoming more evenly distributed through space. By 45 minutes following dye addition, concentrations of dye at the different stations converged. No pesticide data from inside the bath were available for this treatment.

Flushing of this cage was very rapid. Near-surface current speeds during this treatment ranged from 5.1-29.9 cm/s (Table 3). No dye was detected inside the cage following seven minutes after the removal of the tarp at all four of the fluorometry stations. The net had been changed approximately four weeks prior to this treatment and was relatively free of bio-fouling.

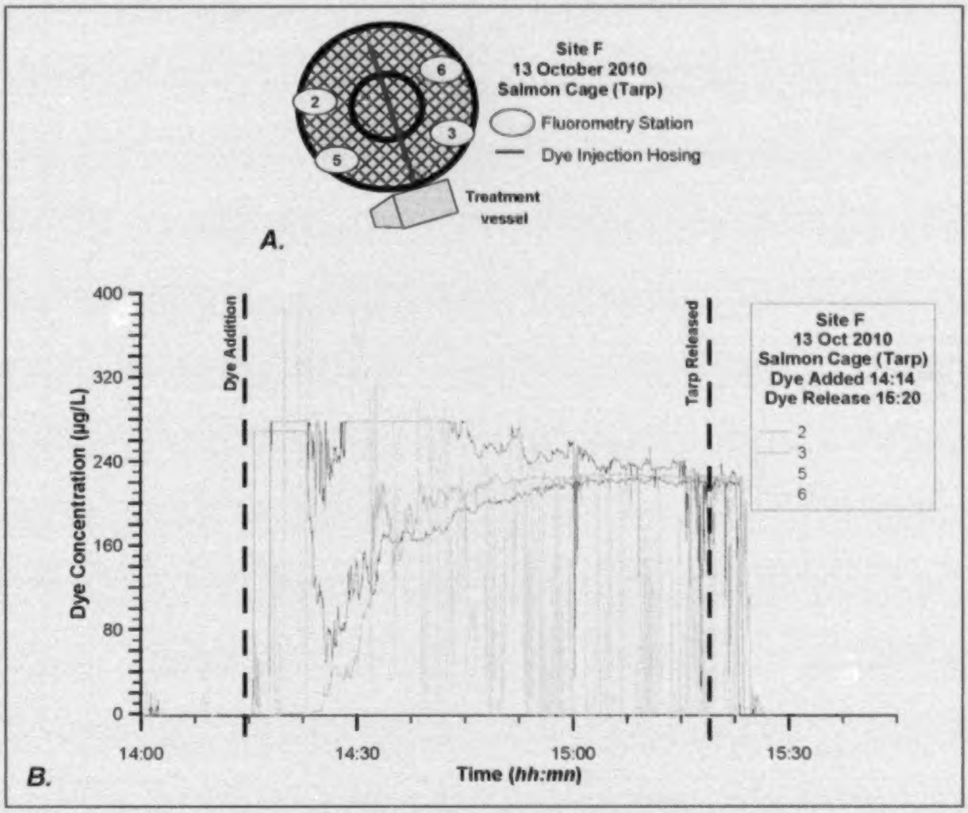

Figure 10. Dye measurements inside the tarped treatment cage at Site F, the 13th of October 2010. Fluorescence plateaus during treatment because dye concentrations exceed the detection limit of the fluorometers. A (top left). Diagram of sampling stations and treatment equipment inside the treatment cage. B (bottom): Time series of dye concentrations throughout treatment and flushing.

Site C – 27th of October 2010

Figure 11 shows the relative location of the recording fluorometers and the time series of dye concentrations recorded at each location during the 27th of October 2010 treatment. In this treatment, deltamethrin was the chemical treatment used and the dye-chemical mixture was added in one pulses; a high concentration of dye pulse was added in order to follow the plume after release into the receiving water. Near-surface current speeds during this treatment ranged from 0.2-29.9 cm/s (Table 3). Following addition of the dye there was a time lag of five minutes before either of the two functioning fluorometers deployed inside the cage detected dye. As dye was added only once to the cage, and in large amounts, concentrations of dye quickly exceeded the fluorometer detection limits. No pesticide data were available for inside the bath.

Flushing of this cage was occurred over a 30 minute period. This time to flush was similar for the two stations.

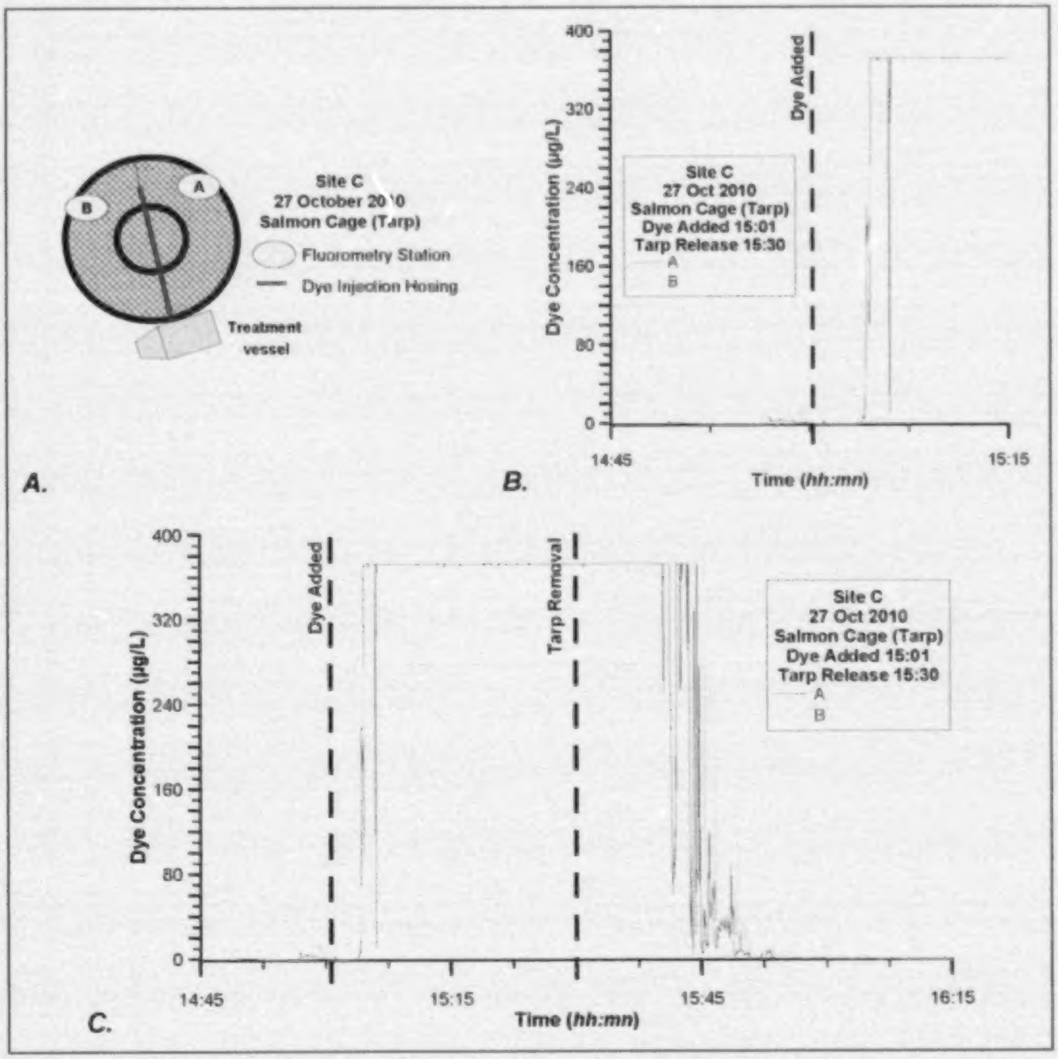

Figure 11. Dye measurements inside the tarped treatment cage at Site C, the 27th of October 2010. Fluorescence plateaus during treatment because dye concentrations exceed the detection limit of the fluorometers. A (top left): Diagram of sampling stations and treatment equipment inside the treatment cage. B (top right): Time series of dye concentrations during mixing (before dye concentrations exceeded instrument limitations). C (bottom): Time series of dye concentrations throughout treatment and flushing.

Site B, with use of Skirt – 22nd of September 2010

Figure 12 shows the relative location of the recording fluorometers and the time series of dye concentrations recorded at each location during the 22nd of September 2010 treatment. In this treatment, azamethiphos was the chemical treatment used and the dye-chemical mixture was added in one pulse; a low concentration of dye pulse was added in an effort to ensure the upper detection limit of the fluorometers would not be exceeded in order to assess the mixing in the skirt for the duration of the treatment. Following the addition of dye to the skirted cage, fluorometers at all but one stations detected dye within the first 20 minutes (A-2 did not detect dye until the treatment was over). Photos taken from the treatment barge (the opposite side of the cage from A-2) show the water in the cage becoming gradually greener as the dye was added and mixed; however, there may have been a zone that dye did not reach in the cage where fluorometer A-2 was located. The dye did not become well mixed (or uniform) inside the skirt during the treatment, with concentrations at the end of treatment ranging between <5 µg/L and 75 µg/L.

Near-surface current speeds during this treatment ranged from 0.8-22.8 cm/s (Table 3). Flushing the cage completely of dye took over 150 minutes, beyond when the instruments were removed, though concentrations in the cage were <20 µg/L. There was similarity in the flushing times among stations, with the exception of A-2 which hardly detected any dye at all throughout the entire study. The net on the cage was highly fouled.

Pesticide was detected at all of the pesticide sampling stations along the cage periphery. Pesticide concentrations just prior to release varied between 40 and 80 µg/L. The target concentration for Salmosan® in skirts is 150 µg/L. Therefore the average concentration of pesticide in the cage prior to release was roughly one third of the target concentration.

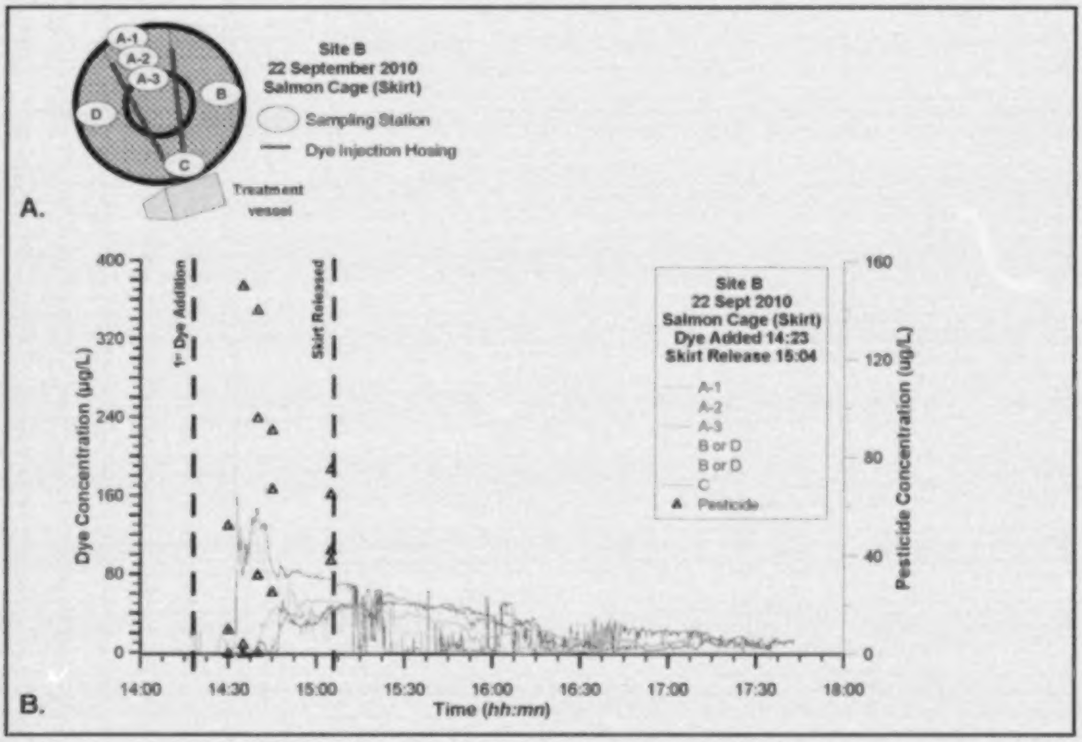

Figure 12. Dye and pesticide concentrations inside the treated cage at Site B, the 22nd of September 2010. Fluorescence plateaus during treatment because dye concentrations exceed the detection limit of the fluorometers. A (top left): Diagram of sampling stations and treatment equipment inside the treatment cage. B (bottom): Time series of dye and pesticide concentrations throughout treatment and flushing.

Site J, with use of Skirt – 6th of October 2010

Figure 13 shows the relative location of the recording fluorometers and the time series of dye concentrations recorded at each location during the 6th of October 2010 treatment. In this treatment, azamethiphos was the chemical treatment used and the dye-chemical mixture was added in one pulse; a low concentration of dye pulse was added in an effort to ensure the upper detection limit of the fluorometers would not be exceeded in order to assess the mixing in the skirt for the duration of the treatment. Following the addition of dye to the skirted cage, fluorometers at all stations detected dye within the first 5 minutes. Interestingly, dye concentrations appeared to become well mixed approximately 40 minutes into the treatment, with concentrations at each of the individual fluorometer stations converging at 30 µg/L; however, the concentrations of dye at all of the stations gradually decreased from that point until the end of the treatment. Concentrations at each of the stations at the end of treatment were roughly 10 µg/L.

Flushing the cage completely of dye following the end of the treatment took approximately 25 minutes, though the decrease in concentrations suggest that the dye may have been emptying from the cage for some time prior to the end of the treatment when the skirt was removed (see Observations on Vertical Aspects for more discussion of vertical distribution of dye in skirts). Flushing times were similar among stations.

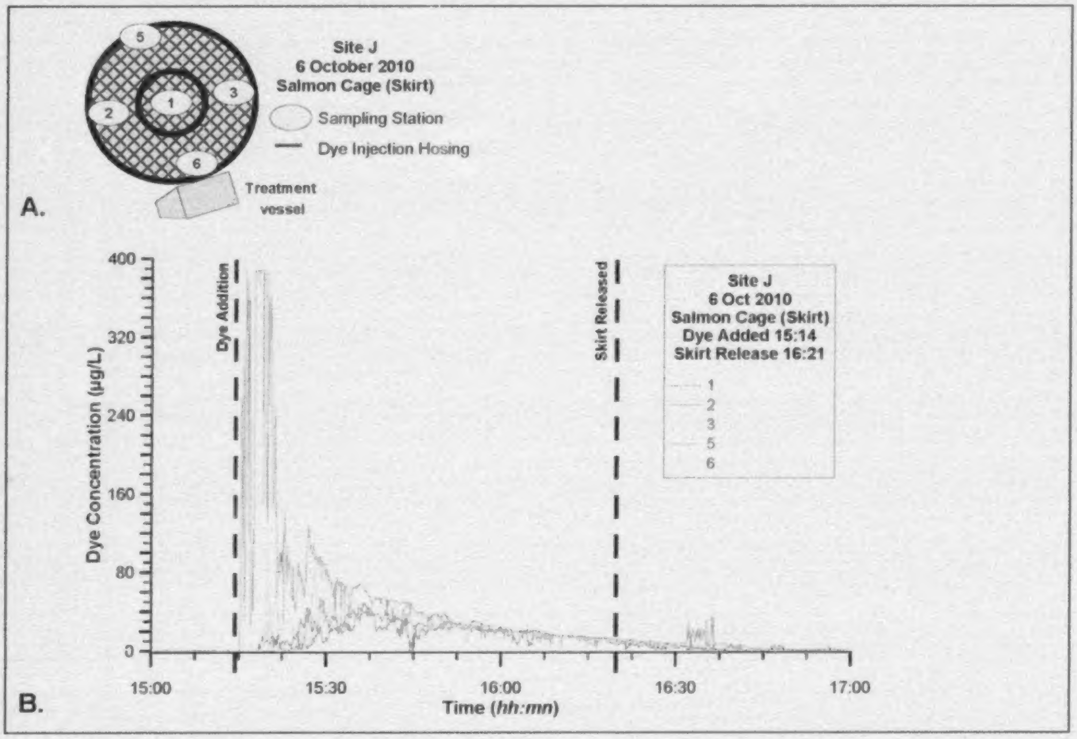

Figure 13. Dye and pesticide concentrations inside the treated cage at Site J, on the 6th of October 2010. Fluorescence plateaus during treatment because dye concentrations exceed the detection limit of the fluorometers. A (top left): Diagram of sampling stations and treatment equipment inside the treatment cage. B (bottom): Time series of dye concentrations throughout treatment and flushing.

Mixing and Flushing Summary

In summary, the observations on mixing within the tarped cages suggest that the mean concentration of azamethiphos at the time of release was within about 25% of the target concentration (100 µg/L), that mixing within the bath volume varies among treatments and is often incomplete within the duration of the treatment. The range in pesticide concentration just prior to release into the environment varied from 20 µg/L to 150 µg/L. For skirts, mixing within the bath volume also varies among treatments and is not necessarily complete within the duration of the treatment, and also the data suggest that dye may escape skirts in some situations. For the one pesticide treatment with data, the average final pesticide concentration was approximately 30% of the target concentration. No tarp or skirt mixing data for Alphamax® were available.

The flushing times ranged from about 7 to 150 minutes for tarps and skirts, times that are sometimes considerably longer than those estimated using simple assumptions of cage diameters divided by ambient current speeds. The exact reason for the range is not known, although it is assumed to be related to variations in mesh size, bio-fouling, ambient current speeds and farm configurations. The flushing rates could not be related to current speeds within the cages because the participating farmers did not want current meters deployed in their cages during bath treatments.

TRANSPORT AND DISPERSAL AWAY FROM NET-PEN

Background

There are several classic reference books that provide entrance into the extensive literature on transport and dispersal processes. These include Fisher et al. (1979), Bowden (1983), Csanady (1973), Lewis (1997) and Vesilind et al. (2010). The overview of the underlying theory presented below draws heavily from these sources. It should also be noted that there appears to be very little literature concerning the specific situation of therapeutant transport and dispersal from fish farms and well-boats and, with the exception of Ernst et al. (2001) and Page et al. (2000), almost no literature specific to the southwest New Brunswick area.

It is also worth pointing out that to a first approximation, the dilution rate is independent of the translation or advection rate. In other words, the rate at which a patch of dissolved substance is diluted is not affected by how fast or how far the patch is carried by the currents. The rate of therapeutant dilution is controlled by the rates of horizontal and vertical mixing in the area of release, as well as rates of chemical behaviour and reaction in the ambient water. Although this report does not address these chemical processes, it should be noted that the empirical dye results reported below were associated with releases of specific chemicals and that water samples taken during the releases support an interpretation that the dye results are indicative of therapeutant transport and dispersal, at least over the short time scales considered here.

There is a considerable amount of literature that is useful to the dispersion component of the transport and dispersal of the therapeutant from the fish cages. However, all of this theory and experience assumes the presence of the fish cages, fish nets and farm infrastructure does not influence the dispersal. As indicated above this may not be a good assumption. A brief overview of the theoretical aspects of dispersal is given next.

The simplest form of dispersion solutions assumes that the material to be dispersed is instantaneously introduced into the dispersing environment, the rate of dispersal is constant over time and the rates of dispersal along orthogonal x,y,z Cartesian coordinates are independent of each other (Csanady 1973, Lewis 1997). This is called Fickian dispersion and in a horizontally and vertically unbounded situation an analytical solution for the case of a point source release has been reported by (Lewis 1997) as

$$c(x,y,z,t) = \frac{M \exp\left[-\frac{1}{2}\left(\frac{x^2}{\sigma_{xt}^2} + \frac{y^2}{\sigma_{yt}^2} + \frac{z^2}{\sigma_{zt}^2}\right)\right]}{(2\pi)^{3/2}\sigma_{xt}\sigma_{yt}\sigma_{zt}} \qquad (6)$$

where $c(x,y,z,t)$ is the concentration of therapeutant at a given position (x,y,z) and time t, M is the mass of the therapeutant, σ_{xt}, σ_{yt}, and σ_{zt} are the temporally varying standard deviations in the x, y, and z directions, respectively. This solution is of limited use to the spread of therapeutant released from a cage since it assumes the initial release has all of the material (M) contained within an infinitely small volume, i.e., the concentration is infinitely large (Csanady 1973). However, it is the foundation of the Fickian dispersion perspective and more useful modifications of the solution have been developed.

A solution that assumes the material is initially distributed over some finite space has been given by (Lewis 1997) as

$$c(x,y,z,t) = \frac{M \exp\left[-\frac{1}{2}\left(\frac{x^2}{\sigma_{x0}^2 + \sigma_{xt}^2} + \frac{y^2}{\sigma_{y0}^2 + \sigma_{yt}^2} + \frac{z^2}{\sigma_{z0}^2 + \sigma_{zt}^2}\right)\right]}{(2\pi)^{3/2}(\sigma_{x0}^2 + \sigma_{xt}^2)^{1/2}\left(\sigma_{y0}^2 + \sigma_{yt}^2\right)^{1/2}(\sigma_{z0}^2 + \sigma_{zt}^2)^{1/2}} \qquad (7)$$

where the initial patch size is incorporated by substituting the values for the standard deviations (i.e., the σs) with the square roots of the sums of the initial and turbulence standard deviations, $\sqrt{(\sigma_0^2 + \sigma_t^2)}$. The initial dimensions are assumed to be a three dimensional Gaussian distribution with σ_{x0}, σ_{y0} and σ_{z0} being the standard deviations of the source distribution along their respective orthogonal Cartesian x, y and z coordinates. Values for these initial standard deviations can be estimated from the length scales (l_x, l_y, l_z) of the initial patch (Lewis 1997) as

$$\sigma_{x0} = \frac{l_x}{4} \qquad (8)$$

$$\sigma_{y0} = \frac{l_y}{4} \qquad (9)$$

$$\sigma_{z0} = \frac{l_z}{2} \qquad (10)$$

The σ_{xt}, σ_{yt}, and σ_{zt} signify the subsequent increase in variance due to water turbulence. The solution for the concentration at the center $(x = y = z = 0)$ of this evolving patch is given by

$$c(0,0,0,t) = \frac{M}{(2\pi)^{3/2}(\sigma_{x0}^2 + \sigma_{xt}^2)^{1/2}\left(\sigma_{y0}^2 + \sigma_{yt}^2\right)^{1/2}(\sigma_{z0}^2 + \sigma_{zt}^2)^{1/2}} \qquad (11)$$

This solution is still of limited use, since it continues to assume the patch is horizontally and vertically unbounded, which is not the case for aquaculture cages floating at the sea surface.

A more appropriate solution in which vertical diffusion is bounded by the sea surface and unbounded below the surface, is given by (Lewis 1997) for the case of a point release

$$c(x,y,z,t) = \frac{M \exp\left[-\frac{1}{2}\left(\frac{x^2}{\sigma_{xt}^2} + \frac{y^2}{\sigma_{yt}^2} + \frac{z^2}{\sigma_{zt}^2}\right)\right]}{\sqrt{2}\,\pi^{\frac{3}{2}}\sigma_{xt}\sigma_{yt}\sigma_{zt}} \qquad (12)$$

and as

$$c(x,y,z,t) = \frac{M \exp\left[-\frac{1}{2}\left(\frac{x^2}{\sigma_{x0}^2 + \sigma_{xt}^2} + \frac{y^2}{\sigma_{y0}^2 + \sigma_{yt}^2} + \frac{z^2}{\sigma_{z0}^2 + \sigma_{zt}^2}\right)\right]}{\sqrt{2}\pi^{\frac{3}{2}}(\sigma_{x0}^2 + \sigma_{xt}^2)^{\frac{1}{2}}(\sigma_{y0}^2 + \sigma_{yt}^2)^{\frac{1}{2}}(\sigma_{z0}^2 + \sigma_{zt}^2)^{\frac{1}{2}}} \qquad (13)$$

for a finite-sized initial patch. In the latter situation, the solution at the horizontal center of the unadvected source $(x = 0, y = 0, z = 0)$ is

$$c(0,0,0,t) = \frac{M}{\sqrt{2}\pi^{\frac{3}{2}}(\sigma_{x0}^2 + \sigma_{xt}^2)^{\frac{1}{2}}(\sigma_{y0}^2 + \sigma_{yt}^2)^{\frac{1}{2}}(\sigma_{z0}^2 + \sigma_{zt}^2)^{\frac{1}{2}}} \qquad (14)$$

The solution changes again when the vertical dispersal is bounded by the seabed or the bottom of a surface mixed layer. When the therapeutant is considered to be vertically well-mixed it continues to disperse horizontally but not vertically and the appropriate solution for the dispersal is given by Lewis (1997) as

$$c(x,y,t) = \frac{M \exp\left[-\frac{1}{2}\left(\frac{x^2}{\sigma_{x0}^2 + \sigma_{xt}^2} + \frac{y^2}{\sigma_{y0}^2 + \sigma_{yt}^2}\right)\right]}{2\pi\,(\sigma_{x0}^2 + \sigma_{xt}^2)^{\frac{1}{2}}(\sigma_{y0}^2 + \sigma_{yt}^2)^{\frac{1}{2}}h} \qquad (15)$$

where h is the depth bounding the vertical dispersal. In this case the temporal reduction in concentration at the center of the patch ($x = 0, y = 0$) is given by

$$c(0,0,t) = \frac{M}{2\pi\,(\sigma_{x0}^2 + \sigma_{xt}^2)^{\frac{1}{2}}(\sigma_{y0}^2 + \sigma_{yt}^2)^{\frac{1}{2}}h} \qquad (16)$$

In all of the above solutions, advection of the patch away from its point of release can be incorporated by replacing x with $x_0 + ut$, y with $y_0 + vt$ and z with $z_0 + wt$, where u, v and w are the water velocities along the x, y and z axes of the Cartesian coordinate system.

Continuous Release into the Environment

All of the above solutions assume the removal of the tarpaulin is fast, i.e., a few minutes, and the therapeutant disperses as though the cage were no longer present. However, as illustrated above the presence of the cage nets sometimes causes the therapeutant to escape from the cage over time. In these situations the therapeutant is continuously released into the receiving waters over a finite duration of time, rather than in one instantaneous dump. During this type of release the concentration at the source decreases with time.

An approximate solution for the horizontally and vertically unbounded dispersion of material released at a continuous and constant rate (Q) into ambient water with a spatially homogeneous flow field moving in a single direction, x, with a velocity u_0, has been given by Lewis (1997) as

$$c(y,z,t) = \frac{Q \exp\left[-\frac{1}{2}\left(\frac{y^2}{\sigma_{yt}^2} + \frac{z^2}{\sigma_{zt}^2}\right)\right]}{2\pi\, u_0 \sigma_{yt}\sigma_{zt}} \qquad (17)$$

In this solution, mixing along the direction of flow (x) is assumed to be small relative to the advection and hence it is ignored. When the solution is assumed to have an initial discharge size of σ_{y0}, σ_{z0} and unit length in the X direction, the solution is

$$c(y,z,t)=\frac{Q\ \mathrm{exp}\left[-\frac{1}{2}\left(\frac{y^2}{\sigma_{y0}^2+\sigma_{yt}^2}+\frac{z^2}{\sigma_{z0}^2+\sigma_{zt}^2}\right)\right]}{2\pi u_0\left(\sigma_{y0}^2+\sigma_{yt}^2\right)^{\frac{1}{2}}\left(\sigma_{z0}^2+\sigma_{zt}^2\right)^{\frac{1}{2}}} \tag{18}$$

The above solution is of limited value to the bath treatment situation since it assumes dispersal of the material is spatially unbounded. As in the case of an instantaneous release, the solution can be modified to account for the presence of the sea surface and hence only horizontal and downward mixing. This solution is given by Lewis (1997) as

$$c(y,z,t)=\frac{Q}{\pi u_0\sigma_{yt}\sigma_{zt}}\exp\left[-\frac{1}{2}\left(\frac{y^2}{\sigma_{yt}^2}+\frac{z^2}{\sigma_{zt}^2}\right)\right] \tag{19}$$

and

$$c(y,z,t)=\frac{Q\ \mathrm{exp}\left[-\frac{1}{2}\left(\frac{y^2}{\sigma_{y0}^2+\sigma_{yt}^2}+\frac{z^2}{\sigma_{z0}^2+\sigma_{zt}^2}\right)\right]}{\pi u_0\left(\sigma_{y0}^2+\sigma_{yt}^2\right)^{\frac{1}{2}}\left(\sigma_{z0}^2+\sigma_{zt}^2\right)^{\frac{1}{2}}} \tag{20}$$

when a finite-sized initial release is assumed.

When it is further assumed that the rate of vertical mixing is sufficient to maintain a vertically homogenous distribution of the material over a surface layer of constant depth h, the solution becomes (Lewis 1997)

$$c(y,t)=\frac{Q}{\sqrt{2\pi}u_0h\sigma_{yt}}\exp\left[\frac{-y^2}{2\sigma_{yt}^2}\right] \tag{21}$$

where u_0 is now the depth average velocity within the surface layer. A solution when the discharge has an initial size in the y direction is

$$c(y,t)=\frac{Q\ \mathrm{exp}\left[-\frac{1}{2}\left(\frac{y^2}{\sigma_{y0}^2+\sigma_{yt}^2}\right)\right]}{\sqrt{2\pi}u_0h\left(\sigma_{y0}^2+\sigma_{yt}^2\right)^{\frac{1}{2}}} \tag{22}$$

These equations indicate that as the rate of flow in the receiving water increases, the concentration in the resulting plume of material decreases. This suggests that therapeutants slowly released from tarpaulins will have lower concentrations at any particular time and relative location than when the therapeutant is suddenly released. It also suggests that exposure time to the therapeutant at a particular location may be extended relative to the instantaneous release.

It should be noted that these equations refer to the situation in which the effluent is passively discharged into the receiving environment and advected away by the ambient flow. Different solutions are required when the discharge is actively pumped into the receiving environment. This latter situation is the case for the well-boat treatments discussed below. Predictions based on these equations have not yet been compared to our observations.

Rates of Eddy Diffusion

In all of the above, the standard deviations along the coordinate axes, σ_x, σ_y, σ_z of dispersing patches are usually assumed to increase with time according to the following relationships (Csanady 1973, Lewis 1997):

$$\sigma_{xt} = \sqrt{2K_x t} \tag{23}$$

$$\sigma_{yt} = \sqrt{2K_y t} \tag{24}$$

$$\sigma_{zt} = \sqrt{2K_z t} \tag{25}$$

or

$$\sigma_{xt}^2 = 2K_x t \tag{26}$$

$$\sigma_{yt}^2 = 2K_y t \tag{27}$$

$$\sigma_{zt}^2 = 2K_z t \tag{28}$$

In the above equations, K_x and K_y are the coefficients of horizontal eddy diffusivity along the horizontal x, y axes and K_z is the coefficient of vertical eddy diffusivity along the vertical, z axis.

Although it is convenient to assume the values of K_x and K_y are constant, it has been well documented that they actually increase with the scale of the patch, which in turn increases with time, so that K_x, K_x, K_z are effectively functions of time (Okubo 1971, Okubo 1974, Bowden 1983, Lewis 1997). Okubo provides a relationship describing the rate of horizontal radial eddy diffusivity, K_{hr}, as a function of patch diameter, l. For patch length scales between 100 and 1000 m the relationship is $K_{hr} = 7.56 \cdot 10^{-5}\, l^{4/3}$ where $l = 3\sigma_{re}$ (Okubo 1974, Page et al. 2000) and σ_{re} is the standard deviation along the radial axis.

Horizontal Transport and Dispersion

Methods

In order to follow the temporal evolution of dye patches as they were transported and dispersed, the outline or perimeter of the patch was estimated by tracing the edge of the patch that was visible from the surface with a small boat that recorded its position at 10 second intervals with a hand held GPS unit. The patch outlines at several time intervals are shown in the figures below for several sites and releases. In general the patch shapes became roughly elliptic with the long axis being in the direction of the mean flow. The length of the major and minor axes of the patch at various times was estimated from the patch outlines. The patch dimensions were also checked with fluorometry transects run through the patch using fluorometers towed at 1-2 m below the surface. The faster increase in the length of the major axis of the patch relative to that of the minor axis (Figure 14) is consistent with shear dispersion. The vertical distribution of the dye was also measured at various times during the evolution of the patch. These data are present in the next section.

Observations

Site A – 10th, 11th and 17th of August 2010

Three dye releases were conducted at Site A. For all three releases, the site contained only one cage and dye was poured into this cage using a bucket. The cage held a net but no fish since at the time of the dye studies the site was being fallowed.

On the 10th of August 2010, the dye was released on an ebbing tide and the dye plume or patch moved away from and elongated in a direction away from the inter-tidal zone and into the main channel at this area (Figure 14). The tracings of the plumes horizontal outline are shown in Figure 14 along with the trajectories of some surface drifters that have been released into the plume once it had cleared the net-pen. Interestingly the drifters tethered to a sub-surface drogue moved in a direction opposite that of the dye and the surface drifters. This is consistent with the dye remaining near the surface (see section below on the vertical distribution of the dye). The photographs of the plume (Figure 15) show several features that are typical of the plumes observed during all of the releases; the plume became elongated in the direction of the prevailing current, the concentration of the dye within the plume was patchy, the edge of the patch was very ragged and sometimes difficult to detect, and the dye appeared to be just below the sea-surface.

On the 11th of August 2010, the dye was released on an ebbing tide and the dye plume once again evolved into an elongated patch that moved in a direction away from the inter-tidal zone and into the main channel (Figure 16). This time both the near-surface drifters and those tethered to sub-surface drogues moved in the same direction as the dye patch.

On the 17th of August 2010, the dye was released on a flooding tide and the dye plume or patch elongated and moved away from the release location in a direction toward the inter-tidal zone and eventually into the inter-tidal area (Figure 17).

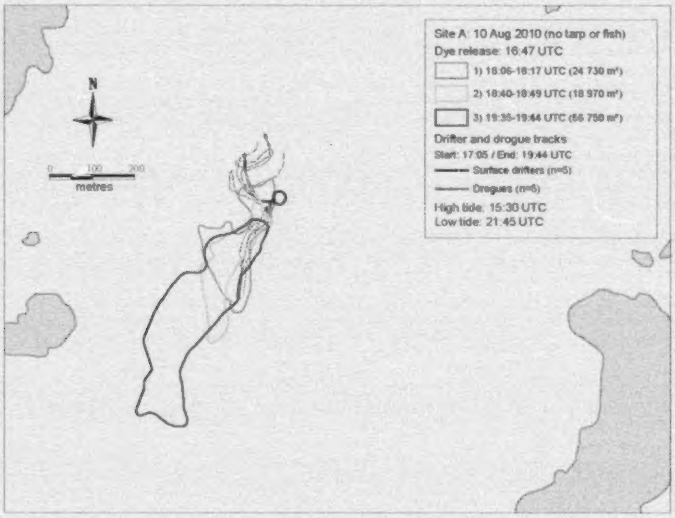
N
0
100
200
metres
Site A: 10 Aug 2010 (no tarp or fish)
Dye release: 16:47 UTC
1) 18:06-18:17 UTC (24 730 m²)
2) 18:40-18:49 UTC (18 970 m²)
3) 19:35-19:44 UTC (56 750 m²)
Drifter and drogue tracks
Start: 17:05 / End: 19:44 UTC
Surface drifters (n=5)
Drogues (n=5)
High tide: 15:30 UTC
Low tide: 21:45 UTC

Figure 14. Map showing the outlines of dye patches (coloured polygons), surface and drogued drifter trajectories (broken lines) and the location of the release cage (circle) for the 10th of August 2010 dye release at Site A. These outlines correspond with the dye plumes shown in Figure 15.

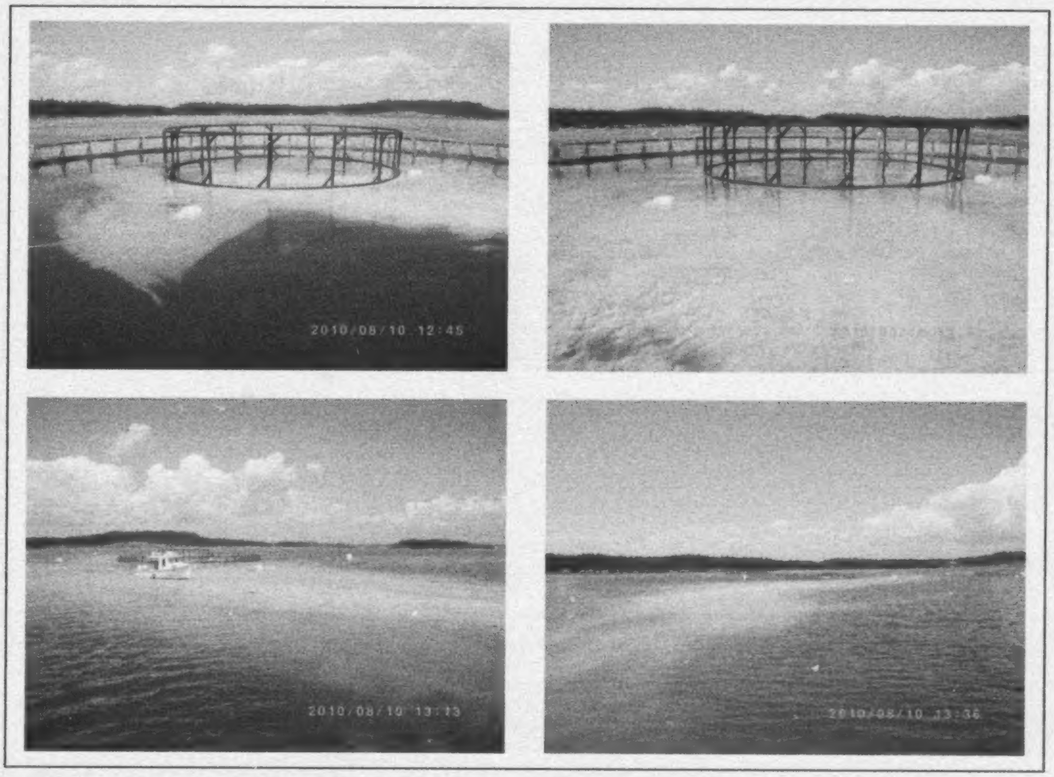
2010/08/10 12:45
2010/08/10 13:13
2010/08/10 13:36

Figure 15. Pictures showing the evolution of the dye plume resulting from a dye release from Site A on the 10th of August 2010.

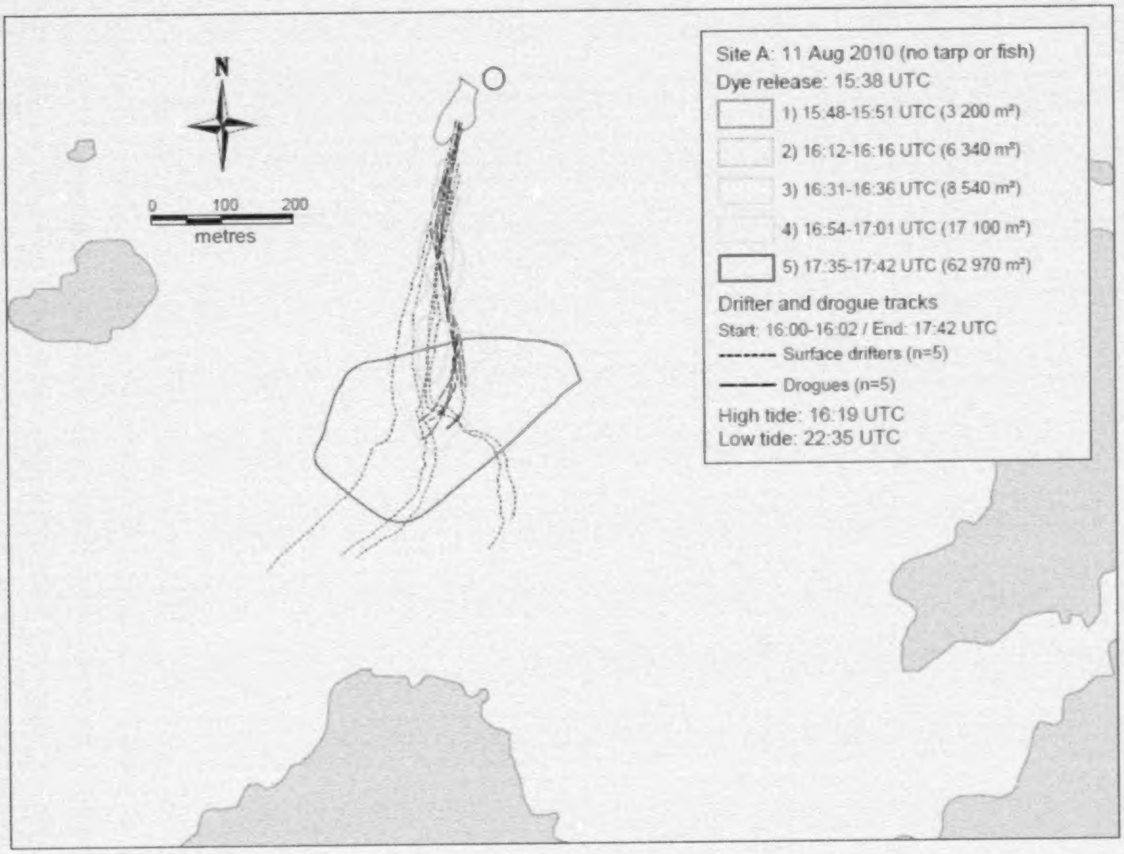
N
0
100
200
metres
Site A: 11 Aug 2010 (no tarp or fish)
Dye release: 15:38 UTC
1) 15:48-15:51 UTC (3 200 m²)
2) 16:12-16:16 UTC (6 340 m²)
3) 16:31-16:36 UTC (8 540 m²)
4) 16:54-17:01 UTC (17 100 m²)
5) 17:35-17:42 UTC (62 970 m²)
Drifter and drogue tracks
Start: 16:00-16:02 / End: 17:42 UTC
Surface drifters (n=5)
Drogues (n=5)
High tide: 16:19 UTC
Low tide: 22:35 UTC

Figure 16. Map showing the outlines of dye patches (coloured polygons), surface and drogued drifter trajectories (broken lines) and the location of the release cage (circle) for the 11th of August 2010 dye release at Site A.

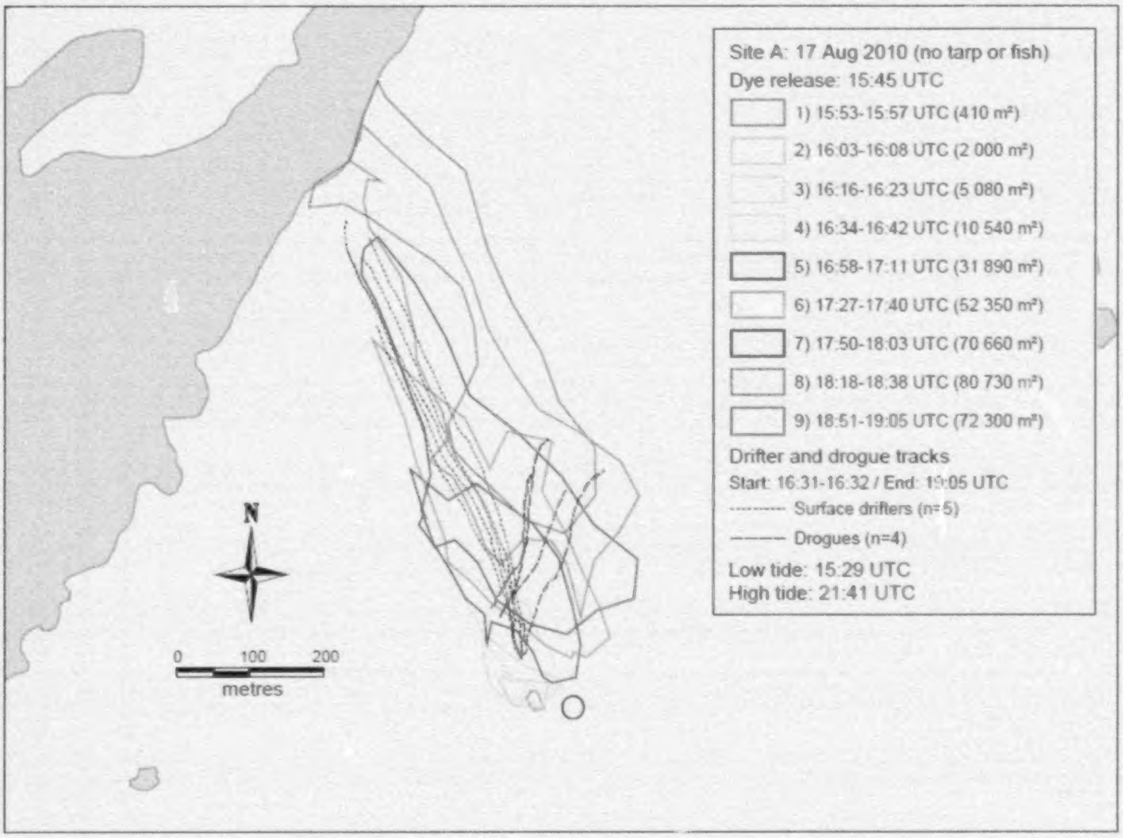
Site A: 17 Aug 2010 (no tarp or fish)
Dye release: 15:45 UTC
1) 15:53-15:57 UTC (410 m²)
2) 16:03-16:08 UTC (2 000 m²)
3) 16:16-16:23 UTC (5 080 m²)
4) 16:34-16:42 UTC (10 540 m²)
5) 16:58-17:11 UTC (31 890 m²)
6) 17:27-17:40 UTC (52 350 m²)
7) 17:50-18:03 UTC (70 660 m²)
8) 18:18-18:38 UTC (80 730 m²)
9) 18:51-19:05 UTC (72 300 m²)
Drifter and drogue tracks
Start: 16:31-16:32 / End: 19:05 UTC
Surface drifters (n=5)
Drogues (n=4)
Low tide: 15:29 UTC
High tide: 21:41 UTC
N
0
100
200
metres

Figure 17. Map showing the outlines of dye patches (coloured polygons), surface and drogued drifter trajectories (broken lines) and the location of the release cage (circle) for the 17th of August 2010 dye release at Site A.

Site B – 8th, 10th and 14th of September 2010

Three dye releases were conducted at Site B. For all three releases the site contained a full array of fish cages and they were all stocked with fish. For each bath treatment a cage was tarped and dye and therapeutant were mixed and added to the bath water.

On the 8th of September 2010, the dye was released on an ebbing tide and the dye plume or patch moved away from and elongated in a westerly direction parallel to the coastline (Figure 18). The drifters moved in a direction and magnitude that was consistent with the movement of the dye patch.

On the 10th of September 2010, the dye was released on an ebbing tide and the dye plume or patch once again moved away from and elongated in a westerly direction parallel to the coastline (Figure 19). The drifters moved in a direction and magnitude that was generally consistent with the movement of the dye patch, although they moved a bit closer to shore than the dye. This was consistent with there being a weak onshore breeze at the time of the study.

On the 14th of September 2010, the dye was released on a flooding tide and the dye plume or patch moved away from and elongated in a northerly direction away from the coastline (Figure 20). Once again the drifters moved in a direction that was generally consistent with the movement of the dye patch.

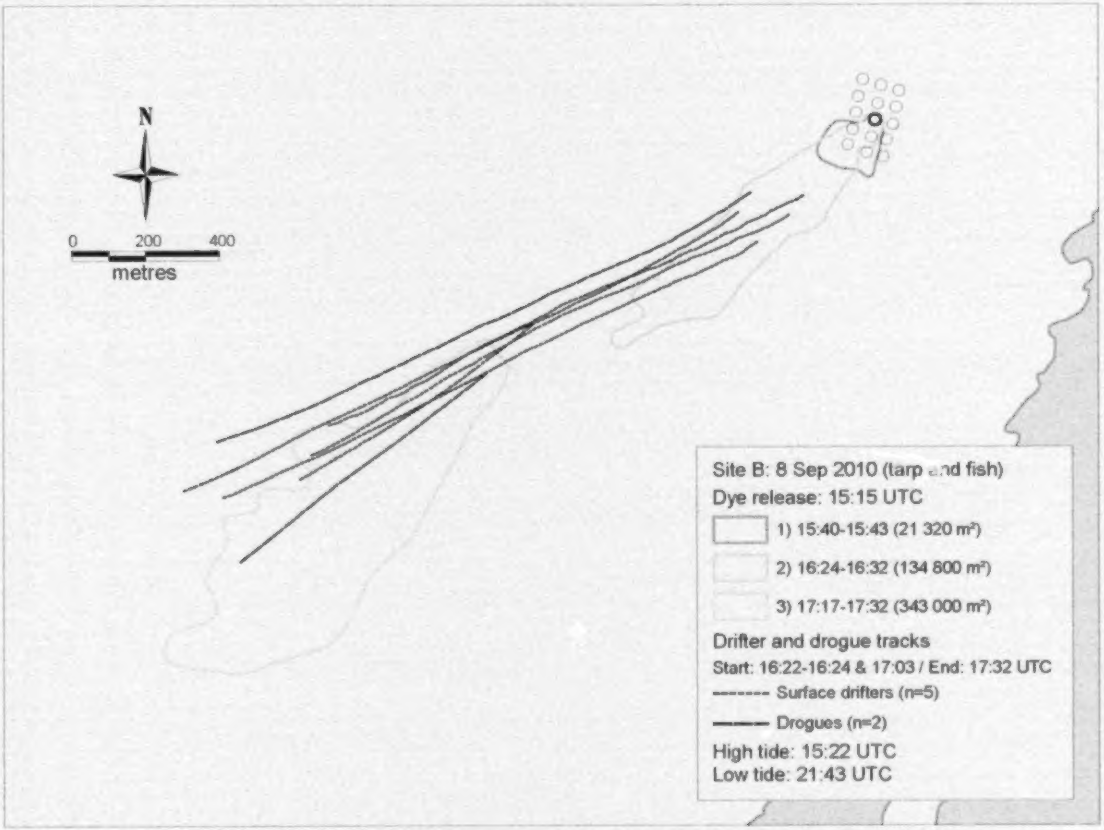
N
0
200
400
metres
Site B: 8 Sep 2010 (tarp and fish)
Dye release: 15:15 UTC
1) 15:40-15:43 (21 320 m²)
2) 16:24-16:32 (134 800 m²)
3) 17:17-17:32 (343 000 m²)
Drifter and drogue tracks
Start: 16:22-16:24 & 17:03 / End: 17:32 UTC
------- Surface drifters (n=5)
——— Drogues (n=2)
High tide: 15:22 UTC
Low tide: 21:43 UTC

Figure 18. Map showing the outlines of dye patches (coloured polygons), surface and drogued drifter trajectories (broken lines) and the location of the release cage (circle) for the 8th of September 2010 dye release at Site B.

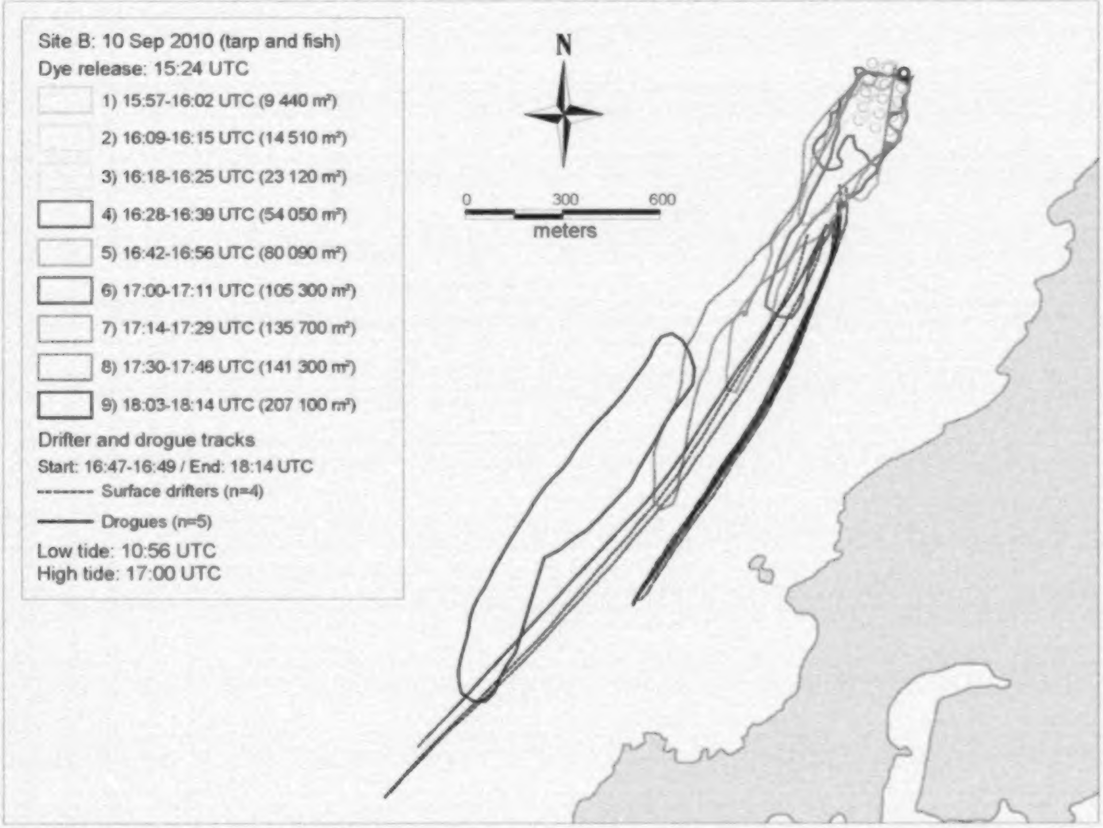
Site B: 10 Sep 2010 (tarp and fish)
Dye release: 15:24 UTC
1) 15:57-16:02 UTC (9 440 m²)
2) 16:09-16:15 UTC (14 510 m²)
3) 16:18-16:25 UTC (23 120 m²)
4) 16:28-16:39 UTC (54 050 m²)
5) 16:42-16:56 UTC (80 090 m²)
6) 17:00-17:11 UTC (105 300 m²)
7) 17:14-17:29 UTC (135 700 m²)
8) 17:30-17:46 UTC (141 300 m²)
9) 18:03-18:14 UTC (207 100 m²)
Drifter and drogue tracks
Start: 16:47-16:49 / End: 18:14 UTC
Surface drifters (n=4)
Drogues (n=5)
Low tide: 10:56 UTC
High tide: 17:00 UTC
N
0
300
600
meters

Figure 19. Map showing the outlines of dye patches (coloured polygons), surface and drogued drifter trajectories (broken lines) and the location of the release cage (circle) for the 10th of September 2010 dye release at Site B.

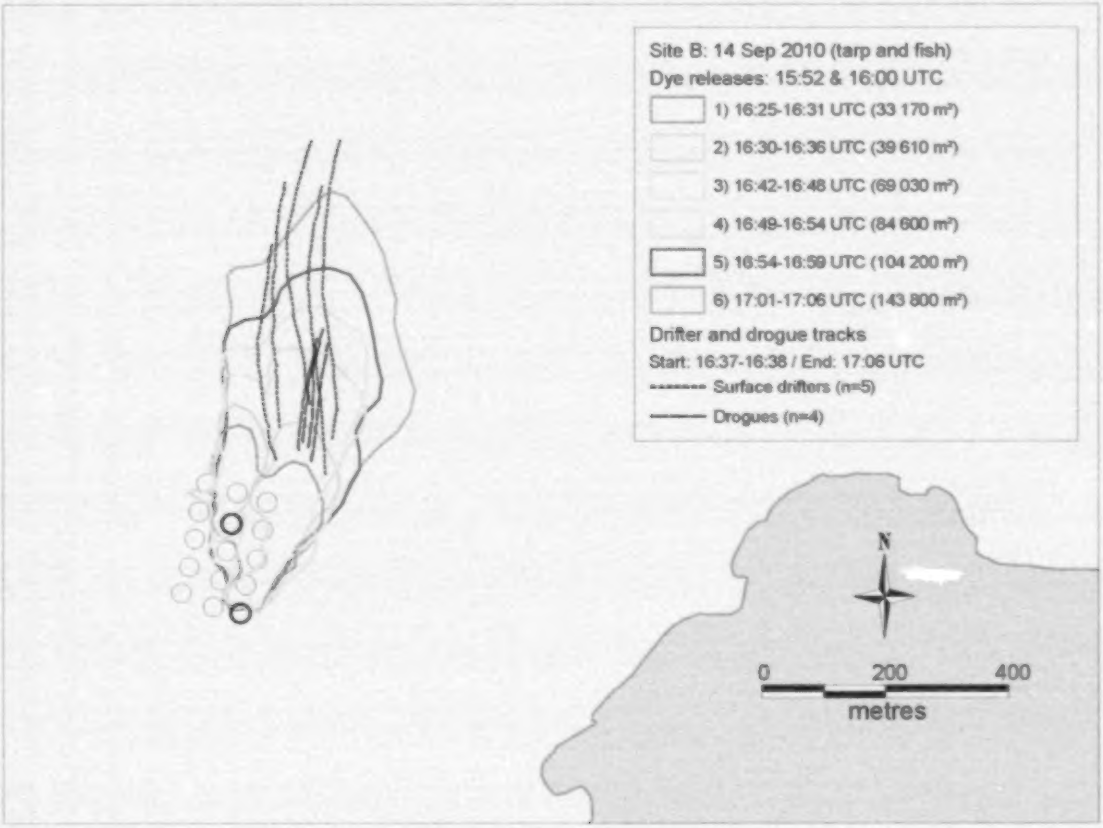
Site B: 14 Sep 2010 (tarp and fish)
Dye releases: 15:52 & 16:00 UTC
1) 16:25-16:31 UTC (33 170 m²)
2) 16:30-16:36 UTC (39 610 m²)
3) 16:42-16:48 UTC (69 030 m²)
4) 16:49-16:54 UTC (84 600 m²)
5) 16:54-16:59 UTC (104 200 m²)
6) 17:01-17:06 UTC (143 800 m²)
Drifter and drogue tracks
Start: 16:37-16:38 / End: 17:06 UTC
------- Surface drifters (n=5)
—— Drogues (n=4)
N
0
200
400
metres

Figure 20. Map showing the outlines of dye patches (coloured polygons), surface and drogued drifter trajectories (broken lines) and the location of the release cage (circle) for the 14th of September 2010 dye release at Site B.

Site C – 27th of October 2010

One dye release was conducted at Site C. The site was located in a narrow channel and contained a single string of fish cages that were stocked with fish. For the bath treatment a single cage was tarped and dye and therapeutant (Alphamax®) were mixed and added to the bath water. The dye was released on a flooding tide and the dye plume or patch moved away from and elongated in a north-westerly direction along the middle of the channel (Figure 21). The drifters moved in a direction and magnitude that was consistent with the movement of the dye patch. During the observed drift period, the dye patch encountered an adjacent fish farm at which point the dye patch went around and through the farm (Figure 21).

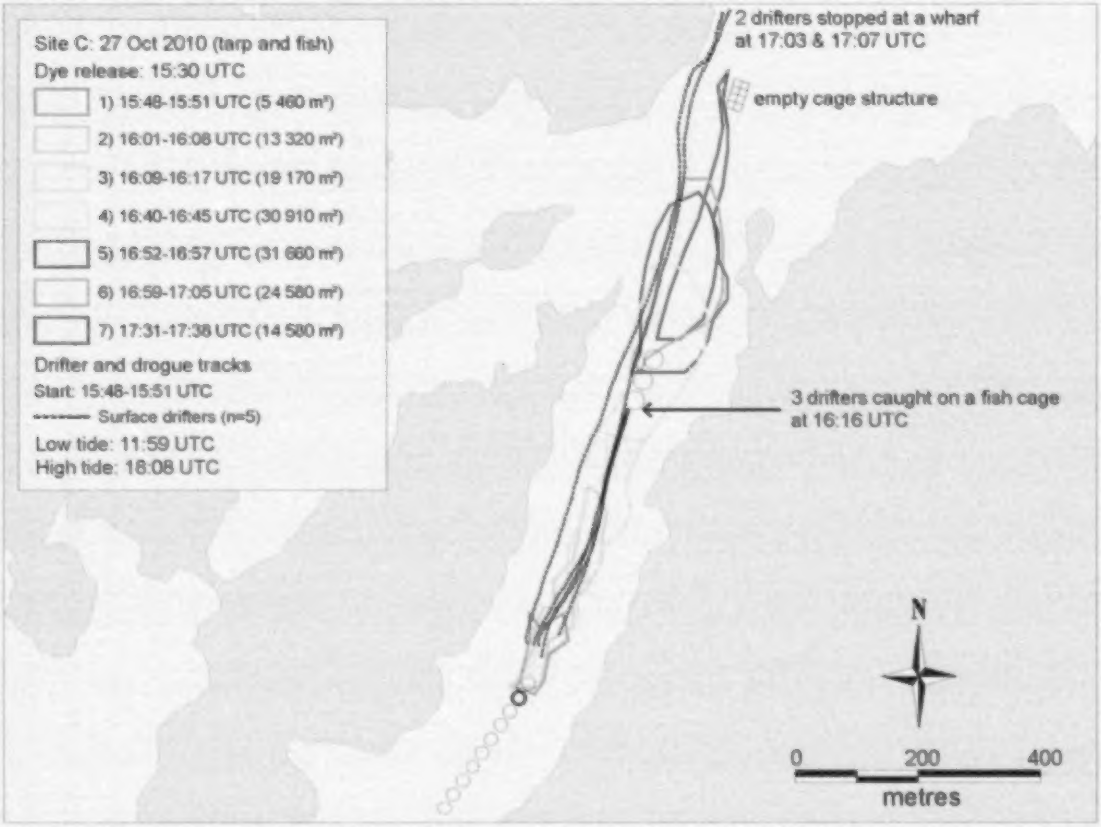
Site C: 27 Oct 2010 (tarp and fish)
Dye release: 15:30 UTC
1) 15:48-15:51 UTC (5 460 m^2)
2) 16:01-16:08 UTC (13 320 m^2)
3) 16:09-16:17 UTC (19 170 m^2)
4) 16:40-16:45 UTC (30 910 m^2)
5) 16:52-16:57 UTC (31 660 m^2)
6) 16:59-17:05 UTC (24 580 m^2)
7) 17:31-17:38 UTC (14 580 m^2)
Drifter and drogue tracks
Start: 15:48-15:51 UTC
Surface drifters (n=5)
Low tide: 11:59 UTC
High tide: 18:08 UTC
2 drifters stopped at a wharf at 17:03 & 17:07 UTC
empty cage structure
3 drifters caught on a fish cage at 16:16 UTC
N
0
200
400
metres

Figure 21. Map showing the outlines of dye patches (coloured polygons), surface and drogued drifter trajectories (broken lines) and the location of the release cage (circle) for the 27th of October 2010 dye release at Site C.

Horizontal Distance Travelled

Tidal current speeds in the southwest New Brunswick area vary with the phase of the tide. In the vicinity of fish farms, the current speeds typically range from 0 to 0.5 m/s (equivalent to one knot). However, in a few locations current speeds may at times be on the order of 1.0 m/s (equivalent to 2 knots). Therapeutant treatments are usually not conducted at times of strong current since the current makes it difficult to deploy the tarpaulin and to keep the tarpaulin from bagging and trapping the fish in a small volume of water. Hence, most tarp treatments are conducted near slack tide when the currents are of order 0.1 m/s (Table 3).

The distance travelled by a patch of chemical released into the water can be estimated as the product of speed and time. A patch would travel from 0 to 3.6 km in one hour and 0 to 11 km in three hours if the current speeds remained constant over these time periods (Table 4). Since the current speeds do not remain constant over time and space, the above distances may overestimate the potential distances that therapeutant patches will travel. The center of mass of patches of dye released from fish farms in southwest New Brunswick shows that patches move a few hundred meters during the first hour after release and several hundred to order one kilometer after two hours (Figure 22). This slow rate of advection is consistent with therapeutant treatments being conducted during period of weak currents. The variation in the distances travelled over the longer time periods is due to variations in the ambient currents and a reflection of an increase in the tidal current speed after the treatments were conducted.

Table 4. Distance traveled over time durations of 1 and 3 hours.

Water Current Speed (m/s)		Distance Travelled (km)	
(m/s)	(knots)	in 1h	in 3 h
0.0	0.0	0.0	0.0
0.1	0.2	0.4	1.1
0.2	0.4	0.7	2.2
0.3	0.6	1.1	3.2
0.4	0.8	1.4	4.3
0.5	1	1.8	5.4
0.6	1.2	2.2	6.5
1.0	2.0	3.6	10.8

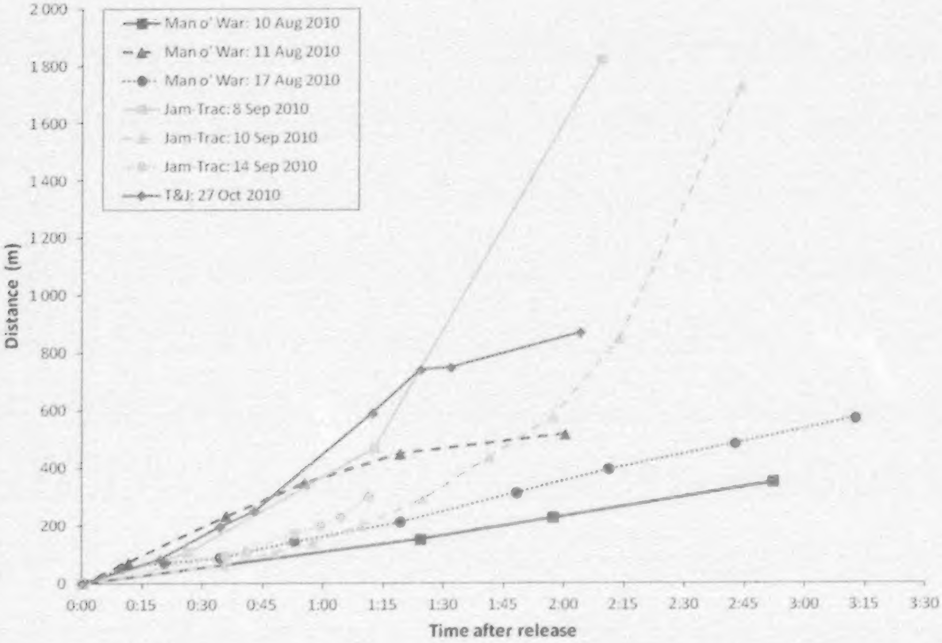

Figure 22. The distance of dye patch centers from the treatment cage vs. time after dye release.

Horizontal Observations and Estimated Rates of Eddy Diffusivity

The rates of horizontal dispersion were estimated from the perimeters of dye plumes generated from the releases. For each plume perimeter, the length of the major (x) and minor (y) axes were estimated by using MapInfo software. The corresponding standard deviations were estimated as $\sigma_x = L_x/4$ and $\sigma_y = L_y/4$. Estimates of the horizontal eddy diffusivities were estimated by assuming $K_x = \partial\sigma_x^2/2\partial t$ and $K_y = \partial\sigma_y^2/2\partial t$. The rates of change in the variance with time were estimated from the slope of a linear regression line relating the variances to the time elapsed since release (Figure 23).

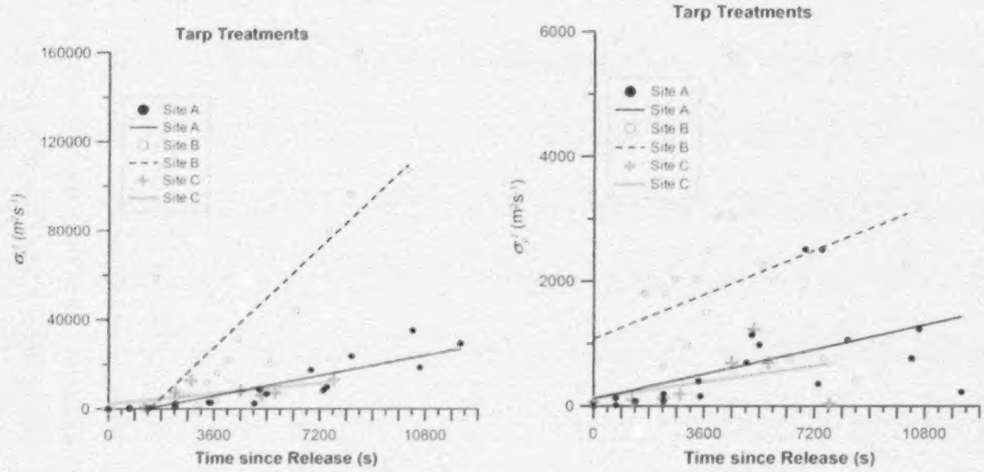

Figure 23. Temporal variation in the variance of dye plumes for tarp treatments. The left/ panel shows the variances along the major axes of the dye plumes. The right panel shows the variances along the minor axes of the dye plumes.

The resulting estimates of horizontal eddy diffusivities are given in Table 5. The release specific horizontal eddy diffusivities along the major axes of the dye plumes, i.e., K_x, ranged from 0.65 to 7.60 m^2/s (Table 5). When the data from all releases at a site were combined the site specific estimates ranged from 0.65 to 6.21 m^2/s (Table 5). In contrast, the release specific horizontal eddy diffusivities along the minor axes of the dye plumes, i.e., K_y, ranged from 0.04 to 0.48 m^2/s (Table 5). When the data from all releases at a site were combined the site specific estimates ranged from 0.04 to 0.10 m^2/s (Table 5). The variances along the minor plume axes were more variable than along the major axes and the K_y values were an order of magnitude less than the K_x values. Both the K_x and K_y rates varied between sites. The values derived for Site B, the more exposed site, were larger than those at the more sheltered Sites A and C; with the values at these sites being quite similar. Although removing apparent outliers and the first 1-3 data points from the calculations made changes to the eddy diffusivity estimates, it did not change the relative order of magnitude of the estimates (Table 5).

Table 5. Summary of horizontal eddy diffusivities estimated from dye releases conducted in southwest New Brunswick during 2010-11. The values were estimated from the lengths of the major and minor axes of each plume perimeter and the associated times since release. The single value for each site was estimated from the composite of all data for the site.

Treatment Method	Site	K_x (m^2/s)		K_y (m^2/s)		K_r (m^2/s)	
None	Site A	0.83	1.26	0.05	0.05	0.41	0.46
None	Site A	0.57		0.15		0.59	
None	Site A	1.55		0.14		0.44	
Tarp	Site B	5.47 (6.21)^{1}	6.21 (7.46)^{3}	0.32	0.10 (0.05)^{3}	2.72	
Tarp	Site B	7.60 (11.03)^{2}		0.04 (-0.06)^{2}		1.40	1.47
Tarp	Site B	3.14 (5.86)^{2}		0.48 (0.71)^{2}		2.47	
Tarp	Site C	0.65 (0.15)^{2}	0.65 (0.15)^{3}	0.04 (0.02)^{2}	0.04 (0.02)^{3}	0.22	0.22

[1] outlier removed from calculation

[2] initial 1-3 data points removed from calculation to account for dye still being influenced by being largely within the treatment cage

[3] outliers and initial 1-3 data points removed

Estimates of Okubo's (1971,1974) apparent horizontal radial eddy diffusivity (K_r) are also given in Table 5. These have been estimated using two approaches. The first approach assumes $\sigma_r^2 = 2\sigma_x\sigma_y$ and $K_r = 0.5\partial(\sigma_r^2)/\partial t$ (Okubo 1971, 1974, Bowden 1983, Lewis 1997). The second calculates the radial variance from the surface area of the patch as $\sigma_r = l_c/3$ (Okubo 1971, 1974). In this approach the length scale (l_c) is the diameter of a circle that has the same area (A) as the observed patch; i.e., $l_c = 2\sqrt{(A/\pi)}$. The length scale is divided by three since 95% of the material is within three radial standard deviations of a radial Gaussian distribution.

Summary of Net-Pen Horizontal Aspects

There was considerable variation in the shape of the observed dye plumes. However, in general the shapes evolved in a manner that was consistent with general expectations of plume dynamic behaviour in the marine environment; i.e., the observed patches of dye were roughly elliptical with the long, or major axis, of the plumes being in the direction of the mean flow and, in general, the plumes were advected parallel to the coastline, although in some cases they were advected perpendicular to the coastline. The length of the major axis increased over time at a greater rate than that of the minor axis. This is consistent with shear induced dispersion. The estimated rates of horizontal diffusivity, K_x and K_y, were consistent with literature values with K_x being in the order of 1 to 10 m^2/s and K_y being in the order of 0.1 to 1 m^2/s. The estimated rates of the Okubo radial diffusivity were for the most part in the order of 1 m^2/s.

Surface drifters deployed within the dye plumes moved in a direction and at a rate that was consistent with the movement of the dye patches.

Vertical Distribution and Mixing

Background

The depth to which therapeutant is mixed depends upon the vertical velocity of the water in the area of release, the density of the solution being released and the rate of vertical mixing in the area of release. For the purposes described in this report, it is assumed the density of the solution being released is the same as the ambient seawater and that there are no vertical water velocities of consequence. Under these assumptions the vertical distance travelled depends upon the rate of vertical eddy diffusivity and the amount of time needed for a solution to vertically mix throughout a depth of h is estimated as $t_v = 0.32h^2/K_z$ where t_v is the vertical mixing time scale (Lewis 1997). At this time, the vertical standard deviation is approximately equal to $\sigma_z \approx 0.8h$.

Assuming a typical rate of vertical eddy diffusivity for vertically well-mixed conditions, i.e., K_z equal to 0.01 m^2/s (Lewis 1997), and a range of water depths, results in the time to mix vertically range from 1 to 32 h (Table 6). Fish farms in the Bay of Fundy are typically in waters with a depth of about 20 m, so for the time scale for the therapeutant to become vertically well mixed is 4 h. However, if we assume the mixing rates may be an order of magnitude stronger due to winds on a particular day or to strong tidal currents, such as those that exist in some areas of the Bay of Fundy, the time to mix vertically may be reduced to less than one hour (Table 6). In either case, the implication is that there is potential for organisms living on the seabed to be exposed to therapeutants that persist in the water for time periods of minutes to hours.

Table 6. Estimated order of magnitude time scales for vertical mixing over a range of depths when K_z has values of 0.01 m^2/s and 0.1 m^2/s.

Water Depth or Depth of Mixed Layer (m)	Time Scale (h) to become well mixed over the depth range when $K_z = 0.01$ m^2/s	Time Scale (h) to become well mixed over the depth range when $K_z = 0.1$ m^2/s
10	1	0.1 (5 min)
20	4	0.4 (21 min)
30	8	0.8 (48 min)
40	14	1.4 (85 min)
50	22	2.2 (133 min)
60	32	3.2 (192 min)

Methods

In order to empirically investigate the vertical distribution and mixing of the therapeutant released from the net-pens, the vertical distribution of dye was measured during many of the dye releases described above. The profiles were obtained over a several hour period at multiple locations inside each temporally evolving dye plume. A summary of the studies where vertical profiles were taken can be found in Table 7. The table contains information such as: the number of vertical profiles collected and number of profiles in the plume, the time elapsed between the release of the dye and the time at which the profiles were taken, the maximum depth estimated from each profile as the depth below which dye concentrations were measured as zero.

The method of vertical profiling consisted of attaching one of two Cyclops fluorometer sensors to a weighted line and gradually lowering the instruments in increments of 1 m, through the water column to a depth at which dye was no longer detected or the end of the cable. A time and location was recorded for each profile. In some instances, the location of the profile may have varied by several meters during profile collection due to vessel drift. When two fluorometers were attached to the same line, they were attached 0.5 m or 1 m apart. Hence, some profiles began at a depth of 0.5 m or 1 m rather than 0 m. The profile recorded by each instrument has been treated as a separate profile.

Vertical profiles of water conductivity (salinity), temperature and density were also collected in the study area, using a Sea-Bird SBE25 Sealogger CTD.

Three dye releases were conducted at Site A. For all three releases the site contained only one cage and dye was poured into this cage using a bucket. The cage held a net but no fish since at the time of the dye studies the site was being fallowed.

Table 7. Summary of data associated with vertical dye concentration profiles obtained during dye releases conducted from salmon net-pen therapeutant treatments conducted in southwest Brunswick during 2010-11. Descriptions of the contents of the columns occur in the text.

Treatment Method	Site Date	Number of Vertical Profiles In the Plume (Total Number)	Range of times elapsed since the beginning of the release (min)	Range of Maximum Depths at which Dye was detected (m)	Comments
None	Site A 10 Aug 2010	3 (3)	110 - 135	3 – 6	Sunny
None	Site A 11 Aug 2010	14 (16)	21 - 65	2 - 10	Sunny
None	Site A 17 Aug 2010	20 (22)	18 - 240	1 - 4	Sunny
Tarp	Site B 8 Sept 2010	4 (8)	34 - 80	6 - 9	Cloudy
Tarp	Site B 10 Sept 2010	10 (11)	13 - 130	6 - 12	Cloudy
Tarp	Site B 14 Sept 2010	14 (14)	54 - 187	5 - 12	Cloudy
Tarp	Site F 13 Oct 2010	0	NAP	NA	Sunny
Tarp	Site C 27 Oct 2010	12 (17)	9 - 150	6 – 18	Cloudy
Skirt	Site B 22 Sept 2010	31 (32)	0 - 75	6	Cloudy
Skirt	Site J 6 Oct 2010	21 (23)	NAP1	6 – 18	Sunny

NAP = Not applicable

[1] All but one of the vertical profiles were taken during the treatment before release.

Observations

Site A – 10^{th}, 11^{th} and 17^{th} of August 2010

Forty one vertical profiles of dye concentration were collected from Site A during three dye releases; one release was conducted on each of the 10th, 11th and 17th of August 2010. Four of these profiles did not detect any dye. The vertical profiles where dye was detected are shown in Figure 24. Maximum depths that dye was detected at Site A ranged from 5 to 11 m below the sea surface, compared to an average site depth at mean low tide of 16 m. There are no CTD data available for this site.

The profiles obtained on the 10th of August 2010 indicate that the highest concentrations of the dye were at the sea surface. The concentrations decreased with depth and no dye was detected below 3.5 to 6.5 m. The concentrations also decreased with time. The maximum depth where dye was detected was 7 m below the water's surface. The vertical profiles are consistent with the occurrence of some vertical mixing, as dye was added to the surface of the water column, and mixed down to three meters over a timespan of two hours.

The profiles obtained on the 11th of August 2010 indicate that the highest concentrations of the dye were below the sea surface. No dye was detected below 6 m with the exception of one set of down and up profiles that detected dye to a depth of about 11 m. The variation in vertical profile characteristics is illustrated by the 16:40 and 16:43 profiles, the profiles with the pronounced subsurface peaks. These profiles were taken within 3 minutes of each other and the depths of maximum concentration vary from 7 to 4 m, respectively. There was no obvious temporal dependence of the evolution of the depth of the dye plume.

The profiles obtained on the 17th of August 2010 include some that have a maximum concentration at the surface and some that have subsurface maximums. In all cases dye was not detected below 3 to 5 m. On this day, the dye plume travelled toward the shore and reached the inter-tidal zone (see Observations on Horizontal Aspects). Once again there was no consistent temporal pattern in the maximum depth of the dye plume.

Profiles of water temperature, salinity and density were not available for this site.

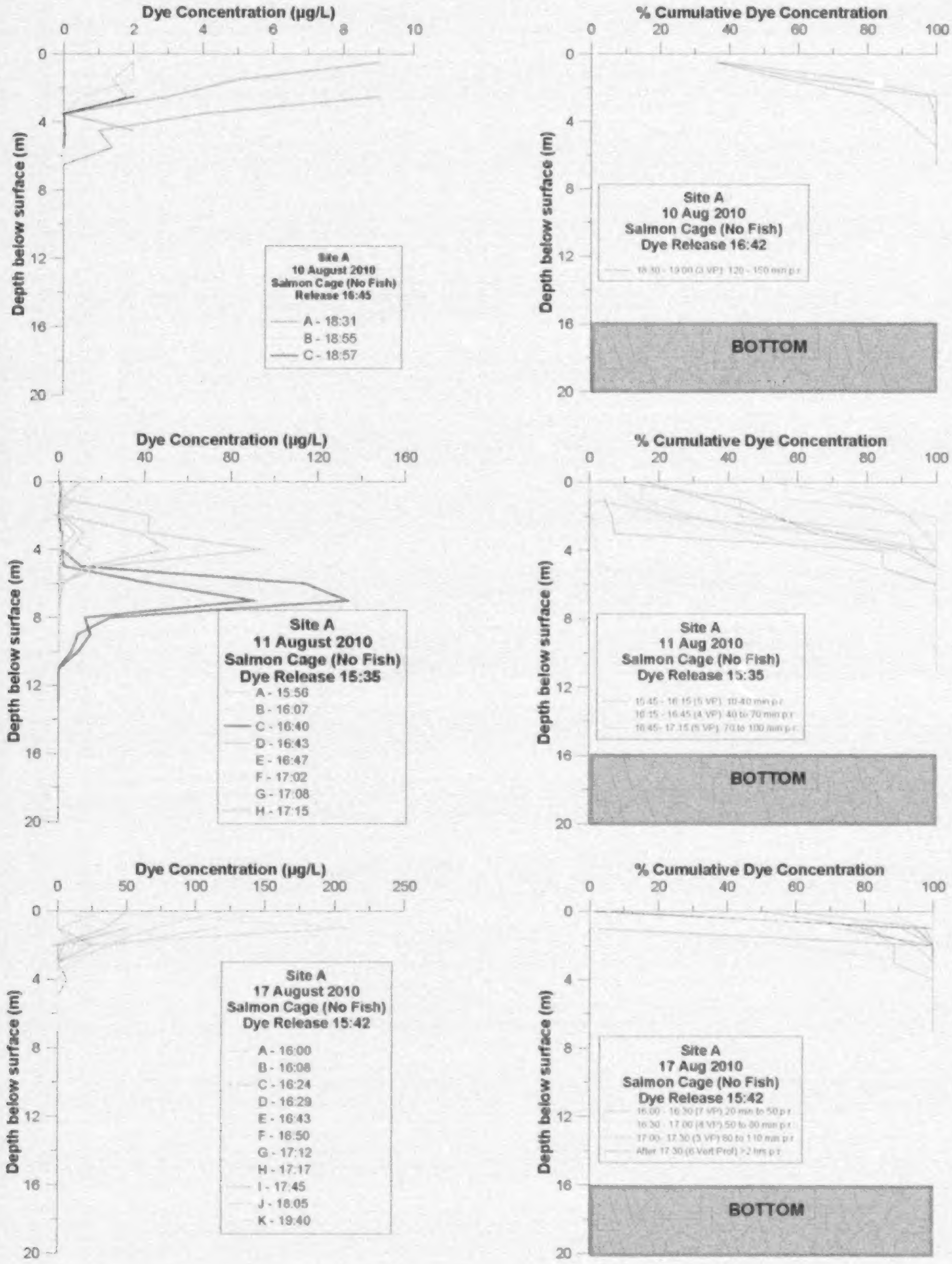

Figure 24. Vertical dye concentration profiles (left panel) and cumulative dye concentration versus depth curves (right panel) associated with dye releases conducted at Site A. The average site depth at mean low tide is 16.2 m. VP = Vertical Profile; p.r. = post release

Site B – 8th, 10th, and 14th of September 2010

Thirty-three vertical profiles of dye concentration were collected from Site B during three dye releases which were conducted on the 8th, 10th and 14th of September 2010. On the 14th of September 2010, two cages were treated simultaneously; dye was added and released from both cages. The dye plumes for the two cages quickly joined to form one plume, hence the two releases on the 14th of September 2010 are considered here together as one release. Five of the profiles collected did not detect any dye. The vertical profiles where dye was detected are shown in Figure 25. Maximum depths at which dye was detected at Site B ranged from 9 to 13 m below the sea surface, compared to an average site depth at mean low tide of 35 m.

One of the two profiles in the plume obtained on the 8th of September 2010 indicates that the highest concentrations of the dye were 2-5 m below the sea surface (profile C). Below 5 m, the concentrations decreased with depth to a maximum depth of around 9 m. The later profile (profile D) did not display any subsurface peaks and was much reduced in concentration. Of the two vertical profiles, dye was measured 2 m deeper during the first profile compared to the profile taken 45 minutes later. Within an hour of the release of the tarp, the depth that dye was detected had roughly doubled from the tarp depth of 4 m to 8 m.

The profiles obtained on the 10th of September 2010 demonstrate variability in the depth of highest concentrations, from the sea surface (profiles B and D) to subsurface peaks between 3 and 5 m depth (profile A), at similar times post release. High variation in the dye detected while the instruments descended and ascended is visible in profile D, with one direction identifying a large surface peak in dye concentrations and the other a much smaller subsurface peak. Below 8 m, the concentrations decreased with depth to a maximum depth of 10 to 13 m. Thirteen minutes after release, dye was recorded to a depth of 9 m. By 40 minutes after tarp release, dye was detected at 12 m.

The profiles obtained on the 14th of September 2010 indicate that initially the highest concentrations of the dye were between 0 and 2 m (profiles A and B). Several later profiles detected more uniform concentrations with depth (profiles E and G). The concentrations generally decreased with depth to a maximum depth of 12 to 13 m. Within 4 minutes, maximum concentrations measured in profiles varied fourfold (profile A and B). Overall, the concentrations also decreased with time. On this day, the maximum depths tended to increase through time. The later profiles (100-130 minutes post treatment) were up to 8 m deeper than the profiles collected one hour post release.

There was no distinct surface mixed layer on any of the days, although there was weak density stratification of the water column, with $\Delta\sigma_T$ ranging from 0.2 to 0.4 over 17 to 30 m (Figure 26).

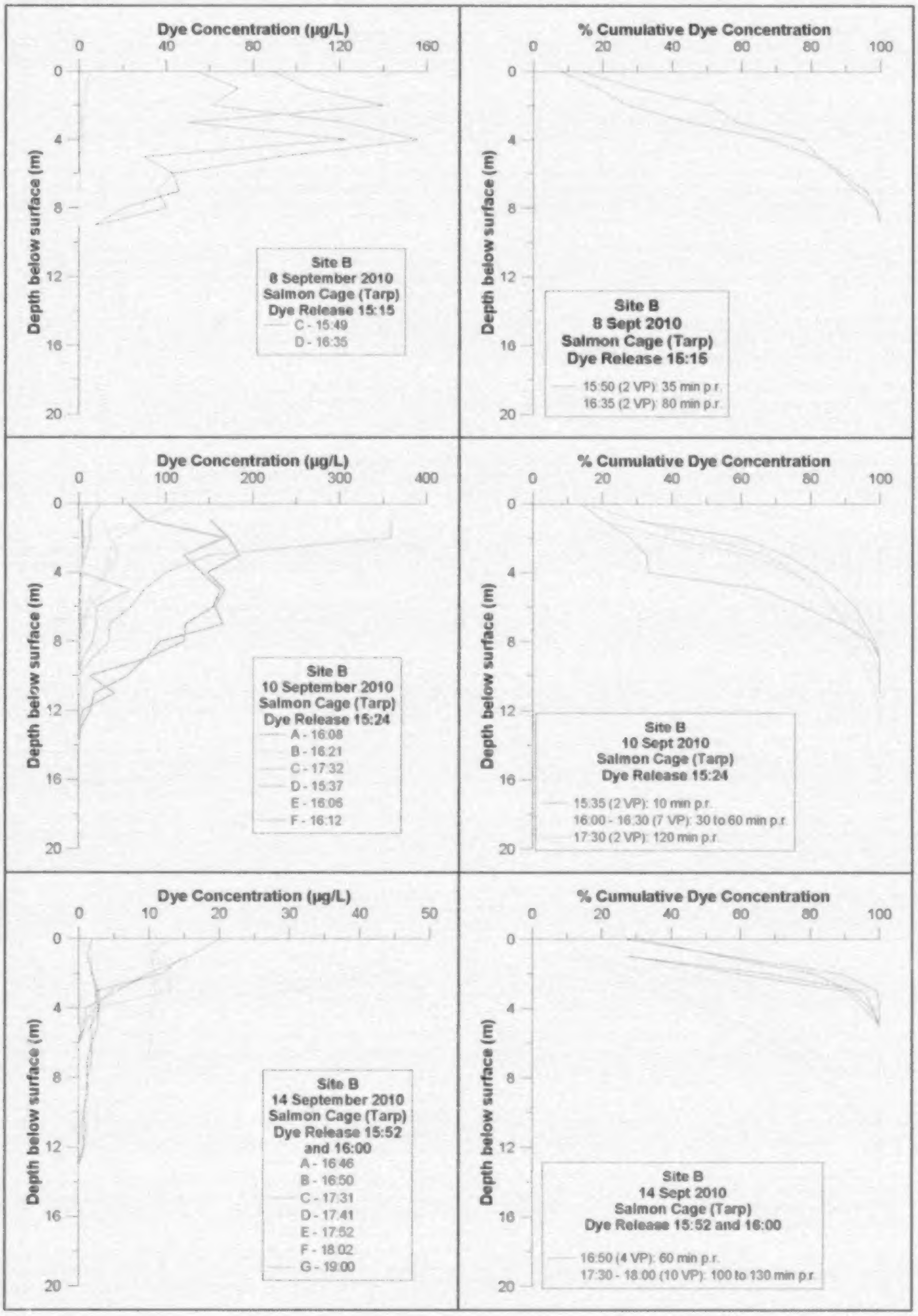

Figure 25. Vertical dye concentration profiles (left panel) and cumulative concentration versus depth curves (right panel) associated with dye releases from tarps conducted at Site B. At Site B, the average site depth at mean low tide was 33.5 m, below the axis of the graph. VP = Vertical Profile. p.r. = post release.

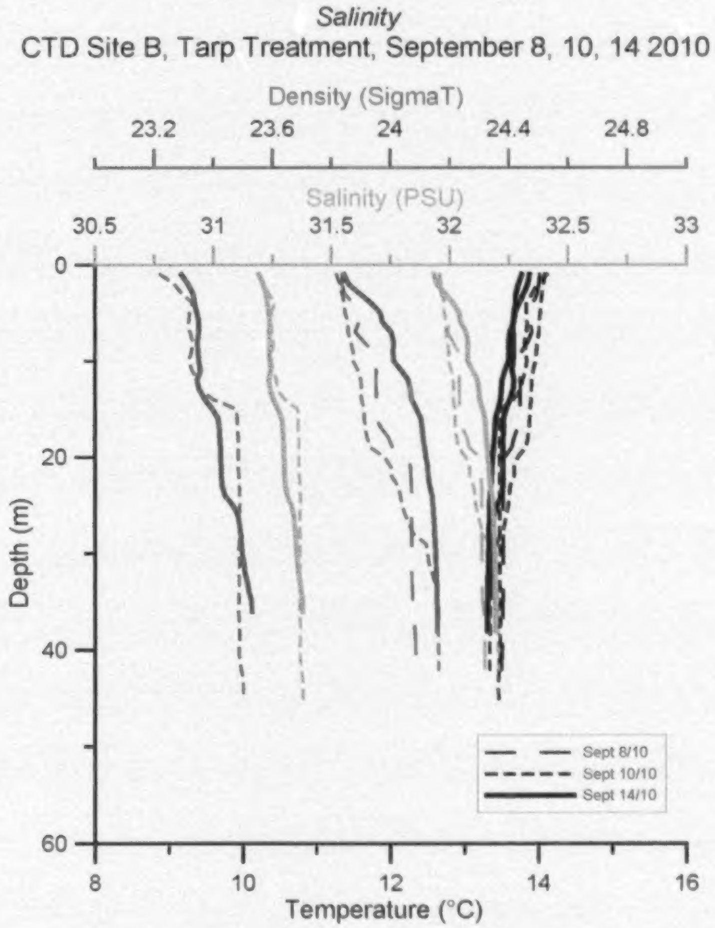

Figure 26. Temperature, salinity and density profiles of the water column collected during tarp dye studies at Site B.

Site C – 27th of October 2010

Seventeen vertical profiles of dye concentration were collected from Site C during a single dye release conducted on the 27th of October 2010. Five of the profiles collected did not detect any dye. The vertical profiles where dye was detected are shown in Figure 27. The maximum depth that dye was detected was 18 m and dye was recorded down to the bottom sediments.

According to the vertical profiles, dye reached depths of 11 m within 15 minutes following tarp removal. The highest concentrations of the dye were detected between 0 - 8 m below the sea surface (profile B). Subsurface peaks were detected between 7 and 11 m (profiles A and P). Below 12 m, the concentrations decreased with depth to a maximum depth of 18 m. Within half an hour of tarp release, dye reached the bottom sediments in several profiles (below 15 m). No temporal pattern in the maximum depth of the dye was distinguishable.

There was weak density stratification of the water column at Site C with a $\Delta\sigma_T$ of 0.2 over 18 m (Figure 28).

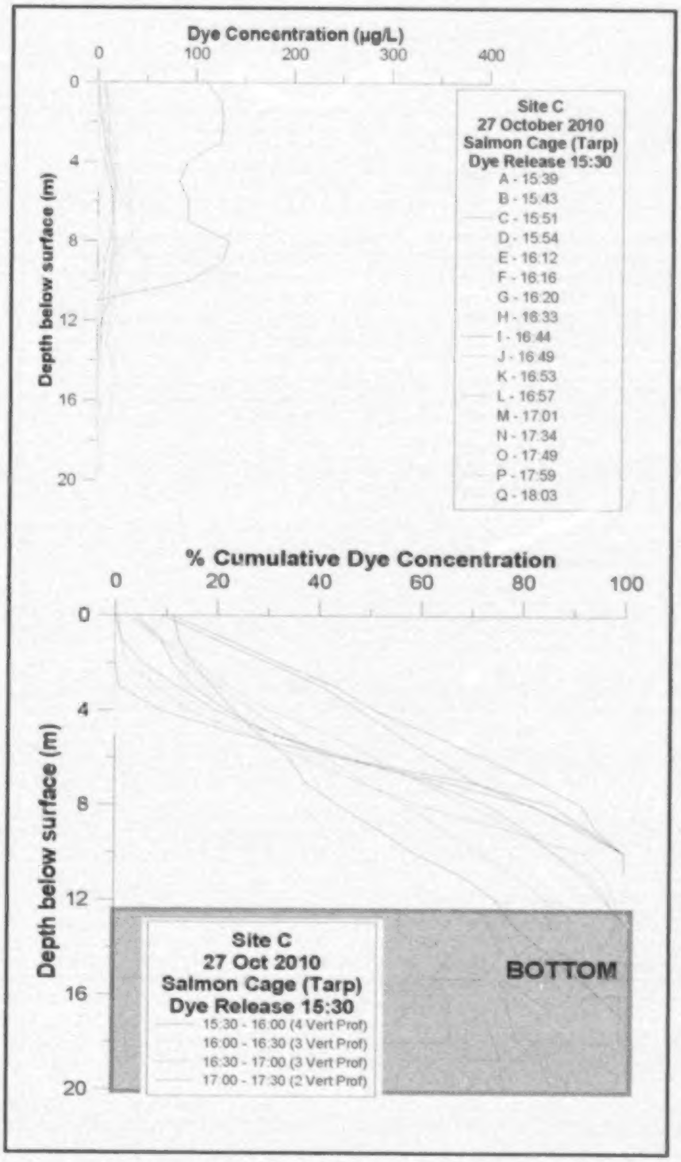

Figure 27. Vertical dye concentration profiles (top panel) and cumulative dye concentration versus depth curves (bottom panel) associated with dye releases conducted at Site C. The average site depth at mean low tide is 12.7 m. VP = Vertical Profile. p.r. = post release.

CTD Site C, Tarp Treatment, October 27 2010

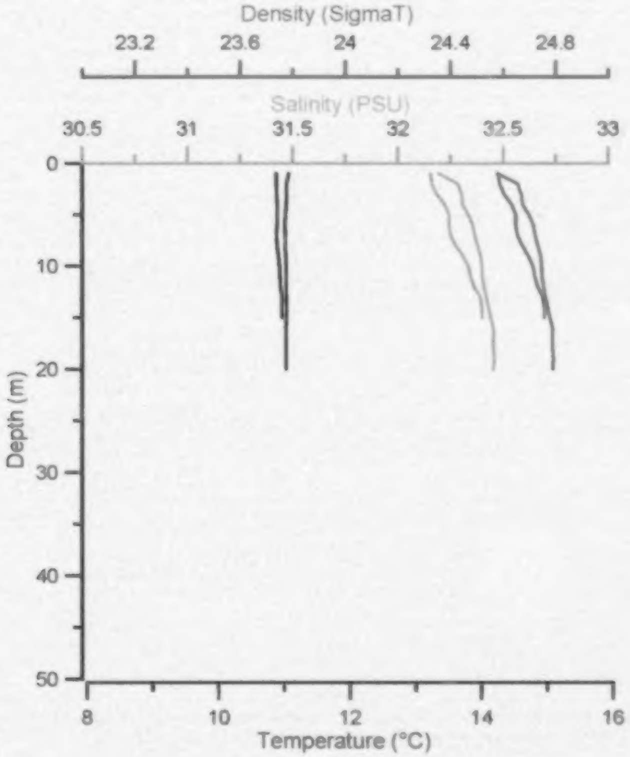

Figure 28. Temperature, salinity and density profiles of the water column collected during tarp dye studies at Site C.

Site J, with use of Skirt – 6th of October 2010

Twenty-three vertical profiles of dye concentration were collected from Site J during a skirt release on the 6th of October 2010. Two of the profiles collected did not detect any dye. The vertical profiles where dye was detected are shown in Figure 29. Dye was detected down to 20 m below the sea surface, compared to an average site depth at mean low tide of 18.3 m.

There was a surface mixed layer from 0-10 m and a pycnocline between 10-16 m with $\Delta\sigma_T$ of 0.4 (Figure 30).

Vertical profiles of dye concentration taken during the treatment at locations between the cage net and the inside of the cage skirt showed the dye descending to depths between eight and 12 meters (Figure 29), while the skirt depth was seven meters. Vertical profiles taken outside of the cage upstream during the treatment detected low concentrations of dye, but profiles taken downstream of the cage recorded up to 20 μg/L of dye (approximately 30-50 % of fluorescence recorded in vertical profiles inside the skirt during treatment) at depths of four to 17 meters (Figure 29). While the skirt was still present, and within 40 minutes from the start of the treatment, dye was mixed down to 17 m.

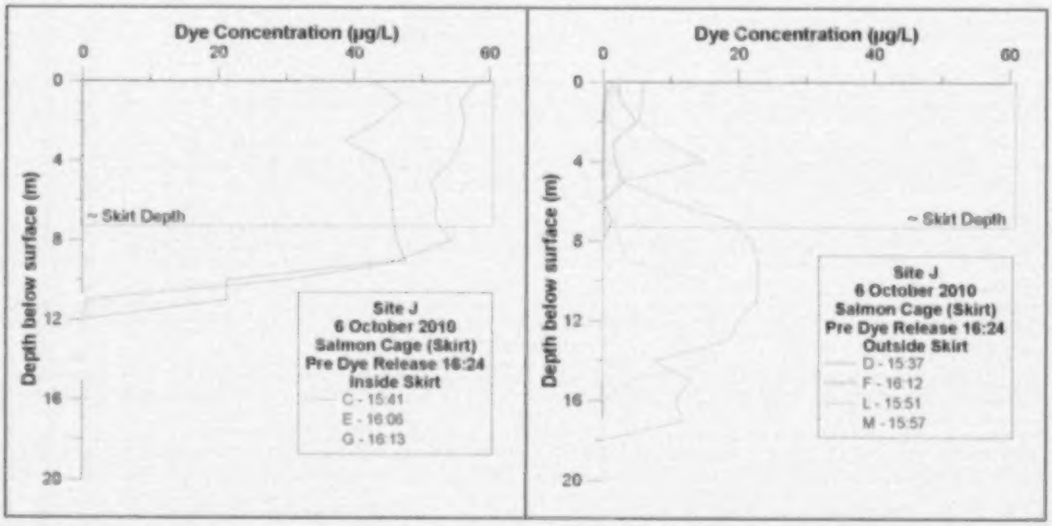

Figure 29. Vertical dye concentration profiles both inside and inside out the skirted treatment cage at Site J. The average site depth at mean low tide is 18.3 m. VP = Vertical Profile. p.r. = post release

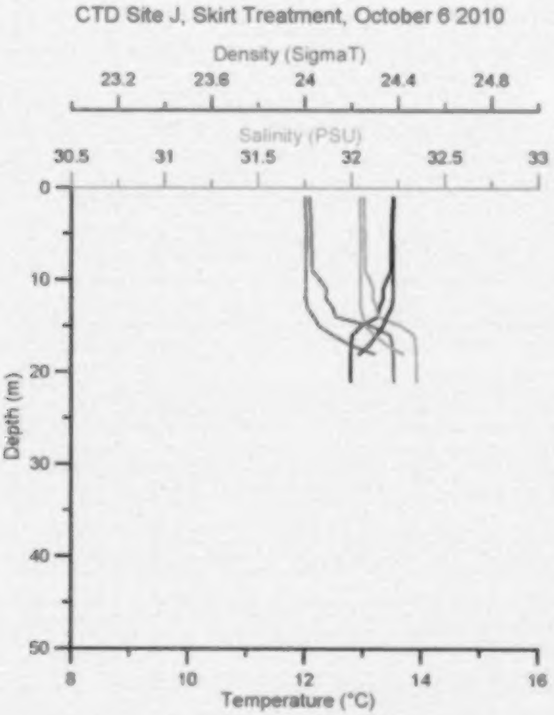

Figure 30. Temperature, salinity and density profiles of the water column collected during a skirt study at Site J.

Site B, with use of Skirt – 22nd of September 2010

Twenty-three vertical profiles of dye concentration were collected from Site B during a dye release from a skirt the 22nd of September 2010. Two the profiles collected did not detect any dye. The vertical profiles where dye was detected are shown in Figure 31. Dye was detected down to 18 m below the sea surface, compared to an average site depth at mean low tide of 35.3 m.

During the treatment, inside the skirt the dye was mostly confined to the upper 6 m of the water column (Figure 31). Outside the skirt, low concentrations of dye were detected over a similar depth range. After the skirt was released, initially dye was still detected over the top 6 m over the water column, but by one and a half hours post release, dye was detected to depths of 18 m. This is consistent with the occurrence of some vertical mixing.

There was little density stratification of the water column, with $\Delta\sigma_T$ of 0.4 over 20 m (Figure 32).

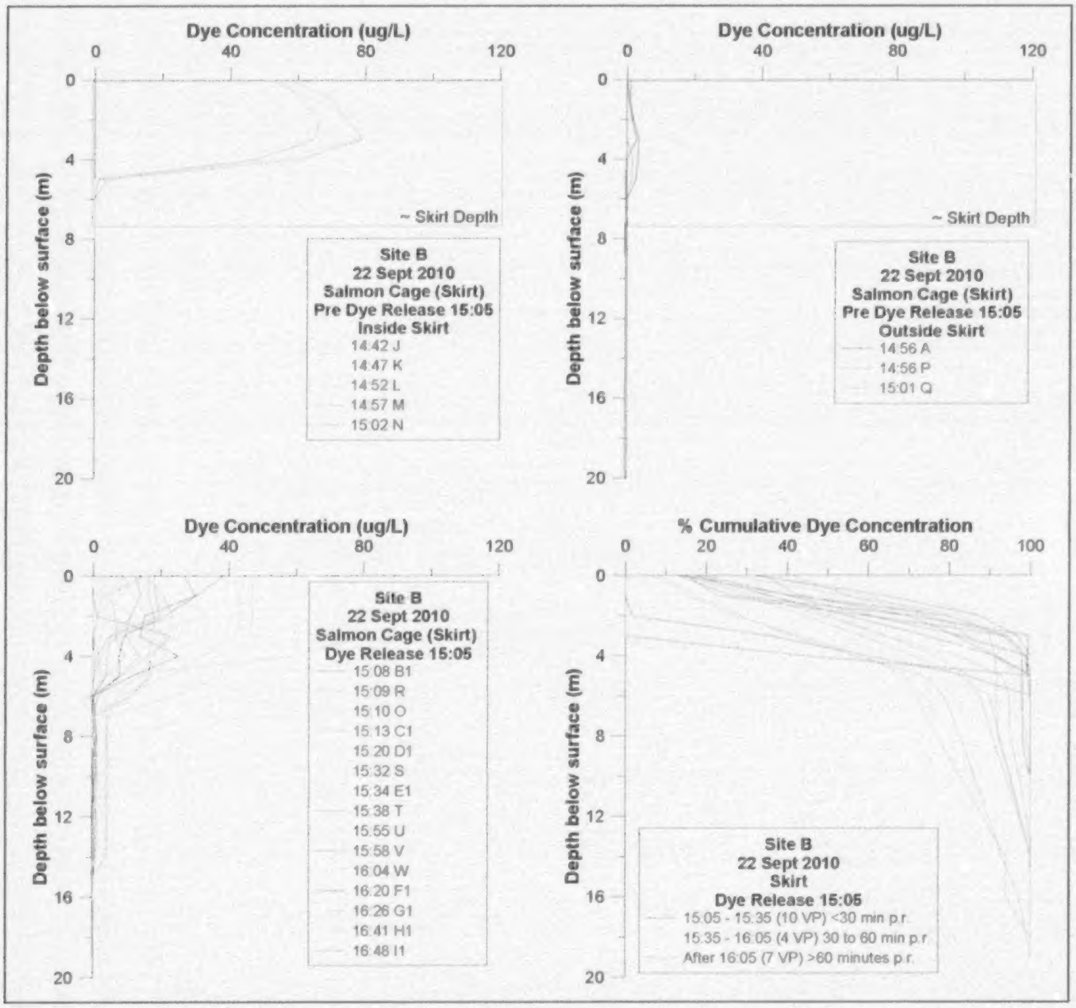

Figure 31. Vertical dye concentration profiles inside and outside the skirt during treatment (top panels), vertical dye concentration profiles post treatment (bottom left panel) and cumulative concentration versus depth curves (bottom right panel) associated with dye released from a skirt conducted at Site B. The average site depth at mean low tide is 35.3 m. VP = Vertical Profile. p.r. = post release

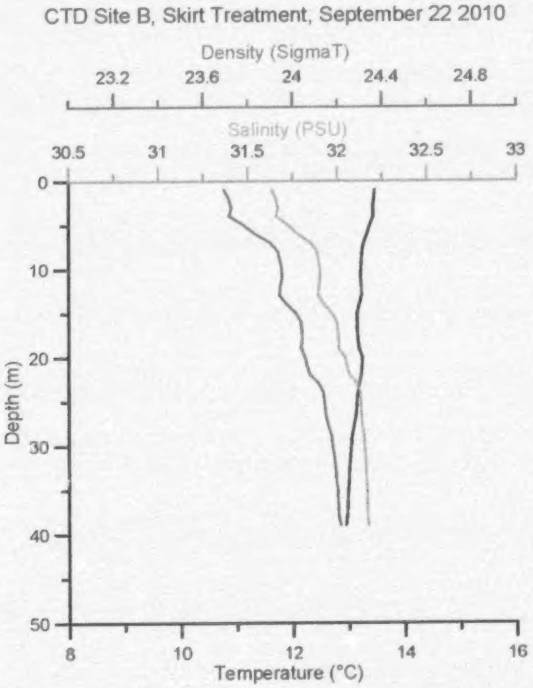

Figure 32. Temperature, salinity and density profiles of the water column collected during a skirt dye study at Site B.

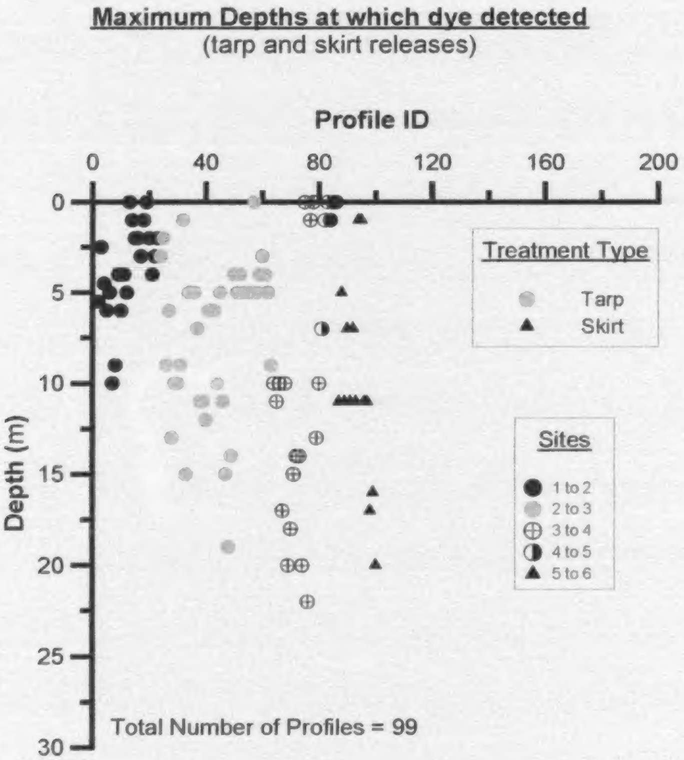

Figure 33. Composite of the maximum depth that dye was detected in each profile taken in association with tarp and skirt releases.

Summary of Net-Pen Vertical Aspects

In summary, vertical profiles of dye concentration showed a lot of variation in terms of absolute concentration, profile shape and maximum depth at which dye was detected. Profiles taken minutes apart sometimes showed very different characteristics. The maximum depths at which dye was detected within each profile are shown in Figure 33. The maximum depths varied from one site to another and there was little difference between the maximum depths observed during tarp and skirt releases, with the exception of the timing: maximum depths of dye from skirt treatments were sometimes reached during treatment.

Over 200 vertical profiles of dye concentration were collected over the full set of treatment studies, and 167 of these were taken from within the dye plumes. The profiles showed considerable variation in terms of absolute concentration, profile shape and maximum depth at which dye was detected; sometimes vertical profiles that were taken only minutes apart showed very different characteristics. This variation is believed to be the result of several potential factors including small scale spatial variation in dye concentrations coupled with point data measurements rather than time averaged measurements; near-surface fluctuations in fluorometer readings due to temporally varying ambient light conditions; and, to confound matters further, profiles were taken at a series of locations and times.

The maximum depths varied from one site to another and there appeared to be little difference between the maximum depths observed during tarp and skirt releases. The maximum depths at which dye was detected within each vertical profile are shown in Figure 34 as a function of time. No distinct temporal pattern in the distribution of maximum depth of dye concentrations was elucidated. The profiles indicated that for the first few hours after release the dye remained in the upper twenty meters, and often within the upper ten meters. In some cases the dye remained much nearer the surface. In other cases, when releases were conducted at sites located in relatively shallow waters, the dye was detected directly adjacent to bottom substrates. Interestingly the maximum depths observed in association with skirt treatments were sometimes reached during treatment whereas the maximum depths observed in association with tarp releases were post-release. All of the profiles were associated with weak vertical density stratification of the water column.

Unfortunately the data were inadequate for robustly calculating vertical mixing rates. However, the depths reached over the observed timescales were consistent with depths expected based on typical vertical mixing rates of 0.01 to 0.001 m^2/s (Lewis 1997).

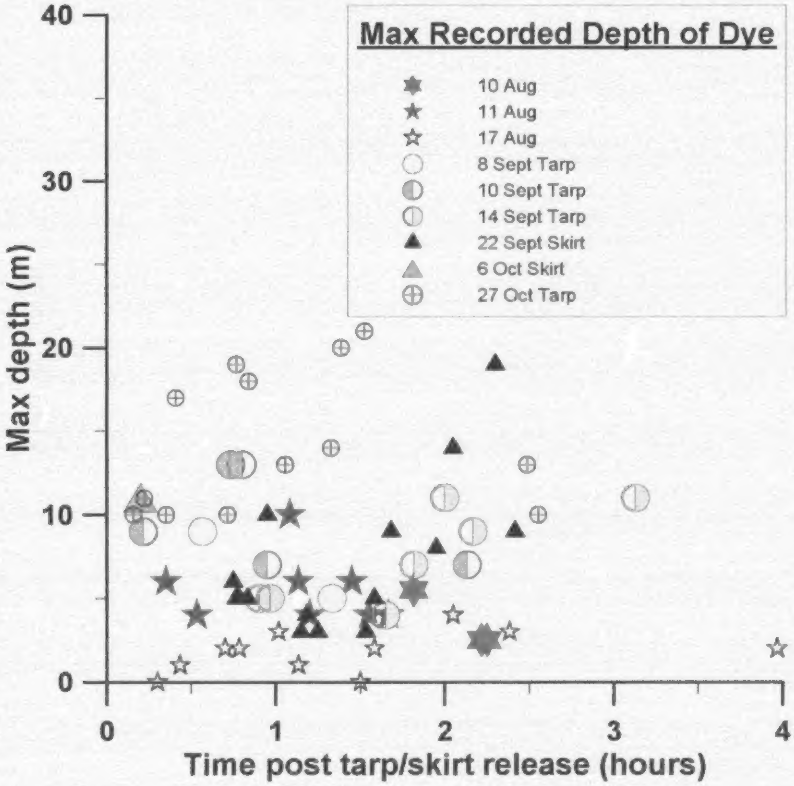

Figure 34. The maximum depth at which dye was detected in vertical profiles of fluorescent based estimates of dye concentration. Only dye concentrations greater than 1 µg/L were considered in this analyses to ensure concentrations were above background fluorescence levels. All profiles included in the analyses were taken post release of tarps or skirts.

THEORY AND MODELS

Dilution of Therapeutant

To illustrate the magnitude of the temporal reduction in the concentration of therapeutant released from the fish cages a time series of predicted normalized concentrations for the situation of a therapeutant treatment in a 100 m circular cage situated in an environment with a shallow mixed layer ($h = 5$ m) is shown in Figure 35. The figure contains two curves, one representing predictions from the above Fickian solution and the other representing a dilution derived from Okubo's (1974) variance relationship. Although the rates of horizontal eddy dispersion vary by an order of magnitude or more (e.g., Lewis 1997), the rates chosen for the Fickian prediction ($K_x = K_y = 0.1$ m^2/s) were selected so that they were consistent with literature values and provided a dilution rate similar to the Okubo-based dilution. We have not yet estimated local rates of dispersion from our data but we have compared the observed sizes of dispersing patches to the Okubo predictions (see below).

The Fickian and Okubo approaches show similar results for about the first hour, but the Fickian approach underestimates the Okubo dilutions after that. This is consistent with the Fickian approach assuming that rates of eddy mixing remain constant over space and time whereas the Okubo approach assumes the eddy mixing rate increases with time. The predicted dilutions are also consistent with the results of Ernst et al. (2001) and the patch scales observed by us in recent dye experiments (see below). The comparisons will become more rigorous as more data are collected and analysed and the modelling matures. In general it appears that average concentrations of therapeutants can be expected to be diluted by an order of magnitude, i.e., a factor of ten, within the first hour, and by a factor of 10 to 100 within three hours after release. It should also be acknowledged that this dilution rate is likely to be quite variable between treatments. A better appreciation and quantification of the level of variability will hopefully be developed as more data are collected and analysed.

The Okubo dilution relationship was derived from Okubo's (1971, 1974) relationship describing the variance in patch size as a function of the cube of time ($\sigma^2 \propto t^3$). For patch sizes characterized by length scales of between about 100 and 1000 m, the equivalent radial variance in the patch size, increases with time according to the specific relationship $\sigma_{re}{}^2 = 2.5 \cdot 10^{-5} t^3$ and for patch length scales greater than about 1 km, the variance increases according to $\sigma_{re}{}^2 = 5.4 \cdot 10^{-6} t^3$ Okubo (1971, 1974). In these relationships, σ_{re} is the size of the patch in terms of the equivalent radius of the patch or the radius that gives an area equivalent to that of the observed patch. Okubo defined the variance of this equivalent patch size as $\sigma_{re}{}^2 = 2\sigma_x\sigma_y$, where σ_x and σ_y are the standard deviations of the concentration weighted distances along the major and minor axes of a patch.

The approximate dilution rate of the average concentration $\bar{C}(t)$ within a patch of therapeutant released from a fish cage can be estimated as the mass (M) of added therapeutant divided by the volume (V) of water it has been mixed into, i.e., $\bar{C}(t) = M/V(t)$. The volume of water can be estimated as the horizontal area ($A(t)$) over which the therapeutant patch is spread times the vertical thickness of the layer ($h(t)$) over which it is spread, i.e., $V(t)=A(t)h(t)$. The area of the patch at the time of release ($t = 0$) is given by

$$A = \frac{\pi d^2}{4} = \frac{\pi(3\sigma_{rc})^2}{4} = \frac{9\pi\sigma_{rc}^2}{4} \qquad (29)$$

where the diameter of the cage is defined as $d = 3\sigma_{rc}$, σ_{rc} is the standard deviation length scale for the radially symmetrical initial distribution and $h(t)$ is specified from local knowledge or estimated from the rate of vertical eddy diffusion. The variance at $t = 0$ is therefore given by $\sigma_{re}{}^2 = 4A/9\pi$, the standard deviation of the initial patch is given by $\sigma_{re} = \sqrt{(4A/9\pi)}$, $\sigma_{re}{}^2 = d^2/9$ and $\sigma_{re} = d/3$. In the Okubo relationship, the time at which $\sigma_{re}{}^2 = d^2/9$ is given by $\sigma_{re}{}^2 = d^2/9 = 2{\cdot}10^{-5}t_0{}^3$ which rearranged gives

$$t_0 = \sqrt[3]{\frac{\sigma_{rc}^2}{2.5 \cdot 10^{-5}}} = \sqrt[3]{\frac{\pi d^2}{9 \cdot 2.5 \cdot 10^{-5}}} \tag{30}$$

In this equation d has units of centimetres and t_0 has units of seconds. The variance of the patch at times subsequent to t_0 are therefore given by $\sigma_{re}{}^2 = 2{\cdot}10^{-5}(t_0 - \Delta t)^3$, where Δt is the time in seconds elapsed after release. The average concentration of therapeutant therefore decreases in time according to

$$\begin{aligned}\bar{C}(t) &= \frac{M}{V} = \frac{M}{Ah} = \frac{M}{\pi\left(\frac{d}{2}\right)^2 h} \\ &= \frac{4M}{\pi d^2 h} = \frac{M}{\pi(3\sigma_{re})^2 h} = \frac{4M}{9\pi\sigma_{re}{}^2 h} \\ &= \frac{4M}{9\pi \cdot 2.5 \cdot 10^{-5}(t_o + \Delta t)^3 h}\end{aligned} \tag{31}$$

Figure 35 shows the predicted decrease in concentration with increasing time for the Fickian (equation 7) and the Okubo (equation 16) models. For each model we have shown the results corresponding with the assumptions that the dye is well mixed over the top 5 and 20 m. We have also shown an intermediate solution for the Okubo model in which the depth of mixing increases from 5 to 10 m over the first hour after release. We have shown the Fickian model for the cases of weak horizontal mixing ($K_x = K_y = 0.1$ m^2/s), the more typical horizontal mixing ($K_x = K_y = 1$ m^2/s) and an intermediate case in which ($K_x = 1.0$ and $K_y = 0.1$ m^2/s).

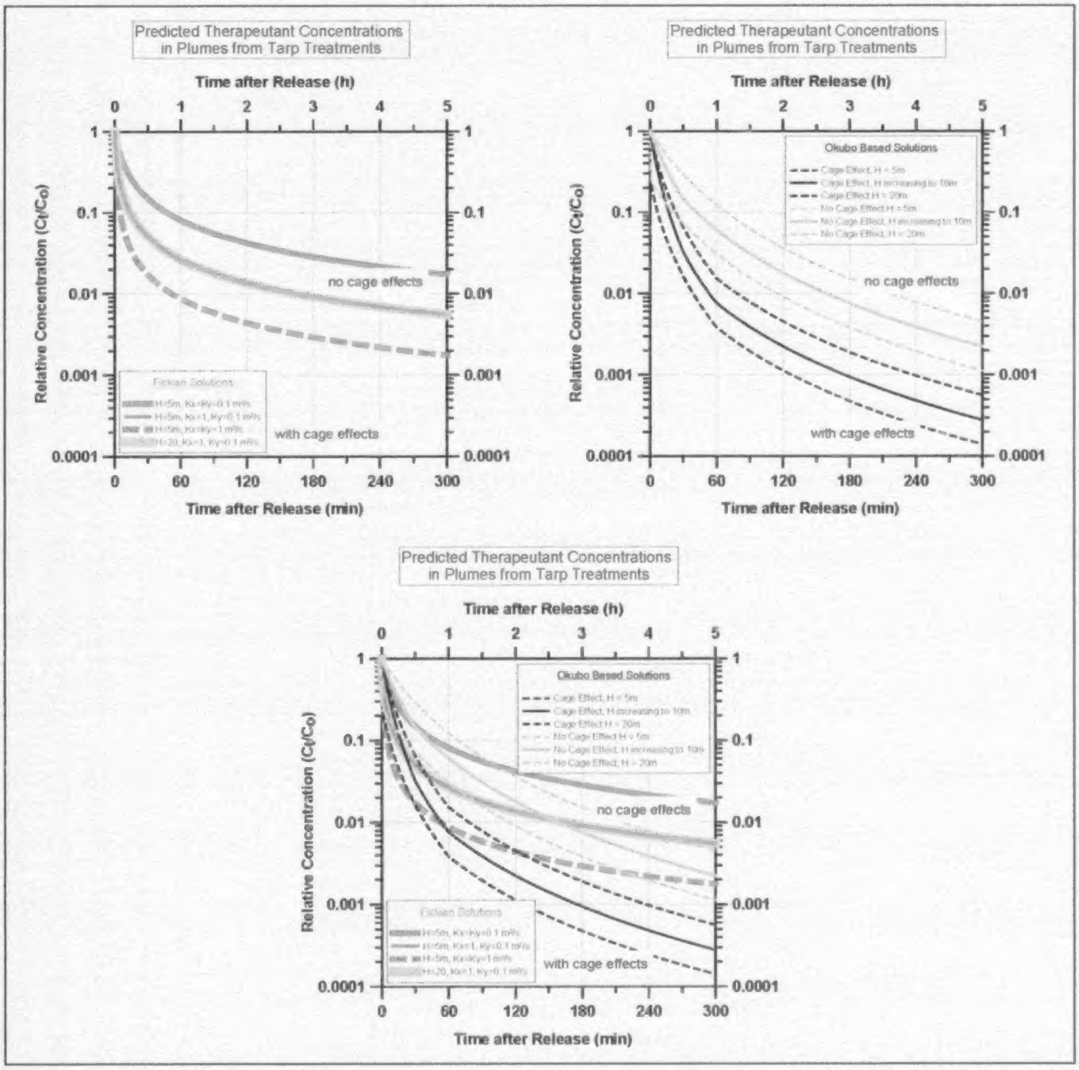

Figure 35. Fickian and Okubo model estimates of the temporal decrease in the standardized dye or therapeutant concentration (C(t)/C(t=0)) after release from a tarped cage. The Fickian curves are based on equation 16. The Okubo curves with no cage effects are based on equation 31. The Okubo curves with cage effect incorporates an initial increase in the rate of horizontal patch spread. Red curves assume a constant depth of 5 m and values of $Kx = Ky = 0.1$ m^2/s. The Okubo dilution assumes an Okubo increase in the horizontal size of the patch and a patch depth that remains at a constant depth of 5 m.

FVCOM Modelling

Model Description

As part of a more sophisticated approach to developing understanding and predictive capabilities of the transport and dispersal of dye and therapeutants from fish cages, we have implemented the FVCOM (Finite Volume Coastal Ocean Model) for the coastal area of southwest New Brunswick.

The Finite Volume Coastal Ocean Model, FVCOM (Chen et al. 2003, 2006), is used to model the sea level and circulation in southwWest New Brunswick. FVCOM is a state of the art four dimensional model, space and time, that solves the primitive equations governing the fluid flow on an unstructured horizontal mesh. Unstructured meshes allow higher resolution in areas of interest while permitting lower resolution in other areas. Unstructured meshes are highly desirable when modelling coastal areas as they allow small scale features to be resolved without requiring high resolution (and hence more computation time) throughout the entire domain.

The model domain used includes the Gulf of Maine and the Bay of Fundy (Figure 36). The grid is that used in Greenberg et al. (2012) with refinements (i.e., higher resolution) in southwest New Brunswick (specifically the Passamaquoddy Bay, Grand Manan and Musquash areas) and St. Mary's Bay in Nova Scotia. The grid has 41,892 nodes and 76,732 cells (triangles) with the largest triangles having sides of length up to 53.7 km and the smallest triangles of 24 m. FVCOM uses sigma layers as the vertical coordinate system. Each sigma level represents a proportion of the depth, with $\sigma = 0$ representing the sea surface and $\sigma = -1$ representing the bottom. In this implementation the vertical depth is divided into 21 layers (sigma levels) such that the levels are geometrically distributed over depth so that there is a higher concentration of sigma levels at the surface and at the bottom.

The Bay of Fundy is known for having some of the largest tides in the world resulting in tidal effects dominating in most of the domain. Large tides give rise to inter-tidal areas in the coastal regions and hence the model is run with wetting and drying in the inter-tidal areas. The model is run in barotropic mode with tides prescribed at the open boundaries. For this study, five tidal constituents are included: M2, N2, S2, K1 and O1. The model domain starts at rest and the tides at the open boundary are ramped-up over the initial 12 hours of the model simulation time. The model is then spun-up for an additional 4.5 days of simulation time.

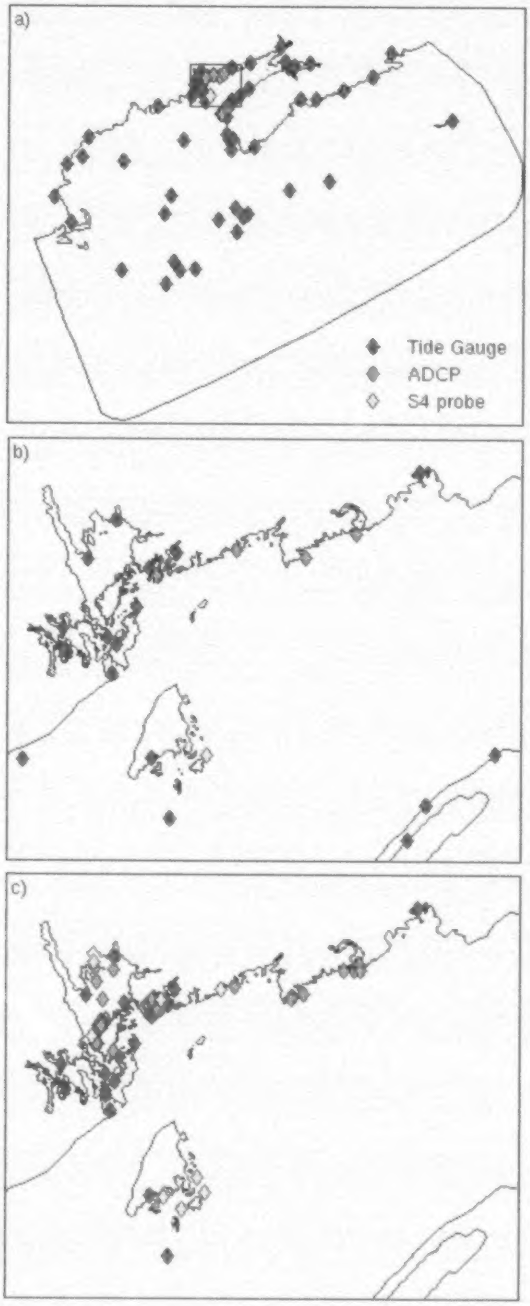

Figure 36. a) FVCOM model grid domain with locations of observation stations used for model sea level and current calibration. The area in the square is enlarged in the other two frames. b) locations of observation stations in southwest NB used for model calibration; c) all stations in southwest New Brunswick.

Before using the FVCOM model for simulating the transport and dispersal of the dye it was calibrated against observations of coastal sea levels and current velocities at locations throughout the model domain, with particular attention being paid to the observations in the areas of specific interest to the dye dispersal, i.e., the dye release areas in southwest New Brunswick.

Observed Data

The observational data were collected from three sources: historic sea level data, Acoustic Doppler Current Profiler (ADCP) data and InterOcean S4 current meter data (Figure 36). There are 60 sites throughout the model domain for which historic data are available. The data consist of tide gauge sea surface heights which have been analysed to give tidal height amplitudes and phases for the important tidal constituents. The ADCP data are from a set of 81 ADCP moorings located primarily in southwest New Brunswick. The ADCP moorings were bottom mounted and collected time series of both sea surface height and horizontal currents throughout the water column. The sea surface heights were broken into their tidal constituents using the tidal analysis program of Foreman et al. (2009). Currents were averaged over the model's sigma layers and then analysed using the same program. The same method was used for analysing the sea surface height obtained from nine S4 probe deployments.

Model Calibration

The initial M2 amplitudes and phases prescribed at the model's open boundary are those from Greenberg et al. (2012). Initial amplitudes and phases for the other four constituents were taken from Dupont et al. (2005). These boundary forcing conditions were then adjusted during the calibration process. The model was calibrated against observed sea surface amplitudes and phases for the five constituents used to force the model. Of the above mentioned observed data sets, all of the historic data, data from 6 of the ADCP moorings and one of the S4 probe moorings were used for calibration. Since the ADCP and S4 probe moorings were concentrated in southwest New Brunswick, a subset of these was used so that the calibration would not be biased towards this area. The model was run for 31 days corresponding to the month of August 2010. Results of the calibrated run are discussed below.

Mean values of the comparisons between the results of the FVCOM run and the observations are given in Table 8. In addition to showing results using the 67 stations used to calibrate the model, results in columns labelled SWNB were calculated using 105 stations located in southwest New Brunswick as this is our area of focus (Figure 36). Overall the model does reasonably well predicting the tidal height amplitudes and phases with the modelled M2 amplitude being within 0.1% of the observed M2 amplitude, the phase within 3.0° and a mean distance between the modelled and observed being 0.162 m. The differences between the results for the calibration data set and the data set for southwest New Brunswick are due to the model being calibrated against observations located over the entire model domain. This will facilitate the future use of the model in other areas in the Bay of Fundy while still giving good results in southwest New Brunswick. The comparisons of the model with observations for the other four constituents are given in Table 8.

Table 8. Mean values of comparisons of tidal amplitudes and phases of FVCOM run with observed values.

Constituent	$A_{mod}{}^1/A_{obs}{}^2$		$\varphi_{mod}-\varphi_{obs}$ (°)		Distance* (m)	
	Calibration[3]	SWNB	Calibration	SWNB	Calibration	SWNB
M2	0.999	0.980	2.1	4.0	0.162	0.208
N2	0.980	0.922	3.0	6.8	0.066	0.128
S2	0.982	1.015	-0.6	3.2	0.032	0.039
K1	0.964	0.908	8.6	4.0	0.022	0.020
O1	0.950	0.931	-9.9	-9.5	0.022	0.022

[1] A_{mod} and φ_{mod} are the amplitude and phase from the tidal analysis of the FVCOM results.

[2] A_{obs} and φ_{obs} are the amplitude and phase from the tidal analysis of the observed data.

[3] The calibration column includes the 67 stations used for calibration whereas the SWNB column is for the 105 stations located in southwest New Brunswick.

* The distance is the length of the error vector between the modelled and observed amplitudes and phases plotted in polar coordinates limits.

Model Validation at Dye Release Sites

As discussed above, overall the model does reasonably well at predicting the tidal amplitudes and phases for the sea surface height. Model performance is evaluated at three of the dye release Sites: A, B and C. Correctly predicting the currents is crucial in modelling the dispersal of therapeutants as the currents determine the trajectory of the therapeutants once they are released into the environment. For purposes of comparisons, only ADCP deployments present during the time of the dye release study are considered: 8, 10 and 4 deployments are in the vicinity of Sites A, B and C, respectively. Although the pressure gauge data from these deployments gave clean records, the currents measured by the ADCPs were often plagued by missing data. This is especially true for deployments located near fish cages. For this reason, care was taken in choosing observations with which to compare. For the results shown here, stations were selected based on three criteria. First, for the results of a tidal analysis at any given sigma level to be considered valid, data must be present for at least 85% of the total time of the deployment. Additionally, for Sites A and B, results of the tidal analysis must be present for at least 10 sigma layer. This criterion was relaxed for Site C as it is located in shallower water. Finally, if plots of the vertical profiles of the tidal ellipse parameters looked suspect, time series plots indicating time and location of valid data were examined. If these plots indicated large gaps in the data or patterns in the missing data, then the ADCP data were not included.

Site A

Of the eight ADCPs deployed during the dye release studies at Site A, 4 met the above criteria and are used for comparison with the model results. Here only the results for the M2 tidal constituents are discussed as it is the dominant constituent in the Bay of Fundy. At Site A, the amplitudes and phases for the M2 elevation predicted by the model are in close agreement with the observed values with the modelled amplitude being 98% of the observed and the modelled phase within 3° (Table 9). Results for the M2 tidal currents ellipses are given in Table 10. The predicted major amplitude is within 5 % of the observed values at three of the ADCP deployment locations (A2, A3 and A4). At Site A1, however, the model has a much stronger current than was measured. Predictions of the current ellipses' minor amplitudes were less consistent and vary considerably in their comparison against observations. The modelled inclinations compare well for all but deployment A4 where the predicted inclination differs from the observed by 13°. The phase differences shown in Table 10 indicate that the model is unreliable in predicting the phases of the tidal currents. The results shown in Table 10 are the results at the individual sigma levels averaged in the vertical. The vertically averaged modelled phase lags the observations by as much as 36° indicating that the modelled currents can lag the observations by as much as 1.25 hours. Figure 37 shows the vertical variation in the tidal ellipse parameters for station A4 and illustrates that even when the sea surface elevation amplitudes and phases and the tidal current ellipses amplitudes are all in agreement with the observations, the tidal current phases can still be poorly predicted by the model. This has important implications in the modelling of the dye release when trying to match experimental data.

Table 9. M2 tidal elevation amplitudes and phases from the tidal analysis of sea surface heights from ADCP data and FVCOM model results for deployments located in the vicinity of dye release Site A.

	Amplitude (m)			Phase (°)			Distance*
ADCP	**FVCOM**	**ADCP**	**Ratio**	**FVCOM**	**ADCP**	**Diff**	
A1	2.556	2.617	0.977	99.2	96.1	3.1	0.154
A2	2.556	2.561	0.998	99.2	96.0	3.2	0.142
A3	2.557	2.625	0.974	99.2	95.8	3.4	0.167
A4	2.556	2.621	0.975	99.2	96.0	3.2	0.158
Mean			0.981			3.225	0.155
Stand. Dev.			0.011			0.126	0.010

* The distance is the length of the error vector between the FVCOM and ADCP amplitudes and phases plotted in polar coordinates.

Table 10. M2 tidal ellipse parameters from the tidal analysis currents from ADCP data and FVCOM model results for deployments located in the vicinity of dye release Site A. The results have been vertically averaged over the sigma layers and only include the range of sigma layers for which ADCP data exist.

	A_{maj} (cm/s)			A_{min} (cm/s)			Phase (°)			Inclination(°)		
ADCP	**FVCOM**	**ADCP**	**Ratio**	**FVCOM**	**ADCP**	**Ratio**	**FVCOM**	**ADCP**	**Difference**	**FVCOM**	**ADCP**	**Difference**
A1	7.62	5.08	1.50	-1.41	-0.89	1.58	11.9	4.9	7.0	53.3	54.0	-0.7
A2	13.23	13.95	0.95	0.13	-0.64	-0.20	14.2	-4.6	18.8	29.9	32.6	-2.8
A3	7.85	8.00	0.98	0.61	0.94	0.65	25.0	6.0	31.0	43.9	39.0	4.9
A4	8.14	8.19	0.99	-0.61	-0.42	1.45	24.2	5.2	19.0	48.4	61.7	-13.3
Mean			1.11			0.87			18.9			-3.0
Stand. Dev.			0.26			0.82			7.6			9.8

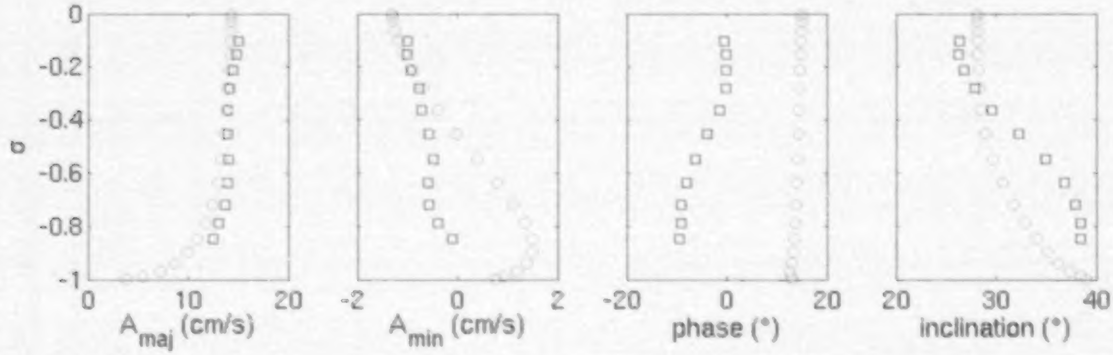

Figure 37. Comparison of M2 tidal ellipse parameters at Site A, ADCP deployment A2. Squares are the results from the tidal analysis of the ADCP data. Circles are the results from the tidal analysis of the FVCOM model run. The vertical axis scale (σ) goes from 0 at the sea surface to -1 at the sea bottom.

Site B

At dye release Site B, data from 7 of the 10 ADCP sites are included in the comparison. Results from the tidal analysis of the ADCP data and the FVCOM model results are given in Table 11 and Table 12 for the M2 elevation amplitudes and phases and the M2 current ellipse parameters, respectively. Unfortunately the currents at Site B are spatially and temporally complex, making it challenging to model the currents in the area. The M2 tides are accurately predicted by the model with the modelled amplitude being, on average, 98% of the observed amplitude and the modelled phase being within 3° of the observed phase. The maximum distance between any two of the ADCP deployments is 2.6 km. In spite of the small area being considered, there is quite a variation in the differences between the modelled results and the observations with some currents being too large and other too small. Of note are the results for ADCP deployments B5 and B6. Both of these were located at the cage site. Deployment B5 was approximately 45 m from the cage site and B6 was approximately 140 m from the site. The ADCP data show a drop in the current amplitude at B5 which is likely due to the presence of the cages adding extra drag. As no extra drag has been included in the model, the modelled current amplitude does not show this behaviour. Other than this trend for stations close to the cage site, the comparison between the modelled and observed major amplitude shows no specific trend. The modelled current amplitude along the semi-minor axis is generally underestimated but has quite a large scatter when compared with the observations. The modelled M2 tidal currents' inclinations are with 10° of the observation but often do much better than this indicating that the currents' directions are on the whole faithfully reproduced by the model. As with dye release Site A, the model has problems accurately predicting the currents' phases. The vertically averaged values indicate that the modelled currents lag the observed currents by up to 19° but the difference between the modelled and observed phases at a given sigma level can be as large as 25° which can result in the modelled currents lagging the observed currents by approximately one hour. The vertical variations of the M2 tidal current ellipse parameters at B2 are shown in Figure 38 and show that even when the vertically averaged variables agree well, there are vertical variations that may not be reproduced by the model.

Table 11. M2 tidal elevation amplitudes and phases from the tidal analysis of sea surface heights from ADCP data and FVCOM model results for deployments located in the vicinity of dye release Site B.

	Amplitude (m)			Phase (°)			Distance*
ADCP	FVCOM	ADCP	Ratio	FVCOM	ADCP	Diff	
B1	2.669	2.763	0.966	106.8	103.8	3.0	0.171
B2	2.667	2.719	0.981	106.8	103.8	3.0	0.148
B3	2.672	2.730	0.979	106.8	103.9	2.9	0.148
B4	2.674	2.666	1.003	106.8	104.1	2.7	0.129
B5	2.672	2.766	0.966	106.8	104.3	2.5	0.152
B6	2.671	2.700	0.990	106.8	104.2	2.6	0.127
B7	2.670	2.714	0.984	106.8	104.9	1.9	0.100
Mean			0.981			2.7	0.139
Stand. Dev.			0.013			0.4	0.023

* The distance is the length of the error vector between the FVCOM and ADCP amplitudes and phases plotted in polar coordinates.

Table 12. M2 tidal ellipse parameters from the tidal analysis currents from ADCP data and FVCOM model results for deployments located in the vicinity of dye release Site B. The results have been vertically averaged over the sigma layers and only include the range of sigma layers for which ADCP data exist.

ADCP	**A_{maj} (cm/s)**			**A_{min} (cm/s)**			**Phase (°)**			**Inclination(°)**		
	FVCOM	**ADCP**	**Ratio**	**FVCOM**	**ADCP**	**Ratio**	**FVCOM**	**ADCP**	**Diff**	**FVCOM**	**ADCP**	**Diff**
B1	19.75	22.05	0.90	-4.97	-5.49	0.91	16.4	-0.5	16.9	56.0	58.3	-2.3
B2	22.47	25.57	0.88	-2.41	-3.08	0.78	-8.19	-13.2	5.0	49.0	51.7	-2.7
B3	16.55	17.97	0.92	-2.92	-4.59	0.64	29.5	14.4	15.1	51.4	60.7	-9.3
B4	14.75	14.01	1.05	-1.17	-3.12	0.37	42.4	23.5	18.9	40.7	48.0	-7.3
B5	18.73	16.99	1.10	-2.20	-3.72	0.59	24.5	10.3	14.2	50.8	50.3	0.5
B6	18.79	19.34	0.97	-3.38	-4.12	0.82	22.2	7.9	14.3	54.2	55.3	-1.1
B7	18.63	19.80	0.94	-1.89	-2.64	0.71	13.3	0.1	13.2	51.8	49.7	2.1
Mean			0.97			0.69			14.0			-2.9
Stand. Dev.			0.08			0.18			4.4			4.1

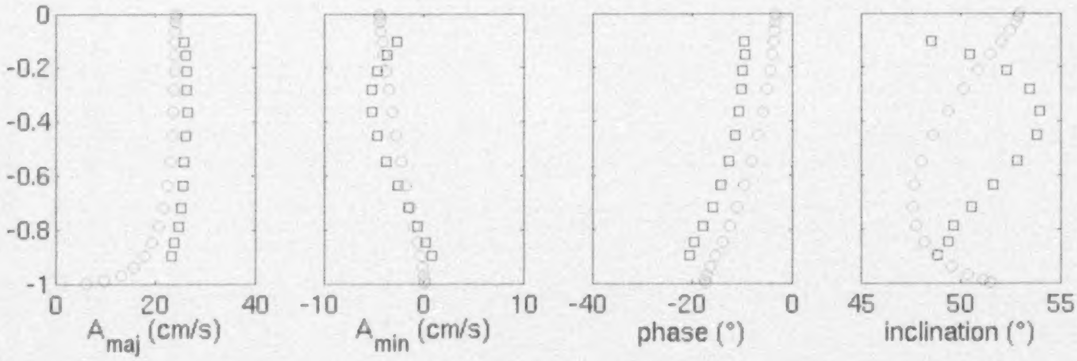

Figure 38. Comparison of M2 tidal ellipse parameters at Site B, ADCP deployment B2. Squares are the results from the tidal analysis of the ADCP data. Circles are the results from the tidal analysis of the FVCOM model run. The vertical axis scale (σ) goes from 0 at the sea surface to -1 at the sea bottom.

Site C

Since there were only 4 ADCP deployments at Site C at the time of the dye release, all four have been included in the comparison between observed and modelled M2 tidal parameters. Results from the tidal analysis of the ADCP data and the FVCOM model results at Site C are given in Table 13 for the M2 elevation amplitudes and phases. The modelled M2 amplitude is 98% of the measured amplitude at all four stations and the modelled phase is within 5° of the observed phase. M2 current tidal ellipse parameters for Site C are given in Table 14. At all four

ADCP sites, the currents amplitude along the major axis is underestimated. In this area, the currents were primarily unidirectional and so the current amplitudes along the minor axis are very small and it is difficult to make a meaningful comparison. This is an area where the model reliably reproduces both the inclination and the phase. The vertical variation M2 tidal ellipse parameters for ADCP Site C1 are shown in Figure 39. When the currents are vertically averaged, the model underestimates the amplitude along the major axis by 15%, but if vertically varying profiles are considered, the modelled major amplitude agrees well with the observations close to the surface.

Table 13. M2 tidal elevation amplitudes and phases from the tidal analysis of sea surface heights from ADCP data and FVCOM model results for deployments located in the vicinity of dye release Site C.

	Amplitude (m)			Phase (cm/s)			Distance*
ADCP	**FVCOM**	**ADCP**	**Ratio**	**FVCOM**	**ADCP**	**Diff**	
C1	2.569	2.614	0.983	99.2	93.8	5.4	0.247
C2	2.568	2.610	0.984	99.2	93.4	5.8	0.263
C3	2.567	2.617	0.981	99.1	93.6	5.5	0.255
C4	2.568	2.630	0.977	99.1	94.1	5.0	0.238
Mean			0.981			5.4	0.251
Stand. Dev.			0.003			0.3	0.011

* The distance is the length of the error vector between the FVCOM and ADCP amplitudes and phases plotted in polar coordinates.

Table 14. M2 tidal ellipse parameters from the tidal analysis currents from ADCP data and FVCOM model results for deployments located in the vicinity of dye release Site C. The results have been vertically averaged over the sigma layers and only include the range of sigma layers for which ADCP data exist.

	A_{maj} (cm/s)			A_{min} (cm/s)			Phase (˚)			Inclination(˚)		
ADCP	**FVCOM**	**ADCP**	**Ratio**	**FVCOM**	**ADCP**	**Ratio**	**FVCOM**	**ADCP**	**Diff**	**FVCOM**	**ADCP**	**Diff**
C1	19.09	23.20	0.82	0.24	0.37	0.65	16.1	10.8	5.2	63.6	66.9	-3.3
C2	18.14	25.81	0.70	-0.05	0.03	-2.15	17.2	10.9	6.3	53.3	53.8	-0.5
C3	19.03	22.39	0.85	-0.39	-0.25	1.57	16.3	9.3	7.0	43.7	43.8	-0.1
C4	22.31	23.91	0.93	-0.09	-0.04	2.50	18.1	12.0	6.1	59.3	54.6	4.6
Mean			0.83			0.64			6.2			0.2
Stand. Dev.			0.10			2.00			0.7			3.3

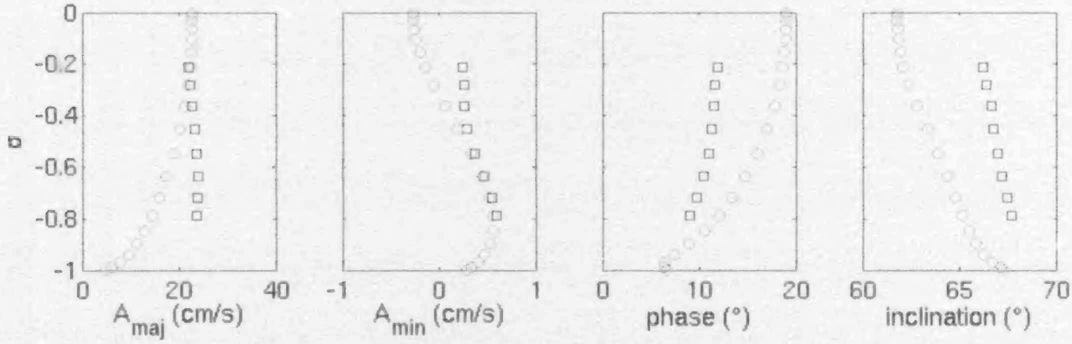

Figure 39. Comparison of M2 tidal ellipse parameters at Site C ADCP deployment C1. Squares are the results from the tidal analysis of the ADCP data. Circles are the results from the tidal analysis of the FVCOM model run. The vertical axis scale (σ) goes from 0 at the sea surface to -1 at the sea bottom.

In summary, the model reliably predicts the sea surface elevation at all the dye study sites examined. It was observed, however, that even when the elevations are accurately predicted, there may be problems in the prediction of the currents particularly both in the amplitude and the phases. In order to get good agreement with tidal height amplitudes and phases throughout the entire model domain, the bottom friction was adjusted during the calibration process. This resulted in a rather large value of the bottom friction being used to get reasonable agreement in the upper Bay of Fundy. This may be causing the large phase lag in the modelled currents and the reduced current amplitude at many of the ADCP sites. Wu et al. (2011) have found that using variable bottom friction improves the model performance in the upper Bay of Fundy. Additionally, at Sites B and C, there were fish cage structures present at the time of the ADCP deployments. The presence of these structures can influence both the amplitude and the phases of the currents. A preliminary FVCOM run including surface drag to model the effect of the cages indicates that the extra surface drag does indeed impact the currents' speeds and phases. These are two model features that merit further investigation.

Modelling the Dispersal of Therapeutants

The purpose of creating a hydrodynamic model for southwest New Brunswick is to create a time and spatially varying velocity field for the use in the study of the dispersion of therapeutants. FVCOM has two modules that are potentially useful for modelling the dispersion of therapeutants: a dye module where the dye conservation equation is solved and a Lagrangian particle tracking module. While the dye module appears to be a natural choice for modelling the evolution of therapeutant concentrations, numerical experiments with the module indicated that the horizontal dispersion rate was too large compared to the dye observations. The experiments also suggested this overestimation was due to having too large a grid cell size since experiments with a finer grid resulted in less horizontal numerical dispersion. Experiments using the particle tracking approach showed that the dispersion was independent of grid size. Additionally, concentration models are known for giving erroneous results near the dye release site (Suh 2006). In the near field, the Lagrangian particle tracking model is the preferred approach as it does not suffer from the same drawbacks as the Eularian concentration approach. Particle tracking models have been used and compared to drifter observations in several studies including those by Spydell and Feddersen (2009), Xu and Xue (2011) and Schroeder et al. (2012). Although Schroeder et al. (2012) found that relative dispersion at submesoscales was significantly underestimated, Xu and Xue (2011) achieved remarkedly good comparison between particle and drifter positions using a similar model grid to the one used. For these reasons the particle tracking approach was chosen.

The Lagrangian particle tracking model is a stand-alone FVCOM module and is run separately from the FVCOM model using the velocity fields predicted by the model as inputs. The particles are advected using this velocity field and a 4th order Runge-Kutta numerical integration scheme. For each dye treatment being modelled, 5000 particles were initially randomly distributed over a cylinder with a radius of 15.92 m whose center was located at the release coordinates. Two values were considered in selecting the depth of the cylinder. When a fish cage is treated, the depth of the cage is reduced from 10 m to roughly 3 m but the cage is allowed to return to its full depth of 10 m after the tarp has been removed. It was found that, at least when visually comparing the horizontal progression of the particle patch, there was not a significant difference between the two sets of model runs. Based on the vertical distribution of the dye, however, the value of 10 m was chosen for the results given here.

In addition to movement due to the advection, the particle tracking model uses a constant rate of horizontal diffusivity. Observations indicate that diffusivity in the horizontal is in the range of 0.04 to 7.6 m^2/s. A value of 0.1 m^2/s was chosen for the model runs discussed here. Although this value is lower than many of those measured from the results of the field work, it was found that when a more representative value of 1.0 m^2/s was used, there was too much horizontal diffusion in the particle patch when compared with the observations. To assess the impact of the horizontal and vertical diffusion used in the particle tracking model, four scenarios were compared: no diffusion, horizontal diffusion only, vertical diffusion only and both horizontal and vertical diffusion. These scenarios were run using initial depths of both 3 m and 10 m. Figure 40 shows the dilution curves for these different configurations of diffusivity and indicates that there is some horizontal diffusion of the particle patch even when no diffusion is added to the model. This is likely a result of the shears in current field used to advect the particles. In the vertical, the particle tracking scheme uses the diffusion from the FVCOM model run. In Figure 41 the vertical cumulative dye concentrations are compared against observations for these runs. Clearly, when the vertical diffusion is included in the particle tracking model, there is too much vertical mixing (Figure 41c, d, g and h). Since the particle tracking model is simply using the vertical diffusion from the output of the FVCOM run, the amount cannot be adjusted. Further work is needed to determine a better model for the vertical mixing. Although the amounts of vertical mixing for the case with no diffusion and the case with horizontal diffusion only are similar (compare Figure 41a and e to b and f, respectively), the results in the horizontal indicated that horizontal diffusion is necessary to get sufficient spread of the particle patch.

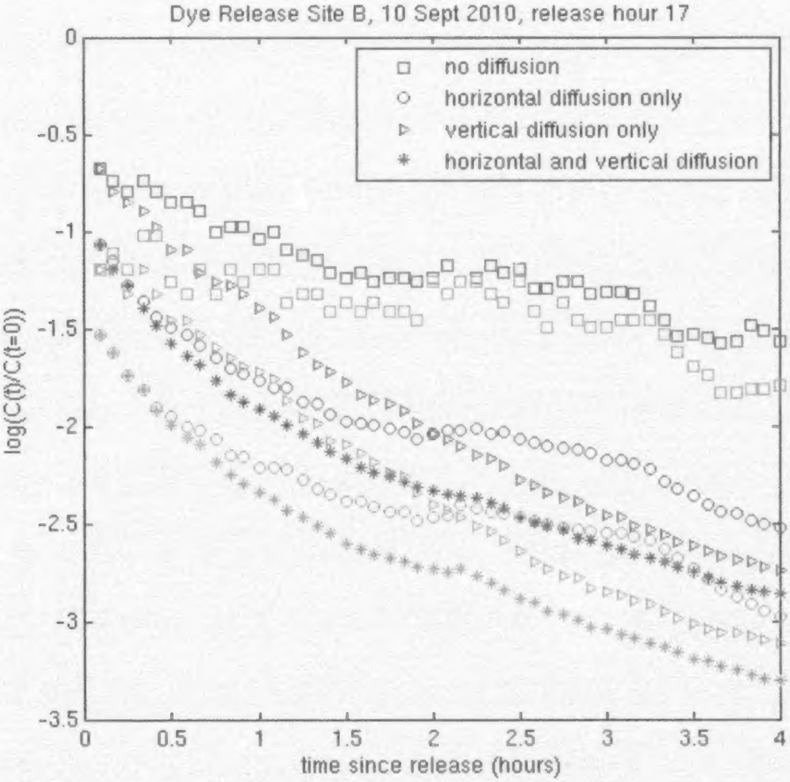

Figure 40. Horizontal dilution curves. Red (blue) symbols are for runs with the particles initially randomly distributed over the surface 3 m (10 m). The concentration at a given time is calculated by multiplying the horizontal surface area occupied by the particles and multiplying them by a constant depth of 10 m. The concentration is divided by the initial concentration C(t=0) which is equal to the total number of particles divided by the volume of the cylinder over which the particles are initially randomly distributed.

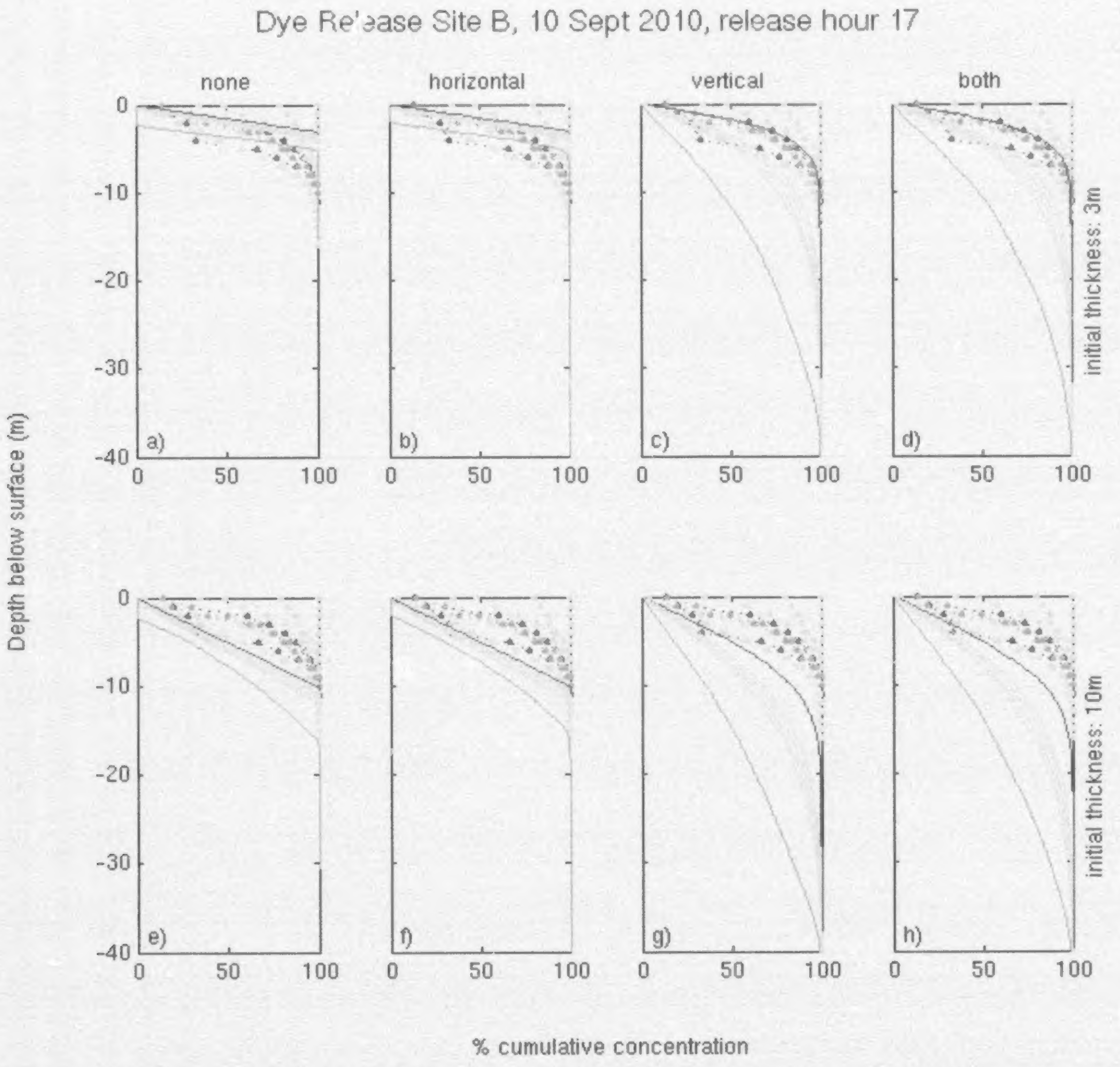

Figure 41. Vertical cumulative concentrations for eight different particle tracking runs comparing the type of diffusion included (no diffusion, horizontal only, vertical only, both horizontal and vertical) and the depth over which the particles are initially distributed (3 m and 10 m). The cumulative vertical concentration for a given depth is computed by determining the number of particles located in the surface layer up to that depth (regardless of horizontal location) and dividing by the total number of particles. Solid lines are the modelled results and dotted lines are the observations. The results are compared at 10 minutes (blue), 40 minutes to 55 minutes (green) and 130 minutes (magenta) post release time.

COMPARISONS BETWEEN MODELS AND OBSERVATIONS

There are several aspects of the dye or therapeutant plumes or patches that need to be predicted: the size (area, depth, length scales) of the plume or patch, the trajectory the patch takes through space and time and the concentration of material within the patch.

Patch Size

From the perspective of patch size, we have compared the temporal evolution of the surface area of the evolving patches to that predicted or expected based on Okubo's (1971,1974) relationship relating the radial variance of the patch to the time since release into the ambient water. Figure 42 shows the computed values of the Okubo variance at specific times after removal of the tarpaulins. The relationship derived by Okubo (1974) is also shown. The first three panels show the comparisons for the dye releases conducted in 2010 at farm sites and the fourth panel shows the relationship for dye releases conducted in the 1990s at a series of locations within southwest New Brunswick where fish farms did not exist. These latter data have been described by Ernst et al. (2001). In general the more recent 2010 data involving dispersal from fish cages with nets (Figure 42 top left panel) and cages within active farm cage arrays (Figure 42 top right and bottom left panels) lie above the Okubo line. However this is due to an initial anomously fast increase in the variance representing the dispersal of the dye from the scale of the cage ($\sigma^2 \approx 100$) to the scale of the farm ($\sigma^2 \approx 1000$). After the initial dispersal of dye through the fish farm, the rate of increase in the variance is consistent with that predicted by Okubo. Interestingly, there is no enhanced initial increase in the variance in the data associated with the Passamaquoddy Bay studies conducted in the 1990s. In the absence of fish cages, nets and fish, the dispersion of dye seems to follow the Okubo relationship more closely.

The rates of Okubo's apparent radial diffusivity (K_a) were also calculated from the data. They were plotted against the size of the patch and they follow the same pattern as discussed above; the data points from the 2010 studies tend to be greater than expected, whereas the 1990s data seems to be consistent with expectations (Figure 43). In all cases, the horizontal diffusivity increased with the size of the patch.

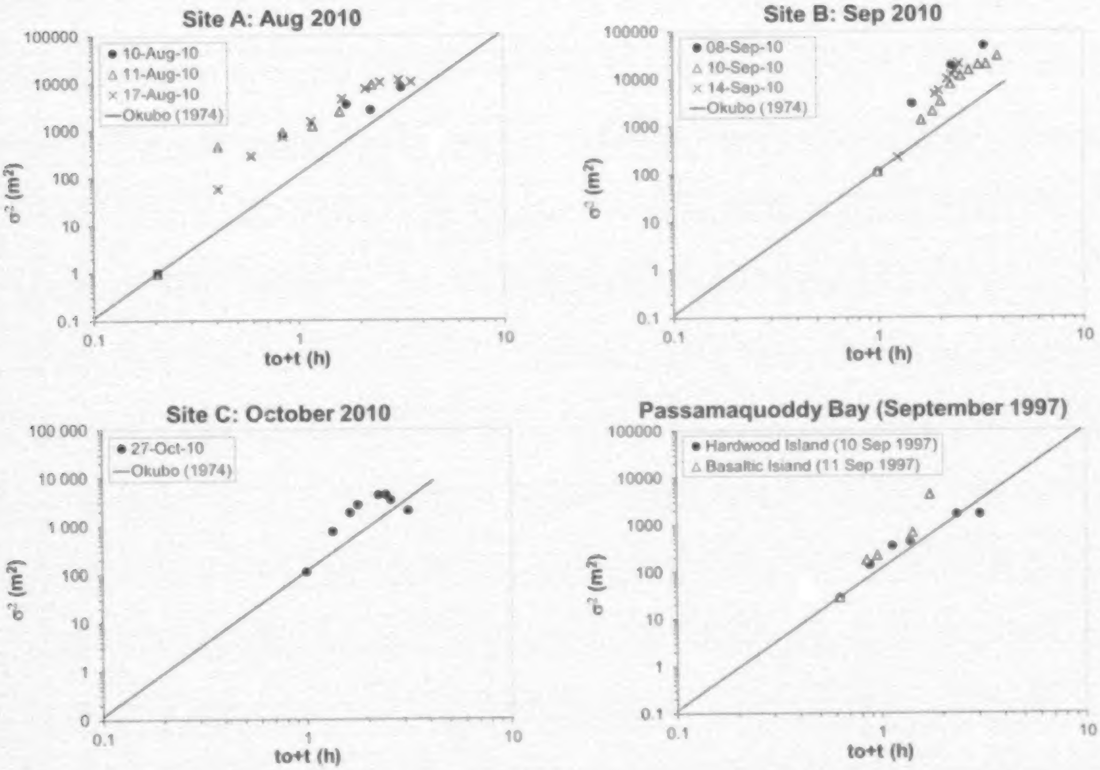

Figure 42. Okubo variance versus time for the dye releases associated with tarpaulin treatments conducted at the three 2010 study sites described here (A, B, C) and the Ernst et al. (2001) study sites (Passamaquoddy Bay).

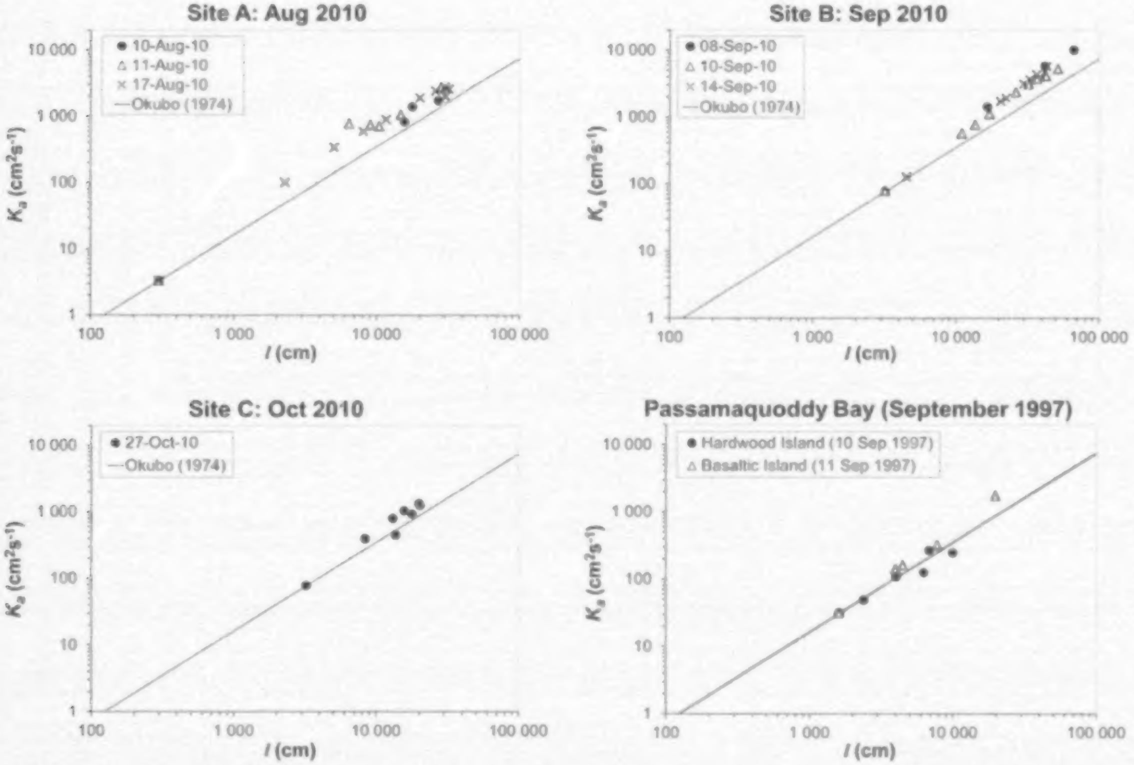

Figure 43. Okubo apparent diffusivity versus time for the dye releases associated with tarpaulin treatments conducted at the three 2010 study sites described here (A, B, C) and the Ernst et al. (2001) study sites (Passamaquoddy Bay).

Patch Trajectories: Current Meters

From the perspective of patch advection or the trajectory of its center of mass through space and time, two approaches were explored. One is to use a single upper water column current meter record from within the vicinity of the release location and calculate the progressive displacement vector from the time of dye release. This approach assumes the current is temporally variable but spatially homogeneous over the spatial scale of the drift track. The results for Sites A, B and C are shown in Figure 44, Figure 45 and Figure 46. Several features are demonstrated in the plots. Firstly, the observed patches are not circular as assumed by the Okubo simulation, though it is possible to set the predicted shape to be ellipsoidal with a specified major to minor axis ratio. Secondly, as indicated above, the predicted Okubo variance at the end of the simulated and observed drift is less than the observed. Thirdly, the predicted trajectories are not always in directions consistent with the drift directions of the dye patches, and the magnitude of the predicted displacements is not always similar to that of the observed displacements. Fourthly, the predictions for a particular dye release vary between current recordings made on the same day but in different locations. Other comparisons that are not shown indicate that the same current meter record can support a good comparison with the observed movement of dye during some releases but give poor agreement on other days. Hence, if only a single current meter record were to be used, one would not know whether or not the predicted dye plume trajectory was realistic. Hopefully, if many trajectories were calculated from a full current meter record, the real trajectory would fall somewhere within the scatter of the potential trajectories. Perhaps this is the way to proceed since in reality multiple treatments will occur over a range of time.

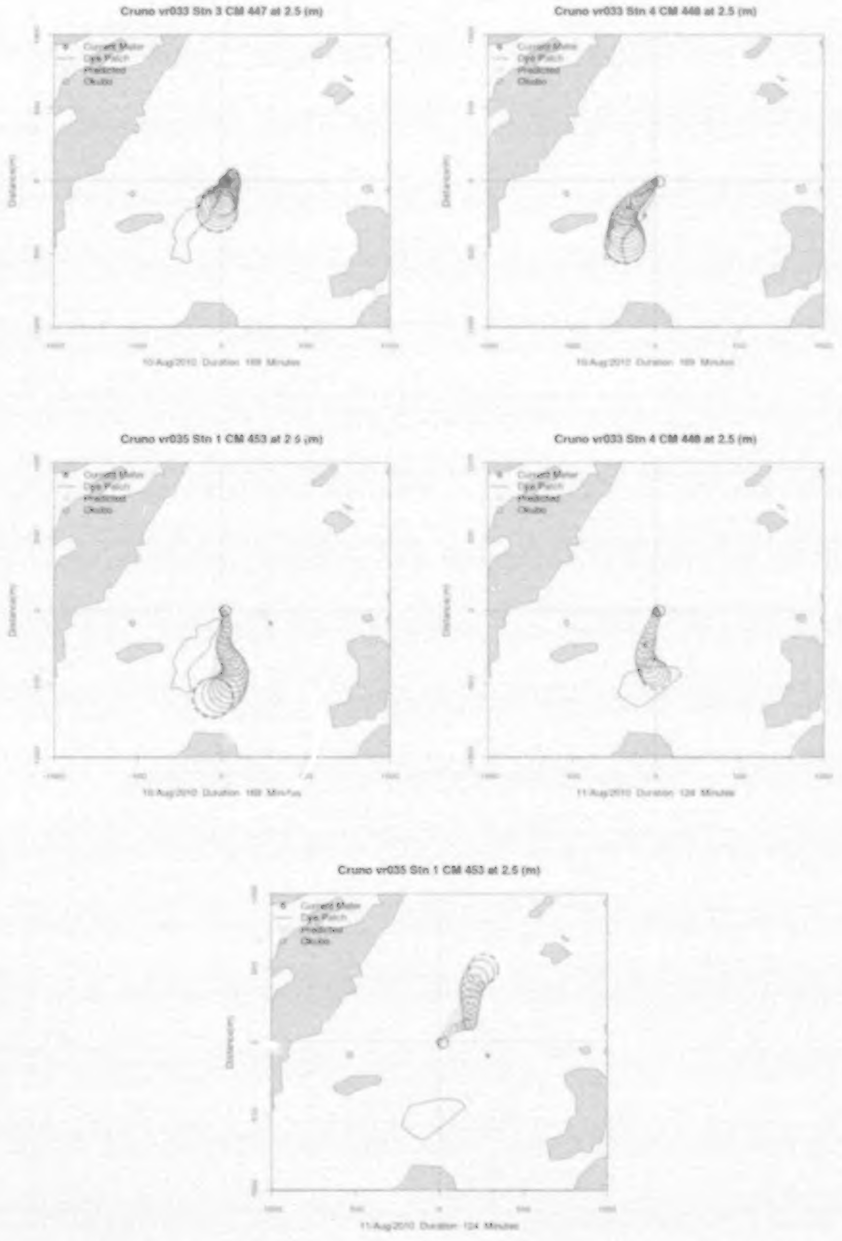
Cruno vr033 Stn 3 CM 447 at 2.5 (m)
Cruno vr033 Stn 4 CM 448 at 2.5 (m)
Cruno vr035 Stn 1 CM 453 at 2.5 (m)
Cruno vr033 Stn 4 CM 448 at 2.5 (m)
Cruno vr035 Stn 1 CM 453 at 2.5 (m)
Current Meter
Dye Patch
Predicted
Okubo
Distance(m)
10-Aug-2010 Duration 169 Minutes
11-Aug-2010 Duration 124 Minutes

Figure 44. Simulations of a dye patch transport and dispersal pattern at Site A using two different current meter records to advect the patch and the Okubo relationship to estimate the evolving area of the patch. The red polygons are the perimeter of the observed dye patches at the end of the simulation. The shaded blue area is the predicted path of advection. The large circles are centered over the advection trajectory and have a diameter that grows with time according to the Okubo (1974) relationship. The circle diameter is $l = 3\sigma_r$.

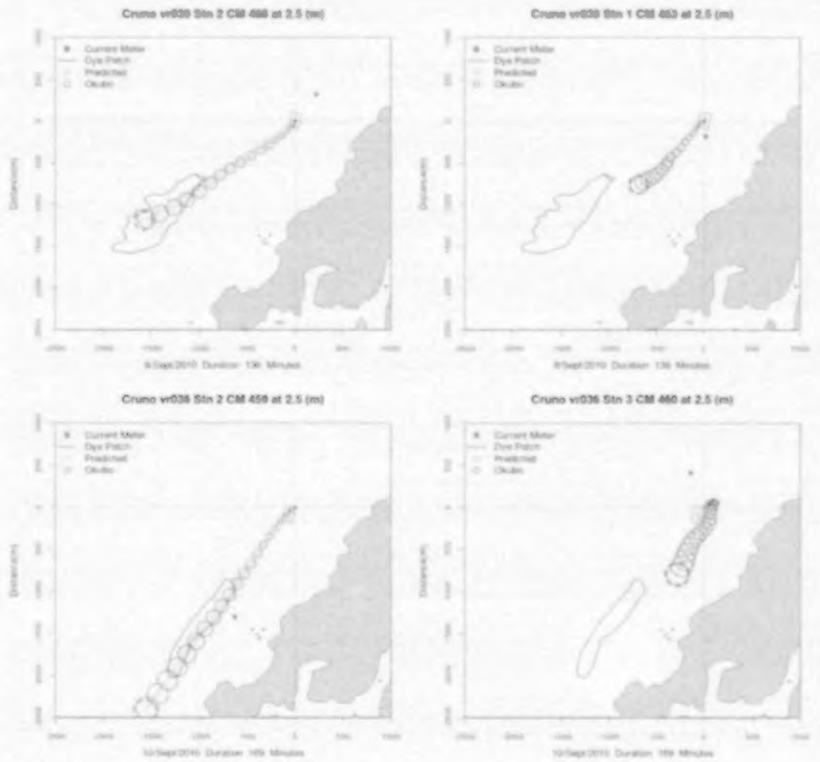

Figure 45. Simulations of a dye patch transport and dispersal pattern at Site B using two different current meter records to advect the patch and the Okubo relationship to estimate the evolving area of the patch. The red polygons are the perimeter of the observed dye patches at the end of the simulation. The shaded blue area is the predicted path of advection. The large circles are centered over the advection trajectory and have a diameter that grows with time according to the Okubo (1974) relationship. The circle diameter is $l\ 3\sigma_r$.

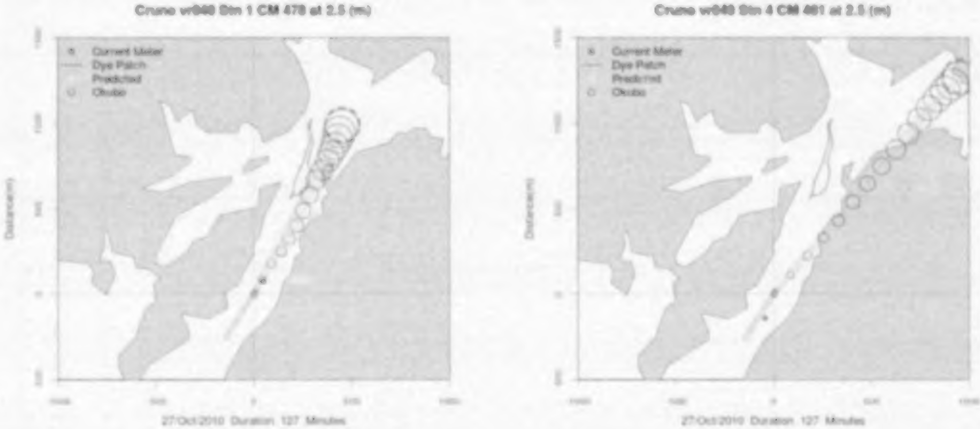
Cruno w040 Stn 1 CM 478 at 2.5 (m)
Current Meter
Dye Patch
Predicted
Okubo
Distance(m)
27/Oct/2010 Duration 127 Minutes
Cruno w040 Stn 4 CM 481 at 2.5 (m)
Current Meter
Dye Patch
Predicted
Okubo
Distance(m)
27/Oct/2010 Duration 127 Minutes

Figure 46. Simulations of a dye patch transport and dispersal pattern at Site C using two different current meter records to advect the patch and the Okubo relationship to estimate the evolving area of the patch. The red polygons are the perimeter of the observed dye patches at the end of the simulation. The shaded blue area is the predicted path of advection. The large circles are centered over the advection trajectory and have a diameter that grows with time according to the Okubo (1974) relationship. The circle diameter is $l = 3\sigma_r$.

Patch Trajectories: FVCOM

The other approach used to predict the trajectory of the dye plumes was to advect particles using the current fields calculated by the FVCOM hydrodynamic model. This approach was described above. The results of the FVCOM hydrodynamic model runs are saved hourly. Since the model did not always predict the current phase correctly, especially at dye release Sites A and B, there is some uncertainty as to what modelled time corresponds to the observed time, in terms of the current direction and amplitude. Additionally, the actual release times did not fall on the hour. Although it is possible to release the particles at any time during the hour, due to the uncertainty in the current phase the particle tracking model was run using three hourly release times for Sites A and B: on the hour on either side of the release plus one additional hour later. For example, if the dye was released at 15:38, then the particle tracking model was run with the particles being released at 15:00, 16:00 and 17:00. The reason for the later run is that the tidal current ellipse comparisons of the phases indicated that the modelled currents could be up to 1.25 hours later than the observed, depending on the site. At Site C, the current phases predicted by the model was fairly close to the observed current phases so for this case the particle tracking model was run on the hour on either side of the release and at the half hour between these two times.

Site A – 10th, 11th and 17th of August 2010

At Site A, there were three different dye release studies conducted on three separate days: the 10th, 11th and 17th of August 2010. Comparisons of model results with the dye perimeter data are shown in Figure 47, Figure 48 and Figure 49. In all three cases, there were significant differences between the modelled and observed trajectories of the dye patches: the predicted displacement of the dye patch for the 10th of August 2010 covered too large a distance, for the 11th of August 2010 the modelled dye patch was too slow to leave the fish farm site, and for the

17th of August 2010 the distance covered by the modelled dye patch was less than the measured distance. Based on the comparisons of the M2 current ellipse parameters from the ADCP data collected in this area, it was expected that the particle tracking simulation with a start time later than the actual release time would give the best agreement with the dye perimeter data. This is certainly the case for the dye studies conducted on the 11th and 17th of August 2010 (Figure 48 and Figure 49 release time 17:00) but for the 10th of August 2010 the simulation that compares best with the observations occurs before the actual time of release (Figure 47, release time 16:00). This result is surprising given the modelled phases lag those of the observed by up to 36°. On this particular day, the dye was released from the cage over a 2 to 3 hour period after the tarp was released. This behaviour is not captured by the model. Based on the comparisons for the 11th and 17th of August 2010, the latest particle release time shown for the 10th of August 2010 will be used in further discussions. For comparisons of the modelled particle patch with the dye perimeters, the modelled particle release times of 18:00, 17:00 and 17:00 are used for the 10th, 11th and 17th of August 2010, respectively.

The dye perimeters collected on the 10th and 17th of August indicate that the dye patches were elongated on those days. The model reproduces this behaviour for the 10th of August simulation only. Although the general shape of the particle patch mimics that of the dye patch, the patch is too long and extends far beyond the area of the dye patch. A possible explanation for the particles being advected too quickly is that the modelled currents at a distance from the release site are too fast, a hypothesis supported by recalling that the model over-predicts the velocity at ADCP deployment A1 (location shown by a black square in Figure 47) by 50% (see Table 10). For the 17th of August 2010, there is no elongation of the particle patch. Additionally, in the field study the dye patch reaches the shoreline. This feature is not captured by the model. For the 11th of August 2010, the particle patch is much slower at leaving the release site than the dye (Figure 48, 35 and 55 minutes post release time) but eventually catches up to the dye patch (Figure 48, 120 minutes past release time) as it passes by the location of the ADCP deployment A1.

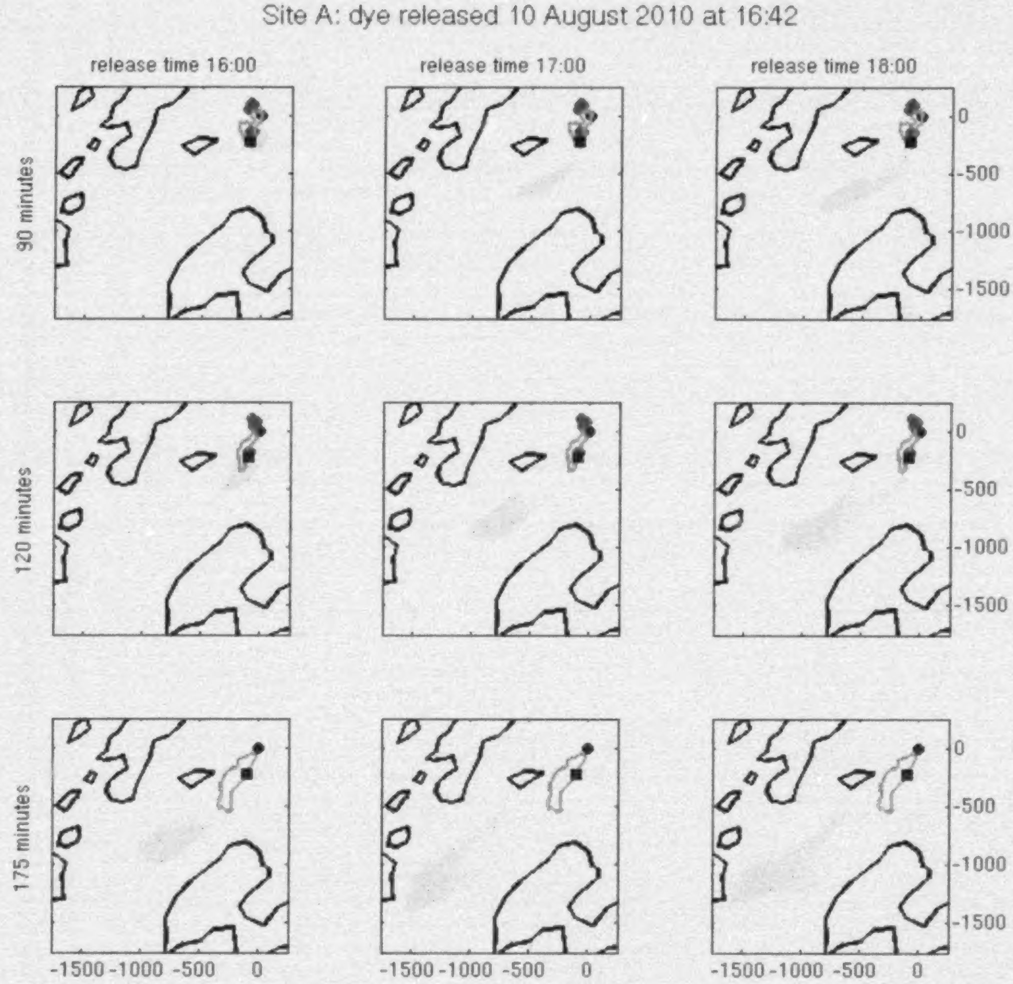
Site A: dye released 10 August 2010 at 16:42
release time 16:00
release time 17:00
release time 18:00
90 minutes
120 minutes
175 minutes
0
-500
-1000
-1500
-1500 -1000 -500 0

Figure 47. Comparison of results of particle tracking model to dye perimeter data for the dye experiment at Site A on the 10th of August 2010. The dye release location is indicated by a black dot. Observational data include the drifter locations (blue circle), the perimeter of the dye (red line) and the location of ADCP A1 (black square). The particle patch is shown in cyan. Times are given in minutes past the release time.

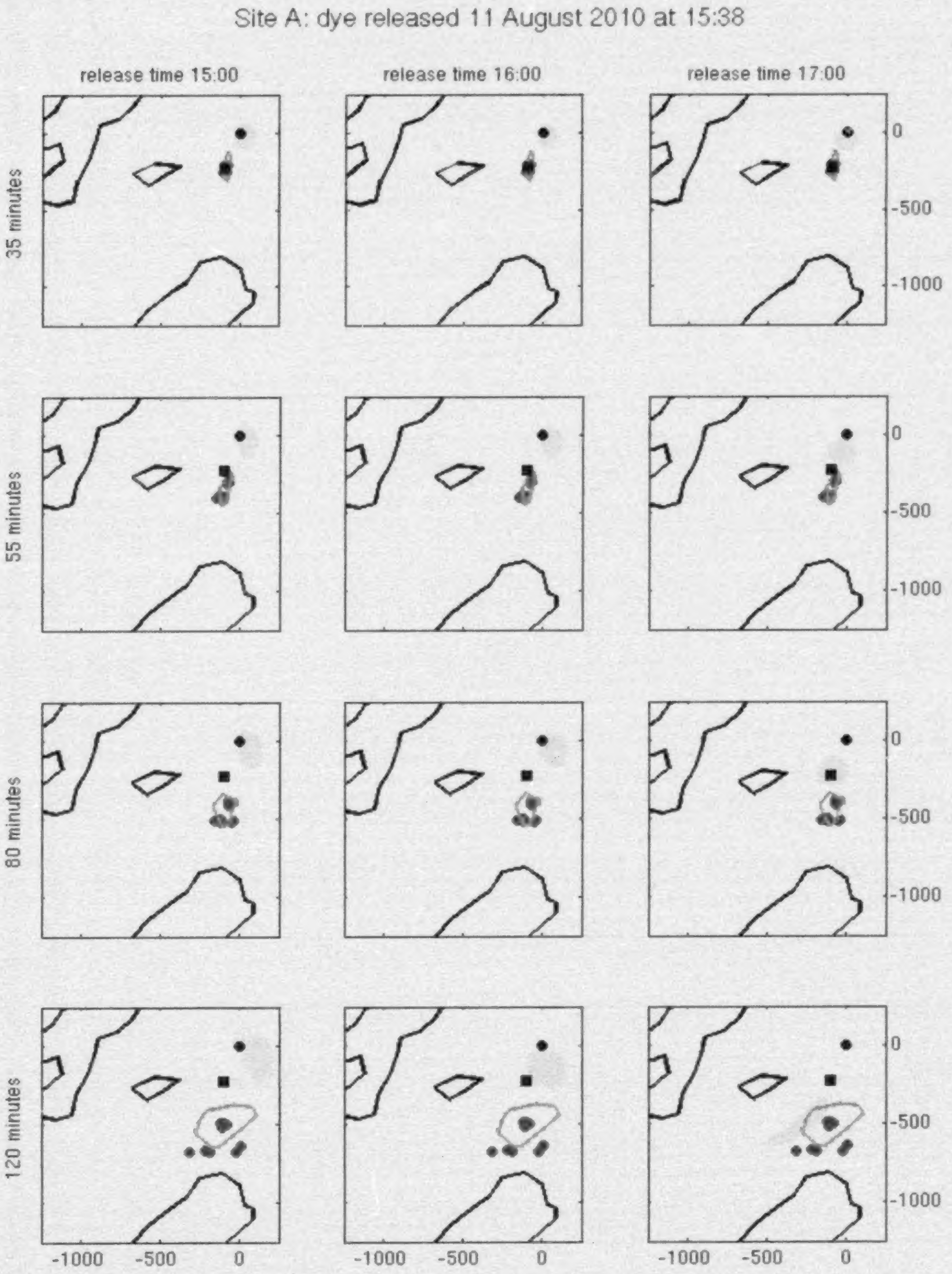
Site A: dye released 11 August 2010 at 15:38
release time 15:00
release time 16:00
release time 17:00
35 minutes
55 minutes
80 minutes
120 minutes
0
-500
-1000
-1000
-500
0

Figure 48. Comparison of results of particle tracking model to dye perimeter data for the dye experiment at Site A on the 11th of August 2010. The dye release location is indicated by a black dot. Observational data include the drifter locations (blue circle), the perimeter of the dye (red line) and the location of ADCP A1 (black square). The particle patch is shown in cyan. Times are given in minutes past the release time.

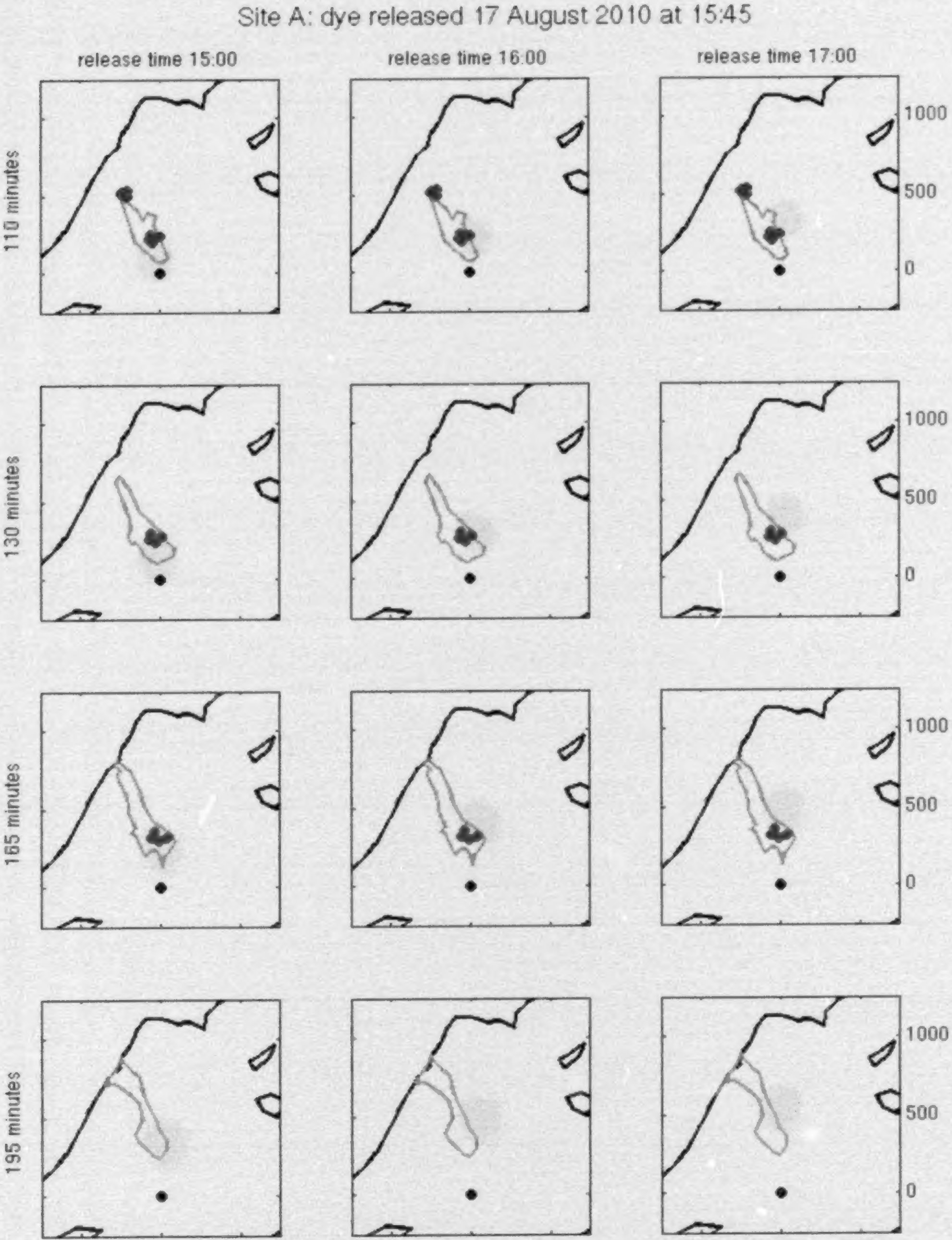
Site A: dye released 17 August 2010 at 15:45
release time 15:00
release time 16:00
release time 17:00
110 minutes
130 minutes
165 minutes
195 minutes
1000
500
0
-500
0
500

Figure 49. Comparison of results of particle tracking model to dye perimeter data for the dye experiment at Site A on the 17th of August 2010. The dye release location is indicated by a black dot. Observational data include the drifter locations (blue circle) and the perimeter of the dye (red line). The particle patch is shown in cyan. Times are given in minutes past the release time.

Site B – 8th, 10th and 14th of September 2010

At Site B, there were three different dye release studies conducted on the 8th, 10th and 14th of September 2010. Comparisons of the model results with the dye perimeter data are shown in Figure 50, Figure 51 and Figure 52. On the 8th and 10th of September 2010 (Figure 50 and Figure 51), the currents at the time of the dye release were going in the same direction. For the 8th of September 2010 release (Figure 50), the particles tracking simulation with the particle release time of 16:00 compare best with the observations in that the head of the particle patch tracks the head of the dye patch in the along-shore distance. The simulations for the 10th of September 2010 (Figure 51) indicate that the particle patch trajectory would best match the observed dye patch trajectory for a particle release time somewhere between 16:00 and 17:00. Results for both the 8th and 10th of September 2010 releases are consistent with the predicted current phase which lags the observations by up to one hour. Although along shore distances travelled by the particle patch are in reasonable agreement with the observations, the modelled particle patch move closer towards shore than the observed dye plume. In both cases, the dye leaks slowly from the cage site resulting in a narrow elongated dye patch. As the model does not have any drag included for the cages, the particles separate immediately from the release site.

On the 14th of September 2010, two cages at the same farm site were treated in close succession. The tarp for the first treatment was removed at 15:52 and that for the second treatment about ten minutes later. Due to the proximity of the release times in the field study, the model was run with particles being released simultaneously from two cages. Similar to the modelled results for the 8th and 10th of September 2010, the results of the simulation for the 14th of September 2010 (Figure 52) do not reproduce the slow release of the dye from the cages. Unlike the simulations for the 8th and 10th of September 2010, the head of the particles patch does not track the head of the dye patch for the expected time based on comparisons of modelled and observed currents (somewhere between 16:00 and 17:00). Instead, the model predicts the particles moving away too quickly from the cage site. The observations made in the field indicate that the dye was slow to move away from the cage site as it was moving through the cages after it was released. In order to reproduce this behaviour, a surface drag needs to be added to the model to account for the presence of the cages and the effect that they have on the water flow.

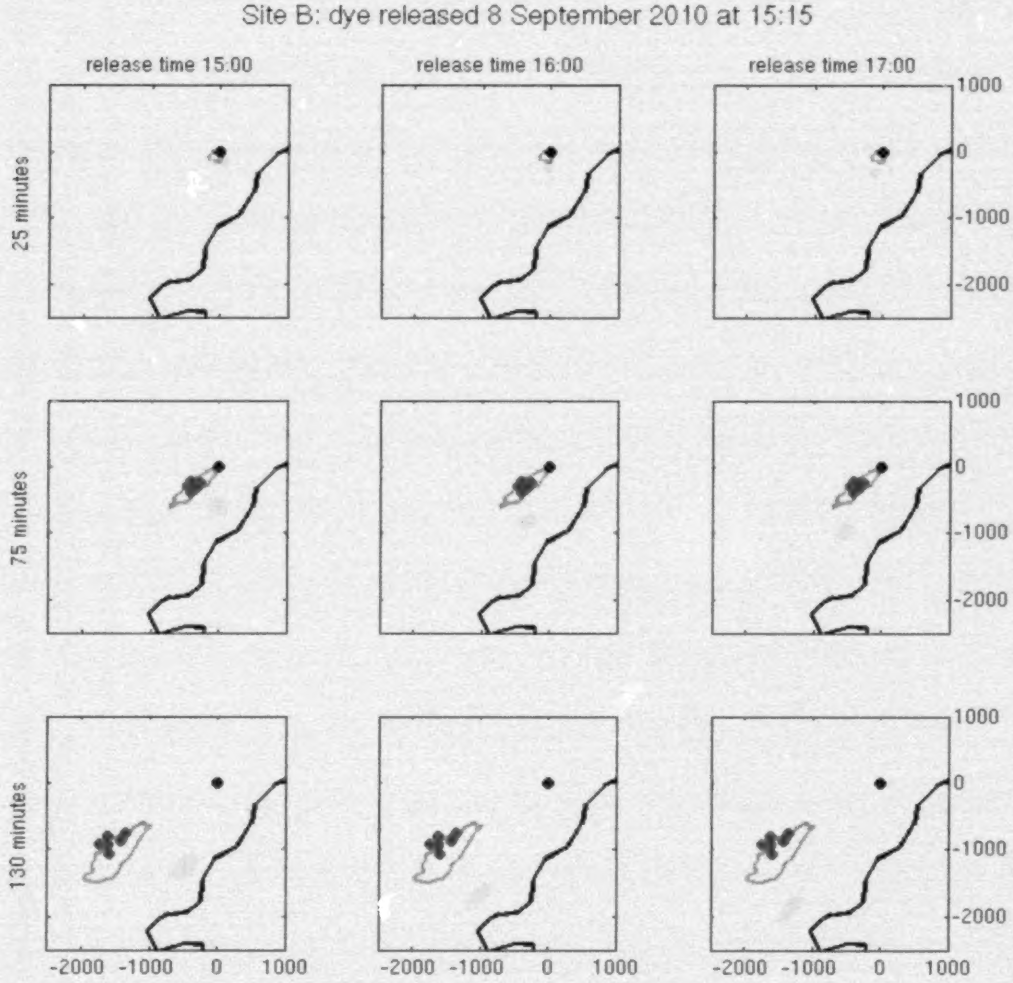

Figure 50. Comparison of results of particle tracking model to dye perimeter data for the dye experiment at Site B on the 8^{th} of September 2010. The dye release location is indicated by a black dot. Observational data include the drifter locations (blue circle) and the perimeter of the dye (red line). The particle patch is shown in cyan. Times are given in minutes past the release time.

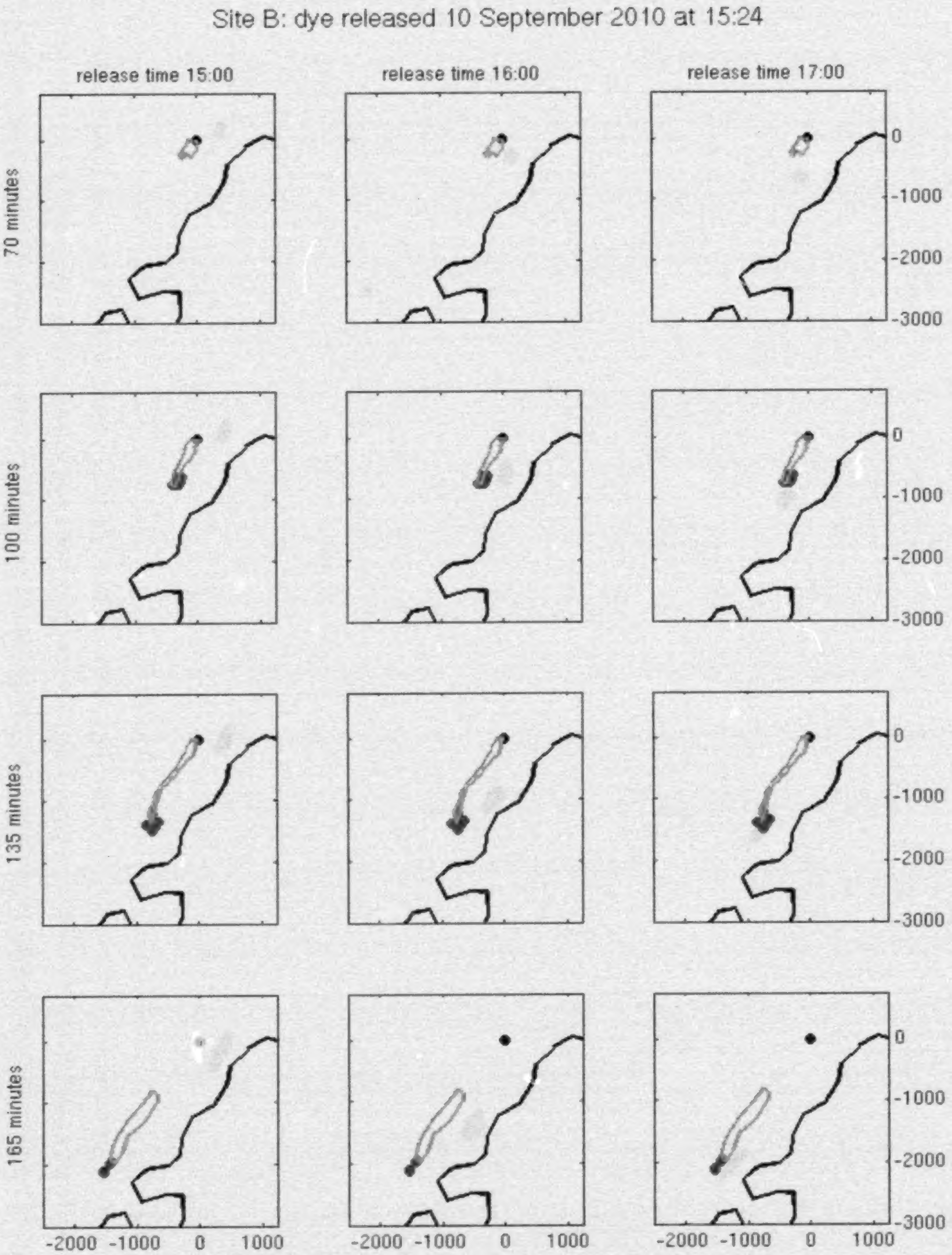

Site B: dye released 10 September 2010 at 15:24

release time 15:00
release time 16:00
release time 17:00
70 minutes
100 minutes
135 minutes
165 minutes
0
-1000
-2000
-3000
-2000 -1000 0 1000

Figure 51. Comparison of results of particle tracking model to dye perimeter data for the dye experiment at Site B on the 10th of September 2010. The dye release location is indicated by a black dot. Observational data include the drifter locations (blue circle) and the perimeter of the dye (red line). The particle patch is shown in cyan. Times are given in minutes past the release time.

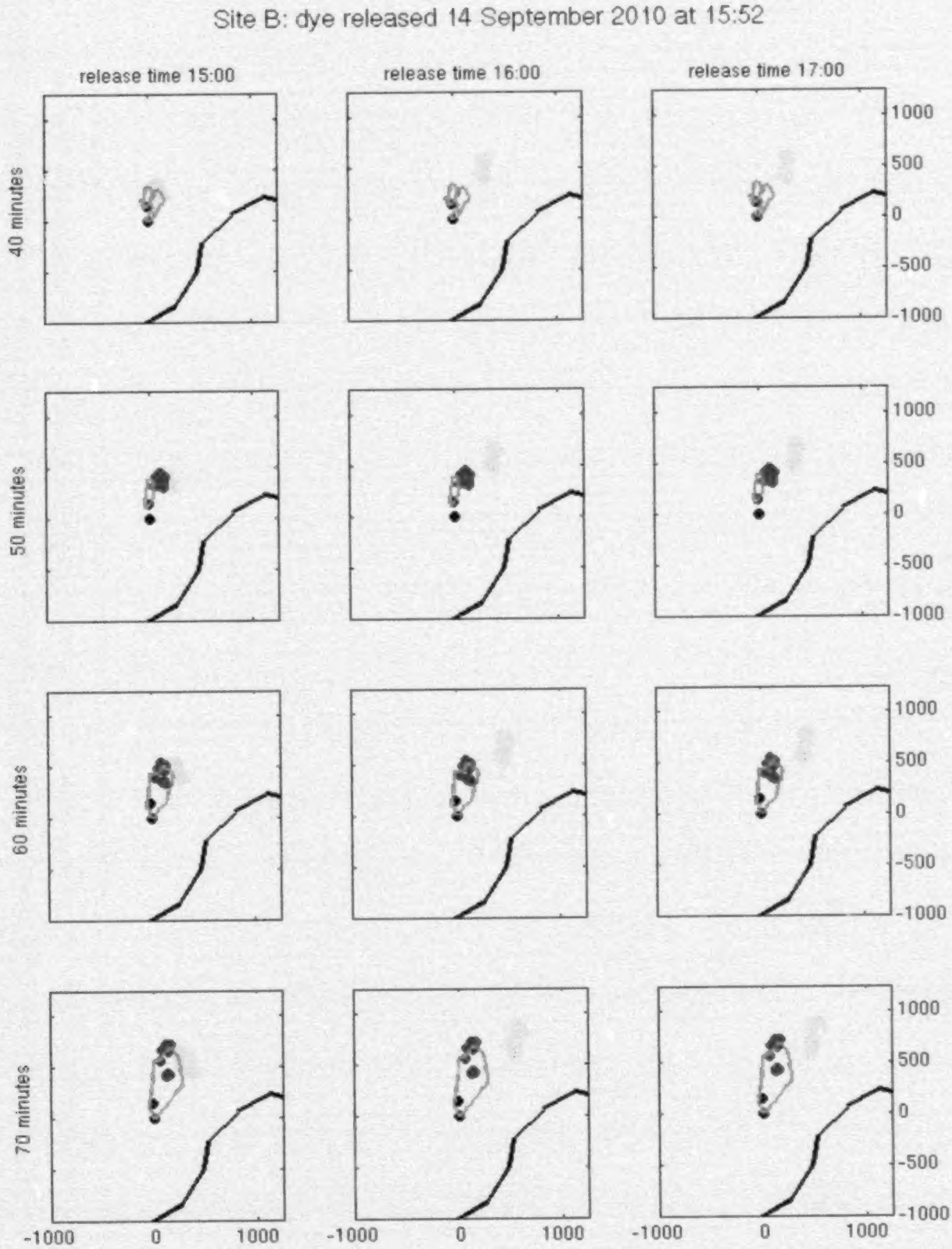
Site B: dye released 14 September 2010 at 15:52

release time 15:00

release time 16:00

release time 17:00

Figure 52. Comparison of results of particle tracking model to dye perimeter data for the dye experiment at Site B on the 14th of September 2010. The dye release location is indicated by a black dot. Observational data include the drifter locations (blue circle) and the perimeter of the dye (red line). The particle patch is shown in cyan. Times are given in minutes past the release time.

Site C – 27th of October 2010

At Site C, a single dye release study was conducted on the 27th of October, 2010. Results of the particle tracking model for this case are shown in Figure 53. The best match between the evolution of the modelled particle patch and the observed dye patch occurs when the particles are released at 15:30. This is the same time that the tarp was removed, and hence the dye was released, in the field study. The matching of the observed and modelled release times is not surprising as the tidal current phases are accurately modelled at this site (Table 14). Initially the particle patch travels too quickly (Figure 53, 40 minutes post release). This is somewhat surprising as results in Table 14 indicate that the modelled current speeds are too slow at this site. However, Figure 39 shows a vertical variation in modelled speed with the bottom speeds being much slower than the surface speeds due to the bottom boundary layer. It is possible that the modelled surface speeds are too high and seems likely in light of the results of the particle tracking model. Unfortunately, due to the shallow depths at this site, the ADCP data does not extend far enough to the surface to verify this hypothesis. Although the head of the particle patch leads the head of the dye patch throughout the simulation, from 70 minutes post release time and onward its position matches the drifter positions. Near the end of the patch trajectory the tail of the particle patch matches the tail of the dye patch reasonably well but the model particle patch is much wider than the observed dye patch.

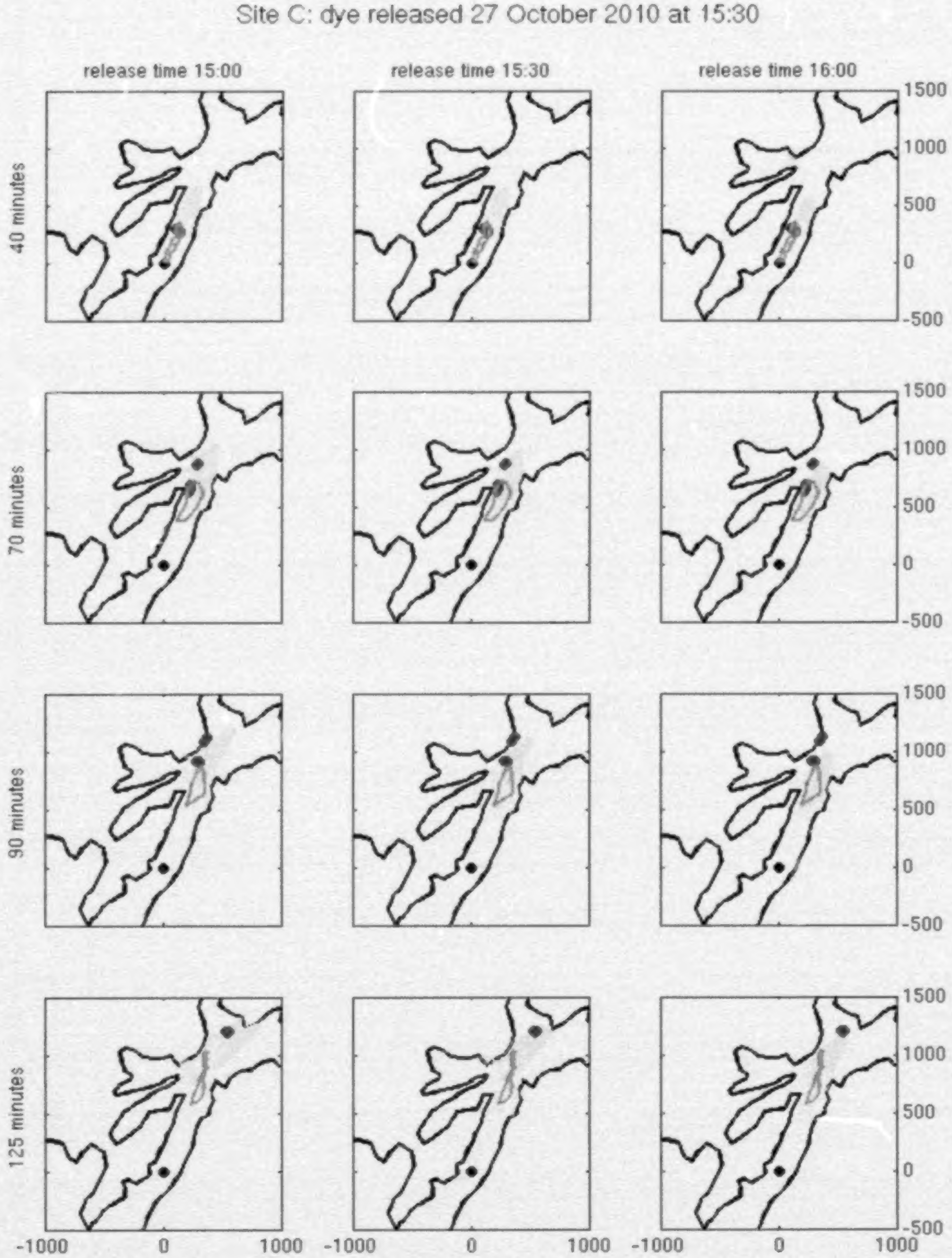
Site C: dye released 27 October 2010 at 15:30
release time 15:00
release time 15:30
release time 16:00
40 minutes
70 minutes
90 minutes
125 minutes
1500
1000
500
0
-500
-1000
0
1000

Figure 53. Comparison of results of particle tracking model to dye perimeter data for the dye experiment at Site C on the 27th of October 2010. The dye release location is indicated by a black dot. Observational data include the drifter locations (blue circle) and the perimeter of the dye (red line). The particle patch is shown in cyan. Times are given in minutes past the release time.

Dilution of Concentrations: Okubo-Based Approach

The following describes comparisons between predicted rates of dilution and observed concentrations of dye and therapeutants.

In the following comparisons dye concentrations were calculated as the depth average of measured concentrations over the depth range from the sea surface to the maximum depth at which dye was observed. The therapeutant concentrations were determined from single point water samples collected near the middle of the evolving dye patches; they include measurements of azamethiphos (Salmosan®) and deltamethrin (Alphamax®).

All models predict the general dilution pattern of dye and therapeutants.

The Fickian-based model, described above, compares favourably with the observations over the initial hour after release whereas at times greater than this it overestimates the concentrations (Figure 54).

The modified Okubo-based model, the model that accounts for an initial increase in patch spreading due to cage infrastructure, fits the observations quite well over the full time range of the observations (Figure 54). The unmodified Okubo model under-estimates the dilution. The latter point is shown in a different way by a scattergram comparing the unmodified Okubo estimate of dye concentrations at various times with near surface average concentrations of dye derived from horizontal fluorescence transects taken through the dye plumes at various times (Figure 55). In the latter approach predicted or calculated average concentrations of dye were based on the amount of dye used in each trial (M) divided by the estimated volume (V) of the plume at a specific time. The volume of the plume was estimated from the area of the plume multiplied by the depth. The area of the plume was based on the patch outlines obtained at various times during each trial. The depth of the plume was based on the vertical profiles of dye concentration taken in the plume at or near the same times as the outline tracks. This approach assumes there is no loss or decay of the dye over the time scale of the observations. These calculated concentrations were then compared with the average measured dye concentration in horizontal transects completed at the same times as the plume outlines. The horizontal transect data were from 1-3 m below the water surface.

Although there is a relatively good agreement between the calculated and measured dye concentrations (Figure 55), there is a tendency for the calculated dye concentrations to exceed the observed concentrations at the lower end of the observed concentration range. There is also an outlier exception, a data point corresponding to the 10th of August 2010 release at Site A. This point had the lowest measured dye concentration and it was much lower than the calculated concentration. Part of the discrepancy at the lower levels of concentration may be associated with the practical issue that when dye concentrations were low, the ability to trace the outline of the patch was hindered due to difficulty in seeing the patch edge. This may have resulted in an underestimate of the patch volume and hence, an overestimate of the calculated dye concentration. Another factor is that, in some cases, horizontal transect data from near surface transects, especially those taken in the top 1 m from the water surface, may have been low, due to dye degradation caused by sunlight.

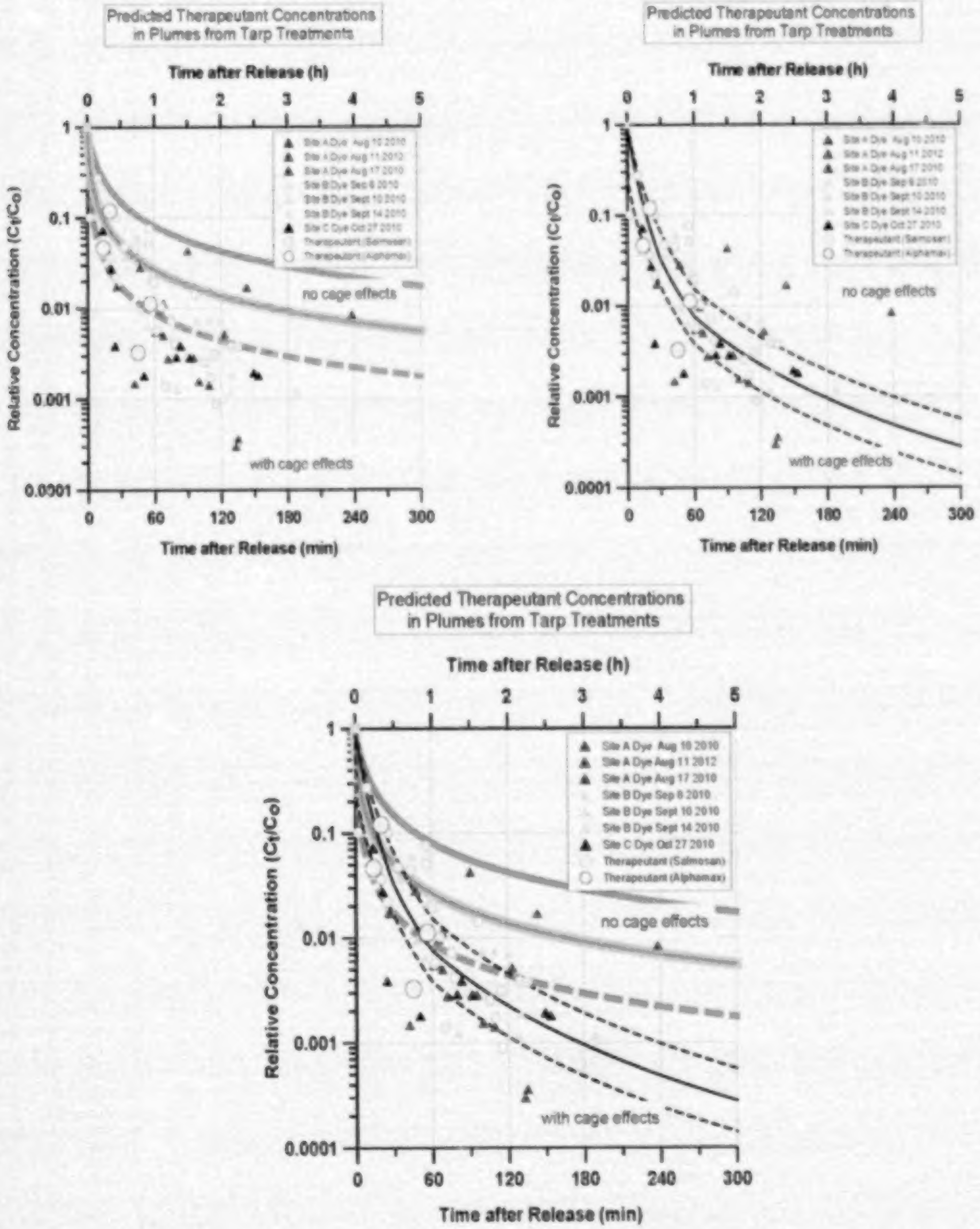

Predicted Therapeutant Concentrations in Plumes from Tarp Treatments

Predicted Therapeutant Concentrations in Plumes from Tarp Treatments

Predicted Therapeutant Concentrations in Plumes from Tarp Treatments

Figure 54. Comparisons of Fickian (red curves) and modified Okubo (black curves) based dilution models with observed concentrations of dye and therapeutant. Fickian and Okubo model estimates of the temporal decrease in the standardized dye or therapeutant concentration ($C(t)/C(t=0)$) after release from a tarped cage. The Fickian curves are based on equation 16. The Fickian curves assume a constant depth of 5 m and values of $K_x = K_y = 0.1$ m^2 s^{-1}. The Okubo curves include an initial increase in the rate of horizontal patch spread due to cage effects and a patch depth that remains at a constant depth of 5 m.

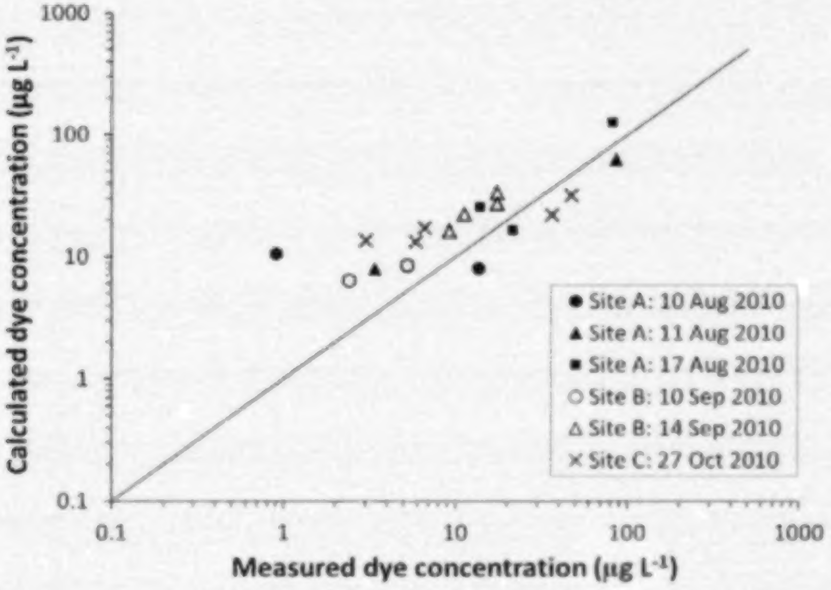

Figure 55. Comparison of measured and calculated dye concentrations in dye plumes resulting from tarpaulin treatments of net-pens.

Dilution of Concentrations: FVCOM-Based Approach

The FVCOM model predictions of depth average concentrations of pseudo dye were also compared to in situ measured concentrations, by plotting each concentration against the time since release on the same plot. FVCOM average concentrations were determined from the model particle tracking outputs for the releases simulating particle transport and dispersal at the study sites. The FVCOM average concentrations were calculated as the total number of particles divided by the volume of water occupied by the particle patch at a given time. Each model run consisted of three releases of particles, one near the actual time of release, another about one hour after the release and a third about one hour before the release. This was to help account for differences in the phasing between model and observed currents. In all cases the particles were initially distributed over the upper 10 m and assumed to be contained within a constant depth of 10 m for the full simulation. The particle tracking model assumed no vertical diffusivity and a horizontal diffusivity of 0.1 m^2/s. No cage friction parameter was added to the model for these comparisons.

The comparison between the observations and the model predictions is shown in Figure 56. The observed concentrations are the same as those shown above for the Comparisons with Fickian and Okubo based predictions, with the exception that the outliers in the observations have not been removed from these plots. The outliers, the data points in the lower left hand corner of the plots, correspond with measurements taken near the outside edge of the dye patches where dye concentrations were very low and patchy. The model seems to be predicting the general magnitude and rate of dilution reasonably well at all three sites, although it may be underestimating the dilution at the longer time scales. Even when the outliers are not shown, the observations show a lot of scatter due to spatial patchiness whereas the model predictions are much less variable.

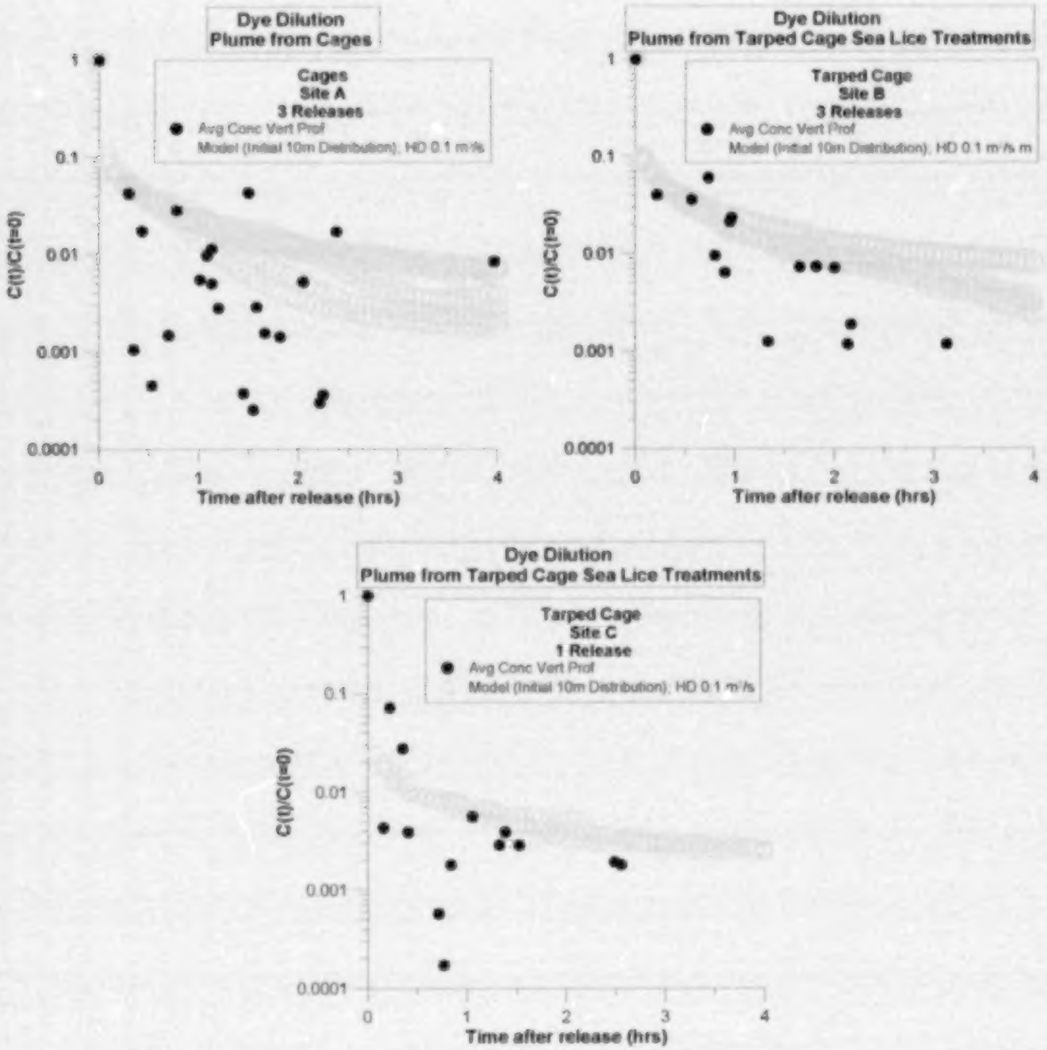

Figure 56. Predicted and measured dilution after salmon cage and tarp releases at three sites. Predicted dilution are based on FVCOM particle tracking model results (see above for more detail). Empirical data are average concentrations measured in vertical profiles from the surface to the maximum depth where less than 99% of the dye is contained.

Model Limitations and Potential Areas for Improvement

The presence of fish net-pens in the water adds an additional friction to the flow which is not included in the FVCOM model. Results of the numerical experiments indicate that this additional friction needs to be included in the model in order to reproduce the slow release of dye from the fish cages (Wu et al. in preparation). This is evident at Site A on the 10th of August 2010 (Figure 47) and Site B on the 8th, 10th and 14th of September 2010 (Figure 50, Figure 51 and Figure 52) where the dye continuously leaves the fish cage site for up to 2 hours past the release time. There are other features that are not captured by the model that cannot be attributed to the lack of the fish cage drag in the model. For example, at Site A the modelled currents at ADCP deployment A1 is over-estimated. At this site, the fish cages had been removed at the time of the dye study with a single cage put in place for the dye release field work. It is speculated that the additional surface drag due to the presence of a single cage with no additional infra-structure is minimal. Hence the over-estimation of the currents at this site by the model is likely due to another mechanism. In contrast, at Site C, it was seen that the modelled current speed was too low. Since adding extra drag to model the fish cages would only slow the modelled current down further, another explanation is needed to account for model under-estimating the current speed at this location.

In terms of improving the physical model there are three areas that may need to be addressed: variable bottom drag, baroclinicity and wind events. Using an FVCOM implementation for the upper Bay of Fundy, Wu et al. (2011) were able to get improved modelled performance by including variable bottom friction. The version of FVCOM used in this study does not have this additional variable bottom friction capability. In the calibration of the physical model it was necessary to use a large value of the bottom friction to get reasonable agreement with the tidal sea surface heights amplitudes and phases in the upper Bay of Fundy. This large bottom drag may result in poor prediction of the currents' phase, especially near the bottom.

In the Bay of Fundy, circulation is predominantly tidal and the waters are vertically well mixed in many areas, particularly in the inner Bay, off southwest Nova Scotia and in areas of southwest New Brunswick. For this reason, initial modeling efforts focused on a barotropic implementation of FVCOM. Work on a baroclinic version of the model is underway since density profiles obtained from CTD casts in the dye study areas indicate that weak stratifications in the surface layer are present at some locations and times. It is unknown if this amount of stratification is sufficient to affect the circulation. Earlier comparisons between barotropic and baroclinic model results using a different model of the area showed little difference in the circulation between the two implementations. Finally, as the therapeutants are released at the surface, the movement of the therapeutants is dictated by the surface currents which in turn are impacted by wind events. Thus, unless treatment only occurs on calm days, the inclusion of wind events may be necessary to adequately model the surface circulation. Fortunately, net-pen tarp and skirt treatments tend to be during calm weather since the treatments cannot be safely and efficiently done in other conditions.

As mentioned above, the inclusion of the effect of the cages is needed for better prediction of the surface currents at the cage sites and, as a result, to properly model the slow release of the dye from the fish cages. One way of modelling the presence of the fish cages is to introduce a surface drag at the fish farm locations. Although the surface drag does not include specific details of the fish cage structure, addition of a drag in the surface layer in areas where fish cages are present is one way of including the effects of fish cages in a larger scale model (Venayagamoorthy et al. 2009, Shi et al. 2011). This method has recently been implemented into FVCOM (Wu et al., in preparation) and preliminary runs using this model are presented here. The cage friction drag used in the results presented here was 0.18. This is a value used by Wu et al. (in preparation) which was obtained by initial calibration of model results against ADCP data from Site A from an earlier time when fish cages were present. The value may change in the future as a result of more detailed investigations and model parameterizations. Results of the particle tracking model using velocities calculated by FVCOM including surface cage friction are shown in Figure 57 for Site B on all three days that dye studies were conducted. Compared to the run without cage drag (centre columns of Figure 50, Figure 51, Figure 52), there are substantial differences. When the cage drag is included, the particles leave the cage more slowly, and underestimate the displacement of the dye patch and drifter trajectories.

By including a surface drag to model the presence of the fish cages, it was seen that the model results are substantially changed indicating this route needs to be further investigated. The main obstacle in implementing this method is determining what value of drag to apply to the surface. Wu et al. (in preparation) determined the value to use by calibrating the model against observations at a single site and time. Further study is needed in order to determine the exact nature of the effect of the cage infrastructure on the flow. There are several possible approaches to this involving field studies, laboratory experiments or the use of numerical models (or computer experiments). In Fan et al. (2009), ADCP data were used to study how the vertical structure of tidal current is changed by the presence of aquaculture raft structures. Using the ADCP data collected throughout southwest NB, this is one way that investigating the effects of fish cages on the currents could proceed. The laboratory offers a controlled environment in which to measure cage drag using a scaled model of the fish cage structures in a flow tank. On the numerical side, computational fluid dynamics (CFD) methods which solve the full Navier-Stokes equations can be used to model small scale flows around the fish cages themselves. Although work is underway to couple a CFD model with FVCOM (Wu and Tang 2010), this is not likely the direction of choice for this application. CFD models are very costly to run due to their very fine grids. Their use here would be to use results of CFD models of fish cage flow to calculate drag to be used in large scale models like FVCOM.

Although including the cage drag into FVCOM influences the results, it does have the drawback that the model must be re-run whenever a new farm site is to be studied which is time-consuming. With current computing capabilities and using the FVCOM code that includes variable bottom drag and cage friction, a 30-day simulation takes approximately two weeks of execution time. Additionally, to properly include an aquaculture site in the model, the model grid may need to be refined, further increasing the time needed to run the model. An alternative is to include the effects of the fish cages directly into the particle tracking model. As a first approximation, the effects of the fish cages were included into the particle tracking model by reducing the horizontal velocity at the fish cage site by 75% and linearly increasing the velocity to its full value over a distance of 500 m from the cage site. Although this does not include the increases of current below and around the cage site, the particle tracks shown in Figure 58 indicate that there is potential to this approach. This method requires a good understanding of how the fish cages affect the current which, as discussed above, requires further investigation. As mentioned above, inclusion of the cage drag in the FVCOM model influences the flow field and prediction of the particle trajectories. The particle trajectories estimated using the FVCOM plus cage drag velocities enhances the underestimate of the displacement of the dye patch and drifters.

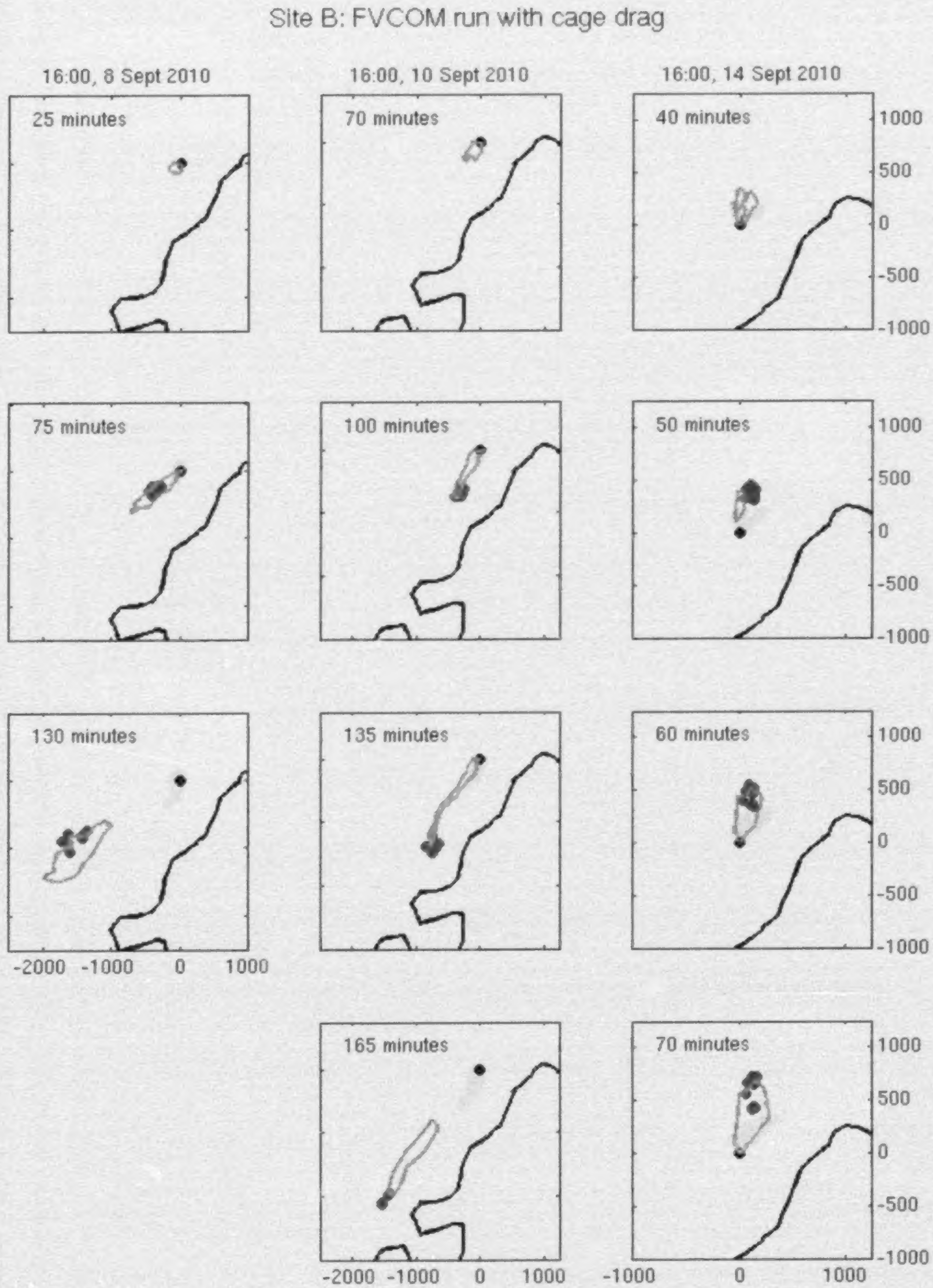
Site B: FVCOM run with cage drag
16:00, 8 Sept 2010
16:00, 10 Sept 2010
16:00, 14 Sept 2010
25 minutes
70 minutes
40 minutes
75 minutes
100 minutes
50 minutes
130 minutes
135 minutes
60 minutes
165 minutes
70 minutes
1000
500
0
-500
-1000
-2000
-1000
0
1000

Figure 57. Comparison of the results of particle tracking model for the dye experiment at Site B when the effects of fish cage drag are included in the model. The dye release location is indicated by a black dot. Observational data include the drifter locations (blue circle) and the perimeter of the dye (red line). The particle patch is shown in cyan. Times are given in minutes past the release time.

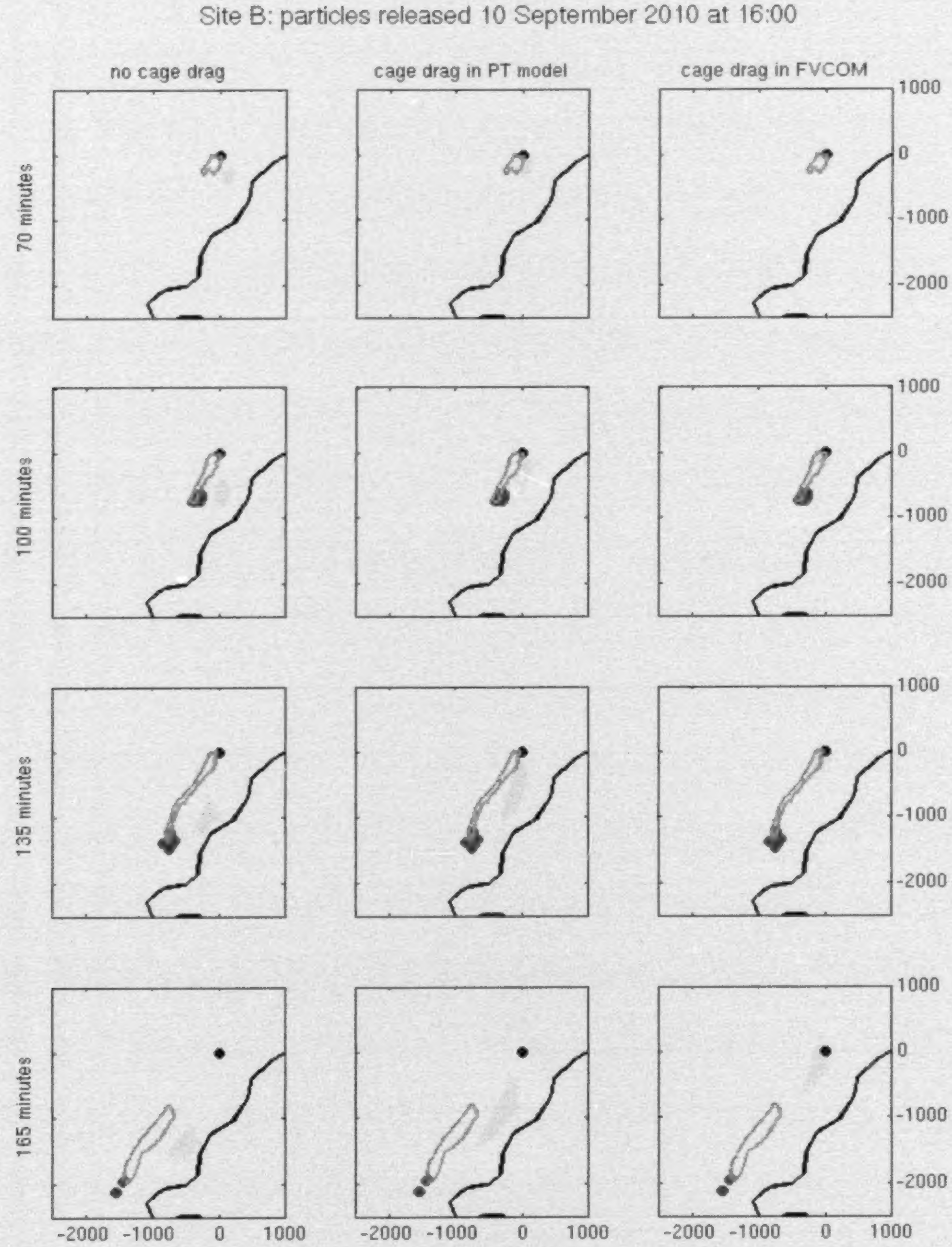
Site B: particles released 10 September 2010 at 16:00
no cage drag
cage drag in PT model
cage drag in FVCOM
70 minutes
100 minutes
135 minutes
165 minutes
1000
0
-1000
-2000
-2000 -1000 0 1000

Figure 58. Comparison of different ways to incorporate effect of fish cage drag on the results of particle tracking model for the dye experiment at Site B on the 10th of September 2010. The dye release location is indicated by a black dot. Observational data include the drifter locations (blue circle) and the perimeter of the dye (red line). The particle patch is shown in cyan. Times are given in minutes past the release time.

Comparison with SEPA Model

The Scottish Environment Protection Agency (SEPA) has developed a management model to simulate the dispersion of soluble sea lice treatment chemicals after their release into the water column from salmon net-pens. This model is being actively used as a guide in determining the licensed quantities of pesticides allowed in the treatment of sea lice in the Scottish aquaculture industry. The SEPA model is the combination of two complimentary models: a short-term model which is only valid for periods of up to 6 hours and a long-term model for chemicals that remain at potentially toxic concentrations for periods greater than a tidal cycle. A comparison is made between the underlying assumptions of the two SEPA models and the two models examined here: the Okubo model and the FVCOM model. Specifically, the assumptions regarding current speed, horizontal dispersion, closed boundaries and vertical mixing are examined.

Current speed: SEPA's short-term model uses the mean current speed whereas the long-term model uses M2-tidal and residual currents. Our implementation of an Okubo-based dispersion model uses near-surface current meter or FVCOM predicted current data, both of these include the mean flow as well as the tidal currents. The current meter data includes all aspects of the flow including the mean, tidal and wind driven flows. For all three models, there is no spatial variation in the current field. The long-term SEPA model and the Okubo model use currents that have temporal dependencies. Since the tides in the Bay of Fundy area are M2 dominated, it is useful to use a time varying current rather than a mean flow as required in the short-term SEPA model. Also, in the Bay of Fundy there is significant variation in the tidal currents due to spring-neap cycles and tidal constituents in addition to the M2, hence the long-term SEPA model will not reproduce.

All models that assume spatial homogeneity of the flow can be of somewhat limited use in a area such as southwest NB, where the bathymetry and coastline varies on short length scales (100s of m) and the flow is interrupted by multiple islands and peninsulas. Examples using the Okubo model (Figure 44, Figure 45 and Figure 46) show that even current meters that are placed within close proximity to each other can yield significantly different results. The FVCOM particle tracking model uses the current predicted to by the FVCOM model which varies both temporally and spatially. It was found, however, that the FVCOM model had difficulties accurately reproducing the currents especially in terms of the phase. In areas where the current fields are fairly spatially uniform, the use of a single current record would likely produce reasonable results.

Horizontal eddy diffusivity: All four models include horizontal eddy diffusivity. For the SEPA short-term model, horizontal diffusivity is proportional to $t^{1/1}$ and is included in the lateral direction only, the direction perpendicular to the direction of major advection. Horizontal diffusivity is assumed to be negligible relative to advection in the longitudinal direction, i.e., the direction of advection. In the SEPA long-term model, FVCOM and Okubo-based models, diffusivity is included in both the lateral and longitudinal directions and the coefficients of horizontal eddy diffusivity are assumed to be the same in both directions. This is in contrast to the measured values for which the rates in the lateral direction are an order of magnitude smaller than the rates of diffusivity in the longitudinal direction. The SEPA long-term model uses a constant coefficient of horizontal eddy diffusivity (i.e., Fickian diffusion) whereas the Okubo model uses a coefficient of eddy diffusivity that increases with the horizontal scale of the dispersal patch and hence with time. The FVCOM particle tracking model uses a random walk model with a constant coefficient of horizontal eddy diffusivity resulting in diffusion that is Fickian in nature. Observations indicate that the diffusivity coefficient for the dye patches follow Okubo's empirical formula when no cage is present but in the presence of fish cages the initial increase in patch size is enhanced as it exits the farm site. Once past the farm site infrastructure, the rate of increase in patch size agrees well with the Okubo relationship. It should be noted that none of the models discussed here include this initial enhanced mixing due to the presence of the aquaculture farm site infrastructure. It should also be noted that the scale dependent increase in diffusivity that is observed may to some extent be captured by the models that include the spatial variation in the current.

Closed boundaries: Both the short and long-term SEPA models take into account lateral boundaries (i.e., coastlines). Due to the short time scales for which the model is used, the SEPA short-term model has a single closed boundary which represents the shore. If the treatment patch impinges on the shore boundary due to lateral dispersion, one half of the patch ellipse is reduced to the distance to the shore. The SEPA long-term model allows for three different topographic categories: open waters, a strait, or a sea loch which have one, two or three closed boundaries, respectively, from which patches are reflected when they encounter a boundary. The SEPA long-term model does not allow for realistic representation of the coastline and the its three topographic categories are not representative of most of the southwest NB area. The approach is to provide three different schemes which represent the three different types of topography. The FVCOM particle tracking model allows for realistic representation of the coastline. The coastline is treated as a free-slip boundary: when a particle encounters the coastline it cannot pass through the coastline but can move along or away from the coastline depending on the direction of the local current. At this time, the Okubo model does not have the ability to deal with coastlines.

Vertical mixing: Both SEPA models assume that vertical mixing is constrained by stratification and that the treatment patch remains in a fixed depth surface layer. The surface layer depth is the lesser of 10 meters and half of the water depth. It is assumed that all chemicals are vertically well mixed in the surface layer. When calculating the concentration of chemicals within the patch, the FVCOM particle tracking model also assumed that the particles, and hence the chemicals, were confined within a fixed depth surface layer. In this study, the depth of the surface layer was 10 m regardless of the water depth of the study site. This assumption was based on measurements of the dye concentrations within a patch which rarely detected dye below 10 m from the surface. Similarly, in calculation of concentration using the Okubo model, it was assumed that the chemicals are uniformly mixed in a surface layer. The surface layer had an initial depth of 4 m to model the shallowing of the cage during treatment. The surface layer was allowed to increase to a depth of 10 m over a specified period of time after which it was kept constant.

The above comparisons lead to the following classifications of the models: simple (SEPA short-term model), intermediate (SEPA long-term model and the Okubo model) and complex (FVCOM). The use of the simple model in southwest New Brunswick is of limited application as it is an area with complex coastlines and highly variable currents. The long-term SEPA model and the Okubo model are similar in complexity. Differences include the models used for the horizontal eddy diffusion and the treatment of the boundaries. While the Okubo model uses the more realistic time varying model for the coefficient of horizontal eddy diffusivity, it does not include any coastlines. The long-term SEPA model uses a constant horizontal eddy diffusivity coefficient but only allows for three different types of coastlines, none of which are particularly representative of the southwest NB situation. The FVCOM model is by far the most complex model discussed here providing both spatially and temporally varying current fields and realistic coastline representations.

Summary of Net-Pen Model Results

Models are important tools as they can be used to easily assess a wide range of scenarios which may not be feasible to do if one is to rely on field observations alone. That being said, it is important to keep in mind that a model is a representation of reality and, regardless of the complexity of the model, is based on a set of assumptions and simplifications. As a result, it cannot be expected that models will exactly reproduce observed conditions. For this reason, assessment of model performance requires not only empirical data with which to compare but knowledge of the model's assumptions, simplifications and intended use. In this paper, two models were examined, one at each end of the complexity scale.

The simpler model has the advantage of being easy to implement with no calibration required. In the model, the dye patch is assumed to be circular. Its horizontal spread is assumed to be in the radial direction only and its rate is determined by the Okubo model. The Okubo model is an empirical model based on a large data set assembled from numerous dye patch evolution studies. It assumes that the horizontal diffusion increases with the size of the patch. In the absence of any aquaculture farm site infrastructure, the spread of an observed dye patch in southwest New Brunswick agrees well with Okubo's model although the model does not take into account the characteristic elongation of the observed dye patch. When the dye is released from an aquaculture cage site, a modification to the Okubo model is required to take into account the enhanced initial spreading of the dye patch due to the presence of the cage site. Once the dye patch has cleared the cage site, however, the rate of increase of the dye patch size agrees with that of the Okubo model. The horizontal movement of the dye patch is calculated using collected current meter data. Use of the current meter data assumes that the current field is temporally variable but spatially homogeneous. At several of the study sites, the current field has a high spatial variability. At these locations using current meter data from a single location gives predicted trajectories that are not always in directions consistent with observations and magnitudes of the displacements which are not always similar to observations.

At the other end of the spectrum is the coastal ocean circulation model, FVCOM, with its accompanying particle tracking module. FVCOM is a state of the art model which solves the equations governing the fluid flow. It allows for realistic representations of the coastline and bathymetry and can include effects such as winds and river discharges. FVCOM computes both temporally and spatially varying current vector fields and sea surface heights. Due to the strong tidal nature in the Bay of Fundy, the FVCOM implementation for southwest New Brunswick assumes the flow is barotropic, neglects wind forcing and the open boundaries are forced with the five principal tidal constituents: M2, N2, S2, K1 and O1. Assessment of the FVCOM model results indicate that although the model faithfully reproduces the sea surface heights, it had problems accurately predicting currents in some areas especially in terms of the phase.

Particle patches were used as a proxy for the dye. The particles were advected using the FVCOM current fields. It was found that the particle tracking model did not adequately represent vertical dispersion of the particles and vertical dispersion was not included, dispersal was only due to horizontal processes. In the horizontal, diffusion was modelled using a random walk method which results in a Fickian type of diffusion. The shape of the particle patch depended on both the current field and the value of the constant horizontal dispersion parameter. Comparisons between observed and modelled dye patches show differences in the shape of the plumes, direction of drift and magnitude plume displacements.

Although results of both models indicate that there are challenges in modelling single dye releases, there is potential in using the models to determine the total area of potential exposure. Using the FVCOM current fields and the particle tracking model, if particles are released at all phases of the tide, then the exposure envelope generated by the model encompasses the majority of the areas exposed during dye release studies (Figure 59).

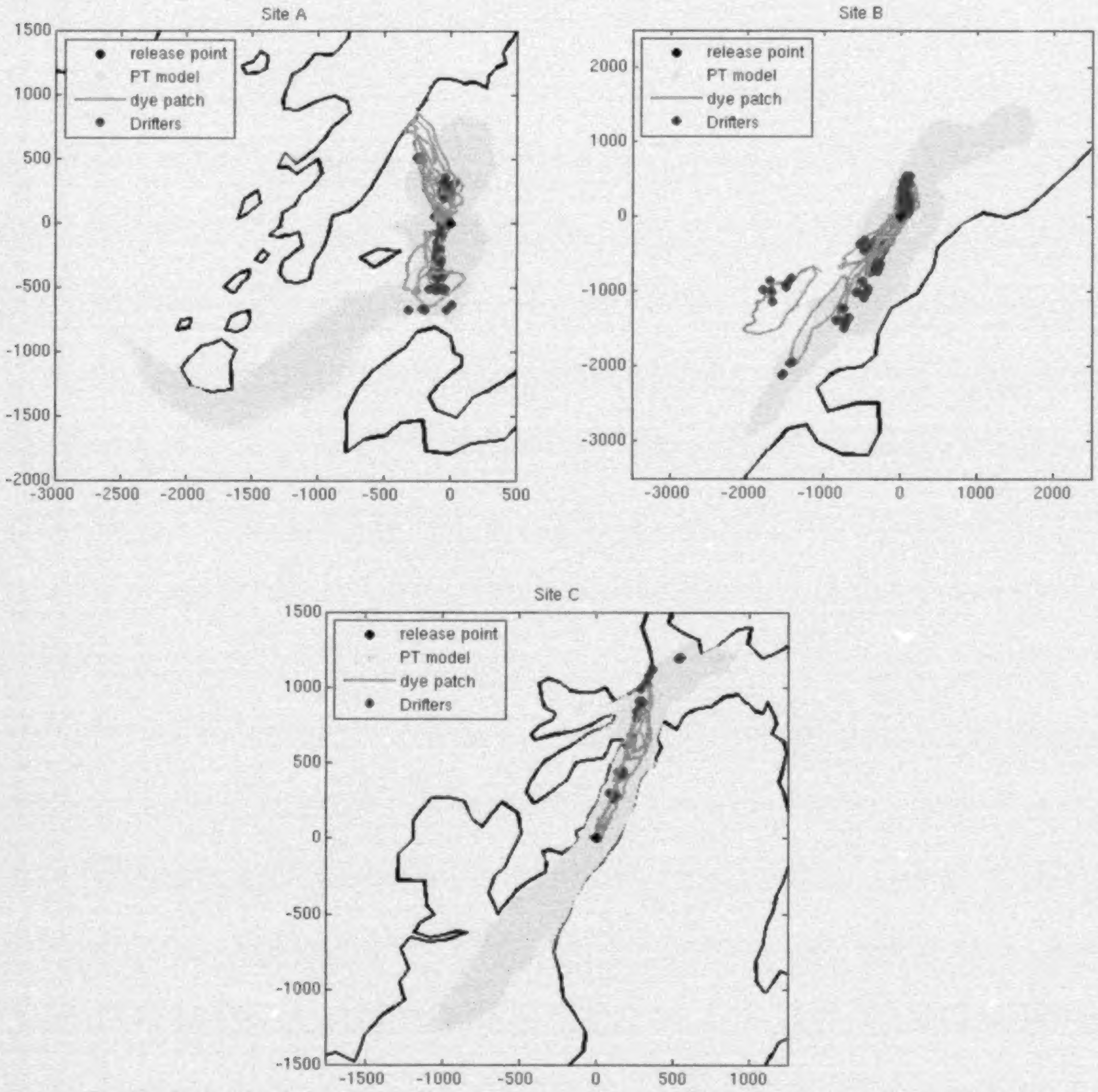

Site A
release point
PT model
dye patch
Drifters
1500
1000
500
0
-500
-1000
-1500
-2000
-3000
-2500
-2000
-1500
-1000
-500
0
500
Site B
release point
PT model
dye patch
Drifters
2000
1000
0
-1000
-2000
-3000
-3000
-2000
-1000
0
1000
2000
Site C
release point
PT model
dye patch
Drifters
1500
1000
500
0
-500
-1000
-1500
-1500
-1000
-500
0
500
1000

Figure 59. Comparison of results of FVCOM particle tracking model with particles released over entire tidal cycle with all observed dye patch perimeters at studies Sites A (top left), B (top right) and C (bottom left).

WELL-BOATS

BACKGROUND

Well-boats operating within the southwest New Brunswick area of the Bay of Fundy are used to conduct chemical therapeutant bath treatments for sea lice. There are two fundamentally different flushing discharge scenarios; one in which the discharge is directed away from the side of the vessel and into ambient sea water (Figure 60) and one in which the discharge is from the side of the ship adjacent to a fish cage (Figure 60). The former discharge initially carries the therapeutant away from the cage but in certain circumstances the ambient flow field may carry the discharge back into the farm. The latter discharge forces a portion of the discharge into an adjacent cage. This latter situation is not explored extensively here.

There are three well-boats operating in southwest New Brunswick. Although the general principles of how each vessel is operated are similar, each vessel has some unique characteristics that influence the manner and rate in which chemical therapeutants are mixed within the well and discharged into the environment.

The Treatment Process

A typical well-boat bath treatment in southwest New Brunswick proceeds as follows. The well-boat fills its wells with ambient water while steaming to the fish farm site. Once at the site the vessel ties up to a fish cage and pumps the fish, previously pursed together and close to the vessel, into the wells. The water within the wells is continuously recirculated for as long as the fish are in the well. The recirculation water is pumped from one end of the well to the other so water is continuously flowing throughout the well. The fish are monitored visually through the well hatch and via real time underwater video cameras located at each end of the well. The concentrations of dissolved oxygen in the well are also continuously monitored by permanent sensors within the well and by hand held sensors lowered through the well's hatch. Oxygen is injected into the well if needed. Measurements of water temperature and salinity are also taken at the beginning of each treatment. The on site fish health supervisor uses this information to determine if the treatment should be undertaken, determine what the desired concentration of therapeutant should be and what the duration of the treatment should be.

At the beginning of each treatment the therapeutant is injected in to one end of the well. This injection takes several minutes and it takes several more minutes for the therapeutant to become homogeneously mixed throughout the well. Once the desired treatment duration has occurred, the water within the well is flushed from the well. This entails pumping water in and out of the well at equal rates so the volume of water within the well remains constant. The water pumped out of the well contains therapeutant while the water pumped into the well does not unless therapeutant from a previous treatment happens to be near the intake. The operational duration of the flushing is typically 15-25 minutes. The discharge from one side of the vessel flows away from the cages and that from the other side flows toward and into the cages (Figure 60). In both cases the subsequent transport and dispersal is controlled by the ambient environmental conditions, with the dispersal in the latter situation being highly influenced by the presence of the farm infrastructure. Once the wells have been flushed, the fish are pumped back into an adjacent fish cage. Any residual therapeutant in the well water is discharged into the environment at this time.

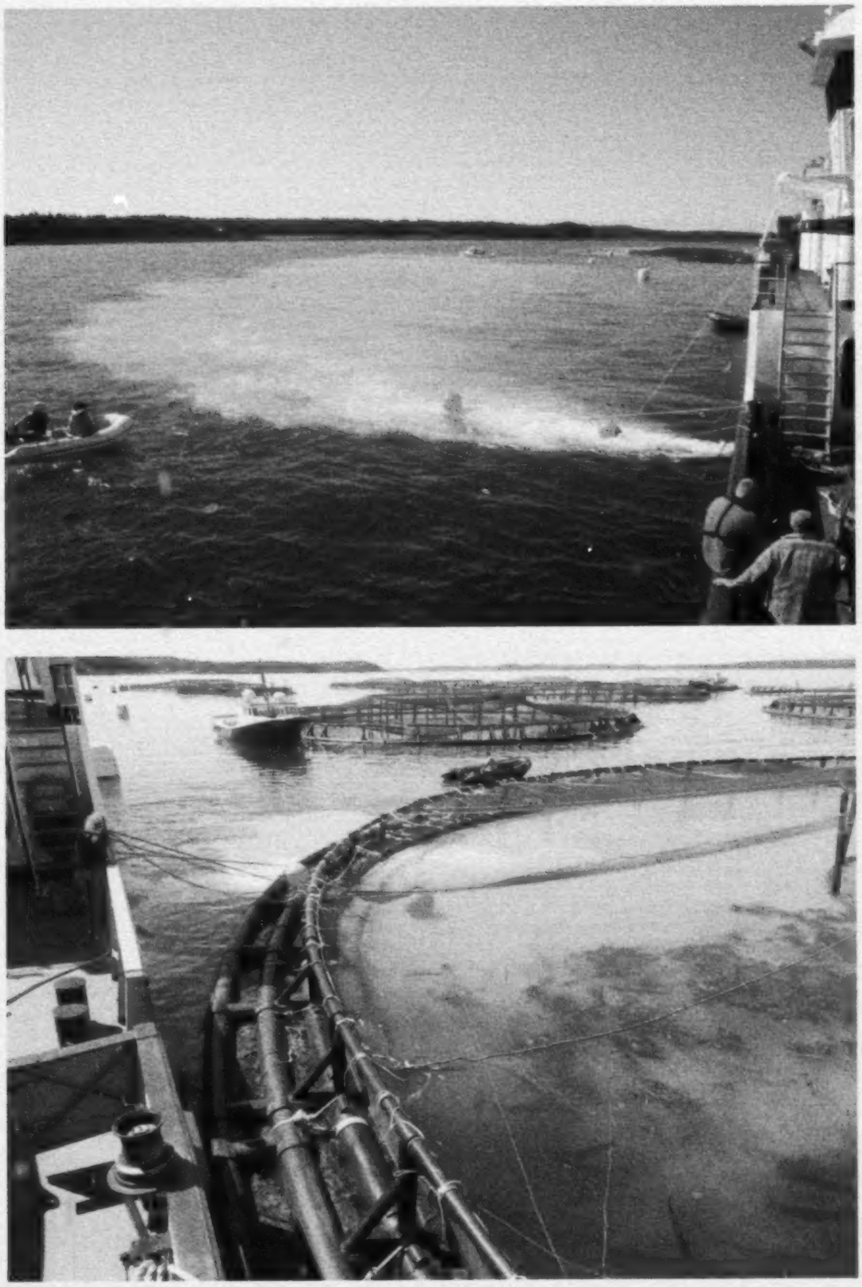

Figure 60. Photographs of a flushing discharge directed away from fish cages (top photo) and one directed into a fish cage (bottom photo).

Initial Distribution within the Well

A consideration of the transport and dispersal of the therapeutant released into the environment as a result of the well-boat bath treatments must first consider the concentration of the therapeutant within the well at the time of flushing. As described above, the concentration is not constant over time. Initially there is no therapeutant in the well and the concentration is zero. Once the therapeutant is injected into the well, the concentration varies in time and space within the well until it is homogeneously mixed. The well mixed concentration (C_0) can be estimated as the mass of therapeutant (M) divided by the volume (V) of the well (i.e., M/V).

Once well flushing begins, the therapeutant concentration within the well decreases with time until the flushing is stopped or the therapeutant is completely flushed from the well. This decrease can be approximated by

$$C(t) = C_0 \exp(-\frac{Qt}{V}) \tag{32}$$

in which Q is the rate at which water is pumped into and out of the well (Vesilind et al. 2010). The ratio V/Q is the e-folding time scale (t_{flush} or the time needed for 63% of the therapeutant in the well to be flushed from the well. Eighty-six percent is flushed in $2\,t_{flush}$ and 95% is flushed in $3\,t_{flush}$.

If for some reason the well was not rapidly mixed, the ambient water might be considered to enter the well as a plug that moves toward the discharge location. Assuming the discharge is drawn from the end of the well opposite to that of the inflow, the time (t_{pl}) needed for the plug to flow through the well and exit the well is called the hydraulic retention time. In this type of flow the time to remove the therapeutant from the well is also estimated as $t_{pl} = V/Q$ (Vesilind et al. 2010) but the concentration in the flushing discharge would be equal to C_0 from the time flushing began until t_{flush} and then it would immediately drop to zero. The V/Q ratio can also be thought of as the time needed to fill (or empty) or empty the well when water is pumped in (or out) at a rate of Q. The design of the well-boats is such that plug flow is not desired and we have not yet seen plug flow in our observations.

Example of Mixing within Well-Boat Wells

In order to determine what type of mixing actually occurs in well-boats a series of dye experiments have been conducted on each of the well-boats. Although each experiment had its challenges and resulted in individual variations, the general characteristics were similar. For this report we describe the results of the dye study conducted on the 14th December 2010, on Well-boat C.

Well-boat C has two wells – a starboard and port well. Each well contains about 330 m^3 of water when filled to operational bath treatment standards. The volume is slightly less when fish are in the well because the fish displace some of the water. Fish were not in the well for the 14th of December 2010 experiment. Once the wells were filled with water, the external water intake was closed, and the water was continuously recirculated within the well with the water being pumped from the stern to the bow at an unknown rate. While the water was being recirculated, 50 g of powdered fluorescein dye was introduced into the vessel's therapeutant mixing tank. This procedure is consistent with commercial therapeutant treatments that use powdered chemicals such as Salmosan®. The mixing tank holds 400-500 L of water. The dye was mechanically mixed with the water with a bladed stirring rod for two sequential periods of 4 minutes, i.e., a total mixing time of 8 minutes. The mixture was injected into one well at a time in a two step process. In the initial step the full volume was pumped into the designated well. In the second step the mixing tank was flushed with 50L of water and this was also then pumped into the designated well. The process was repeated for the each well. The estimated concentration of dye in each well, assuming it was homogenously mixed throughout the well, was 151 µg/L (M/V with M=50 g and V=330 m^3), i.e., mass added divided by the assumed volume of water in the well.

Once the dye was injected into the well, the water and dye mixture was recirculated and mixed for a 20 minute time period. This simulated the time when fish would be exposed to therapeutant. Once this recirculation period was completed, the dye was flushed from the well by pumping water out of the well while clean water was pumped into the well at the same rate so the volume of water remained more or less constant within the well. The water within the wells continued to be recirculated during this flushing period. Once flushing was completed the trial was ended. When fish are in the well and flushing is completed, the water in the well continues to be recirculated until the fish are ready to be pumped back into a net-pen.

Prior to the filling of the wells with sea water a series of four Turner Designs Cyclops-7® fluorescein sensors were hung within the wells. The sensors were hung near the stern, about one third of the way toward the bow, two thirds of the way from the stern (≅one third of the way from the bow) and near the bow of the well. A fifth sensor was deployed through the well hatch cover at various times to obtain additional readings of dye concentration at several depths within the well. The hatch was located near the center of the well.

Figure 61 shows the results recorded by the fluorometers. The concentration of dye inside the well varied over time. Initially there was no dye in the well. Once the dye was injected the concentration increased rapidly. This rate of increase varied with location in the well. In some locations the concentration increased and then decreased to a more or less constant concentration. In other locations the concentration increased steadily to a constant concentration. In all locations the concentration became constant after about 10 to15 minutes. The concentration did not generally achieve the expected homogeneous value of 151 µg/L. Although this may suggest that mixing may have been incomplete, it is more likely that it is measurement error associated with air bubbles sticking to the optical sensor of the fluorometers. This was suggested by the fact that when the sensors were shaken the concentration values increased. This is indicated by some of the sudden increases in concentration seen in the time series. Unfortunately, in this case only the mid-bow sensor could be shaken vigorously and this resulted in the concentration reading just prior to flushing rising to the expected 151 µg/L. This interpretation is consistent with the fact that the mid-bow readings are similar to the values obtained through the well hatch. These latter readings are believed to be affected by bubbles to a much lesser extent since the sensor is constantly being moved up and down in the water column.

Once flushing began the dye concentration recorded by all sensors decreased with time (Figure 61). This decrease is replotted in Figure 62 by standardizing ($C(t)/C_0$) the concentration ($C(t)$) to the concentration (C_0) observed just prior to the commencement of flushing. This helps to compensate for the assumed effect of bubbles on the concentrations. The plots indicate that the concentration of dye or therapeutant within the well is reduced by an order of magnitude within about 30 minutes. The plots also show expected rates of decrease based on the volume of the well (V=330 m^3), several estimates of pumping rates (Q) and the relationship described above in which $C(t) = C_0\exp(-Qt/V)$. Although the pumping rate for any given flushing event is not well known, the maximum rate the pumps are rated for is about 3000-3500 m^3/hour (personal communication from the ships engineer). The pumping rate during a flushing event is less than this since the pumps are not run to full capacity (personal communication from the ships engineer). The curves on the plot assumed a maximum pumping rate of 3500 m^3/hour. The 30% of maximum pumping rate curve corresponds to a pumping rate of 1050 m^3/hour and an e-folding flushing time of 19 minutes. The 50% pumping rate is 1750 m^3/hour and an e-folding flushing time of 11 minutes.

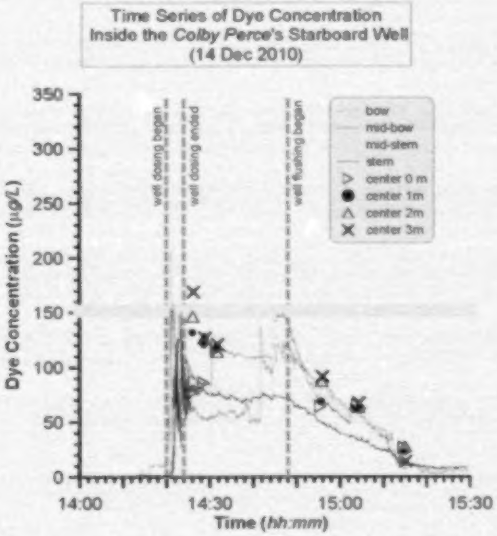

Figure 61. The time series of dye concentration within the starboard well of the Colby Perce as measured by a Cyclops 7 fluorometer hung through the well hatch on the 14th of December 2010. The amount of dye added to the well was 50 g so the homogeneous concentration would have been 151 µg/L.

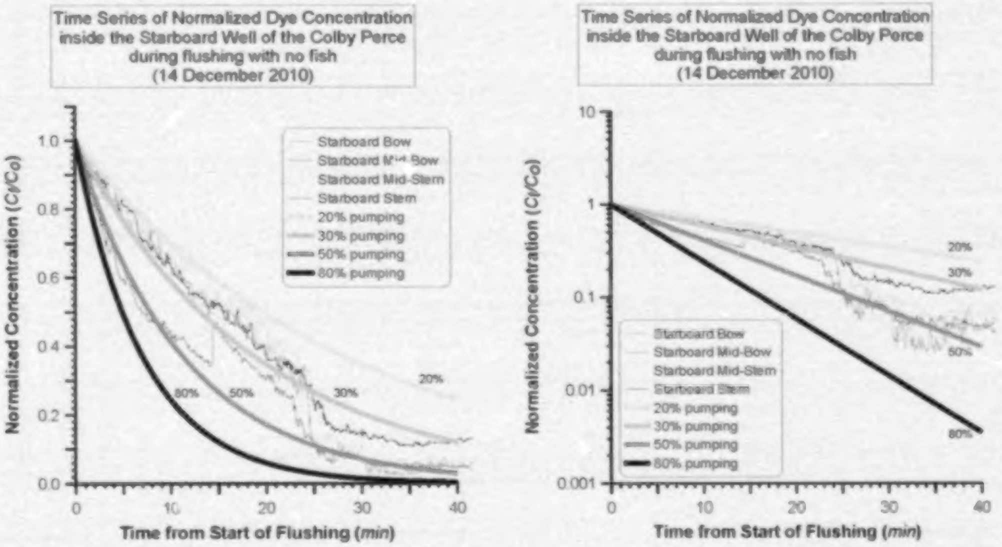

Figure 62. The time series of normalized dye concentration within the starboard well of the Colby Perce during the flushing period conducted on the 14th of December 2010. The two plots show the same data as in Figure 61. The data in the left panel are plotted on an arithmetic scal;, that in the right panel on a logarithmic scale.

TRANSPORT AND DISPERSAL ONCE RELEASED INTO THE RECEIVING ENVIRONMENT

Background

Well-boats discharge therapeutant solutions into the ambient receiving water by mechanically pumping the bath treatment water through a circular pipe that exits the side of the vessel at an angle normal to the vessel hull. The discharge solution therefore has momentum and it intrudes into the receiving water which usually has similar density characteristics. The flow induced by this type of discharge is termed a jet flow (Fischer et al. 1979). The water exiting the discharge pipe has a velocity and a density and the receiving water has its own characteristic velocity and density. When the density of the discharge water is less than the density of the ambient receiving water, the jet is termed a buoyant jet and the discharge tends to rise toward the surface. When the density of the discharge water is greater than the density of the ambient receiving water, the jet is termed a sinking jet and the discharge tends to sink toward the bottom. Buoyant or sinking jets are not discussed here since it is assumed the water from most well-boat discharges has a density equal to that of the receiving waters.

One of the distinguishing features of jet flows is that as the jet exits into and flows through the receiving waters, ambient water is entrained into the jet. This entrainment helps dissipate the momentum of the jet and dilute the therapeutant contained in the discharged water.

For circular discharge pipes discharging below the water surface, the steady state velocity $u(x,r)$ parallel to the main axis of the jet may be approximated by the following equation (Cushman-Roisin 2014).

$$u(x,r) = u_{\max}(x)\exp\left(-\frac{50r^2}{x^2}\right) \tag{33}$$

where $u_{\max}$ is the velocity along the main axis of the jet. In this equation x is the distance from the infinitely small or virtual jet source along the main axis of the jet and r is the radial distance perpendicular to the main axis. The velocity at distance x along the center of the jet ($r = 0$) is defined as

$$u_{\max}(x) = \frac{5d}{x}U \tag{34}$$

where d is the diameter of the discharge pipe, and U is the cross-sectional average of the exit velocity of the water at the end of the discharge pipe (Cushman-Roisin 2014). The axial velocity therefore decreases with distance from the discharge origin such that when $u_{\max} = 0.1U$, $x = 50d$ and when $u_{\max} = 0.01U$, $x = 500d$. Commensurate with the decrease in axial velocity with increasing distance from the discharge point, is an increase in the width or radius (R) of the jet. The effective radius is approximated as $R = 0.2x$ (Cushman-Roisin 2014).

The above equations use a distance x that is from a virtual infinitely small diameter discharge pipe. The distance at the end of an actual discharge pipe that has a specific diameter is given by $x = 5d/2$ where d is the diameter of the actual discharge pipe. For practical purposes the distance from the mouth or end of the actual discharge pipe is therefore given by $x' = x - 5d/2$.

In addition to the velocity, the steady-state concentration of therapeutant $c(x,r)$ within a jet has also been approximated and is given by

$$c(x,r) = c_{\max}(x)\exp\left(-\frac{50r^2}{x^2}\right) \tag{35}$$

(Cushman-Roisin 2014). The concentration of therapeutant at any given distance along the axis of the jet is a maximum when $r = 0$. This concentration ($c_{\max}$) is given by

$$c_{\max}(x) = \frac{5d}{x}c_0 \tag{36}$$

where c_0 is the concentration constantly leaving the discharge pipe.

In order to apply the above relationships to discharges from well-boats, the diameter of the discharge pipe and the flow rate of water through the pipe must be known. Measurements of the diameter of the discharge pipes on the well-boats used in southwest New Brunswick indicate that a typical diameter for the well-boat discharge pipe is approximately 0.5 m and discussions with the Well-boat Captain's indicated that the discharge pumping rates were typically about 3000 m^3/h. Under these assumptions, the virtual location of the discharge is $x = 5 \cdot 0.5/2 = 1.25$ m and U is approximately 4 m/s, i.e., $U \approx Q/(\pi d^2/4)$. When $Q = 1000$ m^3/h, $U = 1.4$ m/s. At the higher discharge rate $u_{\max}$, is about 1 m/s at a distance of 10 m from the discharge exit and 0.1 at a distance of 100 m. At the slower discharge rate of 1000 m^3/h, $u_{\max}$ is about 0.35 m/s at a distance of 10 m from the discharge exit and 0.035 at a distance of 100 m. These velocities are consistent with measurements taken by in the discharge jets from one of the well-boats. The radius of the discharge jet is 2 m at x=10 and 20 m at x=100 m.

These calculations suggest that discharges directed vertically downward from a well-boat can be expected to interact with the seafloor when the well-boats are operating in waters of less than about 50 m in depth. The calculations also suggest that predictions of the transport of therapeutants discharged from well-boats must take into consideration the water velocities generated by the discharge jet as well as those in the receiving waters, at least for the first 100 m or so from the discharge point. Tidal velocities in the vicinity of fish farms in the coastal waters of southwest New Brunswick typically range from 0 to 1 $m \cdot s^{-1}$ (Page, Losier et al., personal knowledge). Hence, the velocities associated with well-boat flushing discharge jets can be expected to rival or exceed those of the tidal currents within 100 m or so of a well-boat.

From a dilution of therapeutant perspective, the concentration equations suggest that for the same diameter discharge pipe as above, the concentration of therapeutant exiting the discharge pipe will be reduced by a factor of ten when $x = 25$ m (i.e., $c_{\max} = 0.1c_0$ and $x = 50d$), by a factor of 100 when $x = 250$ m (i.e., $c_{\max} = 0.01c_0$ and $x = 500d$) and by a factor of 1000 when $x = 2500$ m (i.e., $c_{\max} = 0.001c_0$ and $x = 500d$). In general, the distance at which the concentration will be equal to a specified value ($c_{threshold}$), such as an LC50, is estimated as $x = 5dc_0/c_{threshold}$ (Cushman-Roisin 2014). It should be noted that the distance is dependent only on the discharge concentration and not the discharge velocity and that the distances are overestimates since the effect of ambient turbulence is not taken into consideration.

Although the above solutions are steady state solutions, a quasi-time dependent concentration within the discharge jet might be approximated by replacing c_0 in the above equations with $c_0(t) = (M/V)\exp(-Qt/V)$ so that

$$c_{\mathrm{max}}(x,t) = \frac{5d}{x}\left(\frac{\mathrm{M}}{\mathrm{V}}\right)\exp\left(-\frac{Qt}{V}\right) \tag{37}$$

At the time of this writing a true time dependent solution has not been found.

From a dispersion perspective, Cushman-Roisin (2014) indicates that the above relationships correspond to an effective rate of cross-axis dispersion that is approximated as $D = 0.0125dU$. The effective rate of cross-axis dispersion associated with the above discharge characteristics is therefore 0.006 m^2/s ($D = 0.0125(0.5\ \mathrm{m})(1\ \mathrm{m/s})$). This is about an order of magnitude less than a typical rate of cross-flow eddy dispersion and similar to typical rates of vertical eddy dispersion. Therefore the estimated reductions in concentration are underestimates since the mixing processes in the receiving waters will enhance the dispersion generated by the jet.

Although the above theory gives some insight into the magnitudes of jet velocities, magnitudes of concentration dilutions and the length scales of jet influence, it should be noted that the dilution rates are likely underestimates of dilution since the ambient eddy diffusivities in the receiving waters are not included in the calculations. It should also be noted that in one of the well-boats the discharge is at a height of a few centimetres above the sea surface. The effluent therefore needs to fall into the sea before the jet is established. This dynamic is not accounted for in the above equations since they assume the discharge is completely submerged and unaffected by boundaries.

Although the above equations refer to the steady-state situation, the spin up time for the jet, particularly in the near-field, is short, on the order of a minute, and the observations on dye concentration shown below indicate that the equations give a reasonable first approximation to the observed concentrations of dye within the jet.

Methods

In order to empirically investigate the flushing discharge from the wells and the transport and dispersal within the receiving waters, fluorescein dye was injected into the wells on a number of occasions (Table 15). The observations were taken from three different well-boats, Well-boat A, Well-boat B and Well-boat C. The vessels are quite similar in terms of well size and recirculation of water within wells but they are different in terms of their angles and positions of discharge. Well-boat C discharges through the side of the vessel via at a depth encompassing the sea surface and through a pipe that is angled parallel to the sea surface. The Well-boat A discharge is similar to that of Well-boat C with the exception that the discharge is angled 45° downward from the horizontal. The Well-boat B discharge is underneath the vessel and angled vertically downward. The therapeutants used during the well-boat studies were Salmosan®, Alphamax® and hydrogen peroxide.

Table 15. Summary of fieldwork on dye dispersal from well-boats.

Well-boat Name	Farm Site	Date	Angle of Discharge	Dye added (g)	Chemical added	Plume Followed (Y/N)	Weather	Current speed[1] (cm/s)
A	L	20 Sept. 2010	45°	50	Interox Paramove®	N	Sun and cloud	NAV
A	D	30 Sept. 2010	45°	500 + 500	Salmosan®	Y	Cloudy	0.8-17.0
A	B	22 July 2011	45°	1500 +1500	None	Y	Mostly Sunny	NAV
B	E	14 Oct. 2010	90°	1000	Salmosan®	Y	Sunny	NAV
B	G	8 Dec. 2010	90°	1000 +1000	Alphamax®	Y	Cloudy	NAV
C	H	16 Dec. 2010	0°	1000 +1000	Alphamax®	Y	Cloudy	NAV
C	B	5 Aug. 2011	0°	1500 +1500	Interox Paramove®	Y	Sunny	0.7-31.5
C	K	17 Nov. 2011	0°	1500	Interox Paramove®	Y	Sun and cloud	4.5-8.2

1 Current range is from 30 minutes prior to commencement of the treatment to 30 minutes post-treatment. These values were obtained from 1 to 2 current meters deployed within 100 m of the well-boat (unpublished data).

2 NAV = Not available

When the therapeutant used during a well-boat study was Interox Paramove hydrogen peroxide, no chemical measurements were taken since the dye interfered with the chemical measuring technique.

For sampling methodology used to collect dye data, please refer to the methods for the tarps and skirts. As with the tarp and skirt treatments, vertical profiles of the dye concentration were obtained at various times and places near the well-boats and within the plumes associated with the above well-boat releases. The profiling methodology was the same as for tarps and skirts.

To collect dye data directly in the discharge jet, fluorometers were attached to buoys and anchored in the discharge plume (Figure 60).

Time series of dye concentrations were compared to predicted concentrations and therapeutant dilution was predicted as a function of time and distance of discharge pipe (details in upcoming text).

Observation

Near Field: Discharge Jets

Well-Boat C – 5th of August 2011

On the 5th of August 2011, a dye release was conducted from Well-boat C. In this release 1.5 kg of dye was injected into the well. A larger mass of dye was added than in the previous example to facilitate the tracking of the dye in the discharge jet and beyond. As with the case of the lower dose of dye described in the previous example, the time series of the concentration of dye inside the well showed that prior to dye injection there was no appreciable concentration of dye in the well (Figure 63). Once the dye was injected (t=-20) a rapid increase in concentration was recorded until the upper threshold of the fluorometer was exceeded. However, unlike the above example, the temporal evolution of the dye concentration within the well could not be followed since the concentration quickly exceeded the fluorometer maximums. In this case, the particular Cyclops instrument topped out at about 316 µg/L. The calculated average dye concentration within the well, after it was well mixed was 4545 µg/L (M/V = 1.5 kg/330 m^3).

Flushing began 20 minutes after the dye injection. A decrease in dye concentration was not detected until 10-15 minutes after the commencement of the flushing (t=0); it took this long for the concentration to be reduced below the upper 316 µg/L threshold of the instrument. The decrease continued exponentially until flushing was stopped 55 minutes after it began. The concentration had been reduced by a factor of 0.01 (i.e., 100 times less concentrated) after 30 minutes of flushing. When the flushing was stopped after 55 minutes the dye concentration within the well was 0.003 times the initially well mixed concentration (i.e., almost 1000 times less concentrated).

The concentration within the flushing discharge jet during the above treatment is shown in Figure 64 for a depth of 0.5 m and a distance of approximately 6 m from the point of discharge along the major axis of the discharge jet. The concentrations for the first ten minutes or so after the commencement of flushing are higher than the upper threshold (~395 µg/L) of the instrument (Note: this was not the same instrument as was used inside the well and as such has a different upper threshold); after this the concentration decreased with time. The concentration was always less than that measured inside the well at a comparable time. The scatter or high frequency variation in the concentration within the discharge jet is assumed to be evidence of the entrainment of ambient water into the jet. This variation was considerably greater than that recorded inside the well where ambient water was not available for entrainment.

The reduction in concentration inside the discharge jet relative to that inside the well is consistent with the expectation generated by applying a dilution factor to the time series of the smoothed concentration observed within the well during the flushing time period (Figure 64). The dilution factor (d_f) was based on the assumption that the dilution is caused by the entrainment of ambient water into the discharge and that this could be approximated by $d_{fac} = c_{\max} / C_0 = 5d/x$. For the data discussed here the dilution factor was 0.46 since the distance (x) from the discharge point was 6 m and the diameter of the discharge pipe was 0.56 m.

The measured maximum concentration inside the discharge jet is also consistent with that predicted by equation 37 when the pumping rate (Q) was assumed to be 2400 m^3/h, i.e., about 80% of the maximum rate (of 3000 m^3/h) estimated for the ships discharge pumping system (pers. comm. ship's Captain and engineer). When the estimated maximum pumping rate of 3000 m^3/h^{-1} was used, concentrations tended to be underestimated. The predicted concentrations do not equal the homogeneous concentration at the time of flushing initiation because they represent the concentrations at a distance from the discharge. The prediction for a distance of zero ($x = 0$), i.e., the mouth of the discharge, at the time of discharge initiation would be equal to the homogeneous concentrations.

The predicted dilution factor, equal to the ratio of the predicted concentration to the homogeneous concentration within the well just prior to discharge, as a function of time after the beginning of flushing discharge and distance from the mouth of the discharge pipe is shown in Figure 65. After about 20 minutes the concentration of therapeutant within 10-50 m of the discharge pipe is between 100 and 1000 times less concentrated than the initial concentration within the well at the time of flushing initiation.

Figure 66 uses the maximum concentration inside a jet predicted by equation 37 to illustrate the decrease in therapeutant concentration within the discharge jet as a function of time since flushing begins and distance from the point of discharge. The plot suggests that after twenty minutes the therapeutant concentration at a distance of 50 m from the vessel is reduced by two to three orders of magnitude.

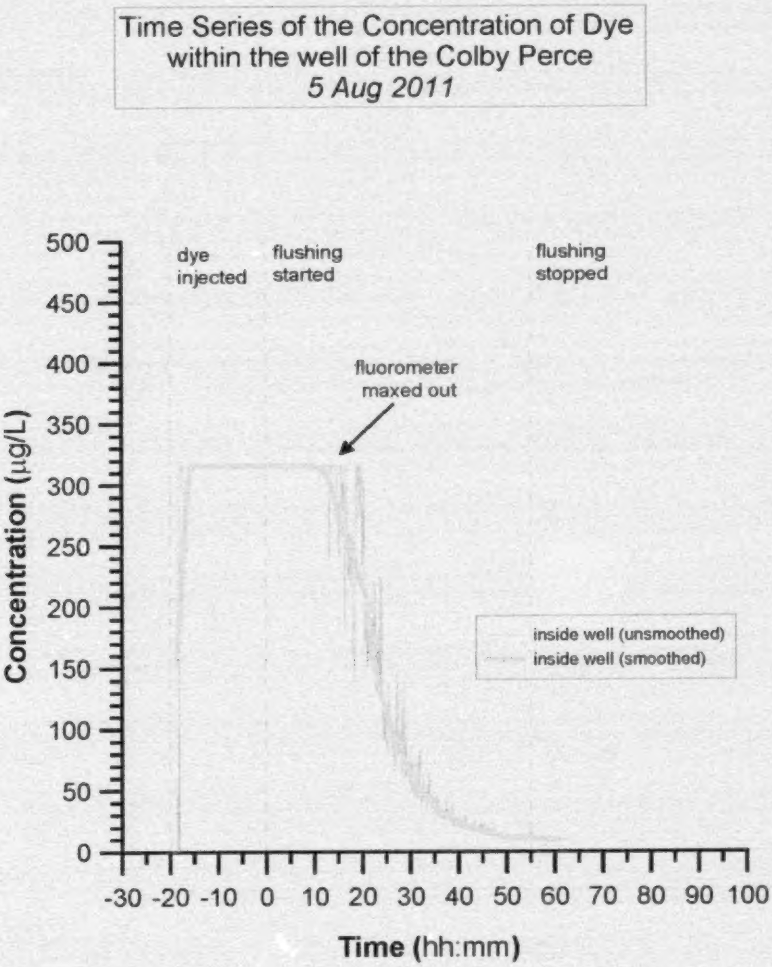

Figure 63. The time series of dye concentration within the starboard well of Well-boat C as measured by a Turner Designs Cyclops 7 fluorometer hung through the well hatch on the 5th of August 2011. The grey line is the unsmoothed data and the green line is the data smoothed by a 5 minute running mean. The amount of dye added to the well was 1.5 kg so the estimated homogeneous concentration would have been 4545 μg/L, a value well above the upper detection limit of the fluorometer.

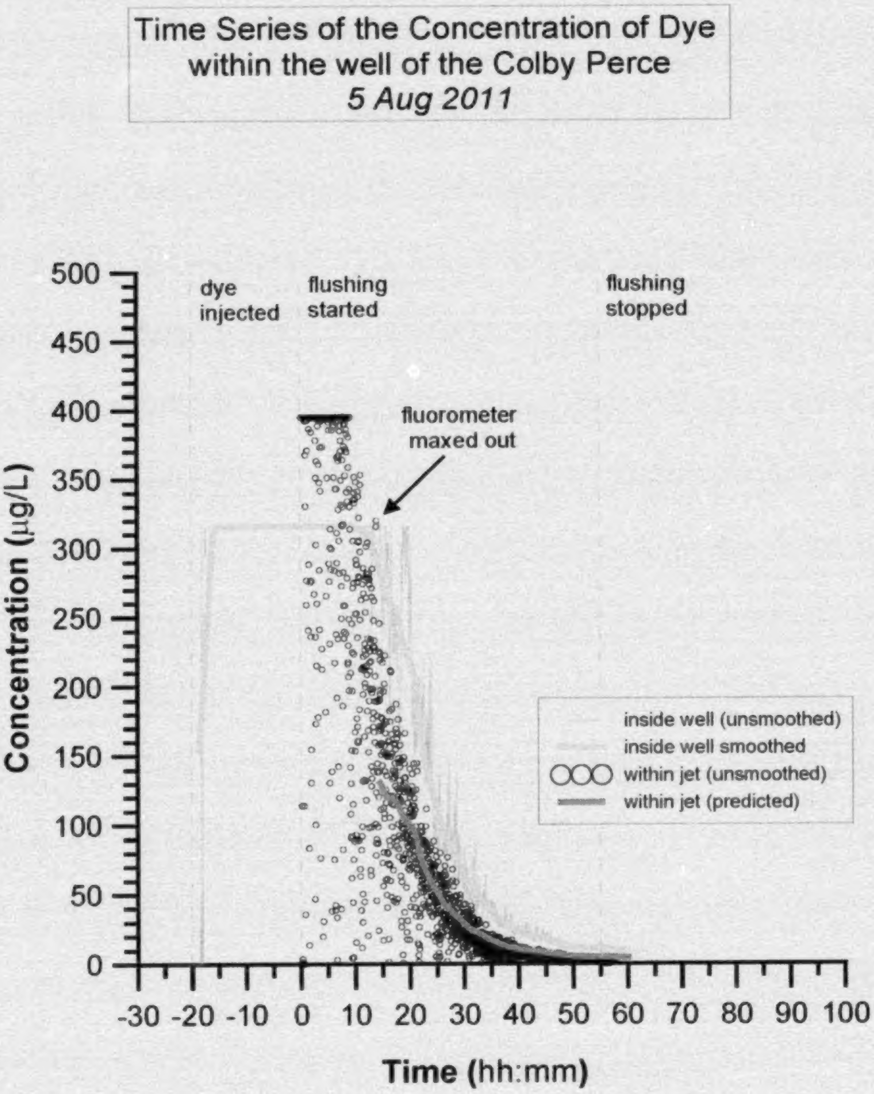

Figure 64. The time series of dye concentration within the flushing discharge jet associated with the starboard well dye treatment conducted on the Well-boat C on the 5th of August 2011. The open black symbols are the unsmoothed time series of dye concentration at depth of 0.5 m and a distance of 6 m from the point of discharge. The heavy red line is the predicted time series of concentration (see text for details). The thin grey and heavy green lines are the concentrations within the well and are the same as those shown in the previous Figure 63.

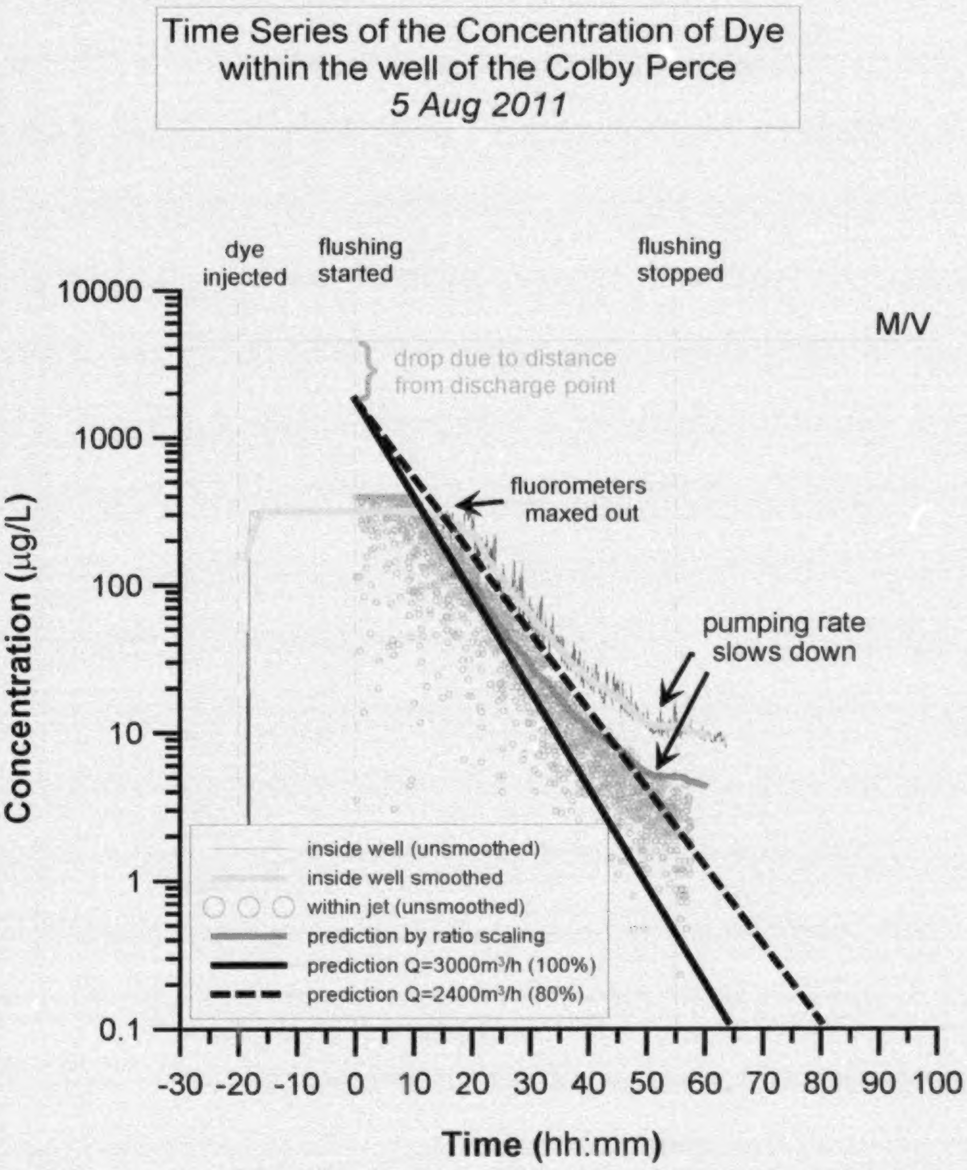

Figure 65. The time series of observed and predicted dye concentrations within the well and flushing discharge jet at a distance of 6 m from the discharge pipe. The observations are associated with the starboard well dye treatment conducted on the Well-boat C on the 5th of August 2011. The straight line predictions (heavy black lines) are based on equation 37. The heavy red line prediction is a scaled version of the smoothed observations taken from inside the well (green line). The blue line is the time series of observations taken from within the well. The open black symbols are the unsmoothed time series of dye concentration at depth of 0.5 m and a distance of 6 m from the point of discharge.

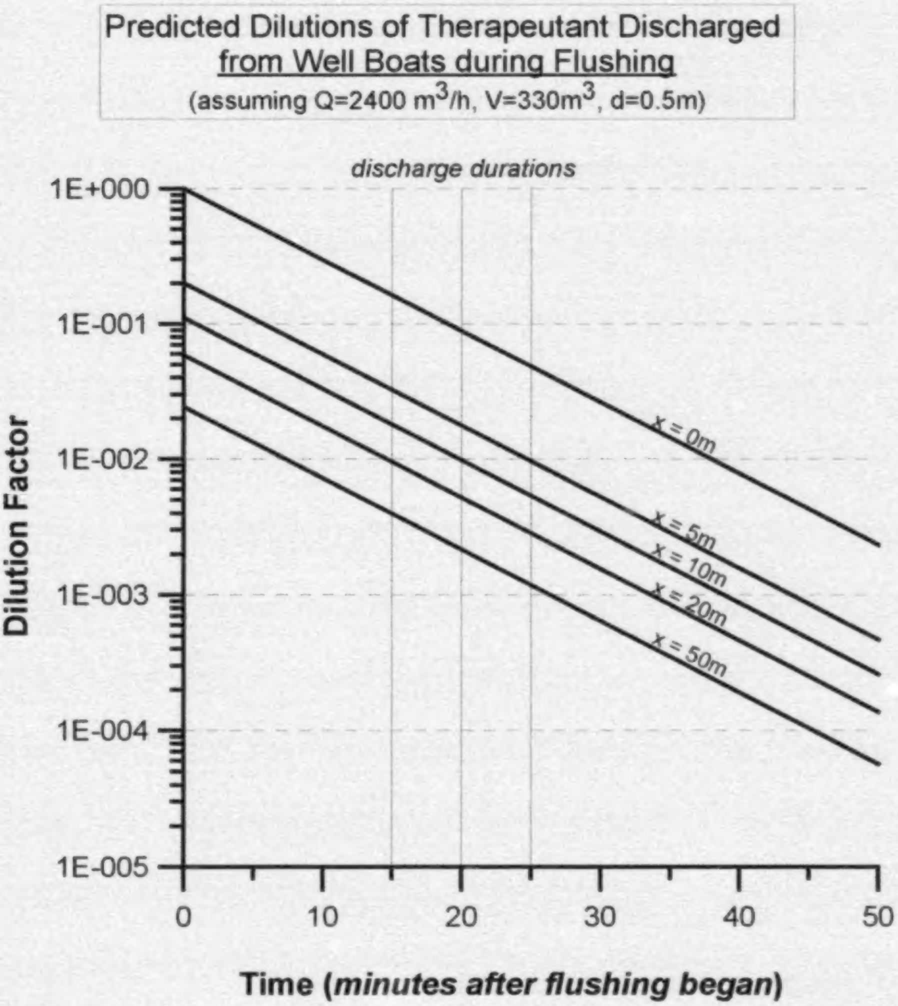

Figure 66. Predictions of therapeutant dilution as a function of time and distance (x) from the mouth of the discharge pipe. The predictions are based on the equation 37.

Far Field: Horizontal Observations of Discharge Plumes

Well-Boat C – Site B – 5th of August 2011

Two well-boat bath treatment releases, one treatment per well, were conducted on the 5th of August 2011 at Site B. The first release was directed away from the fish cages and the second release was directed into the adjacent fish cage. The dye plume associated with the first release (Figure 67) elongated and moved toward the southwest and south. The second release moved into the adjacent cage and eventually emerged to form a plume moving toward the east (Figure 68).

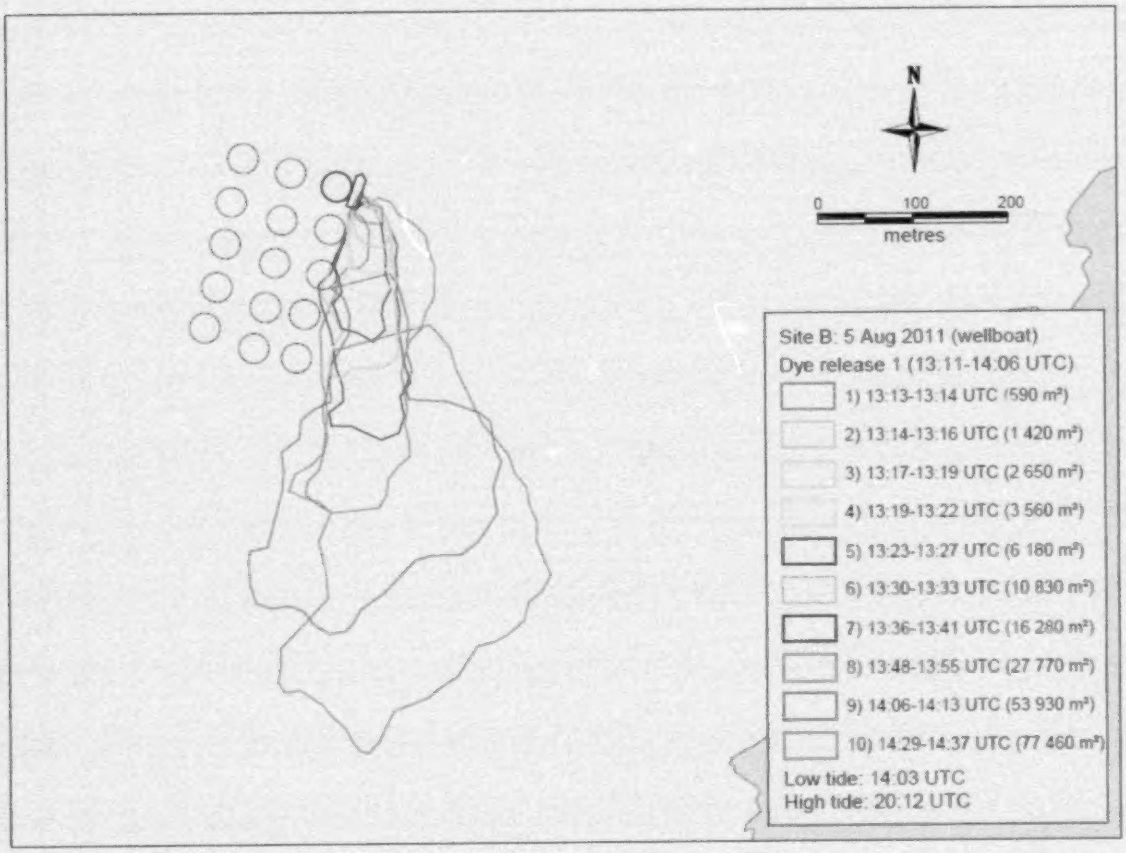
N
0
100
200
metres
Site B: 5 Aug 2011 (wellboat)
Dye release 1 (13:11-14:06 UTC)
1) 13:13-13:14 UTC (590 m²)
2) 13:14-13:16 UTC (1 420 m²)
3) 13:17-13:19 UTC (2 650 m²)
4) 13:19-13:22 UTC (3 560 m²)
5) 13:23-13:27 UTC (6 180 m²)
6) 13:30-13:33 UTC (10 830 m²)
7) 13:36-13:41 UTC (16 280 m²)
8) 13:48-13:55 UTC (27 770 m²)
9) 14:06-14:13 UTC (53 930 m²)
10) 14:29-14:37 UTC (77 460 m²)
Low tide: 14:03 UTC
High tide: 20:12 UTC

Figure 67. Map showing the outlines of dye patches (coloured polygons), and the location of the release (circle) for the 5th of August 2011 dye release from a well-boat treatment at Site B.

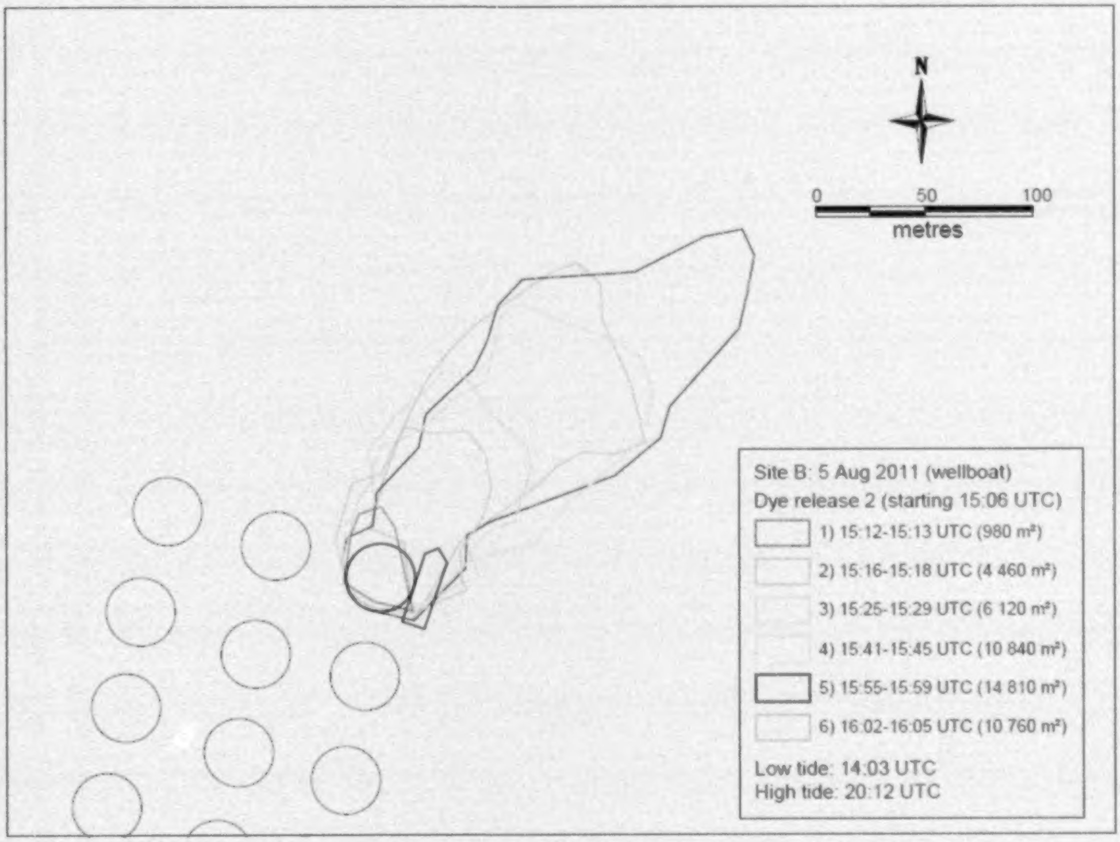
N
0
50
100
metres
Site B: 5 Aug 2011 (wellboat)
Dye release 2 (starting 15:06 UTC)
1) 15:12-15:13 UTC (980 m²)
2) 15:16-15:18 UTC (4 460 m²)
3) 15:25-15:29 UTC (6 120 m²)
4) 15:41-15:45 UTC (10 840 m²)
5) 15:55-15:59 UTC (14 810 m²)
6) 16:02-16:05 UTC (10 760 m²)
Low tide: 14:03 UTC
High tide: 20:12 UTC

Figure 68. Map showing the outlines of dye patches (coloured polygons), and the location of the second release (circle) for the 5th of August 2011 dye release from a well-boat treatment at Site B.

Site K – Well-boat C – 17th of November 2011

Dye was released from the starboard well of Well-boat C, in the direction pointing away from the salmon cage to which the well-boat was moored. Although the discharge plume spread out horizontally, it only moved a short distance toward the southeast (Figure 69).

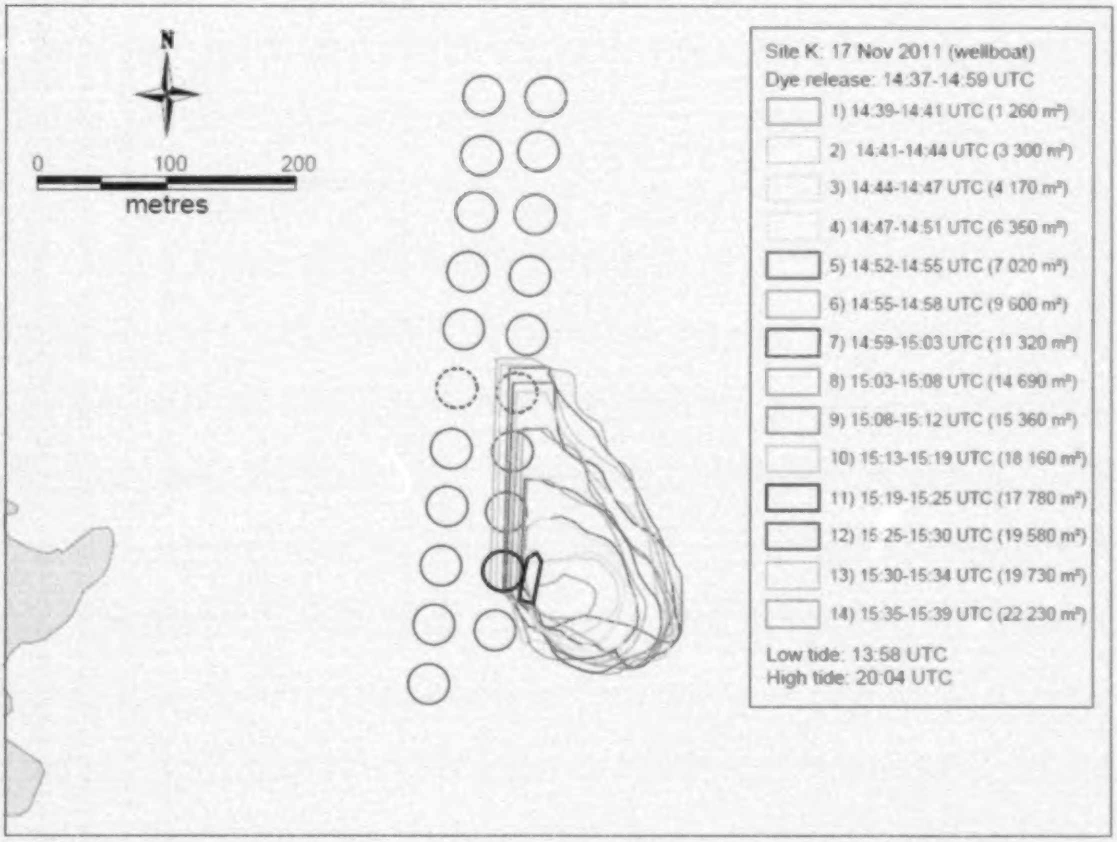
N
0
100
200
metres
Site K: 17 Nov 2011 (wellboat)
Dye release: 14:37-14:59 UTC
1) 14:39-14:41 UTC (1 260 m²)
2) 14:41-14:44 UTC (3 300 m²)
3) 14:44-14:47 UTC (4 170 m²)
4) 14:47-14:51 UTC (6 350 m²)
5) 14:52-14:55 UTC (7 020 m²)
6) 14:55-14:58 UTC (9 600 m²)
7) 14:59-15:03 UTC (11 320 m²)
8) 15:03-15:08 UTC (14 690 m²)
9) 15:08-15:12 UTC (15 360 m²)
10) 15:13-15:19 UTC (18 160 m²)
11) 15:19-15:25 UTC (17 780 m²)
12) 15:25-15:30 UTC (19 580 m²)
13) 15:30-15:34 UTC (19 730 m²)
14) 15:35-15:39 UTC (22 230 m²)
Low tide: 13:58 UTC
High tide: 20:04 UTC

Figure 69. Map showing the outlines of dye patches (coloured polygons), and the location of the release (circle) for the 17th of November 2011 dye release from a well-boat treatment at Site K.

Far Field: Vertical Observations in Discharge Plumes

Site H – Well-boat C – 16th of December 2010

Eighty vertical profiles of dye concentration were collected from Site H during two dye releases from Well-boat C the 16th of December 2010. There was a strong pycnocline in the upper 10 m of the water column with a $\Delta\sigma_T$ of 10 over the 0-10 m depth range (Figure 70) but no surface mixed layer. Extremely heavy rainfall in the days just prior to the 16th of December 2010 is thought to be the cause of the strong pycnocline.

Seventeen of the vertical dye profiles collected did not detect any dye. The vertical profiles where dye was detected are shown in Figure 71. Dye was detected down to 8 m below the sea surface, compared to an average site depth at mean low tide of 33.7 m.

The profiles obtained on the 16th of December 2010 show that for both releases, the dye was primarily in the upper 5 m of the water column, with the exception of one profile demonstrating a subsurface peak at 6 m. The highest concentrations were predominantly found in the upper 2.5 m. The vertical distributions are consistent with the angle of discharge of the well-boat (0º) and the water density properties, with the dye being injected directly into the upper metre of the water column and contained in the upper few metres by the strong stratification of the water column.

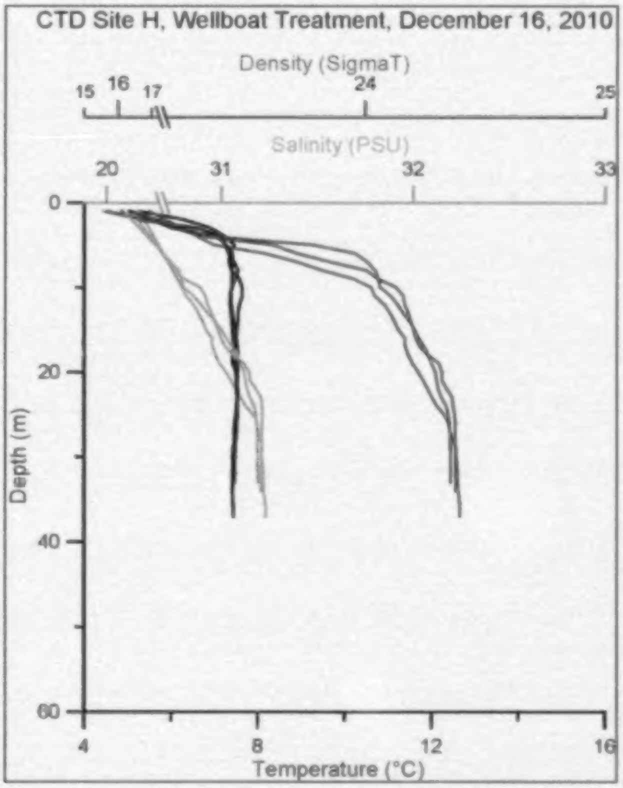

Figure 70. Temperature, salinity and density profiles of the water column collected during a well-boat dye study at Site H from well-boat C on the 16th of December 2010.

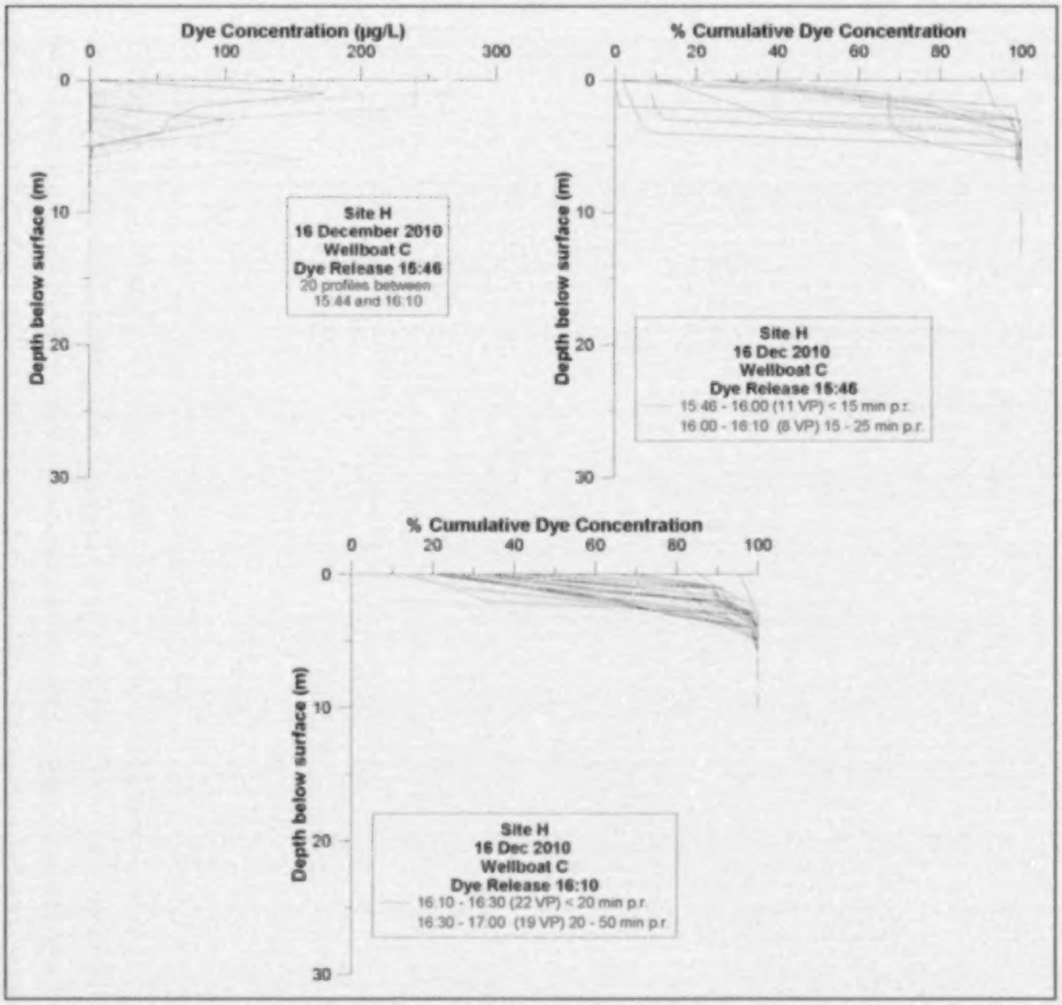

Figure 71. Vertical dye concentration profiles (left panel) and cumulative concentration versus depth curves (right panel) associated with two dye releases from Well-boat C at Site H on the 16th of December 2010. The average site depth at mean low tide is 33.7 m. VP = Vertical Profile. p.r. = post release

Site K – Well-boat C – 17th of November 2011

Three vertical profiles of dye concentration were collected at Site K during a single dye release conducted on the 17th of November 2011. All of the profiles collected detected dye. The concentrations of dye as a function of depth are shown in Figure 72. All three profiles identified a subsurface peak at around 2.5 m. Dye was detected only within the top 5 m below the sea surface, compared to an average site depth at mean low tide of 8.2 m. There are no CTD data for this day.

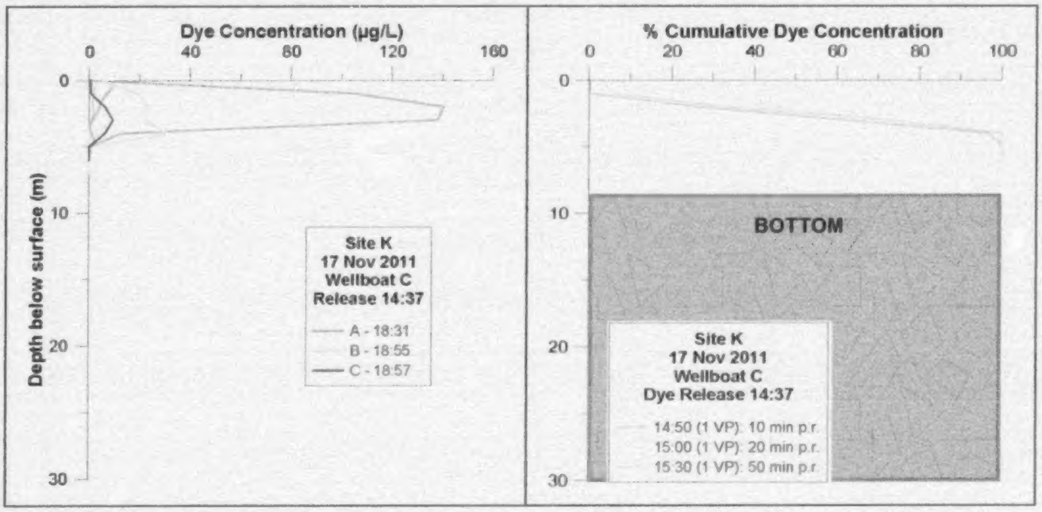

Figure 72. Vertical dye concentration profiles (left panel) and cumulative concentration versus depth curves (right panel) associated with dye releases from Well-boat C conducted at Site K. The average site depth at mean low tide is 8.2 m. VP = Vertical Profile, p.r. = post release

Site B – Well-boats A and C – 22nd of July 2011 and 5th of August 2011

Thirty-three vertical profiles of dye concentration were collected at Site B during four dye releases held on the 22nd of July 2011 and the 5th of August 2011. On the 22nd of July 2011 there were two port releases with the effluent jets pointing away from the salmon cage. On the 5th of August 2011 there was a port and starboard release, one release pointing away from the salmon cage and one release directed toward the salmon cage. Nine of the profiles collected did not detect any dye. The vertical profiles where dye was detected are shown in Figure 73 and Figure 74. Dye was detected down to 25 m below the sea surface, compared to an average site depth at mean low tide of 35.3 m.

There was a continuous increase in density of the water column in the upper 10 m both days, with a $\Delta\sigma_T$ of 0.4 on the 22nd of July 2011 and 0.2 on the 5th of August 2011 (Figure 75). One of two CTD profiles on the 5th of August 2011 showed a surface mixed layer of 7 m, followed by $\Delta\sigma_T$ of 0.2 between 7 and 10 m.

For the first release from Well-boat A on the 22nd of July 2011, the highest recorded concentrations were measured between depths of 5 and 15 m, and for the second release, at approximately 12 m. For both releases, dye was detected below 20 m within fifteen minutes post release. A few of the profiles were not able to go deep enough to detect the maximum depths to which the dye had been dispersed. Hence, the maximum depths recorded are underestimates and the cumulative depth profiles skewed. Only following the second release was there dye located at the water's surface. The detection of a subsurface plume is consistent with the angle of discharge of Well-boat A (45°) and the lack of stratification of the water column.

On the 5th August 2011, Well-boat C was used. For the first release, over an hour after the dye began being released, the maximum depth at which dye was detected was 10 m, while for the second release, dye reached depths of 15 m in less than 15 minutes. The increased depths of the dye plume following the second release relative to the first release may have been due to forcing of the plume downward by cage infrastructure. The first release was directed away from the cage site into open water, while the second release was directed into a salmon cage only a couple of meters away. The effects of the cage infrastructure are visible due to minimal stratification of the water column that day.

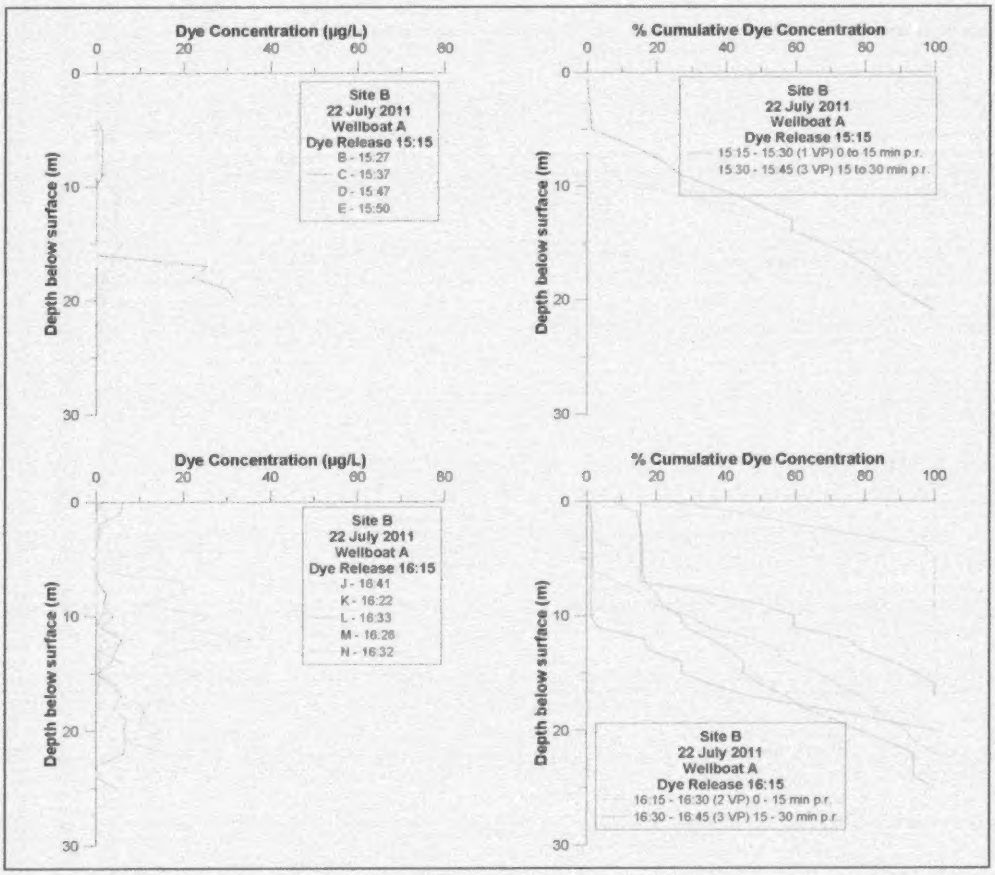

Figure 73. Vertical dye concentration profiles (left panel) and cumulative concentration versus depth curves (right panel) associated with dye releases from Well-boat A at Site B. The average site depth at mean low tide is 35.3 m. NOTE: Cumulative profiles for the incomplete profiles (B and C) are presented in this figure; insufficient dye data at deeper depths may skew the cumulative profiles. VP = Vertical Profile, p.r. = post release

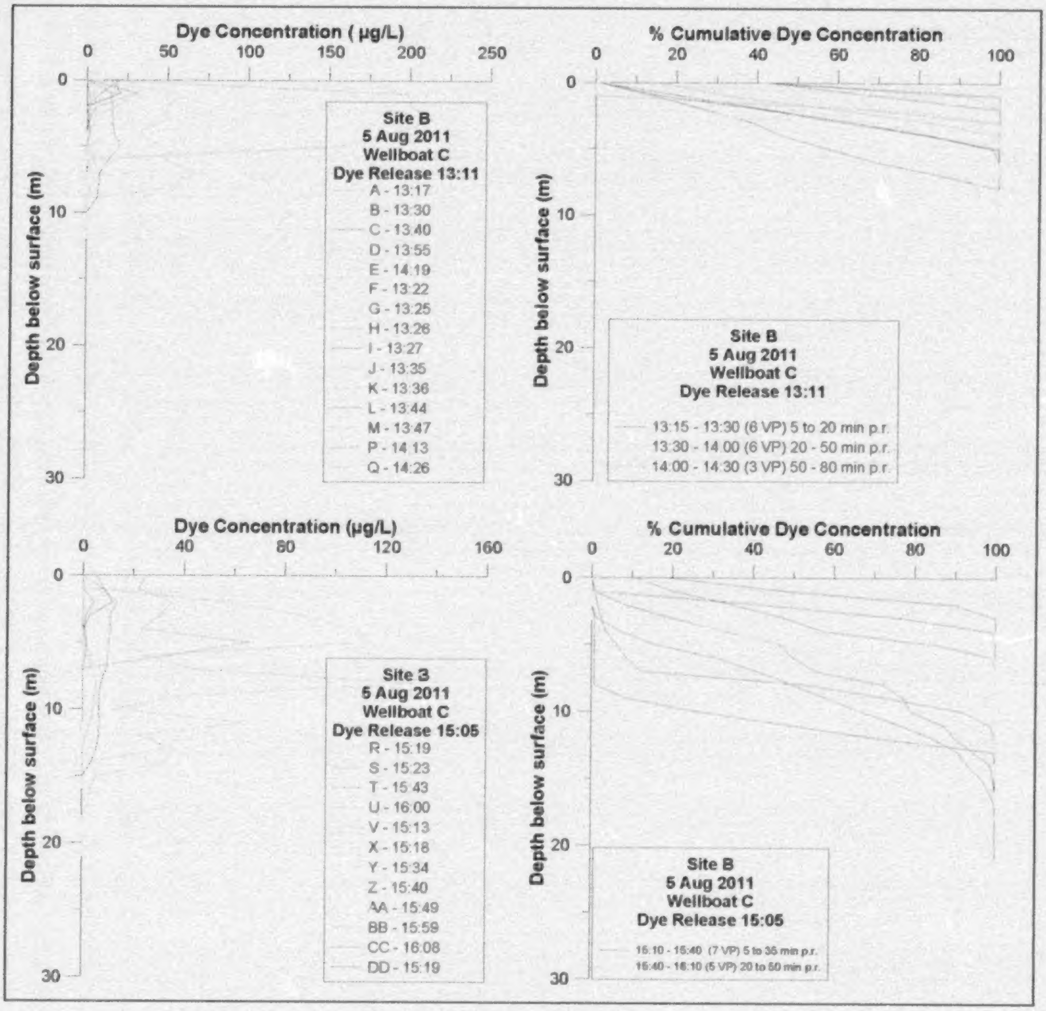

Figure 74. Vertical dye concentration profiles (left panel) and cumulative concentration versus depth curves (right panel) associated with dye releases from Well-boat C at Site B. The average site depth at mean low tide is 35.3 m. VP = Vertical Profile, p.r. = post release.

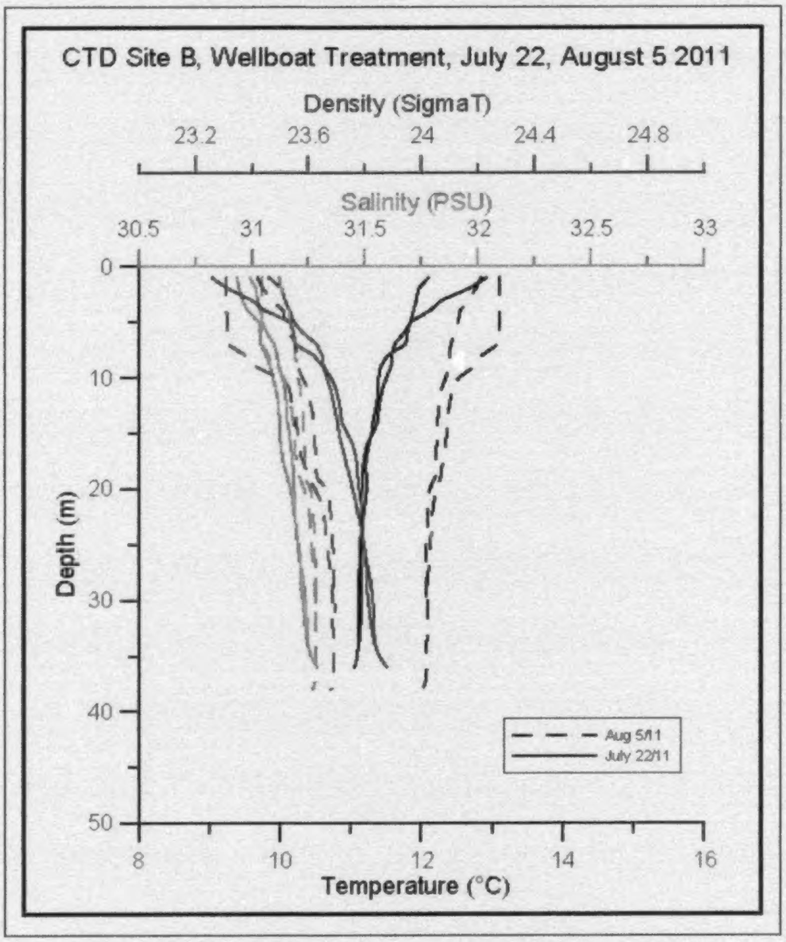

Figure 75. Temperature, salinity and density profiles of the water column collected during well-boat dye studies at Site B.

Site D – Well-boat A – 30th of September 2010

On the 30th of September 2010, forty vertical profiles of dye concentration were collected from Site D during two dye releases from Well-boat A. Dye was released from the port tank of the well-boat first and subsequently the starboard tank; the port side of the vessel was facing away from the salmon cage, and the starboard side of the vessel was facing into to the salmon cage. Ten of the profiles collected did not detect any dye. The vertical profiles where dye was detected are shown in Figure 76. Of these, only four vertical profiles were collected after the second release (profiles E and N), and could not be attributed decisively to the first or second release. Therefore the data for the two releases are pooled. Dye was detected down to 20 m below the sea surface, compared to an average site depth at mean low tide of 20 m. There was a continuous increase of density to a depth of 10 m resulting in a $\Delta\sigma_T$ of 0.8 between 0-10 m (Figure 77).

The profiles obtained on the 30th of September 2010 indicate that the dye plume was between 5 and 15 meters below the sea surface. The majority of the dye was located above the base of the pycnocline. The highest concentrations were detected at a depth of 11 m in profile G at the base of the pycnocline (unfortunately the profile does not continue until the bottom of the dye plume). The presence of the dye at subsurface depths and lack of dye at the surface is consistent with the angle of discharge of the effluents from Well-boat A (45º).

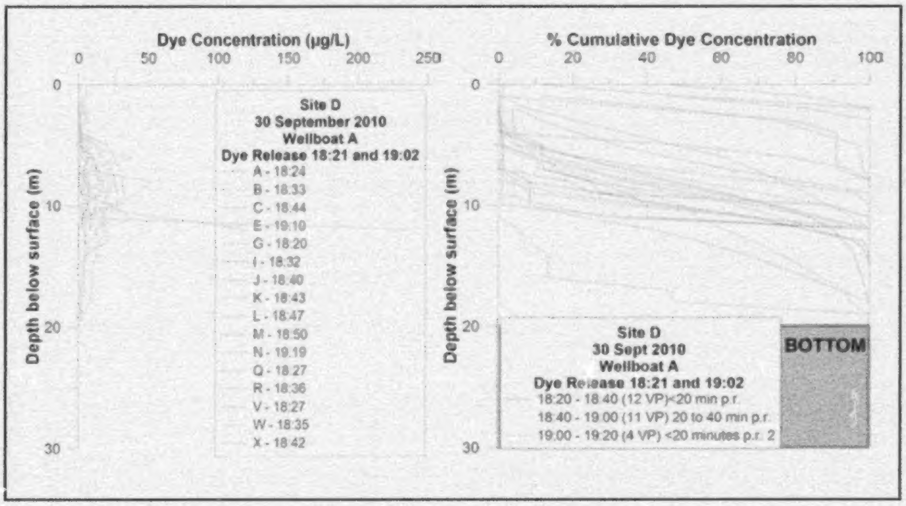

Figure 76. Vertical dye concentration profiles (left panel) and cumulative concentration versus depth curves (right panel) associated with dye releases from Well-boat A conducted at Site D. At Site D, the average site depth at mean low tide is 20.5 m. VP = Vertical Profile, p.r. = post release

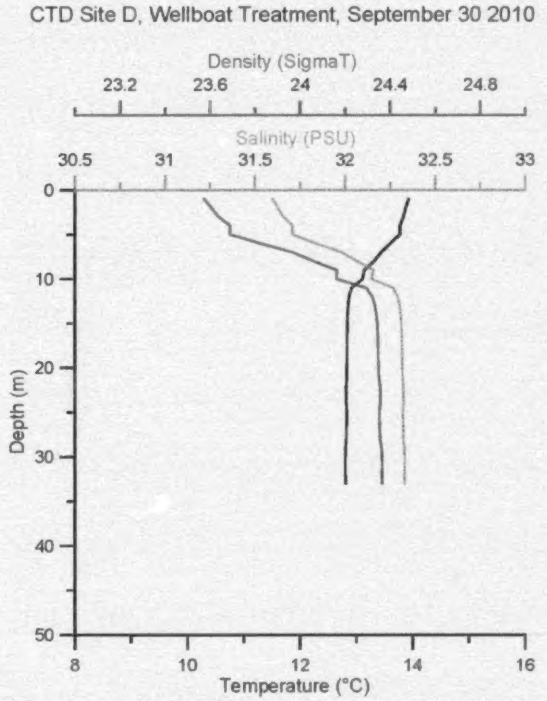

Figure 77. Temperature, salinity and density profiles of the water column collected during well-boat dye studies at Site D.

Site E – Well-boat B – 14th of October 2010

On the 14th of October 2010, fourteen vertical profiles of dye concentration were collected from Site E during a dye release from Well-boat B. Dye was released from the starboard tank of the well-boat, with the dye ejected from the side of the boat opposite the side that was anchored to the salmon cage. Six of the profiles collected did not detect any dye. The vertical profiles where dye was detected are shown in Figure 78. Dye was detected down to 20 m below the sea surface, compared to an average site depth at mean low tide of 15.7 m. The water density increased continuously with depth, with $\Delta\sigma_T$ of 0.1- 0.2 over 0-20 m (Figure 79).

The profiles obtained on the 14th of October 2010 show that the dye plume was located several meters below the sea surface, between 5 and 20 m. The highest concentrations were detected at a depth of 18 m in profile H. Several incomplete profiles (e.g., dye detected at a given depth but no data available at lower depths) indicate that dye may have been present at depths lower than the maximum depth it was recorded (20 m). The presence of the dye at subsurface depths and lack of dye at the surface is consistent with the angle of discharge of the effluents from Well-boat A (90º).

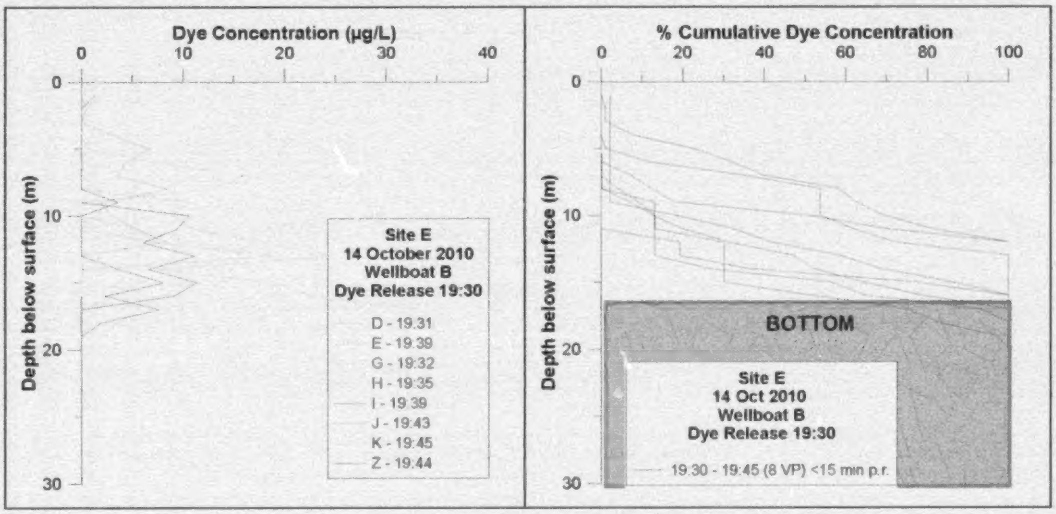

Figure 78. Vertical dye concentration profiles (left panel) and cumulative concentration versus depth curves (right panel) associated with dye releases from Well-boat B conducted at Site E. The average site depth at mean low tide is 15.7 m. NOTE: Cumulative profiles for the incomplete profiles (G and H) are presented in this figure; insufficient dye data at deeper depths may skew the cumulative profiles. VP = Vertical Profile, p.r. = post release.

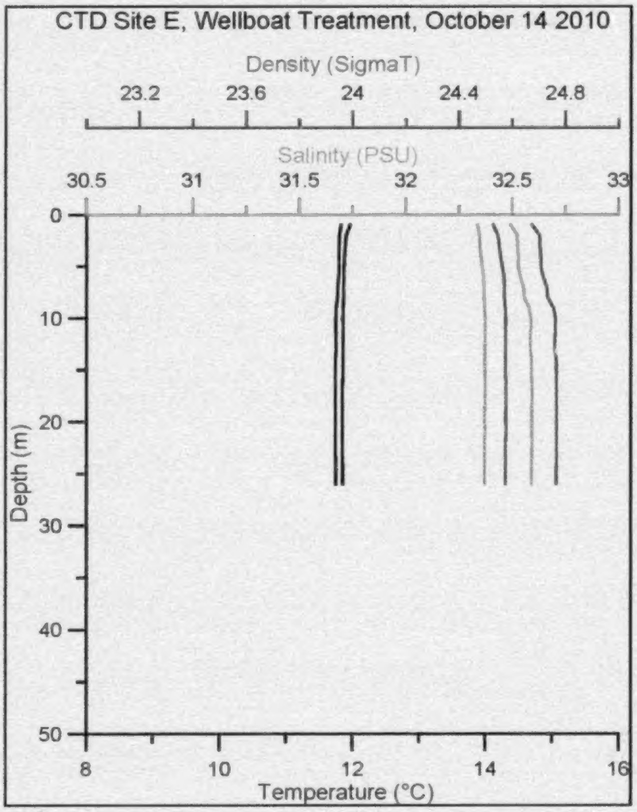

Figure 79. Temperature, salinity and density profiles of the water column collected during a well-boat dye study at Site E.

Site G – Well-boat B – 8th of December 2010

Twenty vertical profiles of dye concentration were collected from Site G during a dye release from Well-boat B the 8th of December 2010. Dye was released from the port tank of the well-boat, with the dye ejected from the side away from the salmon cage the well-boat was anchored to. Seven of the profiles collected did not detect any dye. The vertical profiles where dye was detected are shown in Figure 80. Dye was detected down to 20 m below the sea surface, compared to an average site depth at mean low tide of 20.6 m. The water column was well mixed, with $\Delta\sigma_T$ of 0.1 over 0-20 m (Figure 81).

The profiles obtained on the 8th of December 2010 show that the dye was primarily in the upper 10 m of the water column, with the highest concentrations measured between 0 and 5 m. However, one subsurface peak at 10 m was detected. Variation in the vertical extent of the plume through space and time is evident by comparing profile J to profile I, taken only four minutes apart and at roughly the same position from the well-boat. Profile J detects dye in concentrations of 40 µg/L or greater to a depth of 15 m (no data are available for lower depths) while profile I detected high concentrations of dye (up to 180 µg/L) contained within the upper 5 m of the water column and no dye below.

Given that Well-boat B discharges at a 90 angle from the surface (vertically downward), the observations of the dye plume located in the upper 5 m are not what would be predicted. The observations cannot be explained by density differences either, as the pycnocline was very weak. Photos also recorded a plume at the surface around the same timeframe and the same location that the profiles were collected.

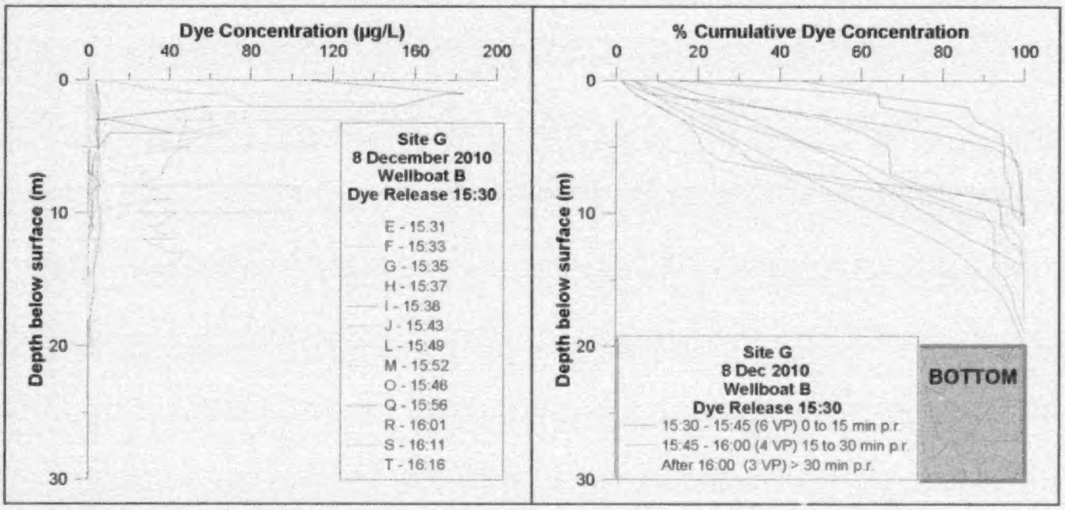

Figure 80. Vertical dye concentration profiles (left panel) and cumulative concentration versus depth curves (right panel) associated with dye releases from Well-boat B at Site G. The average site depth at mean low tide is 20.6 m. VP = Vertical Profile, p.r. = post release

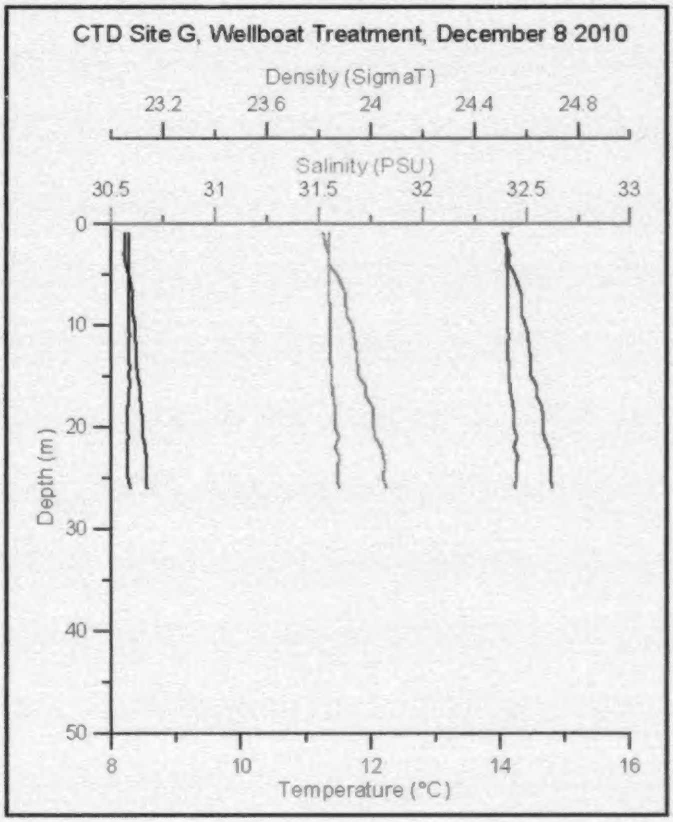

Figure 81. Temperature, salinity and density profiles of the water column collected during a well-boat dye study at Site G.

Transport and Dispersal of Plume once Released into the Receiving Environment

Once the flushing has stopped, the patch of therapeutant created by the flushing process will be transported and dispersed by the ambient velocities and eddy dispersion processes described above. This additional dispersal is the topic of ongoing work and has not been considered extensively in this report.

Observations of Concentrations

To test the efficacy of the sampling program to characterize the dye plumes, we compared the calculated concentration of dye in the plumes (based on the amount of dye used in the trial and the volume of the plume at given times) with measured concentrations in transects within the dye plumes during various dye trials.

The calculated concentration of dye in a plume at given times was based on the amount of dye used in each trial (M) and the estimated volume of the plume at a specific time. For the well-boat trials, well flushing occurred over 20-30 min. We calculated the amount of dye that should be in the plume as the original amount of dye added to the well minus any dye remaining in the well at the selected times. The amount remaining in the wells was based on data from fluorometers placed in the wells; we could only use data collected after the fluorometer readings in the wells had fallen below the maximum calibration levels (about 25 min after the start of flushing).

The volume of the plume was estimated as the area of the plume multiplied by the depth. The area of the plume was based on the patch outlines obtained at various times during each trial. The depth of the plume was based on the vertical profiles of dye concentration taken in the plume at or near the same times as the outline tracks.

The calculated concentration of dye was compared with the average measured dye concentration in horizontal transects completed at the same times as the plume outlines. The horizontal transect data were from 1-3 m below the water surface.

In general the comparison indicates that the measured dye concentrations (Figure 82) are lower than the calculated. This may be due to the fact that the measured dye concentrations may be biased downwards due to interference from sunlight or that the calculated concentrations are too high due to an overestimate of the volume or amount of dye added to the well.

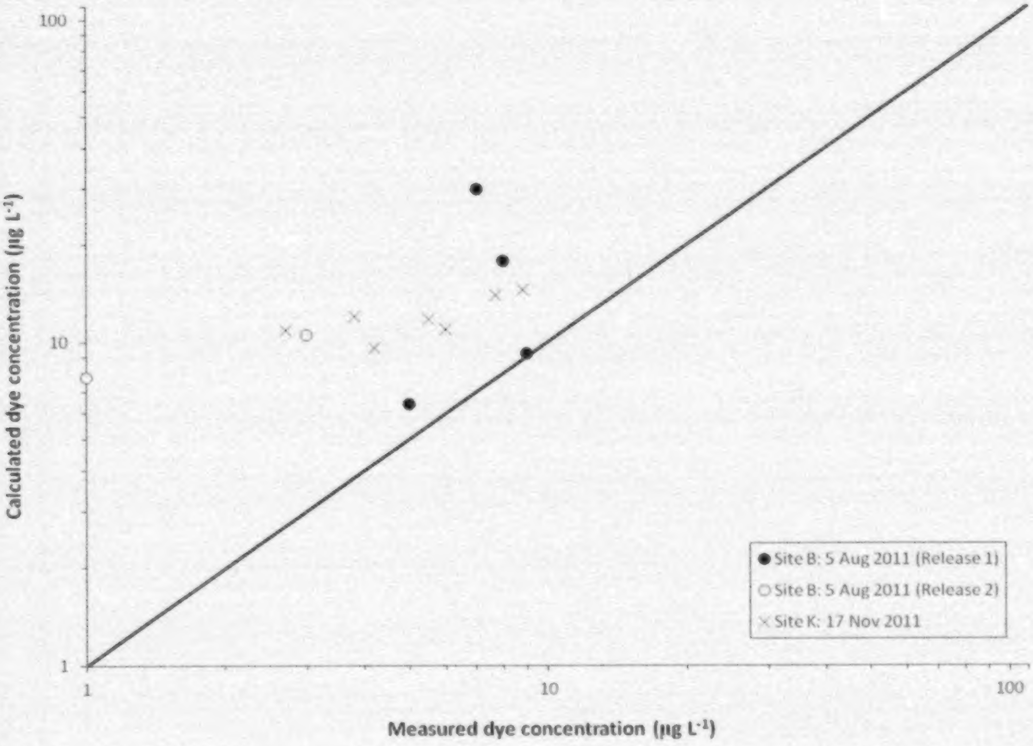

Figure 82. Comparison of measured and calculated dye concentrations in dye plumes resulting from well-boat treatments.

Summary of Transport and Dispersal from Well-Boats

The time series of concentrations of dye in the discharge jet during flushing corresponded closely to the time series of concentrations inside the well. Dilution of dye concentrations in the discharge jet were consistent with predictions based on assumption that dilution is achieved through entrainment of ambient water in discharge. Predicted maximum concentrations inside the discharge jet based on pumping rates were consistent with field observations. Based on predicted dilution factors, at 20 minutes after the start of flushing, in the area 10 to 50 m from the well-boat discharge pipe, concentrations of dye will be diluted by 10x to 100x compared to the concentration inside the well at the time when discharge began. At 60 minutes after the start of flushing, concentrations of dye will be diluted by 100x to 1000x compared to the concentration inside the well at the time when discharge began.

Limited data on the horizontal characteristics of dye patches were available. The horizontal characteristics of the observed dye plumes were consistent with the general nature of plumes. The patches of dye were roughly elliptical, with the long axis in the direction of the mean flow. There was considerable variation in the shape of the dye plumes.

Over 262 vertical profiles were collected over the treatment studies, with 202 defined as within the dye plume. Vertical profiles of dye concentration showed a lot of variation in terms of absolute concentration, profile shape and maximum depth at which dye was detected. Profiles taken minutes apart sometimes showed very different characteristics. The maximum depths at which dye was detected through time are shown in Figure 83. Similarities in the maximum vertical distributions of the dye for releases from a given well-boat are evident, but this observation may be confounded by the presence of pycnoclines and strong density stratification on several of the treatment data as well as interference from cage infrastructure.

For Well-boat A, the plume was largely in the upper 5 m which was consistent with angle of discharge of the well-boat of 45º, but also probably caused by the strong pycnocline.

For Well-boat B, with the 90º discharge angle, the plume depth varied between largely subsurface (as expected) following one release and within the upper 5-10 m for a separate release.

For Well-boat C, the observed plumes from three of the five dye releases were largely in the upper 5 m, consistent with the angle of discharge of the well-boat of 0º, but also consistent with the strong stratification present for at least two of the releases. In a third release which took place in weak stratification, dye was detected to 10 m and to 15 m, possibly due to cage infrastructure.

For 6 of the 7 releases, dye was detected at maximum depths for the release (or within 1 m of maximum depth for that release) within 15 minutes from the start of flushing. At three different sites, the dye was detected at depths of mean low tide.

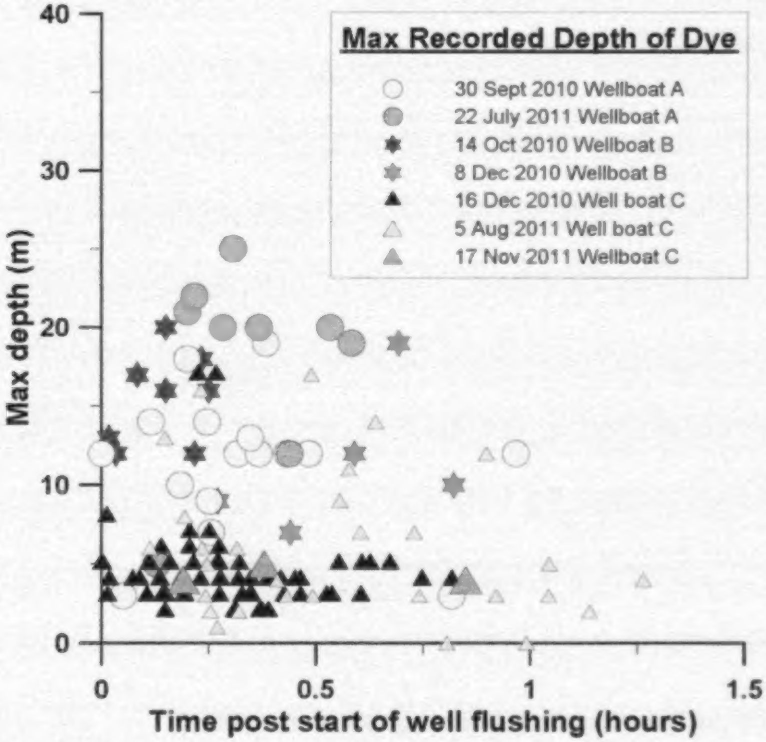

Figure 83. Maximum depth of dye detected through time, post the start of flushing of well. Concentrations greater than 1 µg/L considered.

Models

Methods

In contrast to modelling releases from cages, modelling the release of therapeutants from well-boats has the extra complexity that the treated water has its own momentum as it leaves the well-boat. Furthermore, the direction of the discharge is not necessarily in the horizontal direction. FVCOM has the ability to include river discharges into the model domain. By definition, the river must be on a coastline. In theory this feature can be modified to allow a discharge of water at a non-coastline location in the model domain but in practice this is not a feasible approach. The smallest length scale in the horizontal FVCOM grid used for modelling southwest NB is 24 m whereas the well-boat opening from which the treatment water is discharged is roughly 1 m in diameter. Thus if the existing grid is used with a modified version of FVCOM to allow for well-boat discharge, the momentum from the well-boat discharge is not resolved. Modelling a well-boat discharge requires a very high-resolution grid which is not numerically feasible with the computing resources available at this time.

The particle tracking results simulating the well-boat dye release studies conducted at Sites B and K on the 5th of August 2011 and the 17th of November 2011, respectively, are presented below. The purpose of this exercise is not only to try to recreate the results of the well-boat dye releases, but to learn what limits the model's capability to simulate this scenario and identify areas of further refinement. Recall that the FVCOM run used does not include the extra surface drag due to the fish cages. This may account for some of the differences observed, but not all. Although the additional momentum of the water being discharged from the well-boat is not included, the particle tracking model has been modified to model the continuous release of the treatment water over a given time. Additionally, the decreasing concentration of the dye as it leaves the well-boat is modelled by having an exponentially decreasing number of particles released from the source over the release time period. The particles are initially distributed over a cylinder of volume 330 m^3, having a radius of 3.24 m and a depth of 10 m, to simulate the volume of water in the well-boat.

Comparison between FVCOM Model and Observations

At Site B, two dye releases took place on the 5th of August 2011. The comparison with the particle tracking model and the dye perimeter measured in the field for this day are shown in Figure 84 and Figure 85. Results for the release at Site K on the 17th of November 2011 are shown in Figure 86.

First the results at Site B are examined. Results of tarp treatment dye releases have already been examined at this location. The comparisons of the FVCOM predicted currents with the ADCP measurements indicated that the current's phase predicted by the model lags that of the observations by up to one hour. This indicates that the middle columns of Figure 84 and Figure 85 should give best agreement with the dye patch perimeters measured at the time of the dye release from the well-boat. It is tempting to conclude from Figure 85 that the model actually predicts the evolution of the dye plume reasonably well if one takes into account the fact that there is no surface drag due to the fish cages added to the model. The results in Figure 84, however, show that this is clearly not the case. Here, the dye patch in the middle column is not even moving in the correct direction although the horizontal scale of the dye patch is reproduced by the model. Results at Site K are no more encouraging with the modelled particle patch moving in the wrong direction.

It is not clear from the present results precisely where the model fails although there are certainly areas where the model can be improved upon. As already discussed, it is imperative to ensure that the modelled flow field accurately represents the actual flow in the areas of interest. At Site K, there is one short ADCP record available for the time of the well-boat dye release but that has not yet been compared with the FVCOM results so it is unknown how well the model is predicting the flow field. Ensuring that the model correctly predicts the circulation in fish farm areas may include grid refinement, the use of variable bottom drag, the inclusion of a surface drag in the vicinity of the fish farm cage locations and the use of a nested high resolution model as discussed in Section 2.1.13. Ultimately, however, it will likely be necessary to use a different model to define the initial spread of the plume due to the small spatial scales involved and use this model to initialize the particle tracking model which is forced by the larger scale flow predicted by FVCOM.

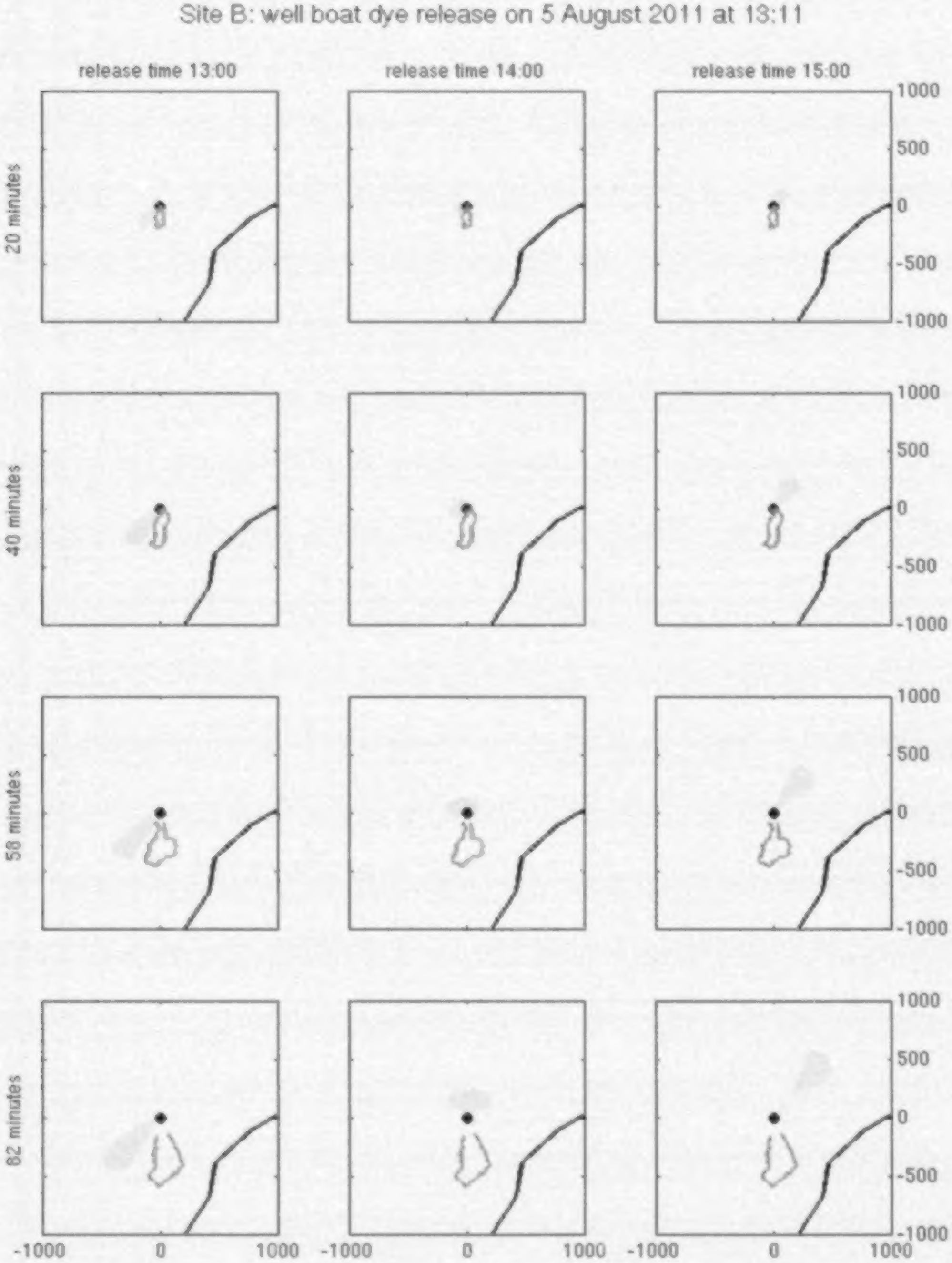
Site B: well boat dye release on 5 August 2011 at 13:11
release time 13:00
release time 14:00
release time 15:00
20 minutes
40 minutes
58 minutes
82 minutes
1000
500
0
-500
-1000
-1000
0
1000

Figure 84. Comparison of particle tracking model with particles continuously released over 55 minutes and well-boat release at Site B on the 5th of August 2011 at 13:11. The dye release location is indicated by a black dot. The red lines indicate the observed perimeters of the dye patches. The particle patch is shown in cyan. Times are given in minutes past the release time.

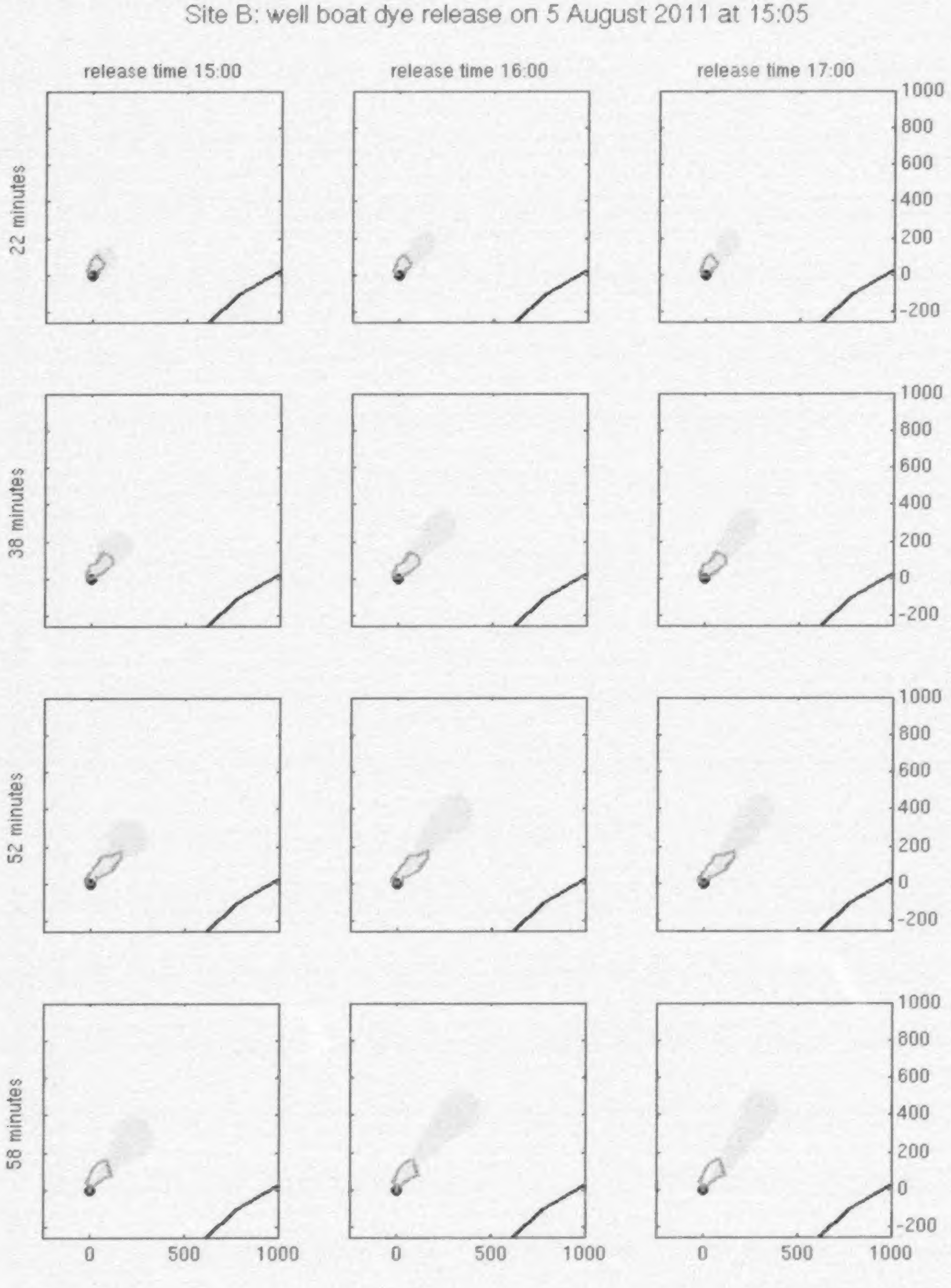

Figure 85. Comparison of particle tracking model with particles continuously released over 63 minutes and well-boat release at Site B on the 5th of August 2011 at 15:05. The dye release location is indicated by a black dot. The red lines indicate the observed perimeters of the dye patches. The particle patch is shown in cyan. Times are given in minutes past the release time.

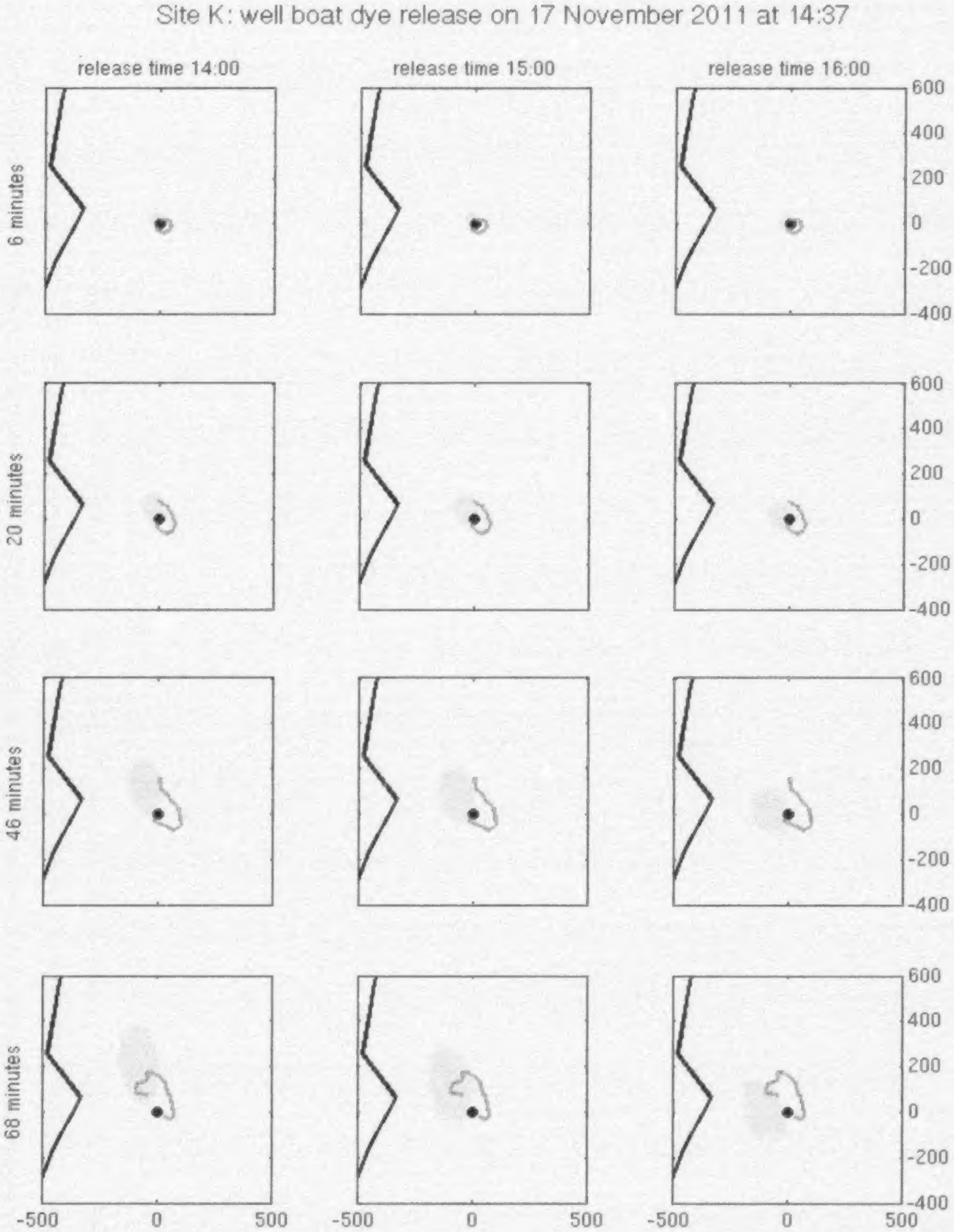
Site K: well boat dye release on 17 November 2011 at 14:37
release time 14:00
release time 15:00
release time 16:00
6 minutes
20 minutes
46 minutes
68 minutes
600
400
200
0
-200
-400
-500
0
500

Figure 86. Comparison of particle tracking model with particles continuously released over 22 minutes and well-boat release at Site K on the 17th of November 2011 at 14:37. The dye release location is indicated by a black dot. The red lines indicate the observed perimeters of the dye patches. The particle patch is shown in cyan. Times are given in minutes past the release time.

CHEMISTRY

Strictly speaking the above information pertains to the distribution, mixing, transport and dispersal of the fluorescein dye. However, the purpose of the work is to gain insight into the distribution, mixing, transport and dispersal of therapeutants. In the absence of contrary information, it can be assumed that the information gleaned from the dye is applicable to the therapeutants.

Previous work has shown that dye is a good proxy for at least some therapeutants, including cypermethrin (Ernst et al. 2001). The work below shows that dye is also a good proxy for azamethiphos. Unfortunately, we could not establish a relationship between hydrogen peroxide or Alphamax® and dye. In the case of hydrogen peroxide, the presence of the fluorescein dye interferes with the techniques we tried for measuring hydrogen peroxide. In the case of Alphamax®, due to circumstances beyond our control, we were unable to conduct sufficient field trials to establish a relationship.

CHEMICAL-DYE RELATIONSHIPS

In order to establish a relationship between the concentration of Salmosan® (a.i. [active ingredient] azamethiphos) and dye, water samples were taken at various locations within the treatment cage just prior to release and at various locations and times within the dye plume as it evolved. For each water sample the concentrations of dye and azamethiphos were determined. A plot of the azamethiphos concentrations against the dye concentrations (Figure 87) shows that there is a linear relationship between the two and that a particular dilution of dye corresponds to the same relative dilution of azamethiphos.

Unlike azamethiphos, we had a more limited dataset with which to establish a dye-chemical relationship for deltamethrin in Alphamax®. However, the data that were available also show a positive relationship between the dye and therapeutant concentrations in that a given dilution of dye corresponds to the same relative dilution of deltamethrin (Figure 88 and Figure 89).

In summary, it seems reasonable to assume that the dye gives a reasonable first approximation to the concentrations of azamethiphos and deltamethrin expected in the field.

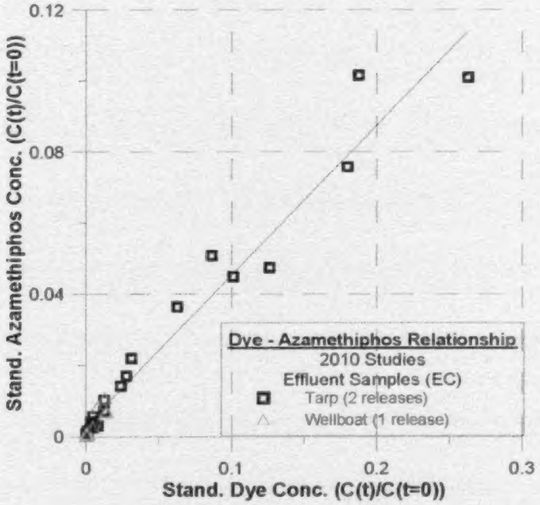

Figure 87. Relationship between dye and azamethiphos concentrations in effluents from salmon aquaculture treatments. Dye concentrations were standardized to the initial concentration (measured concentration/initial dye concentration). The straight line is a linear regression for tarp samples only (R-squared of 0.96).

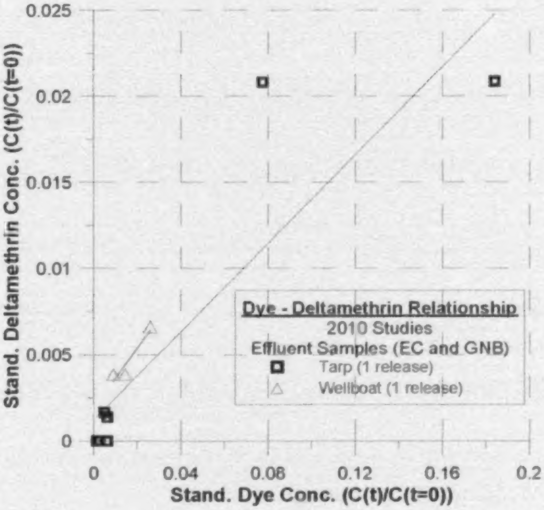

Figure 88. Relationship between dye and pesticide deltamethrin concentrations in effluents from salmon aquaculture treatments. Dye concentrations were standardized to the initial concentration (measured concentration/initial dye concentration). Samples below detection limits are presented as 0. The black regression line through the data includes all of the data.

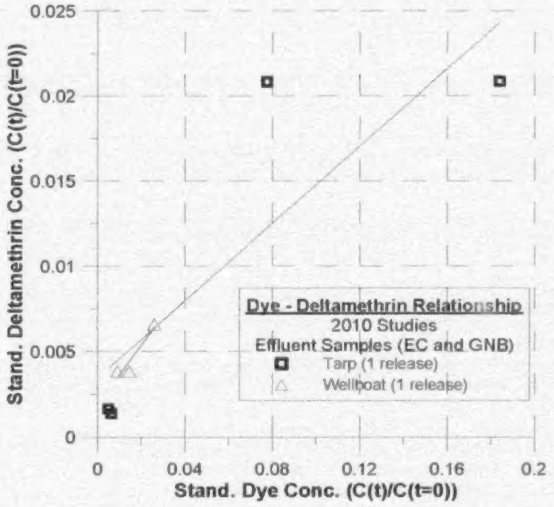

Figure 89. Same plot as in Figure 88, with the exception that the data being designated as having concentrations below the detection limit has been removed from the plot and regression analyses. The black regression line through the data includes all of the data.

CHEMICAL PERSISTENCE

The persistence of Paramove® 50 hydrogen peroxide was tested in the laboratory for several temperature regimes using a temperature controlled mixing bath (Figure 90). In order to estimate the degradation or persistence of the peroxide, water samples were extracted at regular time intervals and the peroxide concentrations determined using the Solvay Interox titration method of analyses. Figure 91 shows that the concentration of Paramove® 50 hydrogen peroxide did not degrade significantly over the 3-h time period in each of the temperatures investigated. The only noticeable difference was at 20°C which showed slightly more degradation. Therefore it can be concluded that Paramove® 50 does not degrade within the period used in well-boat treatments and over the time scales of transport and dispersal considered in this report. Ongoing work is following the peroxide concentration for a longer period of time. So far we have seen relatively little degradation after 19 days.

The degradation rate of Salmosan® was not tested in the laboratory. However, the fact that the dye-chemical relationship between Salmosan® and dye supports the assumption of a 1:1 dilution relationship, i.e., an order of magnitude reduction in dye concentration corresponds to an order of magnitude reduction in therapeutant concentration is consistent with the assumption that the therapeutant is not significantly degrading over the few hour time period represented by these studies.

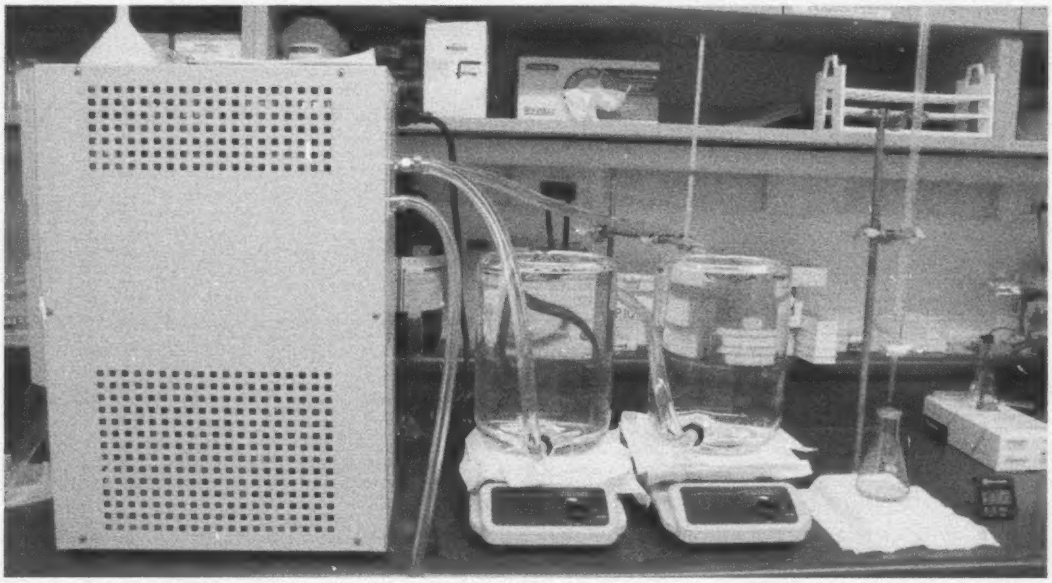

Figure 90. Photograph of the temperature bath system used to determine the change in therapeutant concentration over time. The beakers in the picture are 5-L jacketed beakers containing a stirring bar and they are sitting on top of a magnetic stirring plate.

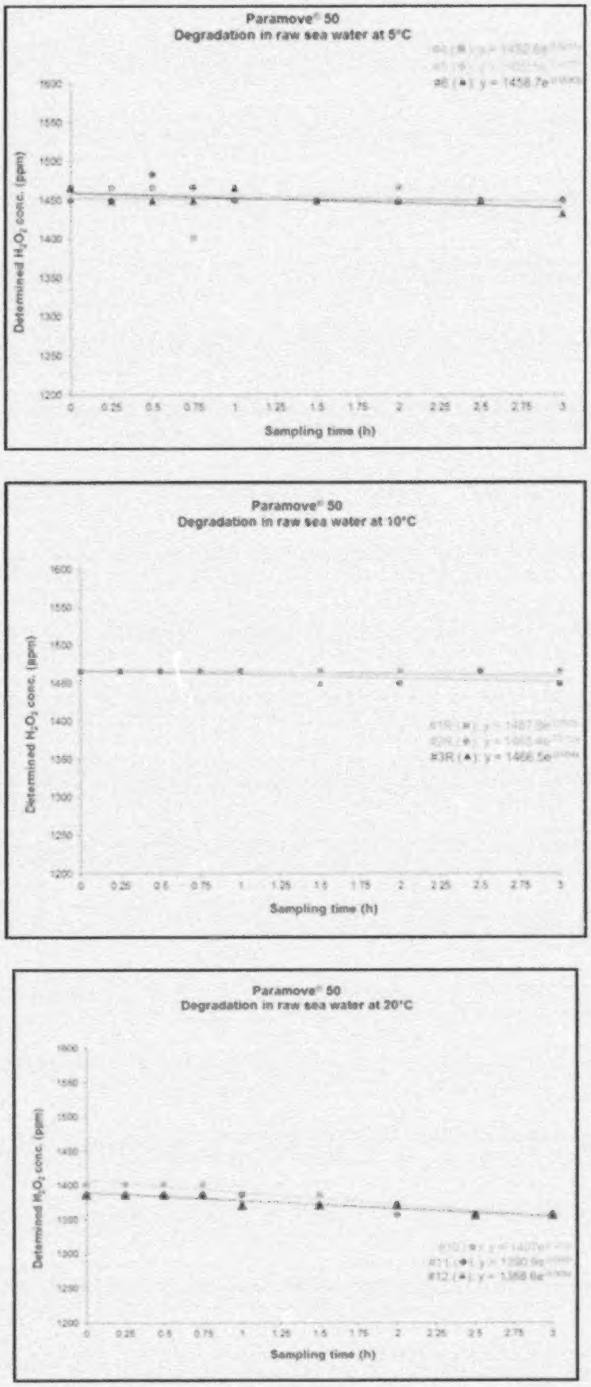

Figure 91. Temporal evolution of the concentration of Paramove® 50 hydrogen peroxide at several water temperatures (5 °C – top, 10 °C – middle, 20 °C – bottom).

SUMMARY AND CONCLUSIONS

The theory and observations presented above give some insight into the characteristics of the transport and dispersal of bath treatment therapeutants released into the aquatic environment. The work also helps to identify and prioritize the many factors that influence the nature of the transport and dispersal of therapeutants from tarped fish cages and well-boats. Even though a considerable amount of work has been done and a foundation has been laid from which additional work can be based, the overall sample size remains relatively small. Additional dye treatments would help augment the present data set and help provide more insight into the actual variations and consistencies of the processes. Also additional equipment would enable dye plumes to be monitored more completely so their horizontal and vertical domains could be more fully characterized.

FACTORS INFLUENCING NET-PEN TRANSPORT AND DISPERSAL

The factors influencing tarp bath treatments include fixed factors such as the:

- scale of the tarped cage (diameter, volume)
- amount of the therapeutant used
- mixing within the bath containment volume
- proximity and nature of nearby cages and other farm infrastructure
- net mesh size and degree of bio-fouling
- treatment procedures (e.g., how tarps are removed, pursing and dropping of nets);

and environmental factors such as:

- rates of mixing in the horizontal (x,y) and vertical dimensions
- rates of horizontal advection
- spatial variation in the flow field
- vertical stratification
- local bathymetry that determines whether the sea bottom and inter-tidal areas are near enough to be at risk of exposure
- weather, wind and waves
- water characteristics such as temperature, salinity, pH, dissolved oxygen content, suspended organic and sediment loads that may infleunce the chemical behaviour of the therapeutant in the ambient water.

FACTORS INFLUENCING WELL-BOAT TRANSPORT AND DISPERSAL

The factors influencing well-boat bath treatments include fixed or controllable factors such as:

- the volume of wells
- the angle of discharge, i.e., horizontal, vertical or at some other angle
- the diameter of the discharge pipe
- the depth or height of the discharge pipe below (above) the sea surface

- the maximum rate of discharge flow, i.e., pumping capacity
- the mass of therapeutant introduced into well i.e concentration of source
- the density of the discharge solution – this is usually the same as the ambient water
- the velocity of discharge (the operator can vary this)
- the direction of the discharge, i.e., into cages or away from cages
- the duration of the discharge
- the proximity of other cages and other farm infrastructure
- the degree of bio-fouling on adjacent fish cages;

as well as environmental factors such as:

- the rates of horizontal mixing in the receiving environment
- the rates of ambient horizontal and vertical mixing in the receiving environment
- the proximity of vertical boundaries in relation to vertical stratification the sea bottom and inter-tidal zones
- the proximity of horizontal boundaries such as the shoreline, bottom and pycnocline
- the weather, wind and waves
- the chemical behaviour of the therapeutant in the ambient water.

Once the plume is some distance from the well-boat and the cage and farm infrastructure, the environmental factors that affect the transport and dispersal from well-boat discharges are the same as those for trap treatments, i.e., the factors that influence local rates of transport and dispersal.

CONCLUSIONS FOR TARP TREATMENTS

Despite the many influencing factors, there are some specific conclusions that the work to date brings to light.

- Cage tarp treatments are restricted to periods of the tidal cycle when water currents are relatively weak, wind speeds are low and wave conditions are calm. This is because site crews are unable to easily tarp the cages in strong currents and want to avoid the billowing of tarps since this will trap the fish in small pockets of water. Health and safety conditions also play a decisive role. Exact limits for these conditions are not available.
- Releases from tarped fish cages are finite size releases.
- Releases may be near instantaneous or spread out over tens of minutes to a few hours.
- The observed increase in the scale of the dispersing patches from tarp treatments appears to be in general agreement with predictions based on Okubo relationships. The rate of increase is suggested to agree more closely when the patches are not influenced by cage infrastructure. When cage infrastructure is involved, the scale of the patch seems to undergo a more rapid increase than predicted by the Okubo relationship. However, after the first hour, observations follow the Okubo rate of increase in patch size.
- The degree of dilution is dominated by horizontal mixing processes since these are an order of magnitude or more larger than vertical mixing processes.

- Concentrations of dye and therapeutant are highly variable and hence numerous measurements need to be made in order to clearly show patterns.
- Dispersal patches or plumes are generally elongated rather than circular, with the major axis of the patch being parallel with the predominate direction of the flow.

CONCLUSIONS FOR WELL-BOATS

- Well-boats can conduct treatments at most if not all phases of the tide and in a wider range of weather conditions.
- Flushing discharges have a finite initial size, a continuous flow for a limited period of time and a concentration of waste in the flow that decreases with time.
- Well-boat discharges are diluted more quickly than tarp discharges because of the mechanical dilution involved in the former.
- Each discharge is different due to variations in the concentration within the discharge, as well as variations in the rates, durations, angles and directions and receiving environments of discharges.
- Fifty percent (50%) of well-boat flushing discharges in southwest New Brunswick are directed away from the farm infrastructure and 50% are directed into fish pens. These two discharge types need to be treated differently. Some theory exists to help with the former type but no theory exists for the latter.
- To a first approximation, observed dye concentrations obtained from within a well during flushing agree with concentrations predicted from a simple single cell reactor mixing model in which the discharge rate of treatment water equals the inflow rate of ambient water.
- The observations and mixing theories appear to be in general agreement with respect to the immediate near-field flushing and jet characteristics.

CONCLUSIONS COMMON TO BOTH TARP AND WELL-BOAT TREATMENTS

- Fish cage infrastructure definitely influences the transport and dispersal of the dye, and by inference, the chemical therapeutant. This influence is complex, not well understood and varies with site design and location. In all cases the infrastructure increases the horizontal mixing.
- Horizontal mixing rates exceed vertical mixing rates by at least an order of magnitude and both vary by one to two orders of magnitude due to specific site and time variations in local flow field conditions.
- No robust theory or prediction capability for the transport and dispersal of therapeutants accounts for the influence of fish cage and farm infrastructure. However, modelling developments that include the effect of cage drag on the flow do seem to improve the ability to model the local flow field and hence the transport and dispersal patterns.
- Each treatment, whether from a well-boat or tarped cage is unique to some degree.
- It appears possible to establish general scales of therapeutant transport and dispersal.
- An effort to model the full spatial and temporal evolution of the transport and dispersal of well-boat flushing discharges is still underway.

- A balance will need to be established that determines the degree of accuracy and site specificity needed. There is considerable variation in the transport and dispersal patterns among treatments and it is unlikely that these will be predicted. Hence, regulation and use of the therapeutants will need to account for this limitation.
- Predictions of transport direction and magnitude are difficult to make. Single current meter records are certainly not sufficient. Models are the only practical way forward and although these seem to give results that are of the correct magnitude they still need further development before they can be considered highly robust.
- Studies in which dye is mixed with the therapeutant are really the only way to empirically determine the transport and dispersal of the therapeutants and hence the only way to guide where water and effects samples should be taken.
- In the studies conducted to date in our area, dye was detected to a depth of at least 20 m.
- In the studies conducted so far there is not strong evidence for the decay of the therapeutants on the time scale of a few hours.
- We did not explicitly consider multiple releases in this document. However, a simple way to consider this aspect is to assume concentrations relating to multiple releases are additive. Hence, the worst case scenario from a concentration perspective is that five releases were conducted simultaneously in both space and time. This would mean the concentrations at any given time and place are five times more than the single release scenario. The other extreme is that the releases are independent and flow in different directions. This would mean the concentrations stay the same but the area occupied by the plumes increase by a multiple of the number of releases. Obviously the real situation is somewhere in between.
- The above work focuses on the transport and dispersal of therapeutants and not on the potential for toxicity. This is considered in the working paper by Page et al. this meeting.

CONCLUSIONS BASED ON THE THEORIES AND OBSERVATIONS EXAMINED

Despite the many variables influencing the transport and dispersal and the limitations of the work conducted to date, the unmodified Okubo approach appears to give a robust and conservative estimate of therapeutant dilution from net-pens over the first few hours after release. The approach has the advantage that the calculations are relatively straightforward and requires relatively little input information; the only information needed is an estimate of the total amount of therapeutant released, the horizontal and vertical extent of the initial release, the expected depth range over which therapeutant will be found and the decay rate of the therapeutant itself. However, the unmodified approach does seem to underestimate the size of the patch, and hence overestimates concentration, when the initial spreading of the patch encounters adjacent farm infrastructure such as other cages. More empirical and modelling work will be needed to better characterize this influence.

From a well-boat perspective the back of the envelope solutions provided here give some guidance but they need more development and more empirical support. The characteristics of the immediate discharge seem to be reasonably well represented by the steady state theory used here although a time dependent solution would be more satisfying. More plume tracking studies need to be conducted and immediate discharge dynamics need to be coupled with the transport and dispersal processes in the receiving environment. Also different vessels have different discharge configurations, pumping rates vary and are not well known, and present discharge procedures in southwest New Brunswick result in fifty percent of the discharges being directed into adjacent cages. These factors result in a complex transport and dispersal environment that has not been well described here.

Finally, although the work was conducted in southwest New Brunswick, the general principles and orders of magnitude dilution are expected to apply elsewhere. The Okubo relationship is based on data collected from many places around the world and it should apply in other areas of Canada as well. What will differ from location to location is the local hydrography, bathymetry and perhaps treatment procedures. The local stratification and current regime will dictate the depth to which therapeutants mix and the direction and magnitude of the therapeutant transport. The bathymetry within the zones of influence will dictate whether the benthic habitat will be exposed. The treatment procedures will influence the initial release characteristics. Because of the local differences it is important that work be conducted in each of the main areas supporting net-pen aquaculture to build confidence that the general relationships do in fact apply there.

ACKNOWLEDGEMENTS

Cooke Aquaculture and the captains and crews of the Colby Perce and Ronia Carrier along with Northeast Salmon and the captains and crews of the Ronja kindly allowed us to work on their vessels during operational bath treatments and at times made the vessel available to us for pure dye release field trials. Jeff Cline helped with sampling operations during some of the field trials. Ian Armstrong introduced well-boat bath treatment technology to southwest New Brunswick and provided valuable insight into well-boat operations. The New Brunswick Salmon Growers Association, now the Atlantic Canada Fish Farmers Association, and Betty House in particular, coordinated the initial access to the Ronia Carrier well-boat. Dr. Leanne Hawkins, the head veterinarian for Cooke Aquaculture, supervised several of the well-boat treatments.

REFERENCES CITED

Bowden, K.F. 1983. Physical Oceanography of Coastal Waters. Ellis Horwood Limited, John Wiley and Sons, 302 pp.

Chen, C., H. Liu, and R.C. Beardsley. 2003. An Unstructured Grid, Finite-Volume, Three-Dimensional, Primitive Equations Ocean Model: Application to Coastal Ocean and Estuaries. J. Atmos. Oceanic Tech. 20: 159-186.

Chen, C., R.C. Beardsley, and G. Cowles. 2006. An Unstructured Grid, Finite-Volume Coastal Ocean Model: FVCOM User Manual. Oceanography 19: 78-89.

Csanady, G.T. 1973. Turbulent Diffusion in the Environment. D. Reidel Publishing Company, Boston, 248 pp.

Cushman-Roisin, B. 2014. Chapter 3: Turbulent Jets. In “Environmental Transport and Fate”.

Dupont, F., C.G. Hannah, and D. Greenberg. 2005. Modelling the sea level in the Upper Bay of Fundy. Atmos.-Ocean 43: 33-47.

Ernst, W., P. Jackman, K. Doe, F. Page, G. Julien, K. MacKay, and T. Sutherland. 2001. Dispersion and toxicity to non-target aquatic organisms of pesticides used to treat sea lice on salmon in net-pen enclosures. Mar. Pollut. Bull. 42: 433-444.

Fan, X., H. Wei, Y. Yuan, and L. Zhao. 2009. Vertical structure of tidal current in a typically coastal raft-culture area. Cont. Shelf Res. 29: 2345-2357.

Fischer, H.B., E.J. List, R.C.Y. Koh, J. Imberger, and N.H. Brooks. 1979. Mixing in Inland and Coastal Waters. Academic Press, 483 pp.

Foreman, M.G.G., J.Y. Cherniawsky, and V.A. Ballantyne. 2009. Versatile harmonic tidal analysis: Improvements and applications. J. of Atmos. and Oceanic Technol. 26: 806-817.

Greenberg, D.A., W. Blanchard, B. Smith, and E. Barrow. 2012. Climate change, mean sea level and high tides in the Bay of Fundy. Atmos.-Ocean 50: 261-276.

Lewis, R. 1997. Dispersion in Estuaries and Coastal Waters. Wiley, 312 pp.

Okubo, A. 1971. Oceanic diffusion diagrams. Deep-Sea Res. 18: 789-802.

Okubo, A. 1974. Some speculations on oceanic diffusion diagrams. Rapp. P.-v. Réun. Cons. int. Explor. Mer 167: 77-85.

Page, F., B. Chang, W. Ernst, G. Julien, and R. Losier. 2000. Research on the dispersion of sea louse pesticides in the marine environment. In: Science Review 1996 & '97 of the Bedford Institute of Oceanography, Gulf Fisheries Centre, Halifax Fisheries Research Laboratory, and the St. Andrews Biological Station. Fisheries and Oceans Canada, Maritimes Region, Dartmouth, NS. 169 pp.

Schroeder, K., J. Chiggiao, A.C. Haza, A. Griffa, T.M. Özgökmen, P. Zanasca, A. Molcard, M. Borghini, P.M. Poulain, R. Gerin, E. Zambianchi, P. Falco, and C. Trees. 2012. Targeted Lagrangian sampling of submesoscale dispersion at a coastal frontal zone. Geophys. Res. Lett. 39: L11608.

Shi, J., H. Wei, L. Zhao, Y. Yuan, J. Fang, and J. Zhang. 2011. A physical-biological coupled aquaculture model for a suspended aquaculture area of China. Aquaculture 318: 412-424.

Spydell, M., and F. Faddersen. 2009. Lagrangian drifter dispersion in the durf zone: Directionally spread, noramally incident waves. J. Phys. Oceanogr. 39: 809-830.

Suh, S.W. 2006. A hybrid approach to particle tracking and Eulerian-Lagrangian models in the simulation of coastal dispersion. Environ. Model. Softw. 21: 234-242.

Venayagamoorthy, S.K, H. Ku, O.B. Fringer, A. Chiu, R.L. Naylor, and J.R. Koseff. 2011. Numerical modeling of aquaculture dissolved waste transport in a coastal embayment. Environ. Fluid Mech. 11: 329-352.

Vesilind, P.A., S.M. Morgan, and L.G. Heine. 2010. Introduction to Environmental Engineering. Third Edition. Cengage Learning, Stamford, USA, 603 pp.

Wu, X.G., and H.S. Tang. 2010. Coupling of CFD model and FVCOM to predict small-scale coastal flows. J. of Hydrodynamics 22: 284-289.

Wu, Y., J. Chaffey, D.A. Greenberg, and P.C. Smith. 2011. Tidally-induced sediment transport patterns in the upper Bay of Fundy: a numerical study. Cont. Shelf Res. 31: 2041-2053.

Wu, Y., J. Chaffey, B. Law, D.A. Greenberg, A. Drozdowski, F. Page, and S.P.A. Haigh. 2014. Three dimensional hydrodynamic model for aquaculture: a case study in the Bay of Fundy. Aquaculture Environmental Interactions 5: 235-248.

Xu, D., and H. Xue. 2011. A numerical study of horizontal dispersion in a macro tidal basin. Ocean Dynam. 61: 623-637.